Recent and active deformation structures in the central-eastern sector of the Betic Cordillera and the Alboran Sea: indentation processes and roll-back

Víctor Tendero Salmerón



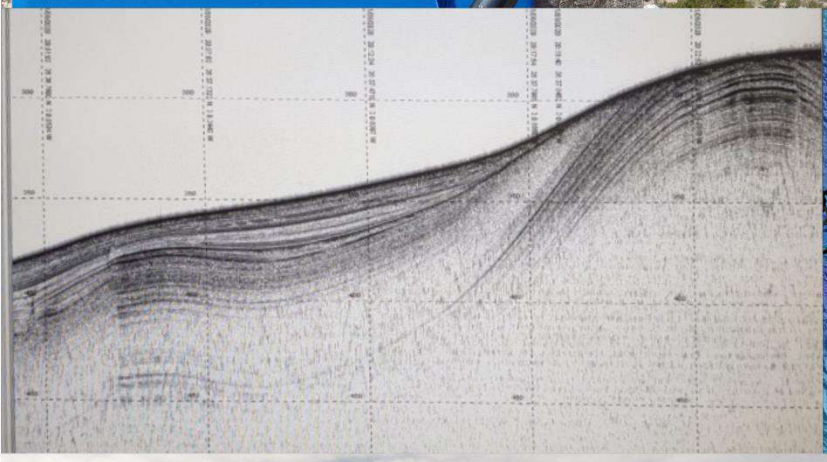
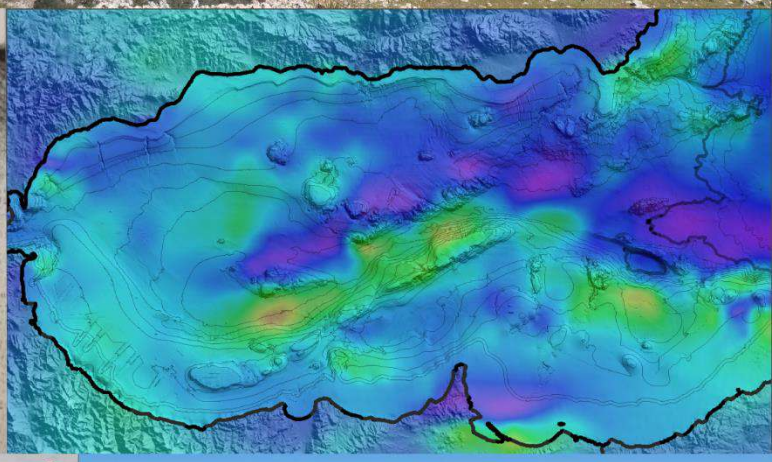

Ph.D. Thesis 2022

UNIVERSIDAD DE GRANADA

IACT INSTITUTO ANDALUZ DE CIENCIAS DE LA TIERRA

CSIC CONSEJO SUPERIOR DE INVESTIGACIONES CIENTÍFICAS

Programa Doctorado Ciencias de la Tierra

Editor: Universidad de Granada. Tesis Doctorales
Autor: Víctor Tendero Salmerón
ISBN: 978-84-1117-352-0
URI: http://hdl.handle.net/10481/75430

Agradecimientos

Tras estos más de cuatro años de trabajo para llegar aquí, he aprendido y evolucionado mucho como geológo y como persona. Ha sido un trabajo arduo en el cual han intervenido muchas personas a las que debo su apoyo profesional y personal. Por ello quiero expresarles mi sincero agradecimiento por haber estado ahí durante todo este tiempo. Menciono muchos nombres, aunque es probable que me deje alguno en el tintero. A todas esas personas, gracias.

En primer lugar quiero destacar el trabajo de mi director, Jesús Galindo Zaldívar, y de mis directoras, Gemma Ercilla Zárraga y Elia d'Acremont. Su difícil labor no solo ha consistido en formarme e introducirme al mundo de la ciencia, sino que me han apoyado y guiado a lo largo de todo este proceso y me han aportado valiosas lecciones en lo profesional y, a veces también, en lo personal. Gracias por la confianza que depositásteis en mí al inicio de este proyecto y en cada uno de los días siguientes.

Como muestran las numerosas coautorías de los trabajos recopilados en esta tesis, en ciencia es frecuente que participen muchas personas para llevar a cabo una investigación y esta tesis no es una excepción. Quiero agradecer a las personas del Departamento de Geodinámica y del Instituto Andaluz de Ciencias de la Tierra su acogida, su apoyo y la ayuda que me prestaron para impartir mis primeras clases universitarias. Agradezco también el trabajo y la colaboración de los compañeros y compañeras geodestas de la Universidad de Jaén. Las campañas de vigilancia de puntos GPS han marcado esta tesis desde su inicio hasta su final y me alegro mucho de haber participado en estas campañas, también junto a compañeros de la Universidad de Alicante. Gracias también a las personas de la oficina del IGME de Granada por su colaboración en los primeros trabajos.

He tenido la inmensa suerte de participar en varias campañas de geología marina (FAUCES 2, RIGEL-2-ÁGORA, ALBACORE) en las que he coincidido con personas de muchas instituciones de investigación; a todas ellas quiero agradecerles haberme enseñado a vivir y trabajar en un buque oceanográfico y todos los momentos que en ellos compartimos. De entre todas esas instituciones, cabe destacar a compañeros y compañeras del CSIC del Instituto de Ciencias del Mar de Barcelona y del Instituto Español de Oceanografía, y a colegas de investigación de instituciones francesas, destacando los provenientes del Institut des Sciences de la Terre de Paris. Me gustaría aquí hacer especial mención a algunas personas por lo vivido en estas campañas. Gracias a Ferran Estrada y a Belén Alonso que me enseñaron a llevar aquella primera campaña, y a Javier Idárraga que me aguantó como compañero de camarote incluso en aquellas noches de mareo inteso. Del IEO, gracias a Nieves y Juan Tomás, de quienes he aprendido mucho, y a Desirée Palomino, quien me ha acompañado de cerca en todas las campañas en las que he participado. A Mª del Carmen Fernández, con quien pasé muy buenas madrugadas trabajando en la campaña RIGEL-2-ÁGORA. A los compañeros y compañeras con las que compartí turno en la campaña

ALBACORE, a Sara Lafuerza por ser una genial jefa junto con Elia, y a mi compañero de camarote Guillem Corbera, con quien me reí mucho.

También he tenido la oportunidad de vivir en otros lugares durante las estancias de esta tesis. Gracias a todas las personas que me acogieron durante mi estancia en París. Un agradecimiento especial merecen Christian Gorini y su pareja, Sandro, que más que unos caseros, fueron unos envidiables compañeros de piso en el Kremlin-Bicêtre. Por parte de la Universidad de Lisboa, gracias a Francisco Martínez por tutorizar mi estancia y por todo lo que me has enseñado en modelización gravimétrica.

Por supuesto, no puede faltar una mención de honor para esos extraños seres con los que he compartido sala, infinidad de alegrías y algunas penurias. Se hacen llaman «doctorandos/as» y se definen como personas que, generalmente de forma voluntaria (márquese este aspecto), decidieron hacer una tesis doctoral y siguen trabajando en ello a pesar de las consecuencias de su decisión. Gracias en especial por el tiempo que he pasado con ellas y sus respectivas parejas, a Cristina A., Ángela, Álex, Asier y Cristina R., y también de forma muy importante a Mayte y a Marcos, aunque para mí llegasen un poco después a la becaría. Incluyo en este variopinto grupo a Lourdes, que no hace tanto que pasó por aquí, y que ha sido un apoyo fundamental en lo personal y lo profesional, además de una excelente mentora de doctorandos. Para terminar este párrafo, quiero agradecer a Manuel Martínez que me acompañara en mis inicios del doctorado y me enseñase todo lo necesario para poder comenzar la tesis.

Reservo este último párrafo para aquellas personas que han apoyado esta tesis desde fuera del ámbito profesional, pero que han sido igualmente imprescindibles. Gracias a Erika por enseñarme a afrontar con filosofía las vicisitudes e, incluso, a mí mismo. Gracias a todas las amistades que me han acompañado estos años, desde las que llevan conmigo mucho tiempo, como Sandra, Isa, Ramón y Gemma (estos sí que son seres extaños e incomprensibles), a compañeros/as de carrera como Antonio María, Álex, Olmo y Ángela, y aquellas que compartieron piso conmigo y me soportaron (nótese que no es poco), como Sandra (otra vez), David, Paola y Sergio. Gracias a Sebas por compartir sus primeros años de doctorado con los míos, aunque nuestros caminos finalmente divergiesen. Gracias a Antonio por ser una pareja extraordinaria, no solo por soportarme en los últimos años de tesis, sino por todo lo demás que me ayuda a desconectar cada día al volver a casa. Gracias a mi madre, mi padre y mi hermano por su constante apoyo, educación y cariño, sin los cuales jamás me habría convertido en lo que soy hoy.

Esta tesis ha sido posible gracias al contrato predoctoral del programa de Formación de Profesorado Universitario (16/04038); a los medios materiales del grupo de investigación RNM148 del Dpto. de Geodinámica (UGR) y del IACT (CSIC-UGR), y a los proyectos de investigación CGL2016-80687-R AEI/FEDER, P18-RT-3275 y B-RNM-301-UGR18.

Abstract

A multidisciplinary study that combines geology, geophysics and geodesy in an integrated land-sea approach is crucial for the analysis of the active and recent tectonic structures in the Alboran Sea and central-eastern Betic Cordillera. Such a study, presented in this Ph.D. Thesis, reveals new insights in the geodynamics of the Gibraltar Arc. The interaction between indentation tectonics caused by the Eurasia-Africa convergence and the active extension, and westwards displacement, related to subduction with roll-back, controls the active tectonics of the central Alboran Domain. To study these structures, geological, geodetical and geophysical methods have been applied, and marine and terrestrial data are integrated.

In the central Alboran Sea indentation, the magnetic anomalies reveal large igneous intrusions related to the AlKaPeCa Domain rift that have conditioned the development of strike-slip faults and the indentation tectonics. In fact, these rigid bodies act as a backstop where the indenter of south Alboran Sea collides and has generated the Alboran Ridge. The magnetic anomalies also point to the inherited origin of the dextral Yusuf fault (north-eastern boundary of the indenter) and a very recent formation of the sinistral Al Idrissi fault zone (western boundary of the indenter).

The southern termination of the Al Idrissi fault zone in the transtensional Nekor basin shows the interaction between the southwestwards motion of the Rif Cordillera and the indentation of the central Alboran Sea. The faults studied at the Al Hoceima Bay (Nekor basin) show a westward migration caused by the SW motion of the Rif.

The deformation of the northern Alboran Sea is characterized by two conjugate sets of strike-slip faults that are propagating towards the coast. In the Campo de Dalías zone, the results of GNSS measurements show that the southern points of the GNSS network move WNW, while the northern ones move WSW. This zone is affected by normal-dextral faults with NW-SE orientation. Their dextral component, together with the GNSS results, implicate an influence of both the ENE-WSW extension, which is dominant in the central Betic, combined with the propagation of the tectonic indentation of the Alboran Sea. Thus, a transition zone can be defined in the western and northern boundaries of the Alboran Sea indentation. Such a transition happens

between the indentation tectonics related to the continental collision in the central Alboran Sea, and the westwards motion with extension due to roll-back in the west Alboran Domain.

In the eastern Betic, the active tectonics is marked by the transpressive and strike-slip faults of the Eastern Betic Shear Zone. A few of these faults, such as the Palomares one, are originated by the Águilas Arc indentation, where a rigid fragment of the Algerian crust collides with the deformed Betic Internal Zones. The gravity modeling next to the Palomares fault shows that the basin geometries are controlled by rotated synforms, whose fragmentation originated the Palomares fault during the indentation. In addition, the length of the Palomares fault is shorter than previously considered and it is constrained by the folding deformation. Consequently, it disrupts the continuity of the EBSZ.

In addition, the data show a NW propagation of the Águilas Arc indentation. The high coupling in the eastern Betics between the Alboran Domain and the underlying Iberian crust favors the stress transmission towards the Iberian massif. This explains the strike-slip seismicity located inside the Iberian basement of the easternmost Guadalquivir foreland basin. Geophysical, seismological and geological data show a NNE-SSW sinistral fault in the Iberian basement and, combined with the compression structures located northwards, support an incipient indentation tectonics. The compression and strike-slip tectonics in the basement combined with the small westwards displacement at the surface, all point to an interaction between the collision tectonics of the eastern Betics and the roll-back in the central Betics.

The boundary zone between areas affected by indentation tectonics and roll-back has variable features. Whilst in the Alboran Sea it is a transition zone, in the central-eastern Betics it manifests as a sharp boundary located west of the Águilas Arc indentation. Alternatively, in the Betic Cordillera, the boundary zone could be an area of progressive transition, eventually affected by other lithospheric processes related to the rupture of the slab between the western and eastern Betics. In the Guadalquivir foreland basin, transitional areas are also observed. The advancement of indentation, and the development of the Gibraltar Arc by roll-back processes, produces a progressive westwards migration of the boundary of the areas affected by these tectonic processes.

Resumen

El estudio multidisciplinar que combina geología, geofísica y geodesia e integra datos tierra-mar es crucial para el análisis de las estructuras tectónicas activas y recientes del Mar de Alborán y del sector centro-oriental de las Béticas. Es el caso de esta tesis, que aporta nuevos datos sobre los procesos geodinámicos que afectan al Arco de Gibraltar. La interacción de indentaciones tectónicas debidas a la convergencia Eurasia-África y la extensión y movimiento al oeste relacionas con la subducción con roll-back controlan la tectónica activa del sector central Dominio de Alborán. Para su estudio se han combinado métodos geológicos, geofísicos y geodésicos y se han integrado datos marinos y terrestres.

En la indentación del Mar de Alborán, las anomalías magnéticas han revelado la presencia de grandes intrusiones ígneas relacionadas con el rift del Dominio AlKaPeCa, las cuales han condicionado el desarrollo de fallas de salto en dirección y la indentación tectónica. De hecho, esas intrusiones actúan como un tope contra el que colisiona el indentador del sur del Mar de Alborán, generando la Cresta de Alborán. Los resultados también apoyan el carácter heredado de la falla dextra de Yusuf (borde noreste del indentador) y la formación muy reciente de la zona de falla sinistra de Al Idrissi (borde occidental del indentador).

La terminación sur de Al Idrissi en la cuenca transtensiva de Nekor muestra la interacción entre el movimiento al suroeste del Rif y la indentación del centro del Mar de Alborán. Las fallas estudiadas en la Bahía de Alhucemas (cuenca de Nekor) muestran una migración al oeste causada por el movimiento al SO del Rif.

La deformación en el norte de Alborán se caracteriza por dos sets de fallas conjugadas de salto en dirección que se propagan hacia la costa. En el Campo de Dalías, los resultados de medidas de GNSS muestran que los puntos del sur se mueven hacia el ONO, mientras que los del norte se mueven hacia el OSO. En esta zona hay fallas NO-SE normales-dextras. Su componente dextro y los resultados de la red GNSS apuntan a la influencia de ambos procesos (la propagación de la indentación tectónica del Mar de Alborán y la extensión ENE-OSO de las Béticas centrales) en las estructuras activas. Así, se puede definir una zona de transición en los márgenes norte y oeste de la indentación del Mar de Alborán entre los procesos de indentación relacionados con la

colisión continental en el centro del Mar de Alborán y el movimiento al oeste debido al roll-back de la zona occidental.

En las Béticas orientales, la tectónica activa está caracterizada por transpresión y las fallas de salto en dirección de la Eastern Betic Shear Zone. Algunas de ellas, como la falla de Palomares, están generadas por la indentación del Arco de Águilas, en la que un fragmento rígido de la corteza argelina colisiona con las deformadas Zonas Internas béticas. Sin embargo, los modelos de gravimetría de las cuencas adyacentes a la falla de Palomares señalan que las cuencas están formadas por sinformes rotados, cuya fragmentación durante la indentación generó la falla de Palomares. Por tanto, la longitud de la falla de Palomares es menor, limitada por la deformación y desplazamiento de los pliegues, y está desconectada de la EBSZ.

Los datos también muestran que la indentación del Arco de Águilas se propaga hacia el NO. Teniendo en cuenta que en las Béticas orientales la corteza ibérica está desconectada del slab y adherida a las Béticas, debe de haber un grado de acoplamiento alto entre ambas que favorece la transmisión de esfuerzos a Iberia. Esto explica la sismicidad con mecanismos focales de salto en dirección en el basamento ibérico de la zona más oriental de la cuenca de antepaís del Guadalquivir. Datos geofísicos, sísmicos y geológicos muestran una falla NNE-SSO sinistra en el basamento que, combinada con las estructuras compresivas localizadas al norte, apoyan la existencia de una indentación incipiente. La compresión y las fallas de salto en dirección del basamento, sumadas a los pequeños desplazamientos al oeste de la superficie, indican una interacción de los procesos de colisión y transpresión que dominan las Béticas orientales y el roll-back en las Béticas centrales.

El límite entre áreas afectadas por la tectónica de indentación y el roll-back es variable. Mientras en el Mar de Alborán es una zona de transición, en el sector centro-oriental de las Béticas parece ser un límite neto, al oeste de la indentación del Arco de Águilas. Alternativamente, en esa zona podría haber una transición progresiva, como en zonas de la cuenca del Guadalquivir, eventualmente afectada por otros procesos litosféricos relacionados con la ruptura del slab entre las Béticas orientales y occidentales. El avance de la indentación y el desarrollo del Arco de Gibraltar por procesos de roll-back generan una progresiva migración al oeste de este límite entre áreas afectadas por diferentes procesos tectónicos.

Index

Abstract i

Resumen iii

Part I

1. Introduction, aims and outlines 3

1.1. Aims and outlines 5

2. Regional setting 9

2.1 Models of the geodynamic evolution of the Betic and Rif Cordilleras 9

2.2 Geological setting 12

2.3 Previous geophysical and geodetical data 25

3. Methods 33

3.1 Geological methods 33

3.2. Geophysical methods 33

3.2.1 Gravity prospecting 33

3.2.2 Magnetic prospecting 36

3.2.3 Electric resistivity Tomography 37

3.2.4 Seismic reflection profiles 39

3.2.5 Throw Backtstripping 40

3.3 Geodetical methods 41

Part II

4. New insights on the Alboran Sea basin extension and continental collision from magnetic anomalies related to magmatism (western Mediterranean) 45

4.1 Introduction 47

4.2. Regional setting 48

4.3 Materials and methods 54

4.4 Results 58

4.4.1 Magnetic anomalies and igneous rocks 58

4.4.2 Forward modeling of magnetic anomalies 61

4.5 Discussion 64

4.5.1 New insights on the geometry and nature of the crustal igneous bodies 64

4.5.2 Geodynamics implications 67

4.6 Conclusions 71

References 73

5. Application of Automated Throw Backstripping Method to Characterize Recent Faulting Activity Migration in the Al Hoceima Bay (Northeast Morocco): Geodynamic Implications 81

5.1 Introduction 83

5.2 Geological setting 85

5.3 Data and methods 90

5.3.1 Data 90

5.3.2 Methods 90

5.4 Results 94

5.4.1 Deformation distribution through time 94

5.4.2 Deformation rate on the main fault zones 97

5.5 Discussion 99

5.5.1 Migration of deformation in Al Hoceima Bay 99

5.5.2 Local deformation into the westernmost Mediterranean geodynamics 102

5.6 Conclusions 105

References 106

6. The Campo de Dalías GNSS network unveils the interaction between roll-back and indentation tectonics in the Gibraltar Arc 113

6.1 Introduction 115

6.2 Geological setting 116

6.3 GNSS equipment and data processing 119

6.4 GNSS network results 120

6.5 Recent offshore active tectonic deformations west of the Campo de Dalías 122

6.6 Discussion 124

6.7 Conclusions 128

References 128

7. Shearing in an indenter boundary: the evolution of the Águilas Arc and its accommodation along the PFZ (Betic Cordillera, Spain) 133

7.1 Introduction 135

7.2 Geological setting 137

7.3 Data and methods 142

7.4 Results 144

7.4.1 Anomaly maps 144

7.4.2 Residual gravity anomaly models 145

7.5 Discussion 147

7.5.1 The Palomares fault zone 147

7.5.2 Geodynamic implications 150

7.6 Conclusions 151

References 152

8. Seismicity in Strike-Slip Foreland Faults (Central Betic Cordillera Front): Evidence of Indentation Tectonics 159

8.1 Introduction 161

8.2 Geological and seismic setting 164

8.3 Methods 167

8.3.1 Seismicity analysis 167

8.3.2 Gravity prospecting 169

8.3.3 Electric resistivity tomography 169

8.4 Seismicity 170

8.5 Deep structures of the southeastern Guadalquivir Basin and the Cazorla Mountain Front 171

8.6 Shallow recent tectonic structures of the Guadiana Menor seismic zone 175

8.7 Discussion 176

7.7.1 Cazorla Mountain Front and Tíscar Fault 176

7.7.2 Guadiana Menor valley and related seismicity 178

7.7.3 Geodynamic implications 180

8.8 Conclusions 183

References 184

Part II

9. General discussion 193

9.1 Strike-slip fault systems and indentation tectonics in the Alboran Sea evolution 193

9.2 Active and incipient indentation tectonics in the central-eastern sector of the Betic Cordillera 195

9.3 Current roll-back influenced zones vs. indentation tectonics zones in the Betic Cordillera and the Alboran Sea: geodynamic implications 197

10. Conclusions 201

10. Conclusiones 205

References 209

Appendix

Appendix A. Supplementary files of Chapter 4 229

Appendix B. Supporting information of Chapter 8 233

Part I

1. Introduction, aims and outlines

2. Regional setting

3. Methods

CHAPTER 1

Introduction, aims and outlines

Plate tectonics is one of the main engines controlling the complex evolution of the Earth. This complexity is well exemplified in the oblique convergence of Eurasia and Africa in the western Mediterranean, where the subduction with slab roll-back of the oceanic lithosphere attached to Africa have controlled its evolution. In recent years many advances have been made for understanding the evolution of this plate tectonic interaction, but, due to this great complexity, it still presents many unresolved issues whose study is a challenge to geologists and geophysicists.

The arc-shaped orogen of the Gibraltar Arc in the Western Mediterranean (Fig. 1.1), formed by the Betic and Rif cordilleras that encircle the Alboran Sea, is a key area for investigation of the Eurasia and Africa plate interaction. Its formation and evolution has been a point of scientific debate. The arc is the result of the convergent collision of both plates and the westward migration the Alboran Domain started since the rupture of the AlKaPeCa Domain. This complex tectonic scenario makes the Gibraltar Arc, an excellent natural laboratory for the study of the interaction between extensional, compressional and transcurrent structures.

The geodynamic evolution of the Gibraltar Arc and the Alboran Domain have led to a wide variety of active structures and both their activity and the tectonic processes involved are still object of scientific discussion. In this scenario, the slow plate tectonics of the oblique plate convergence on the Gibraltar Arc makes it possible to distinguish zones that are affected by different, active geodynamic processes. Thus, it is possible to differentiate sectors conditioned by extension and westward displacement related to the subduction zone from others that experienced tectonic indentation from the continental collision. This Ph.D. Thesis integrates new geological, geophysical and geodetical data from the Betic Cordillera and the Alboran Sea in order to better understand the active and recent deformation distribution along the Eurasia-Africa heterogeneous plate boundary. In particular, this work is focused on how the indentation tectonics (related to the collision of the two major plates, Eurasia and Africa) propagates westwards over the Alboran Domain, while the extension due to the slab-roll back disappears as the subduction seems to be blocked.

This approach is carried out through the study of key strike-slip systems in the central-eastern Betics and the Alboran Sea (Fig. 1.1), some of them related to the Águilas Arc and Central Alboran Sea indentation zones.

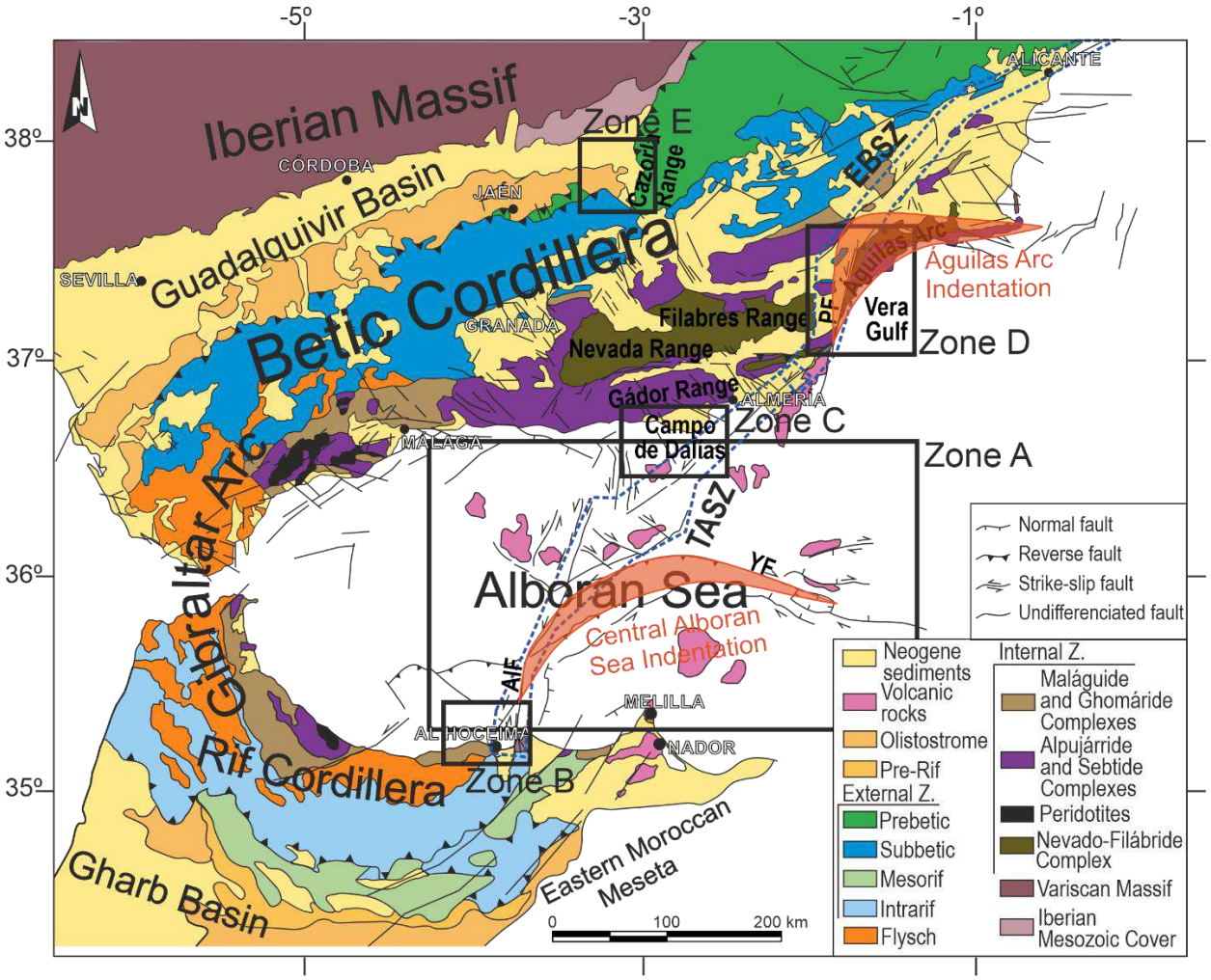

Figure 1.1. Geologic map of the Gibraltar Arc (Betic and Rif Cordilleras) and the Alboran Sea. The study zones (A to E) of this Ph.D. Thesis are depicted. The Trans-Alboran Shear Zone (TASZ) and Eastern Betic Shear Zone (ESBZ) are marked with a blue, dashed line. The two indentation fronts are highlighted in orange colour. AIF: Al Idrissi Fault; PF: Palomares fault, YF: Yusuf Fault.

On the other hand, the Betic Cordillera and the Alboran Sea are important geostrategic areas for investigation because the activity of their tectonic structures can trigger hazardous processes, and cascading events may occur. Therefore, the knowledge of the structural elements likely to produce a disaster is crucial for their prevention and mitigation. In addition, it is an important area of investigation for renewable and non-renewable natural resources industries and for biodiversity and ecosystem functioning, both offshore and onshore.

For all the above mentioned reasons, this Ph.D. contributes to the expansion of scientific knowledge on plate tectonic interaction. More specifically, this research improves the geodynamic models of the Gibraltar Arc and the Alboran Domain, which can be applicable to other arc-shape orogens in oblique continental collisions and final stages of complex subduction zones. Consequently, the results will be of great geoscientific interest and will have multiple practical application

1.1 Aims and outlines

The main objective of this Ph.D. Thesis is to study the recent and active tectonic structures in the eastern-central sector of the Betic Cordillera and the Alboran Sea and determine the influence and interaction of slab roll-back and/or tectonic indentation. The hypothesis is to associate the slab roll-back with the ENE-WSW extension and the westward displacement of the Alboran Domain, while the tectonic indentation is mainly related to the continental collision of rigid blocks between Eurasia and Africa.

According to these research aims, five key zones have been selected and analyzed from the Betic Cordillera and the Alboran Sea (including the Rifian coast) in order to cover the specific objectives proposed (zones A to E, Fig. 1.1):

1. Improve the knowledge on the development of the Alboran Sea, consequence of the early interaction of extension and strike-slip faults in a back-arc context and a later overprinting of tectonic indentation (Central Alboran Sea, zone A).
2. Analyze the recent tectonic activity in the south-westwards termination of the major NE-SW, strike-slip faults that accommodate the Alboran Sea indenter (Al Hoceima Bay, northern Rifian coast, zone B).
3. Characterize the recent tectonic activity of the propagation of the frontal deformation of the Alboran Sea indenter into the indented block and the interaction of folds, strike-slip and extensional fractures (Campo de Dalías, zone C).
4. Discuss the development and interaction of major strike-slip faults and recent folds related to Águilas Arc indentation (the Palomares fault zone and the adjacent basins, zone D).

5. Determine the potential forward propagation of indentation tectonics into foreland basin (Guadiana Menor valley, next to Cazorla Range, zone E).

In order to cover these objectives, multidisciplinary and multiscale approaches were applied, and databases of geological and geophysical information were used. These approaches have included observations ranging from regional to local scale, and also with a land-sea integrated view.

This Ph.D. Thesis is presented as a group of publications, according to the University of Granada prescriptions. As a consequence of being a collection of articles, there are some repetitions, especially in the introduction, geological settings, and methods chapters, as well as in results chapters. The volume is divided into 11 chapters that are grouped into three main parts. The volume is prefaced by a presentation of the Ph.D. Thesis and an abstract.

Part I is introductory and consists of a compilation of the state of the art concerning the knowledge of the studied region. It includes the following chapters:

- Chapter 1. Introduction, aims and outlines.
- Chapter 2. Regional setting. It describes the geological context of the study region and provides an overview of the geophysical and geodetical data available.
- Chapter 3. Methods. It contains a brief description of the methods and databases used in this Ph.D. Thesis.

Part II presents the main results of the Ph.D Thesis that is the collection of publications. It includes the following chapters, which correspond to the specific objectives and the five study zones:

- Chapter 4. New insights on the Alboran Sea basin extension and continental collision from magnetic anomalies related to magmatism (western Mediterranean).
- Chapter 5. Application of Automated Throw Backstripping Method to Characterize Recent Faulting Activity Migration in the Al Hoceima Bay (Northeast Morocco): Geodynamic Implications.

- Chapter 6. The Campo de Dalías GNSS network unveils the interaction between roll-back and indentation tectonics in the Gibraltar Arc.
- Chapter 7. Shearing in an indenter boundary: the evolution of the Águilas Arc and its accommodation along the PFZ (Betic Cordillera, Spain).
- Chapter 8. Seismicity in Strike-Slip Foreland Faults (Central Betic Cordillera Front): Evidence of Indentation Tectonics.

Part III is a comprehensive discussion of all the results obtained and presented in the previous part. It includes the following chapters:

- Chapter 9. General discussions. It integrates the data and interpretations of the previous chapters to improve the geodynamic models of the Alboran Sea and Betic Cordillera and presents a discussion about the current influence of tectonic indentation and subduction with slab roll-back processes.
- Chapter 10. Conclusions. It summarizes the final remarks and conclusions supported by this Ph.D. Thesis.

CHAPTER 2

Regional setting

2.1 Models of the geodynamic evolution of the Betic and Rif Cordilleras

The Gibraltar Arc and the Alboran Basin form a wide deformed area with a complex seismic pattern, where it is not possible to define a simple plate boundary. The slow convergence of Eurasia and African plates (with an estimated velocity of 4 mm/yr, DeMets *et al.*, 2010) is combinaded with subduction processes that have controlled the evolution of the western Mediterranean (Gueguen *et al.*, 1998; Chertova *et al.*, 2014; Malinverno and Ryan, 1986; Royden, 1993; Schettino and Turco, 2011; Spakman *et al.*, 2018). As described in the following sections, the compressive structures are coetaneous of extensional structures. The study of structural evolution is also complicated due to the sequence of extensional and compressional episodes that affect the same structures (*e.g.*, d'Acremont *et al.*, 2020; Galindo-Zaldívar *et al.*, 1989; García-Dueñas and Balanyá, 1986; Martinez-Martos *et al.*, 2017), and the strain partitioning and rotations associated with the arc-shape geometry of the orogen (Crespo-Blanc *et al.*, 2016; Platt *et al.*, 2003; Rosas *et al.*, 2012; Terrinha *et al.*, 2009). In this setting, the compression with orthogonal extension since Late Miocene (Comas *et al.*, 1992; Galindo-Zaldivar *et al.*, 2015; Sanz de Galdeano, 1990) generated large strike-slip fault systems, such as the Trans-Alboran Shear Zone (Fig. 1.1) that continues onshore as the East Betic Shear Zone (Borque *et al.*, 2019; De Larouzière *et al.*, 1988; Silva *et al.*, 1993; Stich *et al.*, 2006). In addition to this geodynamic context, there have been volcanic activity since Middle Miocene to Quaternary, which affected both the thickened crust of the arc-shape orogen and the thinned continental crust that constitutes the Alboran Basin basement. Altogether, the recent geodynamic evolution is in controversy since the 1970s.

First hypotheses explained the Gibraltar Arc shape as a consequence of the westward displacement of the rigid microplate of Alboran (Andrieux, *et al.*, 1971a). The westward motion of Alboran was explained by Tapponier (1977) as consequence of a tectonic scape due to irregular plate boundaries, which explained the presence of dextral strike-slip faults in the Betic Cordillera and sinistral faults in the Rif; later these faults were consider transfer faults (Bourgois, 1978; Dewey *et al.*, 1989; Sanz

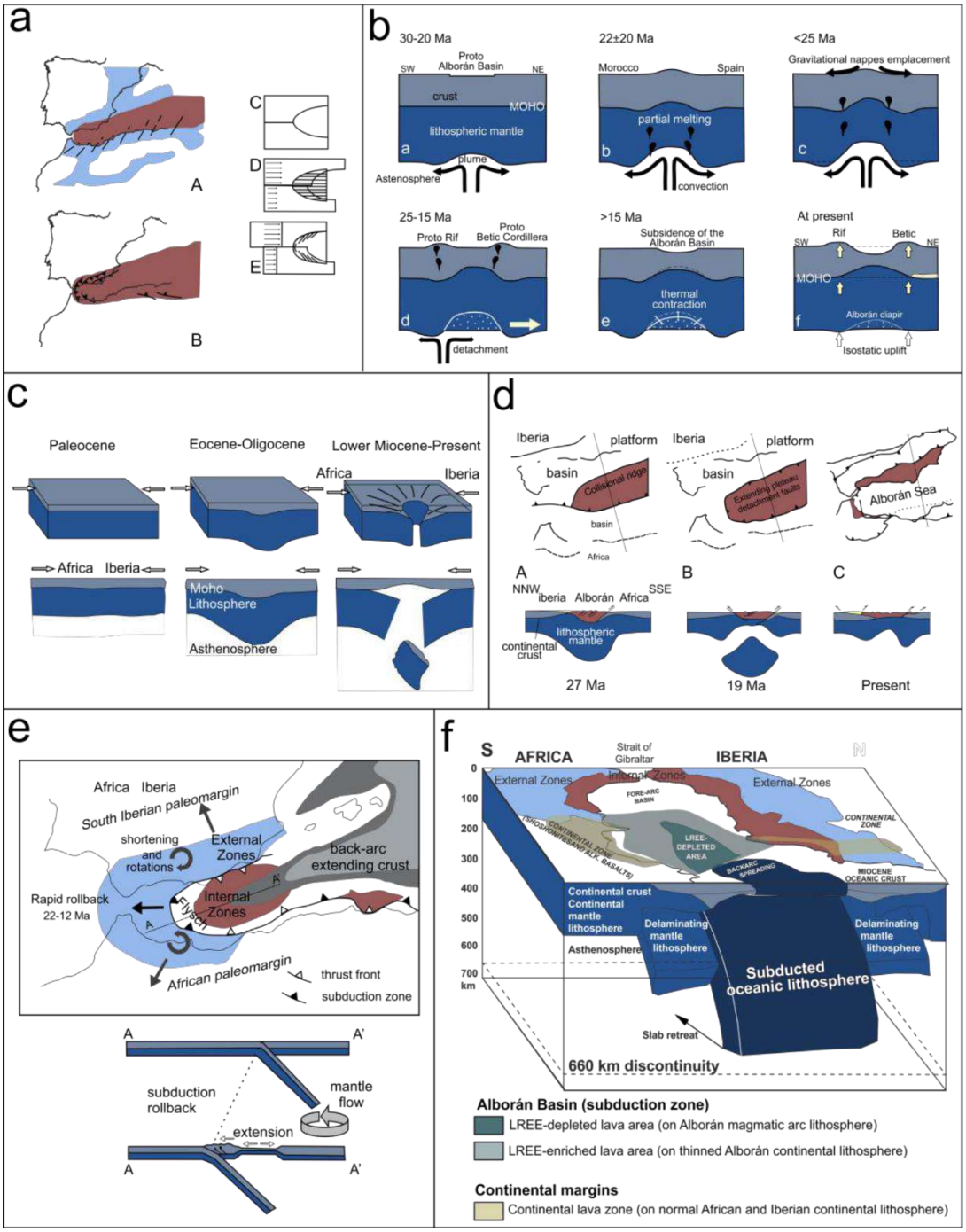

Figure 2.1. Main proposed lithospheric models for the Gibraltar Arc recent geodynamic evolution (modified from González-Castillo (2015). a. Andrieux *et al.* (1971a). b. Weijermars (1985). c. Seber *et al.* (1996). d. Platt and Vissers (1989). e. Lonergan and White (1997). f. Duggen *et al.* (2008).

de Galdeano, 1983). The thinned continental crust of the Alboran Sea was supposed to be the result of mantle diapirism that led to gravitational nappes with radial emplacement followed by the cooling of the Alboran lithosphere (Cloetingh and Nieuwland, 1984; Weijermars *et al.*, 1985). On land, the structure of the Internal Zones was considered as thrusted metamorphic complexes (Egeler and Simon, 1969),

although these faults were reinterpreted as low-angle normal faults in the 1980s (Aldaya *et al.*, 1991; Galindo-Zaldívar *et al.*, 1989; García-Dueñas and Balanyá, 1986; Platt and Vissers, 1989). Thus, the Alboran Domain had to experiment extension while it was westward emplaced during Miocene.

The recent models agree in the existence of the Alboran Domain, but propose different lithospheric hypothesis (Fig. 2.1) to explain the coexistence of shortening and extension, the westwards displacement and the exhumation of metamorphic complexes. These models can be grouped in three lithospheric settings:

1) Detachment and/or delamination of Alboran lithospheric mantle

These models consider that during the Africa-Eurasia convergence a thick and cold orogenic root became unstable (Fig. 2.1c,d), so it were detached during Late Oligocene or Early Miocene through lithospheric delamination (Fig. 2.1c, Calvert *et al.*, 2000; García-Dueñas *et al.*, 1992; Mancilla *et al.*, 2013; Seber *et al.*, 1996) or mantle convection (Fig. 2.1d, Houseman *et al.*, 1981; Platt and Vissers, 1989). Then, the lithospheric removal has caused a radial, crustal extension that finished in the Late Miocene due to the Africa-Eurasia convergence, which became again the dominant geodynamic process in the region. The evidences of these hypothesis are the presence of a SE dipping, intermediate (60-400 km) high velocity body and another deep one (570-650 km) observed in seismic tomographies under the Alboran Sea (Calvert *et al.*, 2000).

2) Subduction of oceanic lithosphere below the Alboran Domain with or without roll-back and/or slab detachment

This hypothesis can be easily related with the consideration of the Alboran Domain as a part of the AlKaPeCa Domain, a landmass that was part of the fore-arc region originally formed during Late Oligocene-Early Miocene on the Eurasian side of the African-Eurasian collision (Bouillin *et al.*, 1986). In this model, the slab was initially attached to the African margin and northwards dipping; then the slab fragmented and the Alboran Domain was displaced westward associated with one of those fragments (*e.g.*, Chertova *et al.*, 2014; Mauffret *et al.*, 2007; Romagny *et al.*, 2020; Rosenbaum *et al.*, 2002; Spakman and Wortel, 2004). The tearing of the slab from Africa as the slab moves westwards has been related to the occurrence of alkaline volcanism along the

African margin (Carminati *et al.*, 1998; Duggen *et al.*, 2005; Hidas *et al.*, 2019; Jolivet *et al.*, 2021; Maury *et al.*, 2000).

On the Iberian margin, the slab would be still attached to the continental crust, which led to a slab dipping eastward to south-eastward with roll-back (Fig. 2.1e) as it is suggested by studies based on seismic tomography (*e.g.*, Blanco and Spakman, 1993; Gill *et al.*, 2004; Hoernle *et al.*, 1999; Royden, 1993; Ruiz-Constán *et al.*, 2011; 2012; Spakman and Wortel, 2004). GPS velocity data also point to the roll-back both in the Rif (Fadil *et al.*, 2006; Pérouse *et al.*, 2010) and in the Betic cordilleras (González-Castillo *et al.*, 2015). Moreover, stress state, intermediate seismicity and seismic tomography in the southern Iberia show a continental subduction of the Iberian Massif below the Betic Cordillera (Marín-Lechado *et al.*, 2017; Morales *et al.*, 1999; Serrano *et al.*, 1998), which supports that the slab is still (at least) partially attached to Iberia. Thus, Alboran Basin is interpreted as a back-arc basin related to a subduction zone westward of Gibraltar Arc (*e.g.*, Blanc and Spakman, 1993; Carminati *et al.*, 1998; Chertova *et al.*, 2014; Comas *et al.*, 1999; Galindo-Zaldivar *et al.*, 1998; González-Castillo *et al.*, 2015; Gutscher *et al.*, 2012; Romagny *et al.*, 2020). Some of the proposals also consider that the subduction is active in present times (González-Castillo *et al.*, 2015; Gutscher *et al.*, 2012; Ruiz-Constán *et al.*, 2011;2012; Thiebot and Gutscher, 2006).

3) Delamination of continental Alboran lithosphere combined with oceanic lithosphere subduction below it

This hypothesis (Fig. 2.1f) was proposed to understand the Neogene magmatism in the region by Duggen *et al.* (2005; 2008). In this model, a delamination of subcontinental lithosphere in Late Miocene under the African and Iberian margins is proposed, but caused by a slab roll-back of an east dipping slab below the Alboran Sea (Duggen *et al.*, 2005; 2008; Martínez-Martínez *et al.*, 2006). Then, a plume (contaminated by the subduction material) of sub-lithospheric mantle would have occupied the space of the delaminated asthenosphere.

2.2 Geological setting

In the westernmost Mediterranean Sea, the Alboran Sea (Figs. 1.1 and 2.2) is located between the Iberian Peninsula and Africa and open eastwards to the Algerian Basin.

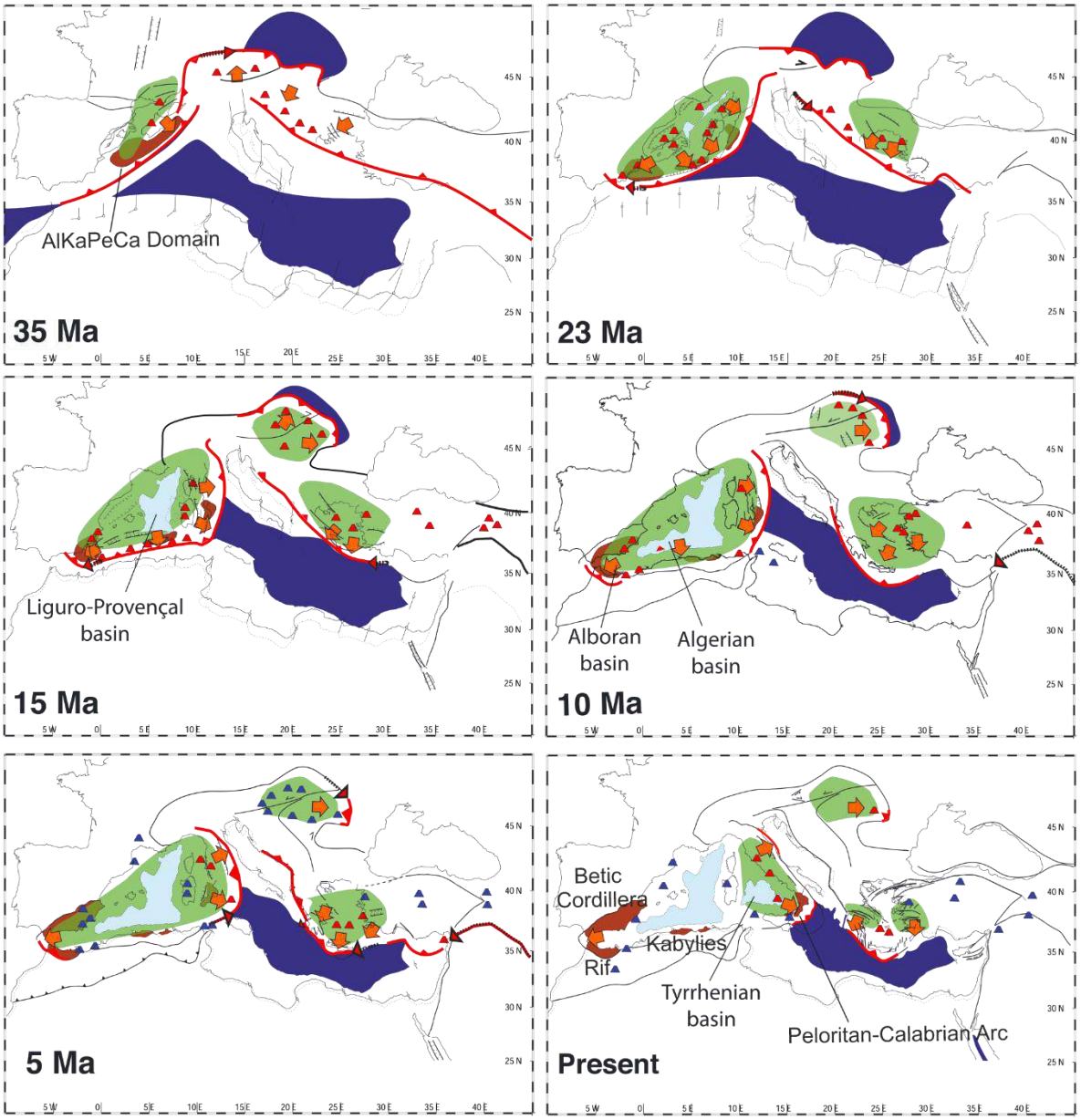

Figure 2.2. Evolution of the Mediterranean and fragmentation of the AlKaPeCa Domain (brown). Green zones: extension areas with stretching direction indicated by arrows. Dark blue zones: oceanic, land-locked basins. Red lines: active subduction zones. Modified from Faccena *et al.* (2014).

It is circled by an arc-shape, alpine orogen, the Gibraltar Arc (Figs. 2.2 and 2.3). This arc presents a northern branch that is the Betic Cordillera, in southern Spain, and a southern branch that is the Rif Cordillera, in northern Morocco (Figs. 2.2. and 2.3). Both cordilleras are the result of the Eurasia-Africa convergence and the westward displacement of the Alboran Domain since the fragmentation of the AlKaPeCa Domain and the opening of the Algerian Basin (Fig. 2.2, Comas *et al.*, 1992; Gutscher *et al.*, 2012; Mauffret *et al.*, 2007; Rosenbaum *et al.*, 2002; Sanz de Galdeano, 1990). That fragmentation led to the opening of the western Mediterranean as a back-arc basin

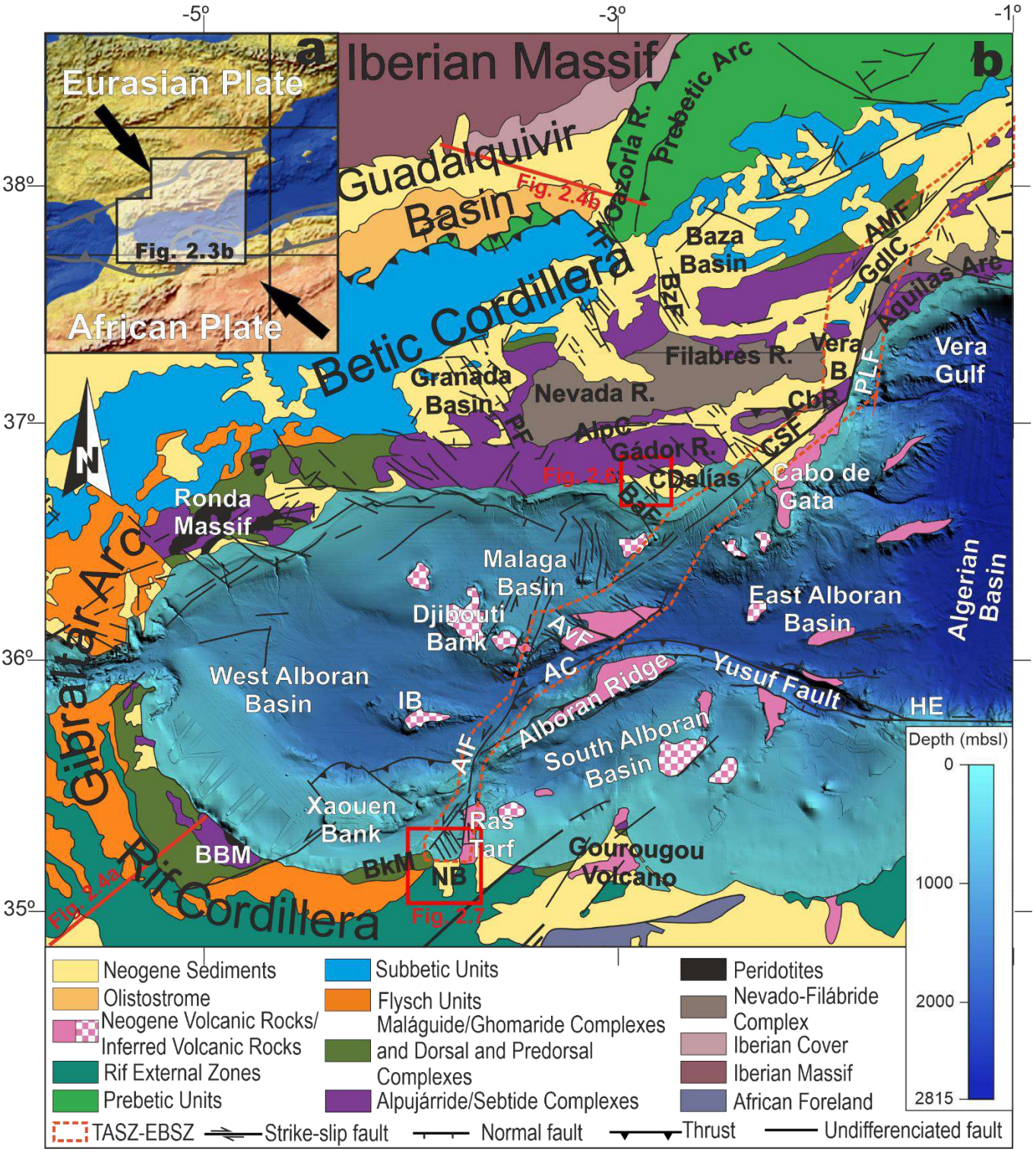

Figure 2.3. a. Location of the study zone in the tectonic boundaries of African and Eurasian plates. b. Geologic map of the Betic and Rif Cordilleras and the Alboran Sea. The location of Figures 2.4, 2.6 and 2.7 are depicted. Trans-Alboran Shear Zone (TASZ) and Eastern Betic Shear Zone (EBSZ) are marked. AC. Alboran Channel; AIF: Al Idrissi fault; AlpC: Alpujarras Corridor; AMF: Alhama de Murcia Fault; AvF: Averroes fault; BaF: balanegra fault; BBM: Beni Boussera Massif; BzF: Baza Fault; CbR: Cabrera range; CSF: Carboneras-Serrata fault; GdlC: Guadalentin Corridor; HE: Habibas Escarpment; IB: Ibn-Batouta Bank; NB: Nekor Basin; PF: Padul fault; TF: Tíscar fault.

and generated (Bouillin *et al.*, 1986) the Alboran Domain, the Kabylie (Algeria), the Peloritan (Sicily) and Calabrian (South Italy) Ranges (Fig. 2.2, Bouillin *et al.*, 1986; Gutscher *et al.*, 2012; Spakman *et al.*, 2018). This led to the collision and thrusting of the Alboran Domain over Eurasia and Africa (Fig. 2.2, Dewey *et al.*, 1989; Gutscher *et al.*, 2012; Sanz de Galdeano, 1990).

The Betic and Rif cordilleras can be divided into three main tectonic domains that constitute stacked nappes: the Internal Zones, which corresponds to the Alboran Domain; the Flysch units, and the External Zones (Comas *et al.*, 1992; García-Dueñas and Balanyá, 1986; Sanz de Galdeano *et al.*, 1990). The Internal Zones are mainly formed by allochthonous metamorphic complexes that include Palaeozoic rocks emplaced during the Eocene-Oligocene Alpine tectonic phase (Fontboté, 1966; Jabaloy-Sánchez *et al.*, 2019; Platt and Vissers, 1989; Sanz de Galdeano, 1990). These rocks form also the basement of the Alboran Sea, which is a thinned continental crust (Comas *et al.*, 1992; 1999; García-Dueñas *et al.*, 1992). Notwisthtanding, recent studies consider that the Nevado-Filabride complex of the Internal Zones is not part of the Alboran Domain and corresponds to a subducted and exhumed sector of the Iberian crust (*e.g.*, Gómez-Pugnaire *et al.*, 2012; Platt *et al.*, 2006; Rodríguez-Cañero *et al.*, 2017). The Flysch units are described as Cretaceous to Miocene marine, deep-water deposits (Durand-Delga *et al.*, 2000). These units appear between the Internal and the External Zones (Figs. 2.3 and 2.4a, Jabaloy-Sánchez *et al.*, 2019; Vitale *et al.*, 2015). The External Zones are sediments from the Iberian and African paleomargins of Mesozoic and Cenozoic age (Andrieux, 1971a; García-Hernández *et al.*, 1980). They are deformed as a fold-and-thrust belt (Figs. 2.3 and 2.4b) and constitute the outer orogenic arc (Andrieux, 1971a; García-Dueñas and Balanyá, 1986; Crespo-Blanc *et al.*, 2016). In the Betic Cordillera, the External Zones are in contact with the Iberian Massif (which is formed by rocks of the Variscan orogeny) in the eastern part and with the Guadalquivir Foreland Basin in the central and western part (Figs. 2.3 and 2.4). In the Rif Cordillera the External Zones are in contact with the Gharb Basin (Figs. 1.1, 2.3 and 2.4a) and Eastern Moroccan Meseta (the African Foreland).

In addition to these domains, there can be found intra-mountain basins and volcanic rocks of Neogene age (Fig. 2.3). These basins are originated by the extensional

episodes that the Alboran Domain experimented (Galindo-Zaldivar *et al.*, 2020). The sedimentary infill of these intra-mountain basins is from Miocene to Quaternary age, as well as the sedimentary infill of the Alboran Sea basin (Comas *et al.*, 1999; Braga *et al.*, 2003; Galindo-Zaldivar *et al.*, 2020; Sanz de Galdeano and Vera, 1992). In general, the infill of these basins starts with marine sediments of Miocene age of marls and calcarenites that change to continental fluvial and alluvial sediments of Pliocene and Quaternary age (Braga *et al.*, 2003; Galindo-Zaldivar *et al.*, 2020; Sanz de Galdeano and Vera, 1992). The volcanic rocks of Miocene to Pliocene age can be found both onshore and offshore (Figs. 2.3 and 2.5). They present a wide variety, including tholeiitic rocks, calc-alkaline series, shoshonites, basanites and alkali basalts (*e.g.*, Duggen *et al.*, 2008).

The study zones are located in the central-eastern Betic Cordillera and in the central Alboran Sea (Fig. 1.1). Zone A comprises the central Alboran Domain. Zone B is the only one located partially in the Rif Cordillera and is contact with units of the three tectonic domains (External Zones, Internal Zones and Flysch units). Zones C and D are located in the Internal Zones of the Betic Cordillera. In particular, Zone D include an intra-mountain basin of the Betic Cordillera. Zone E is located in Guadalquivir Foreland Basin and the External Zones Front.

Guadalquivir Foreland Basin and External Zones

The Guadalquivir Basin is located between the Iberian Massif and the Betic Cordillera, and it constitutes the foreland basin of the cordillera (Figs. 2.3 and 2.4b). The basement of the basin is made of Variscan igneous and metamorphic rocks below a Mesozoic sedimentary cover (Julivert and Fontboté, 1977). The basin is asymmetrical since the Iberian crust is tilted towards the Betic Cordillera due to its load (Fig. 2.4b, García-Castellanos *et al.*, 2002). It is filled with Miocene marine sediments, when the basin was a natural connection between the Atlantic Ocean and the Mediterranean Sea through several straights (García-Castellanos *et al.*, 2002; García-Hernández *et al.*, 1980; Martín *et al.*, 2009). Then, the sedimentary sequence changes progressively to continental sediments of Quaternary age (García-Castellanos *et al.*, 2002; García-Hernández *et al.*, 1980). Mixed with these sediments there is a kilometric scale, olistostromic unit next to the mountain front, favoured by the Triassic Keuper facies

(a layered clay-evaporitic sequence) that act as a detachment level (García-Hernández *et al.*, 1980; Platt *et al.*, 2003; Rodríguez-Fernández *et al.*, 2015).

The External Zones are formed by Mesozoic and Cenozoic sedimentary rocks that were deposited over a marine carbonate continental shelf on the South Iberian passive margin (García-Hernández *et al.*, 1980; Platt *et al.*, 2003). These rocks experimented thin-skin tectonic that deformed them as a fold-and-thrusts belt detached from the Variscan Iberian basement at the Triassic Keuper facies (Platt *et al.*, 2003; Crespo-Blanc *et al.*, 2016). The External Zones are divided into Subbetic and Prebetic domains. The Prebetic corresponds to the shallow shelf next to the continent and contains some continental sediments (García-Hernández *et al.*, 1980). In contrast, the Subbetic was the outermost shelf and it characterized by open sea facies as fine limestones and marls (García-Dueñas and Balanyá, 1986).

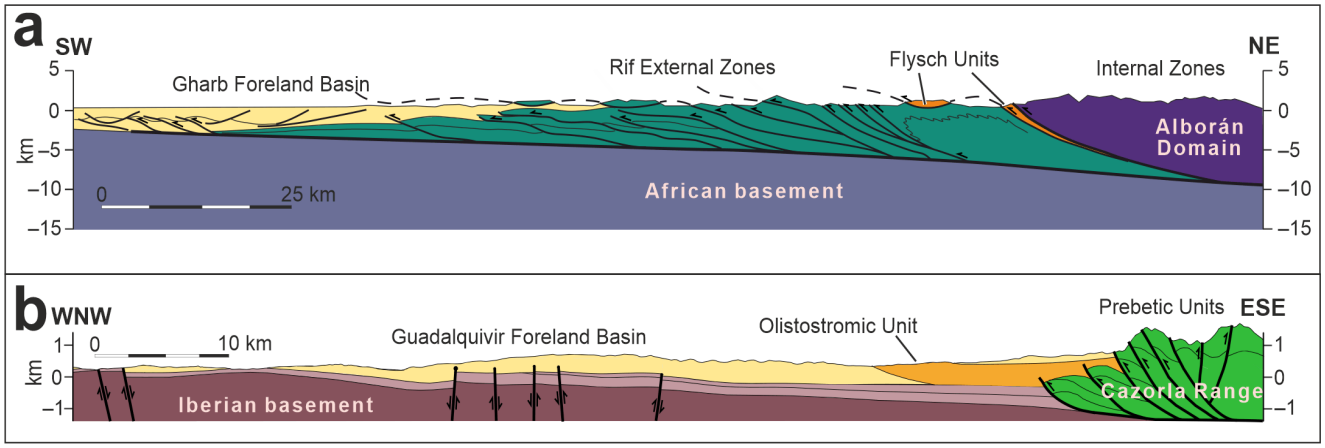

Figure 2.4. Synthetic cross-sections illustrating the structure of the Gibraltar Arc. Locations and colour legend in Figure 3.3. a. Cross-section of the Rif Cordillera (Modified from Platt *et al.*, 2013). b. Cross-section of the Guadalquivir Foreland Basin and the Prebetic mountain front (modified from Marín-Lechado *et al.*, 2017).

In the Rif Cordillera, the External Zones present a similar structure. They are made of sedimentary rocks of Mesozoic to Cenozoic age that were deposited in the African continental margin and experimented thin-skin tectonic during Alboran Domain collision (Andrieux, 1971b; Chalouan *et al.*, 2008; Frizon de Lamotte, 1982). The sequence is characterized by carbonates of Mesozoic to Tertiary age, with detritic rocks of different ages from Triassic to Miocene and an olistostromic unit in the most external subdivision (Andrieux, 1971b).

Internal Zones

The Internal Zones are allochthonous units of metamorphic rocks of Palaeozoic to Mesozoic age that are part of the Alboran Domain (Jabaloy-Sánchez *et al.*, 2019). In the Betic Cordillera, they are subdivided in three metamorphic complexes that are, from bottom to top: Nevado-Filábride, Alpujárride and Maláguide (Blumenthal, 1927; Egeler, 1963; Van Bemmelen, 1927). In the Rif Cordillera only are present (Chalouan *et al.*, 2008): Sebtide (equivalent to Alpujárride) and Ghomaride (equivalent to Maláguide, Kornprobst, 1974; Milliard, 1959). Nevado-Filábride and Alpujárride Complexes present alpine metamorphism and are formed by rocks of Palaeozoic, with a metapelitic sequence that finish with marbles (Fontboté, 1966; Platt and Vissers, 1989; Sanz De Galdeano, 1990). There are also important massifs of peridotites into the Alpujárride (Ronda Massif, Fig. 2.3) and Sebtide (Beni Bousera) complexes (Garrido, 1995; Michard *et al.*, 1992). The Maláguide Complex, in contrast, is not affected by alpine metamorphism and only experimented Variscan metamorphism (Chalouan and Michard, 1990). It is constituted by Variscan low grade metamorphic rocks of Palaeozoic age followed by thin levels of detritic rocks of Mesozoic and Cenozoic age (Milliard, 1959). In addition to these main complexes, the Internal Zones also include the Predorsal and Dorsal complexes, which are carbonate rocks of Triassic to Early Neogene age located between the metamorphic complexes and the Flysch units (Andrieux, 1971b; Frizon de Lamotte, 1982).

Nevado-Filábride and Alpujárride complexes have experimented two important metamorphic episodes, whose age is still debated. The first one is a high-pressure event attributed to crustal-thickening during the thrust-sheet stacking of the complexes that constitute the Internal Zones (*e.g.*, Monié *et al.*, 1991; Platt *et al.*, 2006). The second episode is characterized by a low-pressure high-temperature event followed by cooling, which is associated with the exhumation of the complexes during the extension of the Alboran Domain in the Early Miocene to Middle Miocene (*e.g.*, Monié *et al.*, 1994; Zeck *et al.*, 1992). Low-angle normal faults with top-to-the-west displacement are related to this episode, including the contact between the Alpujárride and Nevado-Filabride complexes (Galindo-Zaldívar *et al.*, 1989; Platt and Vissers, 1989). Contrary, the contact between Alpujárride and Maláguide is interpreted as top-to-the-east low angle normal fault (Aldaya *et al.*, 1991).

Alboran Sea Basin

The Alboran Sea is a Neogene extensional basin developed in a convergent tectonic setting that constitutes the westernmost Mediterranean (Comas *et al.*, 1992; Dewey *et al.*, 1989). It presents a complex bathymetry with numerous highs that separate several sub-basins, being the main ones (Fig. 2.3): the West Alboran Basin (the biggest one, which is 1510 m deep), the Eastern Alboran Basin (opened to the Algerian Basin and reaching 1980 m deep), the South Alboran basin and the Málaga Basin (the last two are considered intra-slope basins, Juan *et al.*, 2016). The major high is the Alboran Ridge (1750 m high) in the central Alboran Sea, next to the Alboran Channel, a narrow trough up to 1800 m deep that connects the West and East Alboran basins. Although a volcanic nature is interpreted by most of the highs, only some of them have been sampled (Fig. 2.3, Duggen *et al.*, 2008). On the other hand, the tectonic origin of some of them have been proved, as the Xauen, Tofiño and Francesc Pagès Banks (d'Acremont *et al.*, 2020), or a combination of tectonism with magmatism, as the Alboran Ridge (Estrada *et al.*, 2018).

The sedimentary infill is Miocene (Aquitanian-Burdigalian) to Quaternary in age and mainly detritic (Comas *et al.*, 1992; Juan *et al.*, 2016). The basement of the Alboran Sea is formed by an asymmetrically thinned continental crust, with16 km of thickness at the northern margin and, progressively, it thickens southwards up to more than 30 km under the Rif (Gómez de la Peña *et al.*, 2020; Suriñach and Vegas, 1993). Seismic refraction profiles and potential field data indicate that the mantle below the Alboran Sea basin is low density and low P-velocity anomalous (Galindo-Zaldivar *et al.*, 1998; Hatzfeld, 1976; Suriñach and Vegas, 1993).

The basement of the Alboran Sea, initially part of the AlKaPeCa Domain, was separated from it in the Late Oligocene-Miocene (Fig. 2.2, Chertova *et al.*, 2014; Comas *et al.*, 1999; Mauffret *et al.*, 2007; Romagny *et al.*, 2020; Rosenbaum *et al.*, 2002). In that period, this domain experimented N-S extension related to southward retreat of the slab and the opening of the Algerian Basin (Fig. 2.2, Faccena *et al.*, 2014; Romagny *et al.*, 2020; Rosenbaum *et al.*, 2002; Schettino and Turco, 2011; Driussi *et al.* 2015). After the opening of the Algerian basin, the extension changed direction to E-W associated to a westward Gibraltar slab retreat, which led to the extension of the Alboran Sea as a back-arc basin (Gutscher *et al.*, 2012; Spakman *et al.*, 2018). The

Alboran Sea Basin is considered as a current back-arc basin with regards to the Gibraltar arc and associated with an eastward subduction (*e.g.*, Chertova *et al.*, 2014; Comas *et al.*, 1999; Gutscher *et al.*, 2012). However, some recent studies interpret an alternative subdivision into three crusts of different origin: a) the West Alboran and Malaga basins together as a Miocene fore-arc basin respecting to b) a magmatic arc whose remains are the East Alboran Basin, the Alboran Ridge and the Alboran Channel, and c) the indenter proposed in Estrada *et al.* (2018) is considered part of the African margin (Booth-Rea *et al.*, 2007; d'Acremont *et al.*, 2020; Gómez de la Peña *et al.*, 2020).

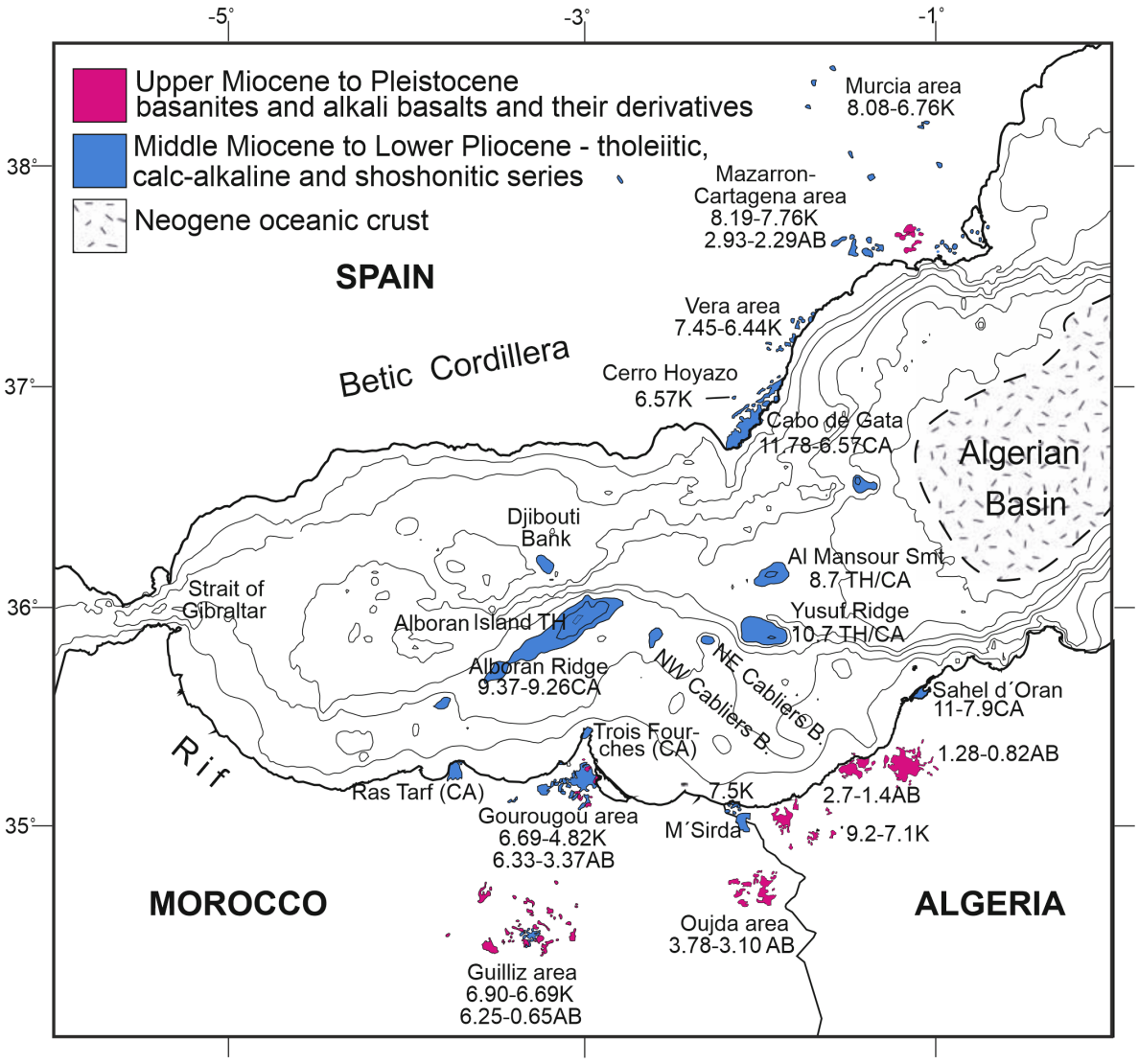

Figure 2.5. Main volcanic outcrops of Alboran Sea region of Neogene and Quaternary age. The number next to the name of the outcrop is the age in millions of years. Modified from Duggen *et al.* (2008). AB: alkali basalts; CA: calc-alkaline series; K: K-rich series; TH: tholeiitic series.

Magmatism

The widespread magmatism that affected the Alboran Domain from Miocene to Pleistocene was due to lithospheric thinning and the related increase in the geothermal gradient, which is still high in the eastern sector (Andrés *et al.*, 2018; Comas *et al.*, 1999; Duggen *et al.*, 2008; Polyak *et al.*, 1996). The geochemical studies of the several types of magmatism cluster them in two major groups (Fig. 2.5): a) tholeiitic, calc-alkaline (mainly basic and intermediate rocks) and shoshonitic series of Middle Miocene to Early Pliocene, that are interpreted as volcanic arc type, located in the central and eastern Alboran Sea; b) and basanites and alkali basalts of Late Miocene to Pleistocene that outcrop in the eastern onshore Alboran Domain (Coulon *et al.*, 2002; Duggen *et al.*, 2004; 2008; Fernández-Soler *et al.*, 2000; Gill *et al.*, 2004; Hoernle *et al.*, 1999). There are several hypotheses to explain the first group of geochemical affinities that are (Duggen *et al.*, 2008): i) MORB-type parental magmas with significant crustal contamination, which produced calc-alkaline lavas similar to subduction settings (Turner *et al.* 1999); ii) crustal magmas without mantle implication (Zeck *et al.*, 1998); and iii) tholeiitic and calc-alkaline series originated in a subduction-modified mantle with some crustal contamination (Coulon *et al.*, 2002; Hoernle *et al.*, 1999).

The last stages of volcanism that correspond to the second group of geochemical affinities (basanites, alkali basalts, hawaiites and tephrites of Late Miocene to Pliocene age) occur offshore in eastern Morocco, northern Algeria and SE Spain. They are caused by intraplate post-collisional magmatism (Duggen *et al.*, 2005). Some of these volcanic zones include rocks of both stages (the calk-alkaline and shoshonitic stage and the late, alkaline stage), such as the Gourougou volcano (Figs. 2.2 and 2.5, El Bakkali *et al.*, 1998).

Main recent and active structures

Since Late Tortonian, the combination of NW-SE compression due to the Africa-Eurasia convergence with orthogonal extension has characterized the activity and generation of tectonic structures in the Betic Cordillera and the Alboran Sea (Comas *et al.*, 1992; Dewey *et al.*, 1989; DeMets *et al.*, 2010; Galindo-Zaldviar *et al.*, 2015). These structures have controlled the evolution of the main chains and basins of the

Betic Cordillera, as well as the reliefs of the Alboran Sea. The External Zones are characterized by the development of fold-and-thrusts belts, with different orientations and axis rotations as the mountain front evolve and strike-slip faults associated with that movements (Crespo-Blanc *et al.*, 2016; García-Hernández *et al.*, 1980; Platt *et al.*, 2003). In the central-eastern part of the Betic mountain front, the Cazorla Range (Figs. 2.3 and 2.4b) is a good example of it. This range is the southern part of the Prebetic Arc (Fig. 2.3) and it is cut at the southern limit by the dextral Tíscar fault. Although these structures generate a relief contrast in the eastern limit of the Guadalquivir Foreland Basin, they are not active (Sanz de Galdeano *et al.*, 2006). Instead, the seismicity is located into the Guadalquivir Basin, whose origin is discussed and raises the possibility of active deformation in the Iberian basement, like Torreperogil seismic swarm with transpressive earthquakes (Marín-Lechado *et al.*, 2017; Morales *et al.*, 2015; Pedrera *et al.*, 2013).

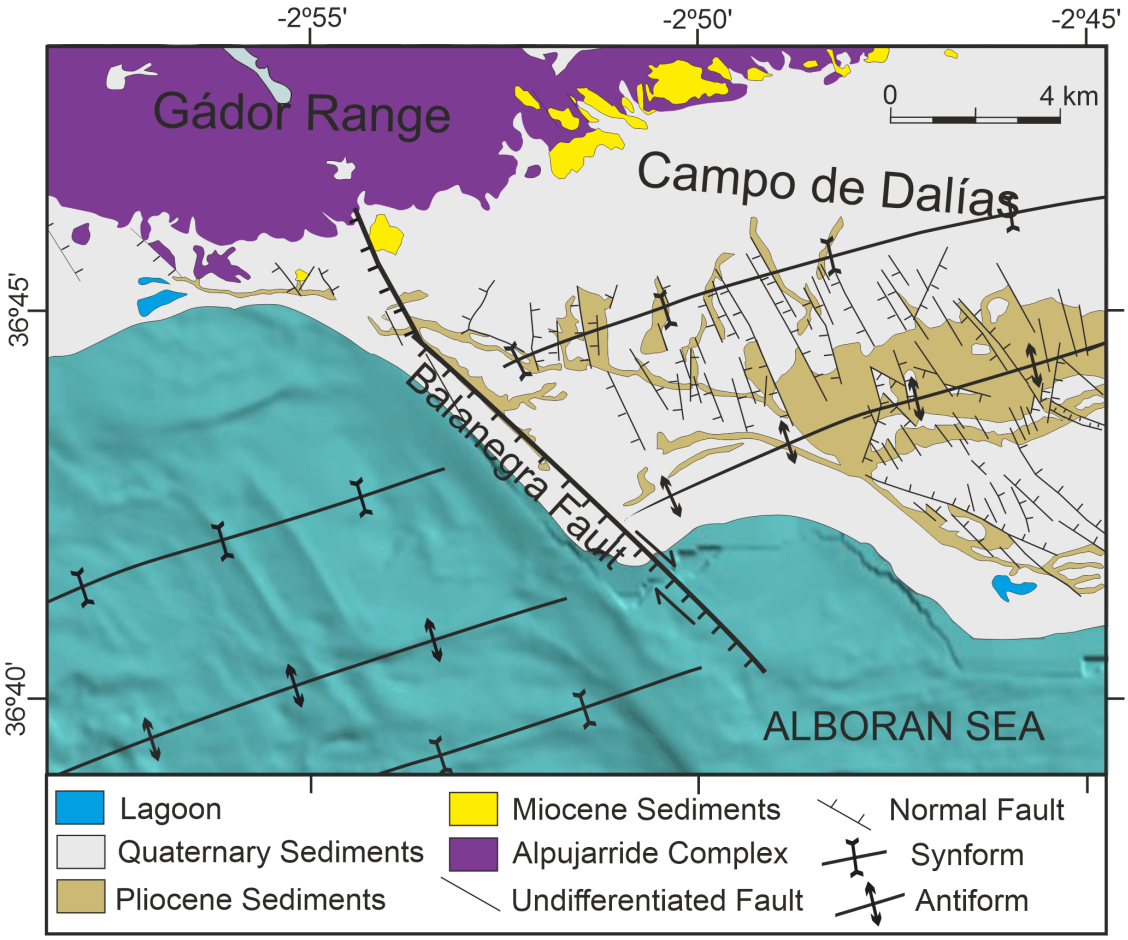

Figure 2.6. Geological map of the Campo de Dalías study zone centred in the Balanegra fault.

The Internal Zones of central-eastern Betic Cordillera, where the highest reliefs are located, are characterized by the development of large E-W to NE-SW oriented antiforms, such as Nevada Range or Gádor Range (Fig. 2.3., Galindo-Zalívar *et al.*, 2003; Sanz de Galdeano and Alfaro, 2004). These ranges are usually separated by the Neogene intra-mountain basins related to extensive fault systems, like the Granada basin (*e.g.*, Galindo-Zaldívar *et al.*, 2003), or to strike-slip systems, like the Alpujarran Corridor (Fig. 2.3, Martinez-Martos *et al.*, 2017). These normal fault systems are NW-SE oriented and active, like the Baza fault in the Baza Basin (Fig. 2.3, Alfaro *et al.*, 2008; Medina-Cascales *et al.*, 2020), the Padul fault (Fig. 2.3., Gil *et al.*, 2017) or the normal faults of the Granada basin that generated a significant seismic swarm during 2021 (Fig. 2.3., Galindo-Zaldivar *et al.*, 2003; Madarieta-Txurruka *et al.*, 2021; Sanz de Galdeano *et al.*, 1995). Another important and seismogenic system of NW-SE fault system is in the Campo de Dalías zone (Figs. 2.3 and 2.6), where these faults condition the western end of Sierra Gádor and the coast line, like Balanegra fault (Figs. 2.3 and 2.6, Marín-Lechado *et al.*, 2005; 2010; Pedrera *et al.*, 2012). In the central sector, there are also scarcer E-W to NE-SW faults, usually with a transcurrent component, related to elongated intra-mountain basins, such as the Alpujarran Coridor (Martínez-Martos *et al.*, 2017 and references therein), and/or to important seismicity, like the Alhama de Granada fault and the Andalucía earthquake of 1884 (Reicherter *et al.*, 2003).

Large strike-slip faults are more common in the eastern Betics, where the East Betic Shear Zone is developed (Bousquet, 1979; García-Mayordomo *et al.*, 2017; Silva *et al.*, 1993). This system of sinistral strike-slip faults, that include the Alhama de Murcia, the Palomares and the Carboneras/Serrata faults (Fig. 2.3), present several associated basins, like Vera basin and Guadalentin Corridor (Fig. 2.3). The seismicity caused by this system until recent times (Lorca earthquake of 2011) is characterized by strike-slip and transpressive tectonics (Borque *et al.*, 2019; Echevarria *et al.*, 2013; Herrero-Barbero *et al.*, 2021; Stich *et al.*, 2006). The Palomares fault (Fig. 2.3) is also part of the tectonic indentation Águilas Arc (Coppier *et al.*, 1989; Ercilla *et al.*, 2022; Silva *et al.*, 1993), which deforms and curve the E-W fold of Cabrera Range and conditions the evolution of the Vera Basin (Booth-Rea *et al.*, 2003; 2004; Coppier *et al.*, 1989; Silva *et al.*, 1993).

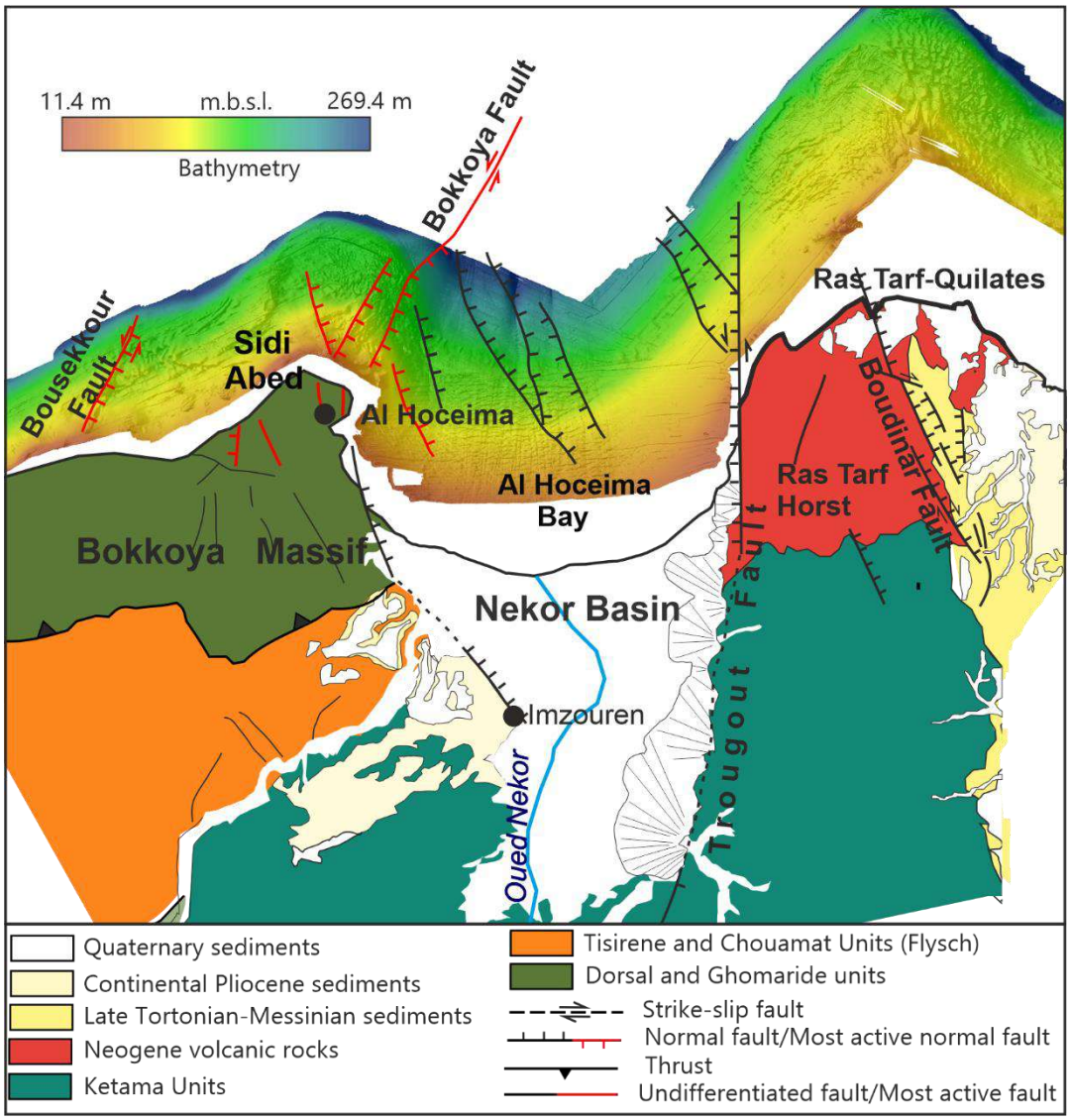

Figure 2.7. Geological map of the Al Hoceima Bay. Swath-bathymetry of the Al Hoceima margin from Marlboro-2 Survey (modified from d'Acremont *et al.*, 2014).

The East Betic Shear Zone is connected to the large strike-slip faults of the central Alboran Sea through the Carboneras fault, which was called the Trans-Alboran Shear Zone (De Larouzière *et al.*, 1988). The main faults of these system are the dextral Yusuf fault, the sinistral Al Idrissi fault and the union of them through the reverse fault at the base of the Alboran Ridge (Fig. 2.3, Ammar *et al.*, 2007; Ballesteros *et al.*, 2008; Comas *et al.*, 1999; Estrada *et al.*, 2018). However, the ages of these faults are different: Al Idrissi fault zone is interpreted as a Pleistocene structure (Lafosse *et al.*, 2020), while Yusuf fault is considered an inherited structure of a STEP fault (Subduction Tear-Edge Propagator) related with the westward displacement of the Alboran Domain during Miocene (d'Acremont *et al.*, 2020). In fact, Yusuf fault has a complex structure with two segments separated by the Habibas Escarpment (Fig. 2.3,

Martínez-García *et al.*, 2011) and it is also a contact between the continental crustal of the south Alboran Sea and the thinned magmatic crust of the East Alboran the Algerian basins (Booth-rea *et al.*, 2007; Gómez de la Peña *et al.*, 2020, Suriñach and Vegas, 1993).

Al Idrissi and Yusuf faults are the lateral faults of a tectonic indentation that contributed to the elevation of the Alboran Ridge (Estrada *et al.*, 2018; Lafosse *et al.*, 2020). The indentation is active and present active seismicity in the Al Idrissi fault zone, including its southern termination in the Al Hoceima Bay, and in the conjugate faults sets located between the Alboran Ridge and the Spanish coast (Figs. 2.3 and 2.6, Estrada *et al.*, 2018; Galindo-Zaldívar *et al.*, 2018; Lafosse *et al.*, 2016; Stich *et al.*, 2006). The fault sets located northwards of the Alboran Ridge are formed by strike-slip faults, some of them with vertical movement in their terminations and with tsunamigenic potential, as the Averroes fault (Fig. 2.3, Estrada *et al.*, 2018; 2021). This faults extended to the coast at Campo de Dalías zone (Marín-Lechado *et al.*, 2005). On the other side, the southern termination of the Al Idrissi fault forms a horsetail splay in the Al Hoceima Bay, part of the transtensional Nekor Basin (Figs. 2.3 and 2.7; d'Acremont *et al.*, 2014; Lafosse *et al.*, 2016). The whole bay is faulted by a set of NW-SE normal faults with the NE-SW left-lateral, normal Bokkoya fault in the western boundary of the bay, and the N-S lefl-lateral, normal Trougout fault in the eastern one (Fig. 2.7, d'Acremont *et al.*, 2014; Calvert *et al.*, 1997; Lafosse *et al.*, 2016). The fault system propagated onshore as the Trougout fault, the Imzouren-Ajdir-Boujibar normal faults and recent and minor fractures and deformations in the eastern part of the Bokkoya Massif (Fig. 2.7, Galindo-Zaldívar *et al.*, 2009; Poujol *et al.*, 2014). The biggest recent earthquakes (M_w 6.4) of the Alboran Sea region are located in this zone, in the western part of the Al Hoceima Bay (Calvert *et al.*, 1997, Van der Woerd *et al.*, 2014).

2.3 Previous geophysical and geodetical data

Precious geophysical data of the Betic Cordillera and the Alboran Sea provided information about the deep structure and characteristics of the region, as well as their geodynamic history and the development of their main features. Geodetical data show the current tectonic movements and help to understand the activity of structures such as faults. This section summarizes the main and most relevant geophysical and

geodetic data of the study zones of this thesis. Geophysical data include seismic prospection data (both refraction and reflection profiles), seismicity, seismic tomography data, gravity data and magnetic data.

Seismic prospection data

Seismic refraction and reflection profiles have been carried out over the Betic Cordillera and, especially, on the Alboran Sea. Deep multichannel reflection profiles have been used to describe the crustal structure and thickness of the both the Betic Cordillera and the Alboran Sea, like the ESCI-BETICAS profiles that cross the central Betic Cordillera (García-Dueñas *et al.*, 1994). ESCI-BETICAS profiles are two profiles that reach 196 km length from the Guadalquivir foreland basin to the coastline, where they are continued through Alboran Sea by the ESCI-ALBORAN profiles. The first of the two ESCI-ALBORAN profiles is 90 km length that continued the ESCI-BETICAS profiles, while the second one is 400 km length and WSW-ESE oriented, towards the Algerian basin (Suriñach and Vegas, 1993). Both ESCI-BETICAS and ESCI-ALBORAN profiles are of poor quality, but enough to interpret the deep structure of Betic and Alboran Sea, in particular the abrupt thinning of the crust at the coastline where the thickness is of 16 km (García-Dueñas *et al.*, 1994; Martínez-Martínez *et al.*, 1995; Suriñach and Vegas, 1993). Recent works have obtained similar results of crustal thickness in the Alboran Sea using wide angle reflection profiles (Gómez de la Peña *et al.*, 2020).

The inland results also show the presence of detachment levels that divide the upper and lower crust and an eastwards thickening of the crust with a maximum thick under Sierra Nevada (Banda *et al.*, 1993). In the Alboran Sea, the crustal thinning is asymmetrical, reaching 30 km at Africa coast from the 16 km thickness of northern Alboran Sea (Gómez de la Peña *et al.*, 2020; Suriñach and Vegas, 1993). The deep seismic profiles, the potential field data and the heat flow point to an anomalous mantle beneath the Alboran Sea (especially in the eastern part) with low density and low P-velocity (Galindo-Zaldivar *et al.*, 1998; Gómez de la Peña *et al.*, 2020; Hatzfeld, 1976; Polyak *et al.*, 1996; Suriñach and Vegas, 1993).

Conventional seismic reflection profiles coverage on Betic basins is irregular. Regarding to the study zones of this thesis, the Campo de Dalías zone is well covered

by old and recent seismic lines (Marín-Lechado *et al.*, 2007) and there are also several seismic multichannel reflection profiles in the eastern Guadalquivir basin (Marín-Lechado *et al.*, 2017). However, the continental Vera basin is not covered by seismic lines or they are not available, although data from cores can be used to study the thickness and characteristics of its sedimentary infill (Booth-Rea *et al.*, 2003).

Conversely, seismic reflection profiles coverage in the Alboran Sea is extensive (Fig. 2.8). The collection of multichannel seismic reflection profiles of the Instituto de Ciencias del Mar (ICM-CSIC, http://www.icm.csic.es/geo/gma/SurveyMaps) covers the whole Alboran Sea and have been used for study its paleoceanography, sedimentology and geomorphology (*e.g.*, Do Couto *et al.*, 2016; Ercilla *et al.*, 2016; Juan *et al.*, 2016). The Al Hoceima Bay study zone is covered by the multichannel high-resolution seismic reflection profiles acquired during the Marlboro-2 survey that were used to describe the faults and sedimentary deposits of the zone (d'Acremont *et al.*, 2014; Lafosse *et al.*, 2016; 2018).

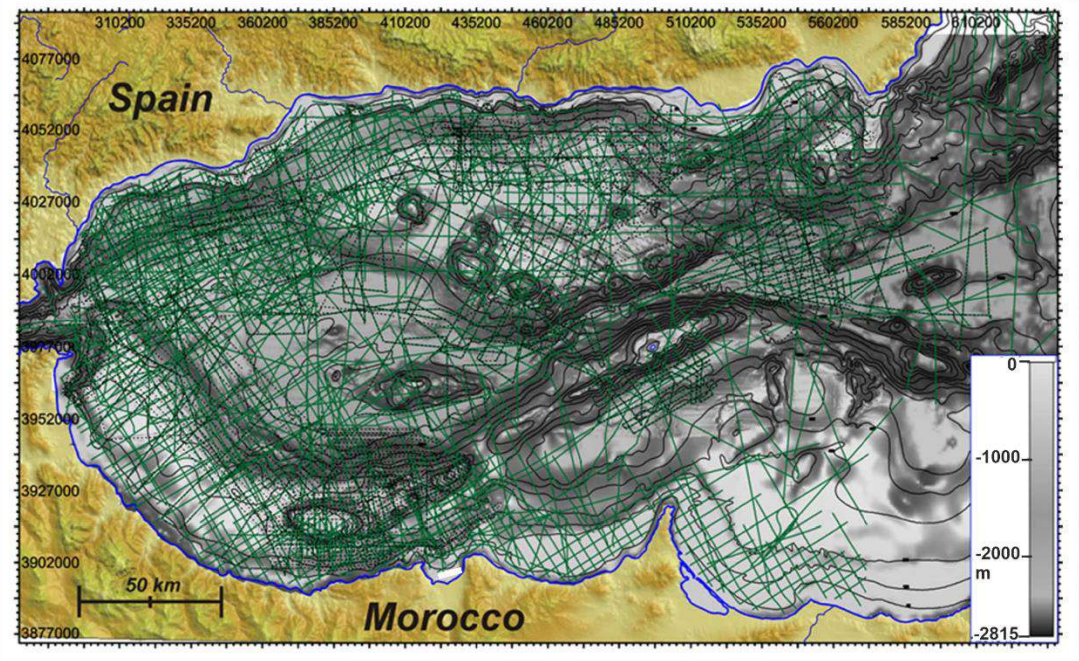

Figure 2.8. Bathymetry of the Alboran Sea with the seismic lines net of the Instituto de Ciencias del Mar database (modified from Ercilla *et al.*, 2016).

Seismicity and seismic tomographies

Seismicity in the Alboran Sea and Betic Cordillera can be divided into three groups: a shallow and widespread seismicity over a 300 km wide band, usually with

earthquakes up to moderate magnitudes (<6); shallow to intermediate earthquakes below the western Alboran Sea, and scarce deep earthquakes (up to 650 km) close to Granada (Buforn *et al.*, 2004; Morales *et al.*, 1999; Stich *et al.*, 2020). Focal mechanisms show a NW-SE compression, but the mechanisms vary all along the region. Reverse faulting is active in the Algerian coast and in the western sector of

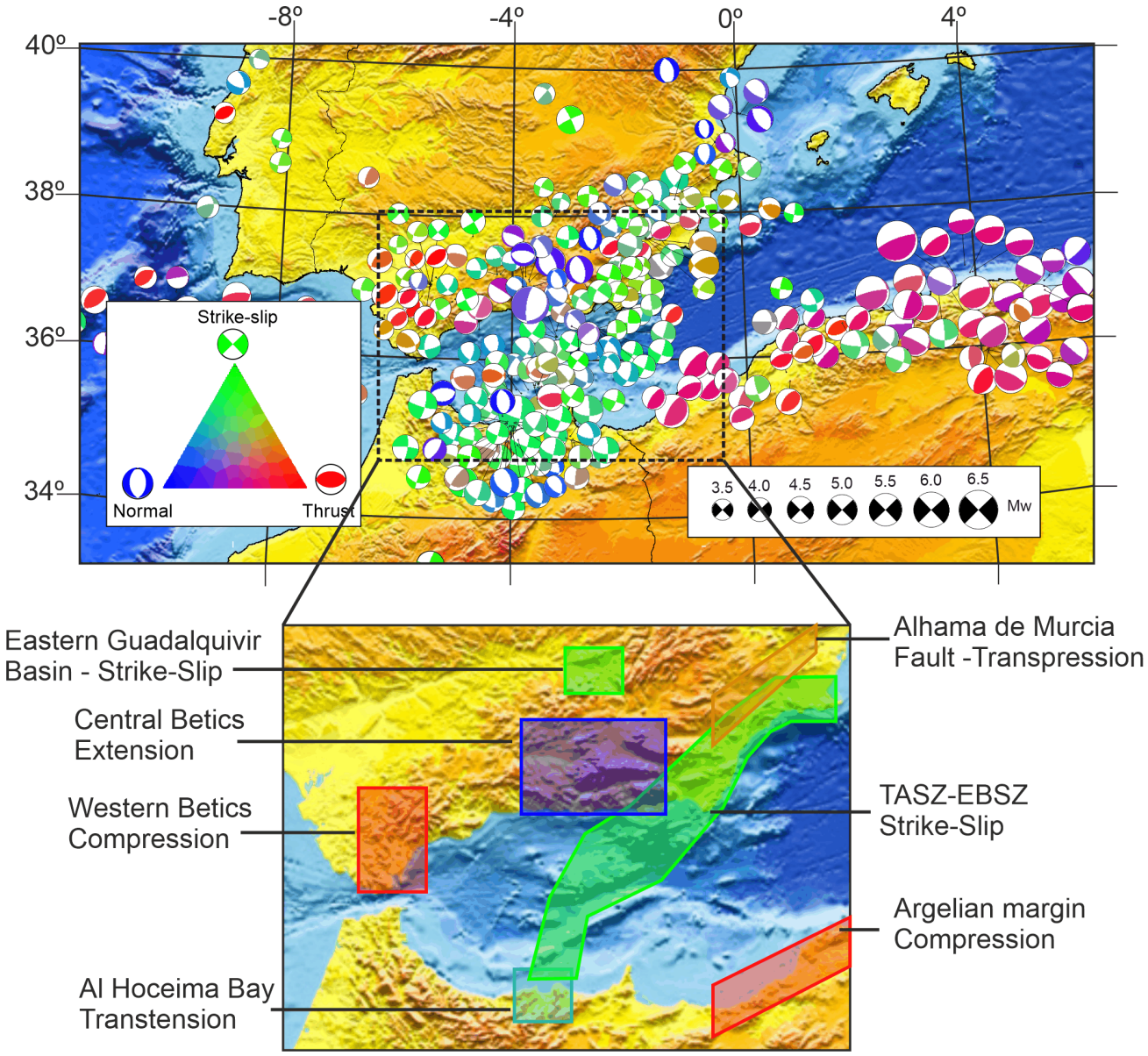

Figure 2.9. Seismic moment tensors from Instituto Andaluz de Geofísica catalog (modified from Martin *et al.*, 2015). The double couple tensor is plotted in the lower hemisphere projection. The lower zoom map summarizes the main seismotectonic zones that can be distinguish from the seismic moment tensors data on the Alboran Sea and the Gibraltar Arc.

Betic Cordillera while normal active faults are dominant in the central part of the cordillera and in some Rifian sectors (Fig. 2.9, Buforn *et al.*, 2004; García-Mayordomo

et al., 2017; Stich *et al.*, 2006: 2010; 2020). Strike-slip mechanisms are concentrated in the Alboran Sea and eastern Betics, where they are combined with normal and reverse faults (Fig. 2.9, Buforn *et al.*, 2004; Stich *et al.*, 2006; 2010; 2020). Some of these areas present a regime of transtension, like the Al Hoceima Bay (Lafosse *et al.*, 2016; Stich *et al.*; 2006; Van der Woerd *et al.*, 2014); while other are under transpression, like the eastern Betics (Borque *et al.*, 2019; Stich *et al.*, 2010).

Natural seismicity has also been used for seismic tomographies in the Alboran Sea and in the Betic and Rif Cordilleras. The data obtained has improved the characterize of the deep crustal structure that is characterized by a thickening of the eastern Betics up to ~40 km and the presence of a slab attached to the Iberian Crust in the western Betics (Carbonell *et al.*, 1998; Dañobeitia *et al.*, 1998; El Moudnib *et al.*, 2015) and upper mantle nature and structure (Blanco and Spakman, 1993; Calvert *et al.*, 2000; Gurria and Mezcua, 2000; Monna *et al.*, 2015; Morales *et al.*, 1999; Serrano et al; 2005; Spakman and Wortel, 2004). Other studies have incorporated the use of receiver functions (Mancilla *et al.*, 2013; 2015; Morales *et al.*, 2022) and seismic anisotropy (Alpert *et al.*, 2013; Diaz and Gallart, 2014). These studies show the presence of a subducting slab, which may have been separated from the Iberian crust by delamination or tearing, in an anomalous, low velocity mantle beneath the Alboran Sea. These studies also show that the fractured slab should occur under the central Betics, while the slab has broken off the Iberian crust under the eastern Betics, being the Iberian crust attached to the Alboran Domain crust.

Gravity data

In the Betic Cordillera, the first regional scale, gravity study was carried out by the Instituto Geográfico Nacional (1976) in order to compute the Bouguer anomaly map of the Iberian Peninsula and the Balearic Archipelago. Later researches are of local scale, many of them focused on the study of Miocene basins and related tectonic structures or local structures (*e.g.*, Alfaro *et al.*, 2008; Do Couto *et al.*, 2014; Madarieta-Txurruka *et al.*, 2021; Marín-Lechado *et al.*, 2007; Martínez-Martos *et al.*, 2017; Martínez-Moreno *et al.*, 2014; Pedrera *et al.*, 2007; Ruiz-Constán *et al.*, 2013). It is also remarkable the gravity data compiled by the TopoIberia project (Ayala *et al.*, 2016; http://info.igme.es/SIGEOF/), which provides gravity measurements of the whole peninsula. Other studies cover the Alboran Sea and/or the Betic Cordillera to

determine the crustal thickness and obtain crustal and lithospheric models, usually by combining gravity and seismic methods (*e.g.*, Casas and Carbó, 1990; Fullea *et al.*, 2006; Galindo-Zaldívar *et al.*, 1998; Hatzfeld *et al.*, 1976; Ruiz-Constán *et al.*, 2012; Torné *et al.*, 2000).

Magnetic Data

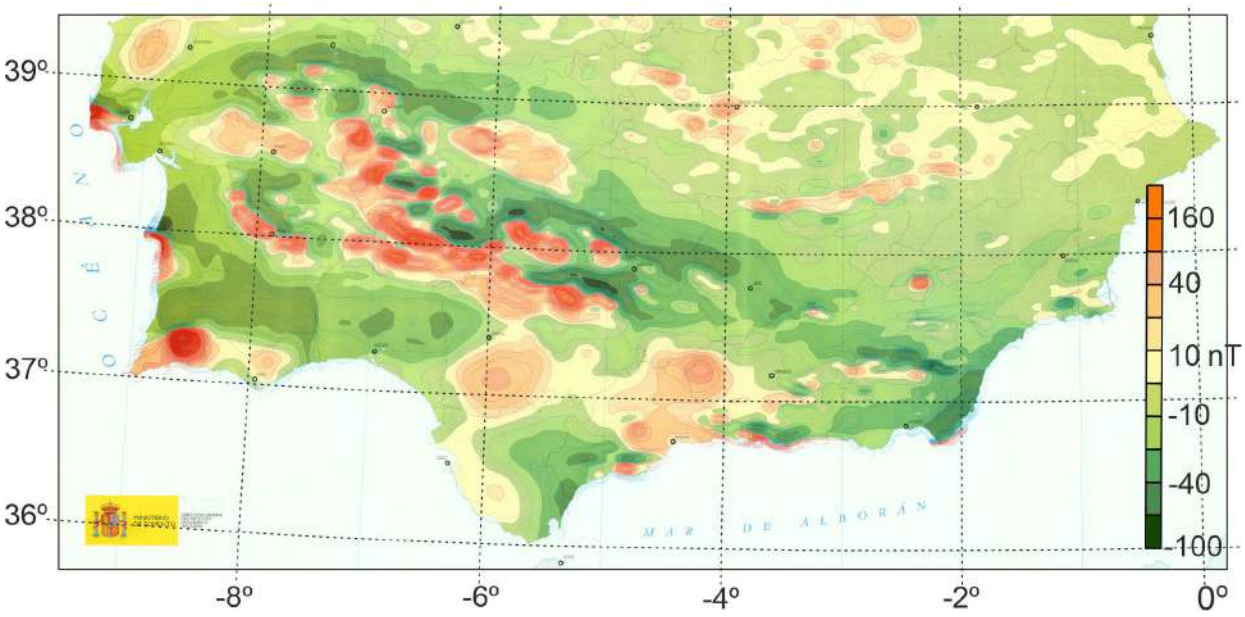

Figure 2.10. Aeromagnetic map of the southern Iberian Peninsula. Modified from Socias and Mezcua (2002).

The Instituto Geografico Nacional provided an aeromagnetic map of the Iberian Peninsula (Fig. 2.10, Socias and Mezcua, 2002). In this map, several magnetic anomalies are shown on the Betic Cordillera and are associated with the Betic structures. To unravel and modeled the origin some of them, detailed magnetic surveys have been carried out and provided information about the mineralized and igneous bodies of the Betic Cordillera (*e.g.*, González-Castillo *et al.*, 2014; Li *et al.*, 2012; Martínez-Martos *et al.*, 2017; Martínez-Moreno *et al.*, 2014; Pedrera *et al.*, 2009; Ruiz-Constán *et al.*, 2013).

The first aeromagnetic map on the Alboran Sea is provided in Galdeano *et al.* (1974). Galindo-Zaldivar *et al.* (1998) modeled the magnetic anomalies of the Alboran Sea combined with gravity data. Some of these anomalies are associated with volcanic highs, while other are displaced from the main volcanic highs, like those located next to the Alboran Ridge. In the Moroccan coast, Anahnah *et al.* (2009) provided magnetic

models of the dipole located over Nador town, both onshore and offshore, which is one of the most intense magnetic anomalies of the Alboran Sea.

Geodetical data

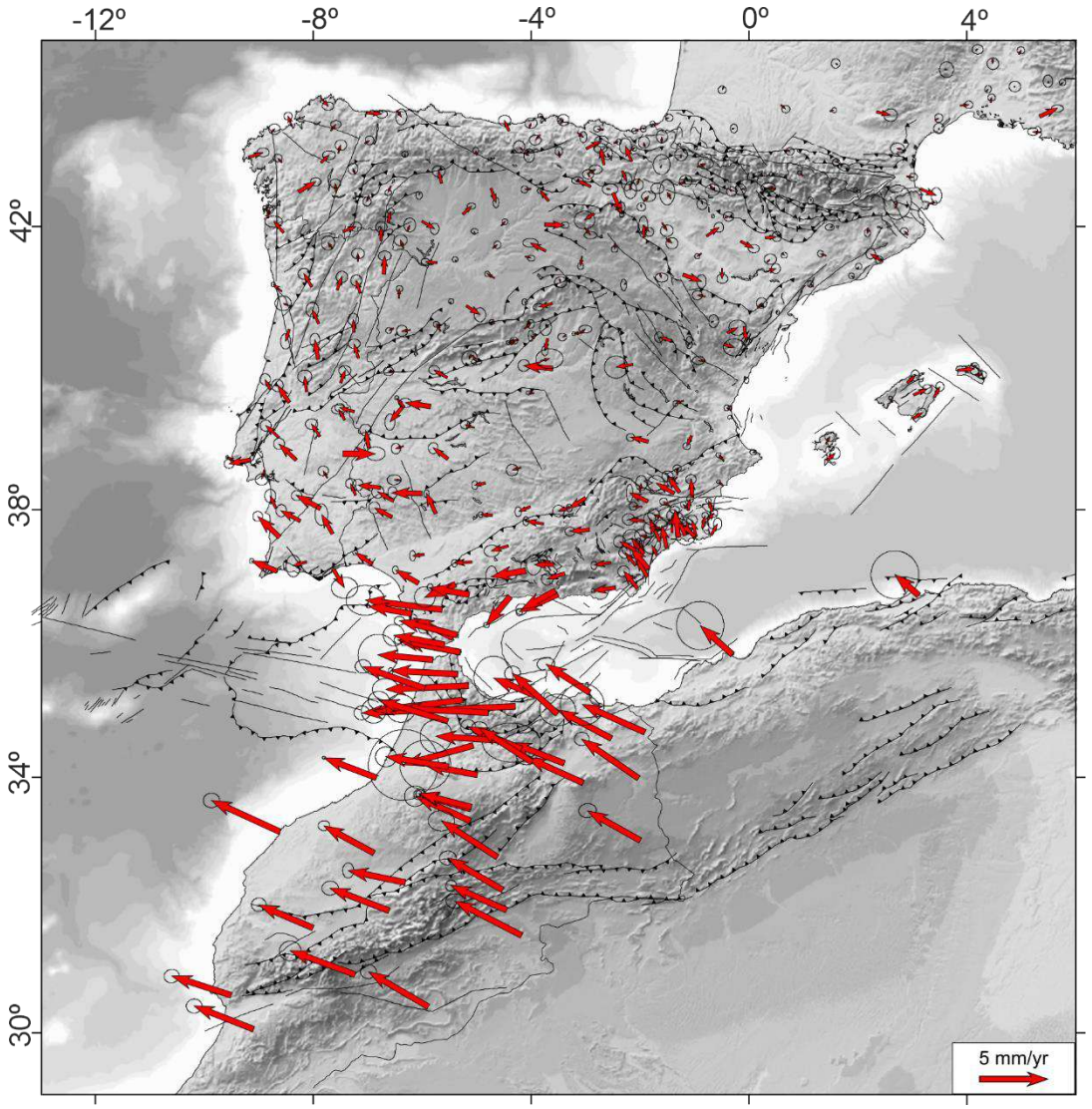

Figure 2.11. GPS velocities with the 95% confidence ellipses considering a fixed Eurasia (modified from Palano *et al.*, 2015).

GNSS networks have been deployed, both temporal and permanent (Ruano and da S. Fernandes, 2020), to characterize the active deformation of the Eurasia-Africa plate boundary over the Alboran Sea, the Iberian Peninsula and northern Morocco. The oblique convergence of 4-5 mm/yr (DeMets *et al.*, 2010), which changes along the plate boundary (Serpelloni *et al.*, 2007), is heterogeneously accommodated through the whole region (Borque *et al.*, 2019; Galindo-Zaldivar *et al.*, 2015, Garate *et al.*, 2015;

Palano *et al.*, 2015; Ruano and da S. Fernandes, 2020). The results show (Fig. 2.11) that there is a WSW displacement of the central and western Betic Cordillera and westwards displacement of the Rif Cordillera respect to stable Eurasia (Galindo-Zaldivar *et al.*, 2015; Garate *et al.*, 2015; Koulali *et al.*, 2011; Vernant *et al.*, 2010). These displacements imply an active extension in central Betic Cordillera (Galindo-Zaldivar *et al.*, 2015), while the eastern Betic presents a transpression regime (Borque *et al.*, 2019; Echeverria *et al.*, 2013).

In addition to these data, local GPS networks and high precision levelling profiles have unraveled the behavior of several active faults. Some examples are the Baza fault in the Guadix-Baza basin (Alfaro *et al.*, 2021), the Balanegra fault in the Campo de Dalías zone (Marín-Lechado *et al.*, 2010) or the Padul fault (Gil *et al.*, 2017).

CHAPTER 3

Methods

In order to obtain the necessary information to unravel and improve the previous knowledge about the active and recent tectonic of central-eastern Betic Cordillera and Alboran Sea, geological, geophysical and geodetical methods have been applied. Several techniques have been combined in each study zone, in addition to previous, available data, to describe the main active and recent faults and relevant crustal bodies and basins. All the methods applied in every study zone are well described in the corresponding chapters of Part II of this Ph.D. Thesis. Complementary, a summary of the methods used and their fundaments is provided in this chapter.

3.1 Geological methods

The geological field work has been focused on the detection of tectonic structures, the characterization of basin boundaries, and identification of the main units and lithologies that may be related with geophysical anomalies. It is remarkable the search and examination of recent faults to determine their kinematics and whether they were still active or not, based on markers like the affected deposits or clastic wedges. For these purposes, the contribution of the database of geological maps from the Instituto Geológico y Minero de España (IGME, Spanish geological and mining survey) has been essential. These maps have been used to plan every field campaign, from the location of the geophysical measurement points to the identification and location of the main tectonic structures and the lithologies used in the modeling.

3.2 Geophysical methods

3.2.1 Gravity prospecting

Gravity prospecting is based in the variation of the gravity acceleration as a result of lateral density contrasts and it consists in measuring the gravity acceleration in several points and the later corrections to obtain the gravity anomalies. A gravity anomaly can be defined as the difference between the gravity value measured in a point and the theoretical gravity value expected for that point according to its geographical position and a standard, homogeneous model of the Earth. Thus, the

origin of the anomaly is not only due to density variations, but also to time and space factors such as the altitude or the topography.

The factors that depend on time are the instrumental drift and the tidal effect. The instrumental drift is due to the slight stretching of the internal mechanism that measures the gravity acceleration after measuring, but it is easily corrected by beginning and finishing every measurement cycle in the same station (called the base station). The tidal effect is due to the gravity modification generated by the Sun and Moon gravity attractions' that are periodical, so they are also easily corrected.

The latitude of the measurement point modifies the gravity measure because the Earth radius decreases from the equator to the poles and the centrifuge acceleration caused by the Earth rotation also decreases from the equator to the poles. This is corrected by applying the Geodetic Reference System empiric formulae to the gravity acceleration observed, g_{obs}, (GRS, 1967):

$$g_l = 978031.849\ (1 + 0.005278895 sin^2\phi + 0.000023462 sin^4\phi)\ (mGal)$$

Where $g_l$the theoretical gravity value is at sea level and ϕ is the latitude in degrees. This formulae is suited for the ellipsoid, so to consider the elevation difference between the ellipsoid and the measurement point, the Free Air (FA) correction has to be applied (0.3086 mGal/m). It is calculated with the following formulae, where h is the elevation in meters above sea level:

$$FA = g_{obs} - g_l + 0.3086\ h\ (mGal)$$

After this correction, the Bouguer correction is computed. It considers the difference of mass in the measurement point due to its elevation difference (the quantity of mass that is between the real altitude and the surface of the ellipsoid). Considering both Free Air and Bouguer corrections, the Bouguer anomaly (BA) is calculated as:

$$BA = g_{obs} - g_l + 0.3086\ h\ - 0.04193\ \rho\ h\ (mGal)$$

Where ρ is the average density of the survey area in g/cm^3.

Finally, it is necessary to quantify the influence of the surrounding topography. To this aim, the Terrain correction (TC) is applied to obtain the Complete Bouguer anomaly (CBA):

$$CBA = g_{obs} - g_l + 0.3086\, h - 0.04193\, \rho\, h + TC\ (mGal)$$

Terrain corrections is computed using digital elevation models (DEM) of the region. The Complete Bouguer anomaly only depends on the density variations of the rocks underneath the measurement point.

Figure 3.1. Gravimeter Scintrex CG-5 Autograve with tripod used to acquire gravity data during this Ph.D. Thesis.

The gravimeter used in the gravity surveys carried out during this Ph.D. Thesis was a Scintrex CG-5 AutoGrav with accuracy up to 0.001 mGal (Fig. 3.1). This gravimeter automatically calculates the tidal correction, stores all the measurements and provides an accurate electronic level to reduce levelling mistakes during measuring. The locations of the measurement points were obtained by means of differential GPS. All the stations were referred to the absolute gravity station of Granada (National Geographic Service of Spain, IGN). Oasis Montaj was used to obtain the Complete Bouguer anomaly, which calculates the Terrain correction using a combination of the methods developed by Kane (1962) and Nagy (1966) up to 160 km of each station applied in a 5 m accuracy DEM provided by the IGN. These data were used to compute Bouguer anomaly maps applying kriging. The residual anomaly maps were derived by the difference between the Bouguer and the regional anomaly maps. After this,

several residual anomaly profiles were modeled using the GRAVMAG v1.7 software of the British Geological Survey (Pedley *et al.*, 1993).

3.2.2 Magnetic prospecting

The Earth magnetic field, which is considered as the field generated by a magnetic dipole, is caused by currents in the outer core produced by different rotation speeds of the inner core respecting to the rest of the Earth. The geomagnetic field is variable in time because of the changes of the inner source (the core) that produces changes in the orientation and intensity of the field, but also due to external variable sources like solar radial. In general, its intensity varies from 60 000 nT in the poles to 30 000 nT in the equator.

Figure 3.2. Magnetometer GSM-8 used to acquire magnetic data during this Ph.D. Thesis.

The magnetic prospection study local magnetic anomalies, *i.e.* deviations of the local magnetic field with regards to the theoretical field at that point, caused to magnetic properties in the rocks. Some rocks present magnetic susceptibility, so when they are under a magnetic field like the geomagnetic one, they acquired an induced magnetic field. This field can be the result of the present day geomagnetic field or it may be associated with a different geomagnetic polarity that induced a magnetic field in the rock when it was formed. This second case is called remnant field. The remnant and the induced magnetization (the field related to the present day geomagnetic polarity) are related by the Könisberger ratio, which tends to be larger in mineralized rocks.

On land, the equipment used to measure the total magnetic field was a GSM-8 proton precession magnetometer with an accuracy of 1nT (Fig. 3.2). Each measurement point was located far from anthropic noise sources such as metallic objects or power lines. To compute the magnetic anomalies, a standard procedure which consists in a reduction to the IGRF 2015 (Thébault *et al.*, 2015) for the measures acquired before 2020 and IGRF 2020 (Alken *et al.*, 2021) was used for the measures acquired after 2020, including 2020. The diurnal magnetic field variation due to the external sources of the geomagnetic field was corrected using the nearest permanent magnetic station that is in San Fernando, Cádiz (Real Instituto y Observatorio de la Armada, Spain).

Regarding to the marine magnetic data used in this Ph.D. Thesis, the data were obtain from the second version of the World Digital Magnetic Anomaly Map Project (http://wdmam.org/). This worldwide map has a 3 nautical miles resolution. The data were gathered at a variety of altitudes, but normalized at sea level for marine surveys (Catalán *et al.*, 2016; Lesur *et al.*, 2016). The magnetic profiles were modeled using the GRAVMAG v1.7 software of the British Geological Survey (Pedley *et al.*, 1993). In addition, Euler deconvolution was applied to estimate the depth of the magnetic anomalies causative bodies combined with the data of the Curie point depth front Li *et al.* (2017).

3.2.3 Electric resistivity Tomography

Electric resistivity tomography (ERT) is a geoelectric prospection method based on induced electric currents. This method is used to detect bodies with different electrical properties. During ERT, an electrical current of known intensity (I) is applied to the ground by two electrodes (called A and B) separated an AB distance. In a symmetric position respect to the half distance between the electrodes (*i.e.*, AB/2) another pair of electrodes (M and N) are located to measure the potential difference (V). Then, the resistivity (ρ) is calculated using all these parameters in a homogeneous and isotropic medium, which is not the case of the ground. Thus, the obtained resistivity is an apparent value due to the different bodies through which the current passes. The equation to obtain the apparent resistivity, depending on the AB distance (r), is:

$$V = \frac{I\,\rho}{2\,\pi\,r}$$

In the ERT several electrode arrangements are deployed, which provides different AB and MN distances; they can be divided into asymmetric and symmetric arrays depending on the M and N electrodes position respecting to the AB/2 position. The asymmetric arrays provide more penetration, but a distortion of the bodies' geometry is generated. On the other hand, symmetric arrays better obtain the morphology of the bodies, but lower penetration.

Figure 3.3. Terrameter SAS 4000 used to obtain the ERT profiles of this Ph.D. Thesis. Lower photos show the dispositive carried out on the field.

In the ERTs carried out during this Ph.D. Thesis, the array used is a gradient array (ABEM, 2006; Loke, 2014) with a 4-channel multiple gradient protocol taking the measurements in two cycles called GRAD4LX8 and GRAD4S8. The equipment used was a Terrameter SAS 4000, which has a 1 μV resolution and an accuracy greater than

1% in the entire temperature range (Fig. 3.3). It has three automatic measurement ranges (±250 mV, ±10 V and ±400 V), with four measurement channels that provide larger amounts of data in a small period of time. After ERT acquisition, the data were downloaded using SAS4000 Utilities software. The positions of each electrode were measured using differential GPS and added to the data files to consider the topography during the data inversion.

The inversion was computed with RES2DINV v.3.59 to obtain real resistivity 2D sections from the apparent resistivity sections. This software makes first a verification of the data; then, it proceeds to the inversion by means of finite elements modeling, which is more suitable in profiles that include the topography. The software applies the least squares method to calculate the real resistivity from the apparent resistivity pseudosection. After that, it calculates the apparent resistivity that would generated the real resistivity section that it has obtained, and compares the results with the field data. This is repeated in several iterations until the root mean squares (RMS) error is acceptable (less than 10%).

3.2.4 Seismic reflection profiles

In this Ph.D. Thesis two groups of seismic reflection profiles has been used (Fig. 3.4). All of them were acquired before the beginning of this Ph.D. Thesis and are based on the same fundaments. A mechanic wave is generated from an artificial source that the ship carries out. The waves experiment different reflections in both the sea bottom and the different discontinuities of the ground, like stratigraphic layers. An array of geophones registers the reflected waves; the number of geophones that the streamer contains is the number of channels. Through different procedures and corrections, the geometry of the reflectors is obtained, but with a vertical exaggeration, because the Y axis is usually in two-way travel times.

The first group of multichannel seismic reflection profiles comprises six lines of regional scale (Fig. 3.4a) were obtained from the database of the Instituto de Ciencias del Mar, Barcelona (ICM-CSIC http://www.icm.csic.es/geo/gma/SurveyMaps). These profiles of deep penetration using airgun source, which have been realized following standard procedures of acquisition and processing, were selected on the basis of their location and position orthogonal to the main magnetic dipoles of the Alboran Sea

(study zone E, see Chapter 9). The second group (Fig. 3.4b) are 265 multichannel high-resolution seismic reflection profiles which cover 190 km2 in the Al Hoceima Bay (study zone D). These data were acquired during the Marlboro-2 survey using a 250-500 J SPARKER source and a six-channel streamer, with a vertical resolution of 1 m.

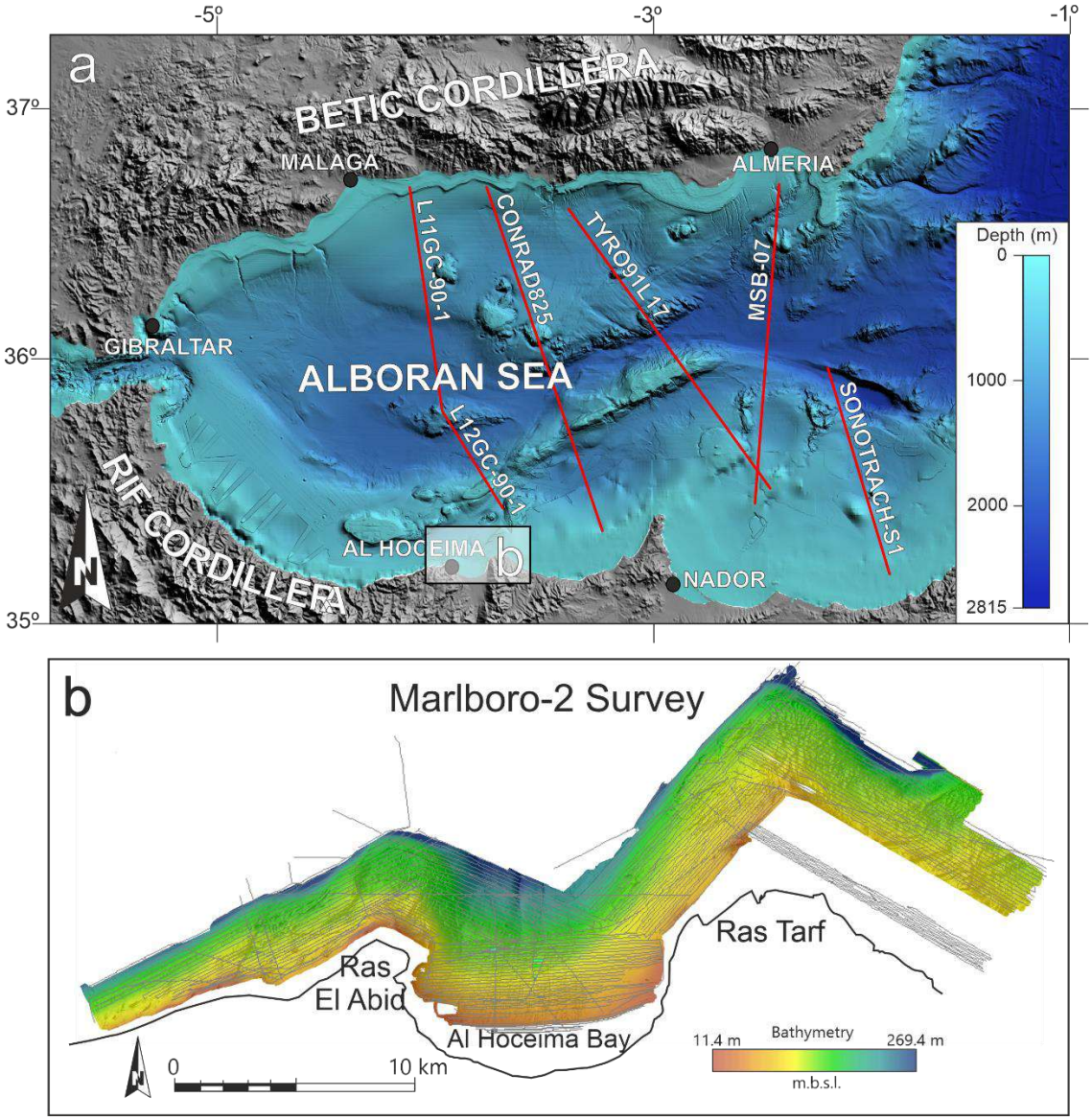

Figure 3.4. Seismic lines traces of the profiles used in this Ph.D. Thesis. a. Regional multichannel seismic reflection profiles from ICM database. b. Multichannel high-resolution seismic reflection profiles of Marlboro-2 Survey.

3.2.5 Throw Backtstripping

The throw backstripping is a method developed by Chapman and Meneilly (1991) to quantify the fault vertical throw/displacement. This method consists in measuring the vertical throw at regular intervals along the fault and across multiple stratigraphic

horizons. It has different variations, but the simplest one makes no assumptions about the patterns of throw accumulation or the style of fault growth (Jackson *et al.*, 2017). The main step is applying the backstripping, that is to say, each throw is calculated by removing the throw accumulated on the youngest horizons, starting with the youngest. By this way, it is possible to quantify the throw of each period of time and also to determine of the activity of the fault through time.

In the study zone D, the Al Hoceima Bay, this method was applied on 672 faults determined by Lafosse *et al.* (2016). Part of these faults have strike-slip components (Lafosse *et al.*, 2016), so the estimation of the vertical throw constitutes an indicator of the deformation and activity of the faults. For this purpose, an automation of the method using ArcGIS software was made. Three very low dipping surfaces (which were considered reference surfaces to measure the vertical throw) were selected and extracted from HIS Kingdom Suite software, as well as the fault traces and the crossing's location between each fault and each seismic profile, called “fault points”. Then, a work-flow were created using the model builder tool of ArcGIS that comprised the following steps (see Chapter 8 for the explanation of each step):

1) Extraction of the depth range at each reference surface for each fault point.
2) Determination of whether each fault point cut each reference surface.
3) Calculation of the throw of each fault point and each interval following the throw backstripping method.
4) Making raster layers of the throw of the area close to the fault traces for each interval.

Finally, throw rates maps were created from the throw maps by transforming two-way travel times into depth and then dividing by the period of time between each reference surface. These throw rates only consider the vertical deformation associated with the faults.

3.3 Geodetical methods

A non-permanent local GNSS network with five sites (labelled as 9400, 9600, 9700, 9800 and 9900), which belongs to a wide regional network (Marín-Lechado *et al.*, 2010) has been used to determine the active tectonics in the western Campo de Dalías (study zone C). This network was built in 2006 and it is formed by self-centring

mounting devices anchored to stable rocks. The records were made through field campaigns every year since its installation with, at least, 96 hours of measurements during each observation and divided in 24 hours and 30 seconds sampling interval RINEX files. The equipments used until 2010 were LEIAX1202 antennas and Leica Geosystem GX1230 receivers and, after that year, LEIAR10 antennas and LEICA Geosystem AR10 receivers. The last ones have been the devices used during this Ph.D. Thesis (field campaigns during November 2017, 2018, 2019 and 2021).

Part II

4. New insights on the Alboran Sea basin extension and continental collision from magnetic anomalies related to magmatism (western Mediterranean).

5. Application of Automated Throw Backstripping Method to Characterize Recent Faulting Activity Migration in the Al Hoceima Bay (Northeast Morocco): Geodynamic Implications.

6. The Campo de Dalías GNSS network unveils the interaction between roll-back and indentation tectonics in the Gibraltar Arc.

7. Shearing in an indenter boundary: the evolution of the Águilas Arc and its accommodation along the PFZ (Betic Cordillera, Spain).

8. Seismicity in Strike-Slip Foreland Faults (Central Betic Cordillera Front): Evidence of Indentation Tectonics.

CHAPTER 4

New insights on the Alboran Sea basin extension and continental collision from magnetic anomalies related to magmatism (western Mediterranean).

Víctor Tendero-Salmerón[a*], Jesus Galindo-Zaldivar[a,b], Elia d'Acremont[c], Manuel Catalán[d], Yasmina M. Martos[e,f], Abdellah Ammar[g], Gemma Ercilla[h]

[a]Instituto Andaluz de Ciencias de la Tierra (CSIC-UGR), 18100 Armilla (Granada), Spain

[b]Departamento de Geodinámica, Universidad de Granada, 18071 Granada, Spain

[c]Sorbonne Université, CNRS-INSU, Institut des Sciences de la Terre Paris, ISTeP UMR 7193, 75252 Paris Cedex 05, France

[d]Royal Observatory of the Spanish Navy, 11100 San Fernando (Cádiz), Spain

[e]NASA Goddard Space Flight Center, Greenbelt, MD 20771, USA

[f]University of Maryland College Park, College Park, MD 20742, USA

[g]Faculté des Sciences, Université Mohammed V-Agdal, Rabat, Morocco

[h]Instituto de Ciencias del Mar, Continental Margins Group, CSIC, 08003 Barcelona, Spain

Published on:

Marine Geology, Volume 443 (January 202)

https://doi.org/10.1016/j.margeo.2021.106696

(Received 14 August 2021, Accepted 4 November 2021, Available online 14 November 2021)

JCR(2020): 3.548 (Q1)

Abstract

In the Alboran Sea there are a few well exposed Neogene and Quaternary volcanic zones, often geographic highs, which are generally associated with magnetic anomalies. . In this paper, we present a characterization of these magnetic anomalies based on a recent and accurate magnetic data compilation for the Alboran Sea area. The anomalies reveal the distribution of magmatism and shed light into the discussion about the origin and evolution of the westernmost Mediterranean. One of the most relevant magnetic anomalies is the Nador dipole, which extends from the Gourougou volcano to the Chafarinas Islands, and is related to an E-W crustal scale intrusion. However, the main NE-SW elongated continuous dipoles of the central Alboran Sea are not related to any surface structure, but they are parallel to the Alboran Ridge, which is the main volcanic high in the Alboran Sea, and are located to the north of it. These anomalies extend discontinuously eastward along the NW-SE dipoles located along the Yusuf fault zone. The results of our 2D magnetic forward modeling suggest that the causative bodies of these main magnetic dipoles are deep igneous bodies. According to the tectonic evolution of the region, and the high magnetic susceptibility values obtained, these igneous bodies probably are made of a basic igneous rocks. Their emplacement may represent the westward tip of the rift axis of the AlKaPeCa Domain, which is related to the Oligocene-Miocene NW-SE extension, and associated with the southern slab retreat stage and oceanic spreading of the Algerian basin. Afterwards, these bodies were displaced toward the west, together with the Alboran Domain, and affected by the STEP fault located at its southern limit. Since the Late Miocene, the north Alboran Ridge elongated intrusions acted as a backstop that conditioned the folding and uplift of the Alboran Ridge in a tectonic indentation setting. In this setting, the STEP fault is deformed and the eastern part of the bodies were segmented along the Yusuf transtensional fault system. Simultaneously, the E-W crustal body related to the Nador magnetic dipole was emplaced, possibly evidencing a slab tearing process. The deep seated basic igneous bodies constitute main crustal heterogeneities that reveal and drive the Alboran Sea tectonic inversion.

Keywords: Magnetic anomalies, igneous basic rocks, rifting, continental collision, Alboran Sea development

4.1 Introduction

Back-arc basins are extensional structures formed in active continental margins generally related to oceanic lithosphere subduction (Taylor, 1995 and references therein). Extension in these basins is the consequence of a slab rollback (Heuret and Lallemand, 2005 and references therein). The rifting and magmatism associated to the spreading of back-arc basins may lead to the emplacement of igneous bodies that may be characterized by magnetic anomalies (Bohoyo *et al.*, 2002; Catalán *et al.*, 2013; Lawver and Hawkins, 1978; Taylor *et al.*, 1996; Weissel, 1981). Therefore, an analysis of the igneous bodies based on magnetic studies can provide clues for decoding the onset and evolution of back-arc basins.

The Western Mediterranean is a relevant area of back-arc basin occurrence, due to the slab rollback of the subducting African plate, which started during the Oligocene, and resulted in the extension and fragmentation of the southwestern margin of Europe (Doglioni, 1991; Gueguen *et al.*, 1997; 1998; Malinverno and Ryan, 1986; Royden, 1993; Schettino and Turco, 2011; Spakman *et al.*, 2018; Spakman and Wortel, 2004). The migration of arcs and collision with the nearby continental margins led to the formation of arc-shaped alpine orogens (Fig. 4.1a) and the extension in the fore-arc and back-arc basins, which ultimately underwent tectonic inversion (Faccena *et al.*, 2014; Gómez de la Peña *et al.*, 2020b; Yelles *et al.*, 2009; and references therein). This is the case of the Gibraltar Arc, formed by the Betic and Rif Cordilleras, which encircles the Alboran Sea (Fig. 4.1, Comas *et al.*, 1992; Corsini *et al.*, 2014). The Internal Zones of the Gibraltar Arc (both those of the Rif and Betic Cordilleras) and the basement of the Alboran Sea basin constitute the Alboran Domain (Fig. 4.1b).

Two main groups of hypotheses have been proposed to explain the origin of the Alboran Domain extension. On one side, the lithospheric delamination hypotheses (*e.g.*, Baratin *et al.*, 2016; Mancilla *et al.*, 2013; Seber *et al.*, 1996; Valera *et al.*, 2008), and on the other the subduction with slab rollback starting from the Miocene (Fig. 4.1a ; *e.g.*, Blanco and Spakman, 1993; Gutscher *et al.*, 2012; Spakman *et al.*, 2018). Tomographic results support a subduction system that is related to the Gibraltar Arc (García-Castellanos and Villaseñor, 2011; Spakman and Wortel, 2004) more in accordance with the model of slab rollback and lithospheric tearing at the edges (*e.g.*, Chertova *et al.*, 2014; Faccenna *et al.*, 2014). Several paleogeographic reconstructions

propose two consecutive stages of slab retreat since the Oligocene (*e.g.*, Driussi *et al.* 2015). The first one is a south-eastern slab retreat that would have led to the displacement and initial extension of the Alboran Domain, as well as to the opening of the Algerian basin as a back-arc process (Fig. 4.1a, Gueguen *et al.*, 1997; Mauffret *et al.*, 2007; Romagny *et al.*, 2020; Schettino and Turco, 2011; Spakman *et al.*, 2018). The second one is a westward slab retreat that would have resulted in the migration of the Alboran Domain, thus causing the fore-arc and back-arc extension during the Miocene (Comas *et al.*, 1999; Chertova *et al.*, 2014; Gutscher *et al.*, 2012; Schettino and Turco, 2011).

In this paper, a new case study based on magnetic anomaly data is presented, which improves the understanding of the geodynamic scenario of the Alboran Sea basin. This was possible through the use of a recent magnetic data compilation for the study of the main magnetic anomalies produced by major igneous crustal bodies. Their structure and significance, in the context of the back-arc rifting, were analyzed in order to reveal new clues on the extensional deformations that created the Alboran Sea basin, as well as the development of the STEP fault (Subduction Tear Edge Propagator fault, Govers and Wortel, 2005), and the recent tectonic indentation. This contribution also highlights the impact that large igneous bodies intruded during the initial continental rifting stages had on the sedimentary basin evolution.

4.2 Regional setting

The Alboran Sea basin is located in the westernmost part of the Mediterranean. It is bounded by the Gibraltar Arc (Betic and Rif cordilleras, Fig. 4.1). The basin can be subdivided into four sub-basins separated by the main highs, which are the West Alboran Basin (the largest one), the Eastern Alboran Basin (which is opened to the Algerian Basin), the South Alboran basin and the Malaga Basin (Fig. 4.1b). The basement is formed by asymmetric thinned continental crust evidenced by deep seismic profiles (Gómez de la Peña *et al.*, 2020a; Suriñach and Vegas, 1993), reaching 16 km of thickness from the northern margin to the Alboran Ridge, and progressively thickening southwards up to more than 30 km under the Rif. Seismic refraction profiles and potential field data indicate that the mantle below the Alboran Sea basin is low density and low P-velocity anomalous (Galindo-Zaldivar *et al.*, 1998; Hatzfeld *et al.*, 1976; Suriñach and Vegas, 1993). The Alboran Sea basin opens eastwards to the

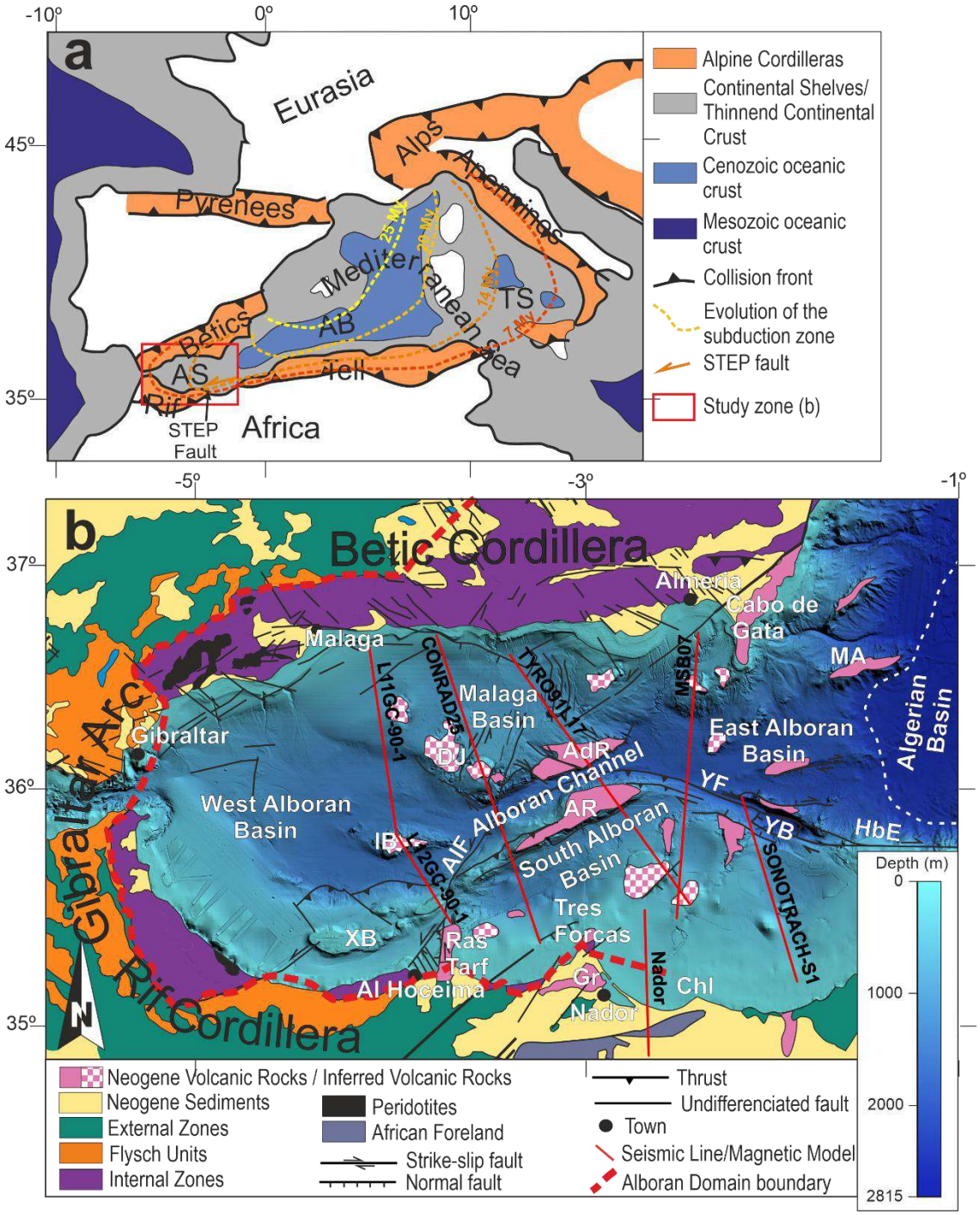

Figure 4.1. Geological context of the study zone. a. Tectonic sketch of the western Mediterranean Sea based on Do Couto *et al.* (2016) that includes the evolution of the subduction zone associated to the opening of the Western Mediterranean (d'Acremont *et al.*, 2019; Do Couto *et al.*, 2016; Faccena *et al.*, 2014; Rosenbaum *et al.*, 2002). AB: Algerian basin, AS: Alboran Sea. b. Simplified geological map of the Alboran Sea based on Hidas *et al.* (2019) and d'Acremont *et al.* (2020). The inferred volcanic rocks correspond to outcrops where there are no dredged or drilled samples to confirm them. The paths of the seismic profiles used to constrain the forward models of magnetic anomalies are included. The approximated boundaries of Alboran Domain are depicted. Eastern boundary is still discussed, so it is not depicted. AIF: Al Idrissi Fault, AR: Alboran Ridge; AdR: Adra Ridge, ChI: Chafarinas Islands, DJ: Djibouti Bank, GR: Gourougou volcano, HbE: Habibas

Escarpment, IB: Ibn-Batouta Bank, MA: Maimonides High, XB: Xauen Bank, YB: Yusuf Basin, YF: Yusuf Fault.

oceanic Algerian basin (*e.g.*, Faccena *et al.*, 2014; Gueguen *et al.*, 1997). The thinned continental crust basement, which constitutes the Alboran Domain, is represented by alpine metamorphic rocks (mainly metapelites) of the Internal Zones of the Betic and Rif cordilleras (Comas *et al.*, 1992; García-Dueñas *et al.*, 1992) that include peridotites (Garrido, 1995). Although the Alboran Sea is considered a current back-arc basin associated to a westward subduction (*e.g.*, Balanya *et al.*, 2012; Chertova *et al.*, 2014; Comas *et al.*, 1999; González-Castillo *et al.*, 2015a; Gutscher *et al.*, 2012), recent studies propose an alternative subdivision into three crustal domains: i) the West Alboran and Malaga basins together representing a Miocene fore-arc basin; ii) the East Alboran Basin, the Alboran Ridge and the Alboran Channel, forming part of a magmatic arc; and iii) the area located southwards of the Yusuf fault and the Alboran Ridge, which is considered part of the African margin (Booth-Rea *et al.*, 2007; d'Acremont *et al.*, 2020; Gómez de la Peña *et al.*, 2020a; 2020b). The sedimentary infill is Miocene (Aquitanian-Burdigalian) to Quaternary in age and mainly detritic (Comas *et al.*, 1992; Juan *et al.*, 2016).

The geological evolution of the Alboran Domain is the consequence of the motion and rifting of the AlKaPeCa Domain (Bouillin *et al.*, 1986) between the Eurasian and African plates, started in the Late Oligocene-Miocene (Chertova *et al.*, 2014; Comas *et al.*, 1999; Mauffret *et al.*, 2007; Romagny *et al.*, 2020; Rosenbaum *et al.*, 2002). The AlKaPeCa Domain is described as a landmass that, before the Miocene, was part of the fore-arc and accretionary prism that originally formed on the Eurasian side of the African-Eurasian collision (Bouillin *et al.*, 1986). Its name refers to the domains that were formed by its fragmentation (Bouillin *et al.*, 1986): the Alboran Domain, the Kabyiles (Argelia), the Peloritan Range (Sicily) and Calabria (South Italy). The AlKaPeCa Domain experienced at least 200 km of roughly N-S extension (or even more, Faccena *et al.*, 2014), which started during the Late Oligocene (27-25 Myr) and was related to the southward retreat of the slab. This N-S to NW-SE extension was characterized by a top-to-the north detachment (Jolivet *et al.*, 2021 and references therein) and led to the beginning of the oceanic spreading of the Algerian basin during the Early Miocene (Faccenna *et al.*, 2014; Romagny *et al.*, 2020; Rosenbaum *et al.*, 2002; Schettino and Turco, 2011; Driussi *et al.* 2015). After the opening of the

Algerian basin, the extension changed direction to E-W, in relation to a westward Gibraltar slab retreat and, therefore, to a westward motion of the Alboran Domain. During the Miocene, the westward displacement of the subduction zone has been accommodated by a STEP (Subduction Tear Edge Propagator) fault in the southern limit of the Alboran Domain (*e.g.*, d'Acremont *et al.*, 2020). STEP faults are subvertical, lithospheric-scale tear faults located at the edges of a segmented slab (Govers and Wortel, 2005).

The extension of the Alboran Domain was followed by compression since the Late Tortonian (Comas *et al.*, 1999; Do Couto *et al.*, 2016), when the westward retreat of the Gibraltar slab decreased (d'Acremont *et al.*, 2020). The NW-SE oblique Eurasian-Africa plate convergence was combined with the orthogonal extension associated to the westward motion of the Alboran Domain (Comas *et al.*, 1992; Corsini *et al.*, 2014; DeMets *et al.*, 2010; González-Castillo *et al.*, 2015a; Neres *et al.*, 2016; Watts *et al.*, 1993). Strike-slip faulting has affected the central Alboran Sea since the Late Miocene, forming the main NW-SE dextral and NE-SW sinistral fault sets that cross the basin and continue up to the coast (Fig. 4.1b). Two of the most relevant strike-slip faults of these sets are the Al Idrissi and the Yusuf faults (Fig. 4.1b). While the Al Idrissi fault zone has been considered to be a Pleistocene structure (Lafosse *et al.*, 2020), the Yusuf fault is interpreted as being older, inherited from the STEP fault that accommodated the westward displacement of the Alboran Domain, and deformed by the compression (d'Acremont *et al.*, 2020). The Yusuf fault presents a complex structure with related folds and basins, divided into two segments by the Habibas Escarpment (Fig. 4.1b, Martínez-García *et al.*, 2011). The fault is also considered to be a main contact between the thinned continental crust of the African plate and both the magmatic thinned crust of the East Alboran Basin, and the oceanic crust of the Algerian Basin (Booth-Rea *et al.*, 2007; Gómez de la Peña *et al.*, 2020a; Suriñach and Vegas, 1993). The Al Idrissi and Yusuf faults have been interpreted as being part of a tectonic indentation structure that affects the Central Alboran Sea and causes the elevation of the Alboran Ridge (Estrada *et al.*, 2018; Lafosse *et al.*, 2020). According to this model, the Alboran Ridge uplift above the Alboran Channel would be the consequence of the NNW directed collision of the rigid basement block of the southern part of the Alboran Sea basin, bounded by the Al Idrissi and the Yusuf faults (Fig. 4.1b, Estrada *et al.*, 2018).

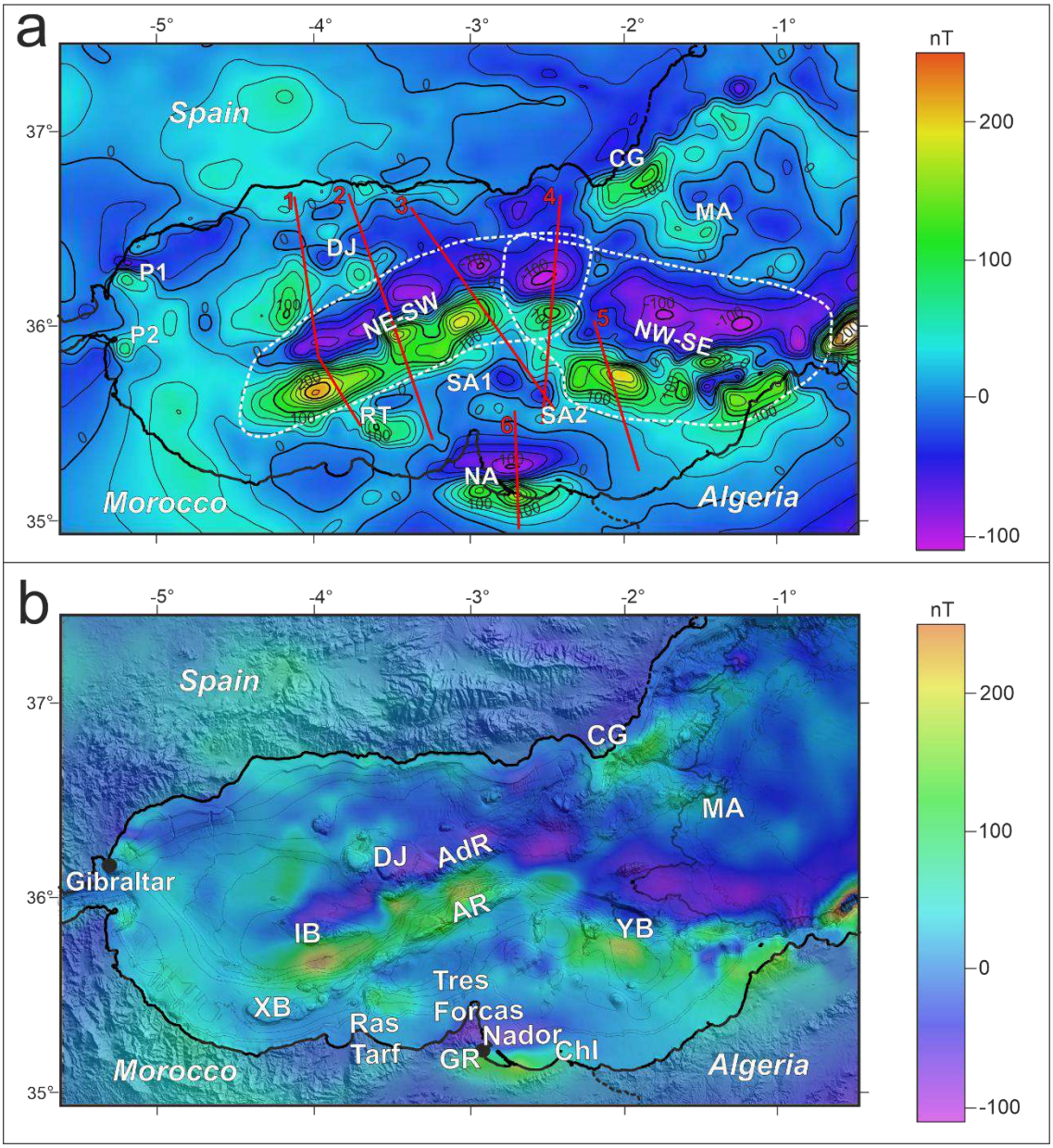

Figure 4.2. Magnetic anomaly maps of the Alboran Sea. a. Magnetic anomaly map of the Alboran Sea at 3 nautical miles resolution. Minor contour lines every 20 nT and major every 100 nT. The paths of the profiles are depicted and numbered as follows: 1. L12GC-90-1- L11GC-90-1, 2. CONRAD825, 3. TYRO91L17, 4. MSB07, 5. SONOTRACH_S1 and 6. Nador. The white abbreviations are the names given to the dipoles (further description in sections 4 and 5). The NE-SW and NW-SE dipole lineations are circled with a dashed line. b. Magnetic anomaly map superimposed over a relief map of the Alboran Sea with bathymetry contour lines every 200 m and the coast line in black. AR: Alboran Ridge, AdR: Adra Ridge, ChI: Chafarinas Islands, GR: Gourougou volcano, IB: Ibn-Batouta Bank, XB: Xauen Bank, YB: Yusuf Basin.

Magmatism

From the Miocene to the Pleistocene, magmatism affected the Alboran Domain due to lithospheric thinning and the related increase in the geothermal gradient (which

continues being high, at least in the eastern part) (Fig. 4.1, Andrés *et al.*, 2018; Comas *et al.*, 1992, 1999; Davis, 2013; Duggen *et al.*, 2008; Polyak *et al.*, 1996). Most of the highs, seamounts and ridges of the Alboran Sea have been considered volcanic outcrops (*e.g.*, Booth-Rea *et al.*, 2007, Comas *et al.*, 1999), mainly made up of basic or intermediate rocks (basalt and andesites, *e.g.*, Duggen *et al.*, 2008; Fernández-Soler *et al.*, 2000). Geochemical studies show a zonation of the magmatism characterized by tholeiitic, calc-alkaline and shoshonitic series (Middle Miocene to Early Pliocene), which are believed to be of volcanic arc type, present in the central and eastern Alboran Sea; while basanites and alkali basalts (Late Miocene to Pleistocene) appear in the eastern onshore Alboran Domain (Coulon *et al.*, 2002; Duggen *et al.*, 2004, 2008; Fernández-Soler *et al.*, 2000; Gill *et al.*, 2004; Hoernle *et al.*, 1999). Three main hypotheses can explain the geochemical affinity of the Alboran magmatism (Duggen *et al.*, 2008): a) MORB-type parental magmas with significant crustal contamination, which generate calc-alkaline lavas similar to subduction-related ones (Turner *et al.* 1999); b) crustal sources without mantle implication (Zeck *et al.*, 1998); and c) tholeiitic and calc-alkaline series from a subduction-modified mantle with different degrees of crustal contamination (Coulon *et al.*, 2002; Hoernle *et al.*, 1999). The last stages of volcanism (basanites, alkali basalts, hawaiites and tephrites of Late Miocene to Pliocene age) occur offshore in eastern Morocco, northern Algeria and SE Spain, and are related to intraplate post-collisional magmatism (Duggen *et al.*, 2005). Some of these volcanic zones include rocks of both stages (the calk-alkaline and shoshonitic stage and the late, alkaline stage), such as the Gourougou volcano (Fig. 4.1, El Bakkali *et al.*, 1998). The occurrence of this volcano has been related to a tearing of the oceanic slab attached to the African margin (Carminati *et al.*, 1998; Duggen *et al.*, 2005; Hidas *et al.*, 2019; Jolivet *et al.*, 2021; Maury *et al.*, 2000).

The magnetic anomalies of the Alboran Sea have been associated with basic igneous rocks since the publication of the aeromagnetic map presented by Galdeano *et al.* (1974). One of the most important anomalies is that of Nador (Figs. 4.1 and 4.2), which was constrained from onshore field observations (Anahnah, *et al.*, 2009) and that continues offshore. In the central basin, Galindo-Zaldivar *et al.* (1998) suggested that the Alboran Ridge is not the causative body of the main observed magnetic dipoles, even though the Alboran Ridge is considered to be made of volcanic rocks (*e.g.*, Booth-Rea *et al.*, 2007). The magnetic models provided in this study improved

the modeling made by Galindo-Zaldivar *et al.* (1998) and support the presence of deep igneous bodies as origin of those magnetic dipoles, although the models are open to alternative interpretations.

4.3 Materials and methods

Magnetic anomaly analysis

To produce the magnetic anomaly map presented with this work we used data from the second version of the World Digital Magnetic Anomaly Map Project (http://wdmam.org/). This worldwide map has a 3 nautical miles resolution. The data were gathered at a variety of altitudes, but normalized at 5 km above sea level on the continents, and at sea level for marine surveys (Catalán *et al.*, 2016: Lesur *et al.*, 2016). The map of the Alboran Sea area has been obtained by combining different line orientations, mainly E-W, NW-SE and NE-SW, with a line spacing smaller than 20 km in most of the zones. This map is suitable for studying magnetic anomalous bodies whose size ranges from several to tens of kilometers, without noise originated by small, shallow bodies. It encompasses data from different international sources whose acquisition times span from 1964 until 2016. The way these data were processed to improve their internal coherency is described in Quesnel *et al.* (2009) and Lesur *et al.* (2016).

After obtaining the magnetic anomaly map (Fig. 4.2), the analytic signal (AS, Fig. 4.3) was calculated. This is defined as the square root of the squared sum of the vertical and two orthogonal horizontal derivatives of the magnetic field anomaly (Nabighian, 1984; Roest *et al.*, 1992; Roest and Pilkington, 1993; Salem *et al.*, 2002):

$$|AS(x,y,z)| = \sqrt{\left(\frac{\partial M}{\partial x}\right)^2 + \left(\frac{\partial M}{\partial y}\right)^2 + \left(\frac{\partial M}{\partial z}\right)^2} \quad (1)$$

where $|AS(x,y,z)|$ is the amplitude of the AS, and M the magnetic anomaly intensity.

Therefore, the resulting 3D AS map summarizes the net variation of the gradient of the magnetic anomaly field intensity in 3D. One of the most attractive aspects of this 3D operator is the fact that its amplitude produces maximum amplitude along the lateral edges of the causative body, regardless of the direction of magnetization, or its induced and/or remanent character (Keating and Sailhac, 2004; Roest et al, 1992;

Roest and Pilkington, 1993). In this sense, there is no need to assume a purely induced magnetization effect hypothesis or to discuss possible remanent vector space orientation. Such a simplistic approach (a purely induced magnetization effect hypothesis) could lead to severe distortion in environments where remanent effects play an important role.

Magnetic techniques were used in order to identify deep structures. To this end, an algorithm based on the Euler deconvolution was applied to estimate the depth to the top of the different magnetic horizons. This procedure was performed by selecting a square window of data from a total field grid and its orthogonal derivatives. Euler's equation was solved using the least squares method, simultaneously for each grid position, within every window (Ravat, 1996; Reid *et al.*, 1990; Thomson, 1982). The equation includes the degree of homogeneity, "N", which usually refers to the structural index (S.I.). This index is a measure of the rate of change with distance of a field.

$$(x - x_0)\frac{\partial M}{\partial x} + (y - y_0)\frac{\partial M}{\partial y} + (z - z_0)\frac{\partial M}{\partial z} = NM(2)$$

where M is the magnetic anomaly intensity at location (x, y, z), caused by a magnetic source at location (x_0,y_0,z_0), and N denotes the structural index.

The results of the Euler deconvolution and the Curie point depth have been used to constrain the maximum depth where the anomalous magnetic bodies may be located. The AS depths (Fig. 4.3) were obtained using the so-called "Standard Euler Deconvolution". This procedure was performed by selecting a square window of data from a total field grid and its orthogonal derivatives. Euler's equation was solved using the least squares method, simultaneously for each grid position, within every window. A value of 2 was used as Structural Index (SI). An index of 2 indicates a body with one infinite dimension. That value was chosen because, in our opinion, it is the option that best represents the geometries of the NE-SW and NW-SE magnetic anomalies: a limited depth and width, with the longest dimension extending along the Alboran Basin. The accepted solutions were only those with a depth tolerance smaller or equal to 15%. A value of 26 km was set as window size, which is the width of the anomalies (according to the AS map) that we are interested in the Alboran ridge and the Yusuf fault zone.

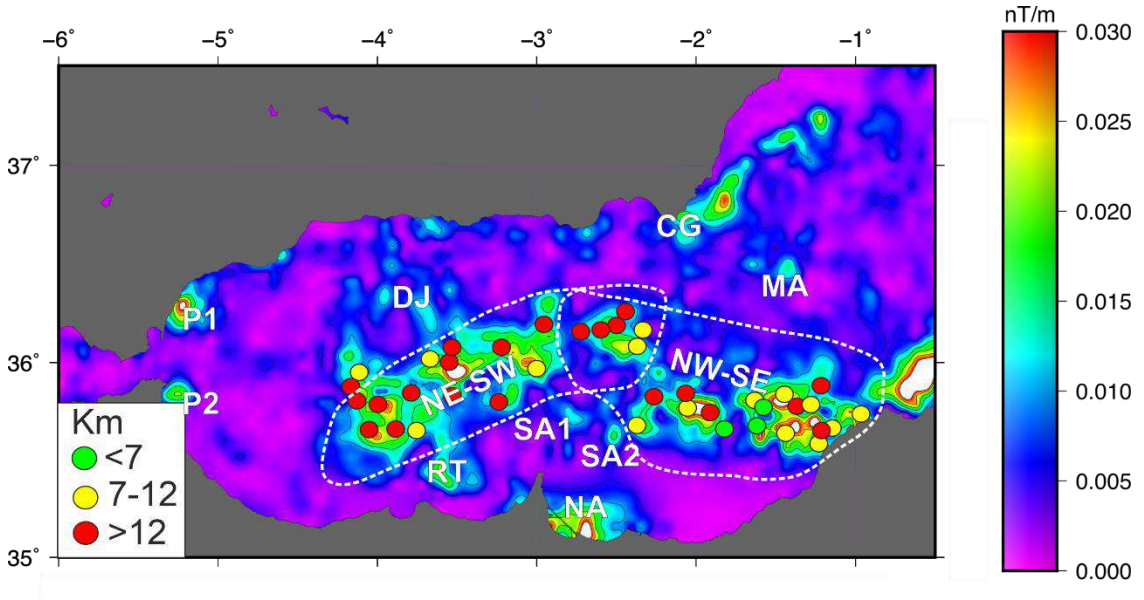

Figure 4.3. Analytical signal map of the Alboran Basin with the depth Euler solutions in km. The names of the corresponding magnetic anomalies are depicted. The white abbreviations are the names given to the dipoles (further description in sections 4.4 and 4.5).

Furthermore, it is necessary to consider the Curie point depth, or Curie depth, the depth at which magnetic minerals lose their magnetic properties due to temperature. Several factors, such as composition variability, could result in uncertainties in the estimation of the Curie depth. For this reason, causative bodies, in order to be safely considered as such, must be emplaced a few kilometers over the Curie depth of the region. These data were obtained from Li *et al.* (2017). It is also important to note that both depths, the Curie depth and the Euler deconvolution depths, are used initially as guiding depths to localize the causative bodies for the forward modeling.

The 2-D forward modeling of the magnetic anomalies (Figs. 4.5, 4.6 and 4.7) was obtained using the GravMag 1.7 software of the British Geological Survey (Pedley *et al.*, 1993). The magnetic susceptibility values of the anomalous magnetic bodies are based on those used in Galindo-Zaldivar *et al.* (1998). Three types of bodies were considered (Fig. 4.5): those with high susceptibility (0.07 SI, basic or intermediate igneous rocks, in black); those with medium values of susceptibility (0.02 to 0.045 SI, areas where there is a mixing of metamorphic and igneous rocks, marked in brown and green); and those with very low susceptibility (< 0.02 SI, sediments and the rest of the basement host rock, respectively marked in yellow and beige). Moreover, for the causative bodies of the major dipoles (bodies in black), which are the main target

of the models, three values of susceptibility (0.05, 0.07 and 0.10 SI) have been considered. This way, the effect of susceptibility on the geometry and depth of the bodies was tested.

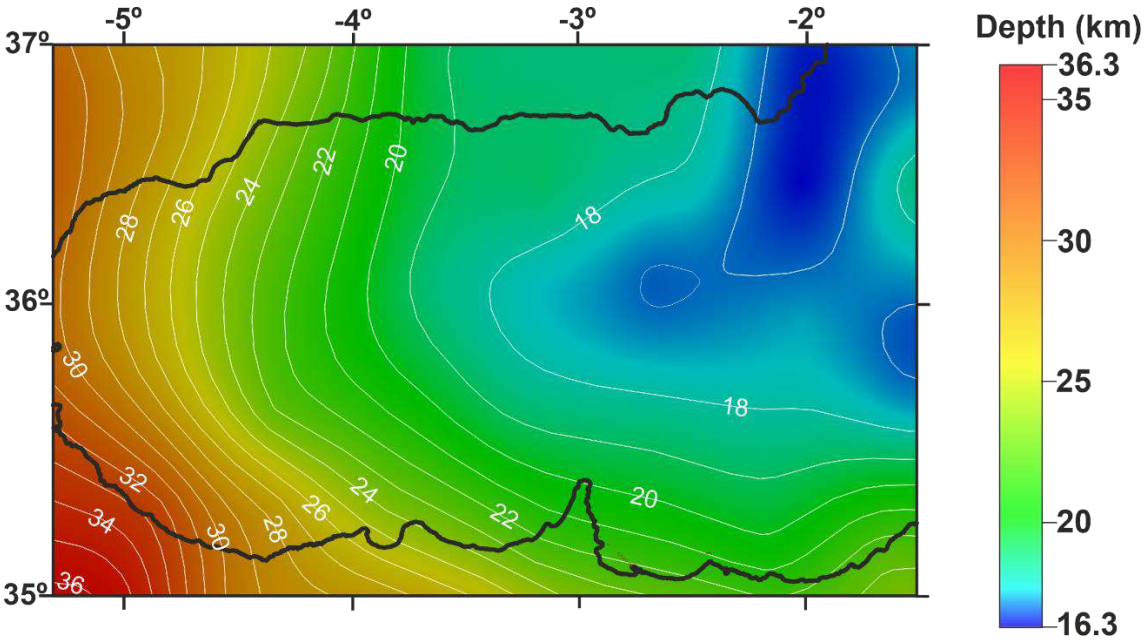

Figure 4.4. Curie depth map for the Alboran Sea based on Li *et al.* (2017) data. Contour lines every 1 km.

The appearance of the magnetic anomalies in the Alboran Sea consists of dipoles that show highs to the south and lows to the north (Fig. 4.2). This polarity is compatible with the induced magnetic anomalies produced by the current Earth's magnetic field in the northern hemisphere (*e.g.*, Telford *et al.*, 1990). Consequently, in the absence of direct information on the remanent magnetization, it was decided not to separate the remanent from induced magnetic contributions in our forward modeling, similarly to what Galindo-Zaldivar *et al.* (1998) did. The susceptibilities should be interpreted as apparent values. The magnetic dipoles that have been modeled are those that present amplitudes > 200 nT, which are also tens to hundreds of kilometers long. The dipoles are considered when magnetic highs and lows with similar size are aligned in a direction close to N-S. During the modeling, as previously mentioned, the deepest anomalous bodies that have been considered were positioned at least a few kilometers over the Curie depth, to avoid possible demagnetization due to high temperatures close to this boundary (Fig. 4.4). The depths obtained from the Euler deconvolution (Fig. 4.3) were used as a guideline during the modeling.

In addition, seven multichannel seismic reflection profiles from the database of the Instituto de Ciencias del Mar (ICM-CSIC http://www.icm.csic.es/geo/gma/SurveyMaps, Figs. 4.1 and 4.5) were selected and analyzed in order to (i) check that the magnetic anomalous bodies were not intruded into the sedimentary infill, and (ii) determine the basement-sediments contact location. These profiles, which have been realized following standard procedures of acquisition and processing, were selected on the basis of their location and position orthogonal to the main dipoles (see Supplementary Files, Appendix A). The profiles L12GC-90-1 and L11GC-90-1 are joined (Fig. 4.6). Only the model of the Nador dipole (Figs. 4.2, NA, and 4.7) is not based on a seismic line, because of the lack of seismic profiles.

4.4 Results

4.4.1 Magnetic anomalies and igneous rocks

This study is focused on the magnetic dipoles of kilometric scale that appear in the Alboran Sea. In order to describe them, two main groups can be considered: dipoles related to the Late Miocene to Pliocene volcanic seafloor outcrops, and those without an apparent link with mapped igneous rocks. The first group of dipoles includes the dipoles CG (Cabo de Gata), DJ (Djibouti Bank), MA (Maimonides High), NA (Nador), RT (Ras Tarf), SA1 and SA2 (South Alboran 1 and 2, Fig. 4.2a). CG is NE-SW elongated and is found close to the Cabo de Gata coast (Fig. 4.2, CG). This dipole has a high of 130 nT and a low of -40 nT, only partially identified offshore. This anomaly is related to the Cabo de Gata volcanic rocks (Fig. 4.1b). To the southeast of this dipole, another smaller dipole is found aligned with the Maimonides High, also of volcanic nature (Figs. 4.1b and 4.2, MA). This dipole ranges from -20 nT to 60 nT. The north-western part of the Alboran Basin is dominated by two elongated positive N-S anomalies (100 and 60 nT) near -4° of longitude. They are geographically correlated with the Djibouti Bank (Fig. 4.2, DJ).

On the other hand, the dipoles located in the southern Alboran Sea (RT, SA1, SA2 and NA, Fig. 4.2) are related to prolongations of the volcanic rocks outcropping at the coastal area. The RT dipole (Fig. 4.2), with a high over 100 nT and a low of -10 nT, is located at the northern prolongation of the volcanic Ras Tarf cape (Booth-Rea *et al.*,

2007; Comas *et al.*, 1999). SA1 and SA2 (with 30 nT in the highs and -40 nT in the lows, Fig. 4.2) occur close to the Tres Forcas Cape Ridge, where the substrate is considered to be volcanic rocks (Fig. 4.1, Martínez-García *et al.*, 2011). To the east of Nador (Figs. 4.1b and 4.2, NA), an E-W 60 km elongated magnetic anomaly dipole is related onshore to the Gourougou volcano, and extends eastwards offshore up to the Chafarinas volcanic islands. This dipole has a high of 170 nT and a low of -100 nT, which puts it close to the highest amplitudes of the Alboran Sea (~270 nT, Figs. 4.2 and 4.7).

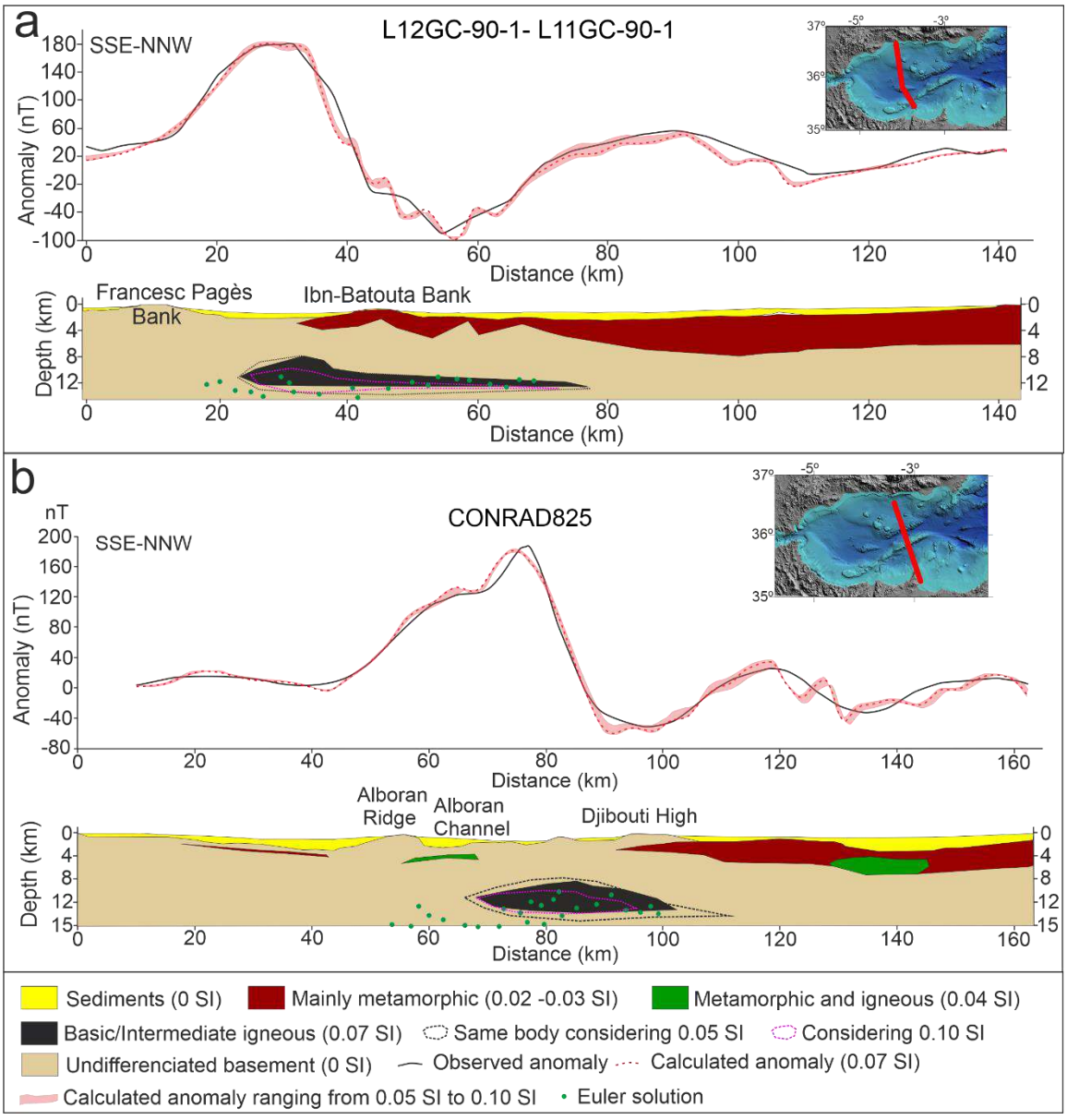

Figure 4.5. Magnetic anomaly profiles and forward models of the NE-SW dipole lineation (L12GC-90-1- L11GC-90-1 and CONRAD825). The inset in the upper right corner shows the position of the profile in the Alboran Sea.

With regards to the group of dipoles that are not related with mapped igneous rocks, they comprise the NE-SW and NW-SE dipole lineations with relatively large scale and amplitude, and the P1 and P2 dipoles, which are smaller in scale and amplitude (Fig. 4.2, P1, P2 and NE-SW and NW-SE dipoles lineations). The NE-SW and NW-SE dipole lineations are parallel to the main structures of the central and eastern Alboran Sea, such as the Alboran Ridge, the Adra Ridge and the Yusuf fault zone (Figs. 4.1b and 4.2). These lineations intersect approximately at 2º30' W in a dipole with values reaching -100 nT and 110 nT (Fig. 4.2). To the west, the NE-SW anomaly shows a continuous plot up to 4º30'W, in line with the western end of Ibn-Batouta bank. Its average intensity is 120 nT along its highs, reaching more than 200 nT at one location. The lows show values of -80 nT. This NE-SW lineation is located north of the Alboran Ridge and of the Xauen Bank (Figs. 4.1b and 4.2, Galdeano *et al.*, 1974; Galindo-Zaldivar *et al.*, 1998). To the east, the NW-SE dipole lineation presents similar values, although there are two significant differences: the geometry is more irregular and formed by different local dipoles, and the lows are generally wider than the highs, which reach up 170 nT (Fig. 4.2). Furthermore, the NW-SE anomaly changes its trend eastwards at 1ºW, becoming parallel to the shoreline (Fig. 4.2), but keeping high amplitudes of more than 200 nT (highs over 140 nT and lows below -100 nT).

The small-scale dipoles P1 and P2, in the Westernmost Alboran Sea, north and south of the Strait of Gibraltar, are not even next to, or parallel to offshore structures. These two small and intense dipoles are located at both sides of the strait close to the coast, with highs of 70 nT (Fig. 4.2, P1) and 90 nT (Fig. 4.2, P2) and lows that reach -70 nT.

The analytic signal map and depth determinations of the magnetic anomalies of the Alboran Sea show the range of depth of the causative bodies for the NE-SW and NW-SE dipole lineations (Fig. 4.3). This depth ranges between <7 km and >12 km along the NE-SW trending magnetic anomaly (Fig. 4.3). 82% of the solutions are deeper than 12 km, and only 9% of them are deeper than 18.6 km. This means that a remarkable fraction of depth from the top lies between 12 km and 18.6 km. For the NW-SE trending magnetic anomaly, our solutions are shallower on average (11.9 km), but they are more scattered, covering a wide range of depths between 5 km to 15 km.

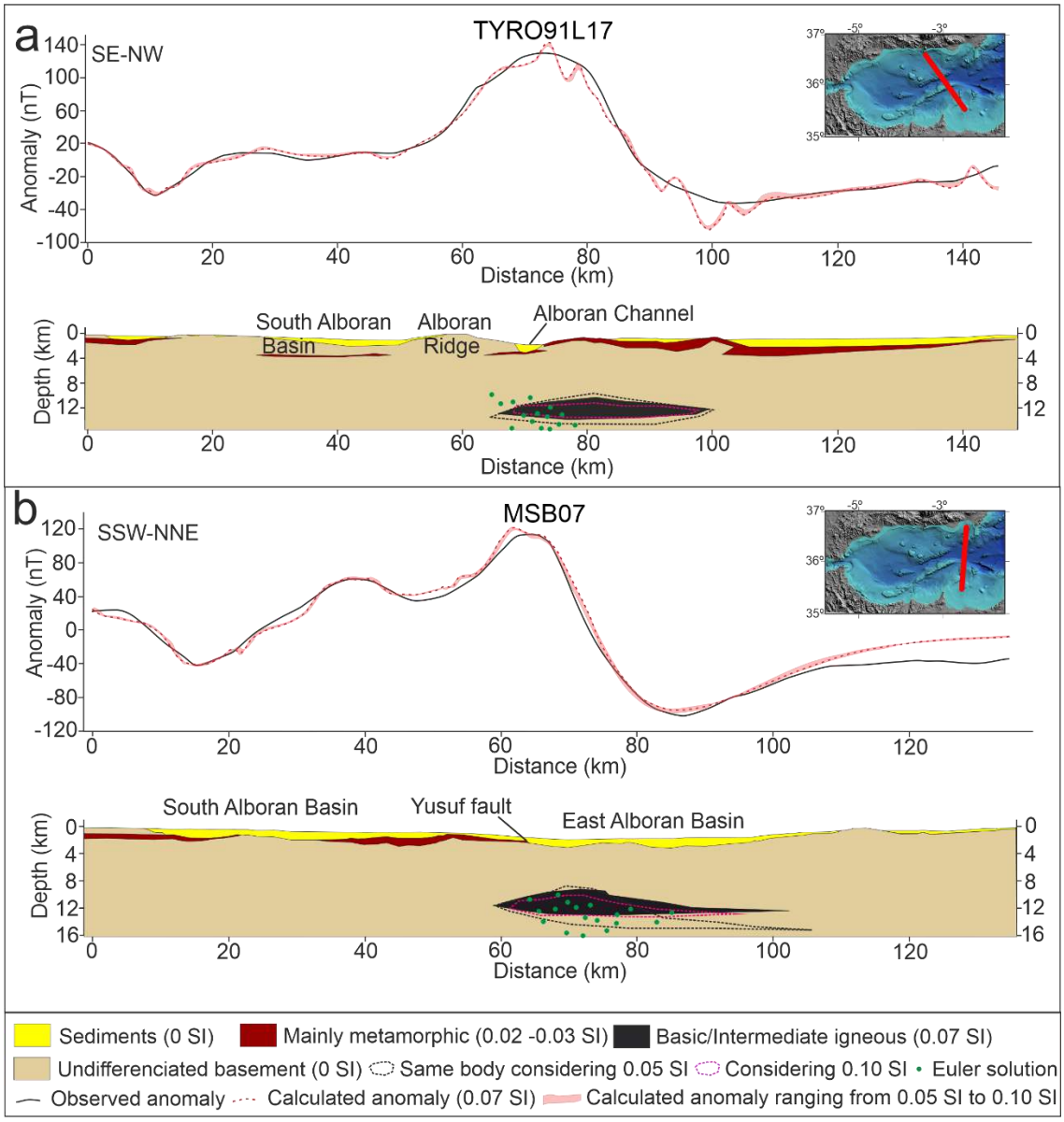

Figure 4.6. Magnetic anomaly profiles and forward models of the NE-SW dipole lineation (TYRO91L17) and of the area where the NE-SW and NW-SE lineations cross (MSB07). Insets in the upper right corner show the position of the profiles in the Alboran Sea.

4.4.2 Forward modeling of magnetic anomalies

The Nador dipole (NA, Fig. 4.2a) and the NE-SW and NW-SE dipole lineations represent the main magnetic anomalies of the Alboran Sea, with amplitudes of ~200 nT or more (270 nT in the case of the Nador dipole). In order to quantitatively constrain the geometry and location of their causative bodies, six 2D forward models have been computed (Figs. 4.5, 4.6 and 4.7); five of them were constrained by seismic reflection profiles to determine the basement-sediments contact depth (see Supplementary Files, Appendix A). The Nador model was performed without

determining the basement-sediments contact because no seismic profiles were available over the whole dipole (Fig. 4.7). The Nador model is located east of the Gourougou volcano and shows a 0.07 SI magnetic susceptibility body of roughly 35 km of width at 5-9 km of depth close to the coast (Fig. 4.7). This body should have an oval shape that wedges northwards. In the northern part of the profile there is a thin body of 0.03 SI magnetic susceptibility, with a 2 km thickness and located at 3.5 km of depth (Fig. 4.7).

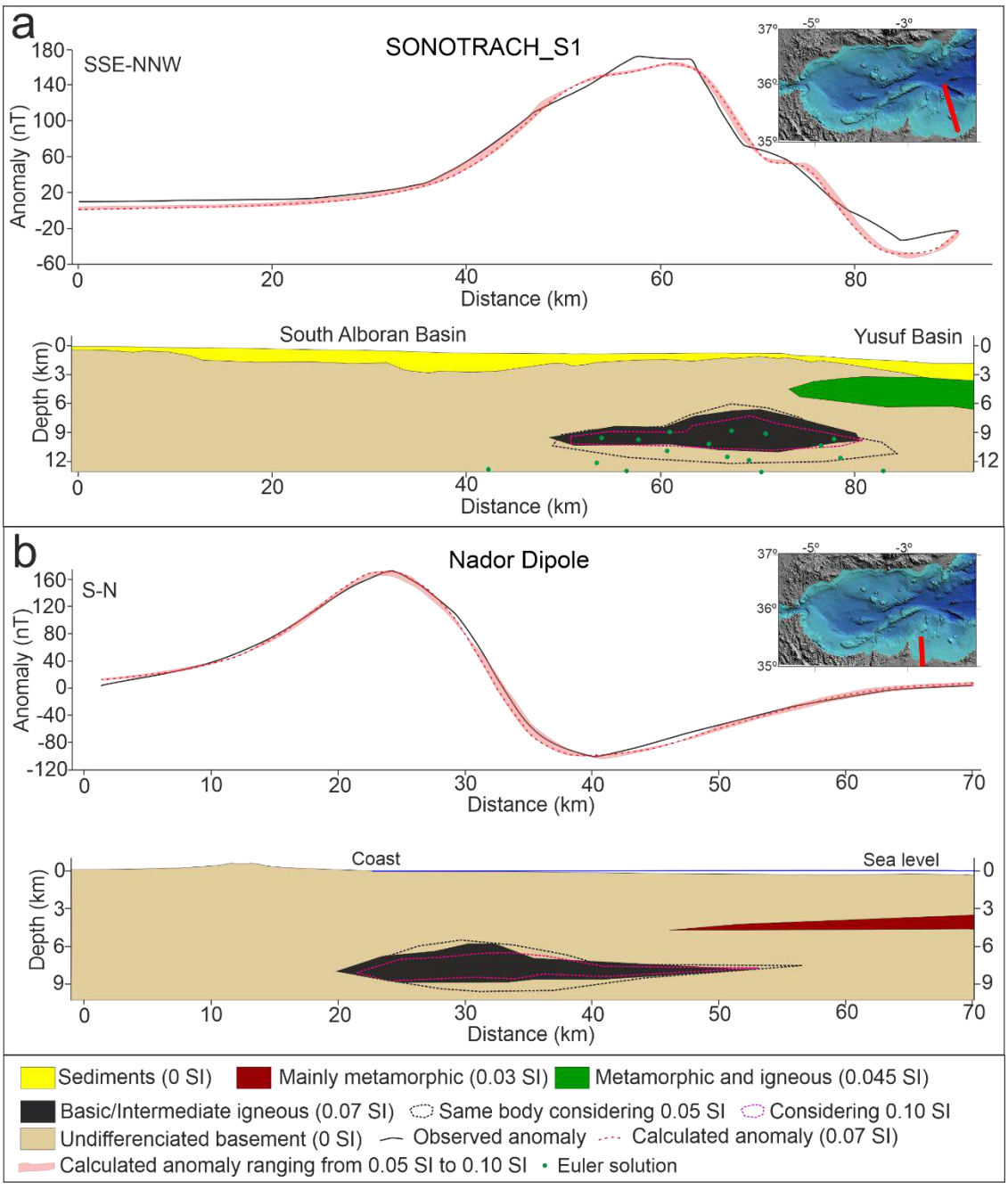

Figure 4.7. Magnetic anomaly profiles and forward models of the NW-SE dipole (SONOTRACH_S1) and of the Nador dipole (Nador). Insets in the upper right corner show the position of the profiles in the Alboran Sea.

Regarding the central and eastern Alboran sea areas, three models are focused on the NE-SW dipole lineation in the central Alboran Sea (Fig. 4.5: associated with the seismic profiles CONRAD825 and the L11-12GC model that joins profiles L11GC-90-1 and L12GC-90-1; Fig. 4.6: the profile TYRO91L17). The model of profile MSB07 is located in the corner of the NE-SW and NW-SE dipole lineations of the eastern Alboran Sea (Figs. 4.2a and 4.6), and lastly, the model of the profile SONOTRACH_S1 (Fig. 4.7) is focused on the NW-SE dipole lineation.

The NE-SW dipole lineation in the central Alboran Sea is related to a deep (8-14 km) body of 0.07 SI magnetic susceptibility (Figs. 4.3, 4.5, 4.6 and 4.8). In the southwestern end of this anomaly, the causative body extends to 8-13 km of depth, slightly south of the Ibn-Batouta Bank, with a thickness of 5 km in the southern part, thinning northwards and reaching almost 60 km of width (L11-12GC model, Fig. 4.5). From the Ibn-Batouta Bank northwards, a shallow crustal body of 0.03 SI magnetic susceptibility is needed to fit the anomaly. This body should be positioned below the sedimentary cover, and have a thickness that increases northwards up to 5 km. In the CONRAD825 model (Fig. 4.5) the deep body is 40 km wide, between the Djibouti High and the Alboran Channel, has a thickness of 6 km and is located at 6-14 km of depth. The shallow crustal body is shorter and thinner than in the L11-12GC model and includes a body of 0.04 SI magnetic susceptibility in the northern part (Fig. 4.5). Two more thin and shallow crustal bodies are needed: one of 0.04 SI magnetic susceptibility under the Alboran Channel, and one of 0.03 SI magnetic susceptibility to the south of the Alboran Ridge. The TYRO91L17 model shows again the main deep body located to the north of the Alboran Ridge, at 9-13 km of depth (Fig. 4.6). This body has a thickness of 4 km and is 40 km wide. The shallow crustal body of the northern half of the profile is thinner (maximum thickness of 2 km) and shifted close to the Alboran Channel. Two thin bodies of 0.03 SI magnetic susceptibility are located in the South Alboran Basin.

The MSB07 model (Fig. 4.6) represents the corner between the NE-SW and NW-SE dipole lineations. In this model, the deep body of 0.07 SI magnetic susceptibility shows a length of 40 km and a thickness of 5 km, in the southern part, while its thickness

decreases toward the north. This body is located at 8-13 km of depth under the boundary of the East Alboran Basin. There are two thin 0.03 SI magnetic susceptibility bodies that are located beneath the sediments of the South Alboran Basin.

In the easternmost Alboran Sea, the SONOTRACH_S1 model (Fig. 4.7) reveals the origin of the NW-SE discontinuous anomaly. At that location, a deep body of 0.07 SI magnetic susceptibility is recognized, roughly 35 km wide, 4 km thick and with a depth of 7-11 km. Moreover, a 4 km thick body underlying the sediments of the Yusuf Basin and characterized by a 0.045 SI magnetic susceptibility is needed in order to fit the model (Fig. 4.7).

4.5 Discussion

4.5.1 New insights on the geometry and nature of the crustal igneous bodies

The magnetic forward models provide new insights on the geometry and nature of the crustal igneous bodies that are associated with magnetic dipoles. The intermediate to low magnetic susceptibility (0.02 to 0.04 SI) large size body is associated to secondary dipoles (less than 100 nT of amplitude). Even though the presence of this body is supported by the available data and the magnetic anomaly models, a detailed definition of its geometry would need higher magnetic resolution data that would account for the effect of local volcanic edifices. In any case, the models indicate that the body, which could be interpreted as a metamorphic layer with dispersed igneous rocks, should be extended over the northern part of the Alboran Sea, and locally in the southern part as well (Figs. 4.5, 4.6 and 4.8). According to the widespread presence of volcanic rocks (Fig. 4.1b) in this region of relatively thin continental crust (Galindo-Zaldívar *et al.*, 1998), this metamorphic layer may be considered one of the sources of the eruptive rocks of the region, favored by crustal thinning (Hatzfeld *et al.*, 1976; Suriñach and Vegas, 1993) and high heat flow (Andrés *et al.*, 2018; Davis, 2013; Polyak, *et al.*, 1996). Conversely, on the southern Alboran Sea, the models reveal a more scattered presence of igneous bodies into the crust (Figs. 4.5, 4.6 and 4.7). Some of these bodies could be related to volcanic rocks, such as the low magnetic susceptibility bodies of the southern part of model TYRO91L17, and the SA2 dipole (Figs. 4.2 and 4.6). Other geometries for these low to medium susceptibility bodies are possible and require data with higher resolution. In any case,

the contrast between the northern and southern Alboran Sea (Fig. 4.8), especially in the Malaga Basin, may also be interpreted as a sign of crustal differences (Alboran versus African domains), as some previous works pointed out (*e.g.*, Booth-Rea *et al.*, 2007; d'Acremont *et al.*, 2020; Gómez de la Peña, 2020b). A special mention should be made of the Nador dipole (Figs. 4.1, 4.2 and 4.7) that highlights the deep connection between the Gourougou and Chafarinas volcanic edifices (Fig. 4.1) by a kilometric scale elongated E-W basic intrusion parallel to the African coast (Fig. 4.7). This deep basic intrusion cannot be related to surface structures, such as faults or folds, which are not E-W oriented (Fig. 4.1).

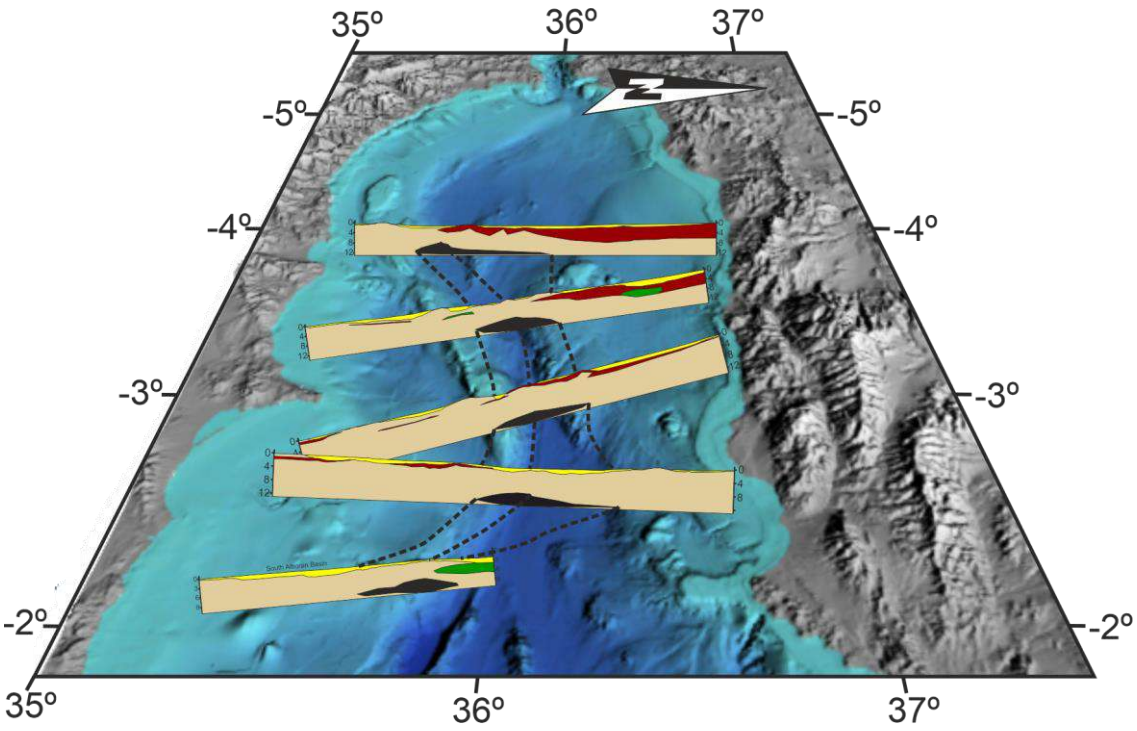

Figure 4.8. Integration of cross sections of the causative body of the NE-SW and NW-SE magnetic anomaly lineations on the bathymetric map of the Alboran Sea. The color legend used are the same as those of the previous figures.

Regarding the group of magnetic dipoles without apparent links with the mapped igneous rocks, their attribution also needs to take into account the geological structures and evolution of the region. The magnetic dipoles P1 and P2 in the western Alboran Sea could be associated with peridotite bodies such as those identified onshore, given their symmetry with respect to the Gibraltar Arc (Fig. 4.2). These bodies could be similar to the outcropping ultrabasic massifs that are located in the western Internal Zones of the Betic and Rif cordilleras (Fig. 4.1, Garrido, 1995). The massifs (Ronda, Beni Bousera) have been correlated with magnetic anomalies in

previous works (Amar *et al.*, 2015; González-Castillo *et al.*, 2015b). For example, in Amar *et al.* (2015) the anomaly related to the Beni Bousera peridotites is extended to the P2 dipole (note that the map displayed in Amar *et al.*, 2015 shows the magnetic anomalies reduced to the pole, a type of processing that maximizes the highs and minimize the lows for positive magnetic susceptibilities).

The main NE-SW dipole lineation located in the central Alboran Sea has a trend parallel to the Alboran Ridge, which is mainly formed by volcanic rocks (Booth-Rea *et al.*, 2007; Comas *et al.*, 1999; Maestro *et al.*, 2007; Polyak *et al.*, 1996; Watts *et al.*, 1993). The NE-SW aligned dipoles (Figs. 4.2 and 4.8), the analytic signal map (Fig. 4.3), and the forward models (Fig.s 4.5 and 4.6) all evidence the presence of a single elongated body made of basic or intermediate igneous rocks. One possible interpretation of this model would involve considering the connection between the causative body of the dipole lineation and the volcanic highs, such as the Alboran Ridge. In this scenario, the body could be formed by a set of aligned magmatic chambers related to the volcanic rocks that are exposed on the surface, which are basic to intermediate composition and can have high magnetic susceptibility values (*e.g.*, Duggen *et al.*, 2008; Fernández-Soler *et al.*, 2000). However, working against this interpretation is the fact that the center of the dipoles is not aligned with the volcanic highs, and that is the point where the bodies should be located. In some sectors, the centers of the dipoles are located north of the Alboran Ridge and of the Alboran Channel, instead (Figs. 4.5, 4.6 and 4.8). Moreover, a dipole has also been identified in the flat areas located at the western tip of the Eastern Alboran Basin (Figs. 4.2 and 4.6, model MSB07), suggesting a break in the correlation between causative body and volcanic high. Altogether, the results suggest no connection between the deep igneous body and the Alboran Ridge, or other outcropping igneous edifices, contrary to what proposed by Galdeano *et al.* (1974). In this setting, the Alboran Ridge could contain heterogeneous volcanic bodies smaller than 1 km, or thin volcanic layers interbedded with non-magnetic rocks, which would not cause relevant magnetic dipoles at a kilometric scale.

An alternative interpretation would be to consider a magnetic mineralization as the causative body of the dipole lineations, similarly to what is observed in the Internal Zones of the Gibraltar Arc, where some iron mineralizations occur (*e.g.*, Torres-Ruiz,

2006). However, the size of these deposits would be much smaller than the calculated size of the causative body associated with the dipole lineations observed in the Alboran Sea, even if a high susceptibility value is used to decrease the size of the modeled body.

The main NW-SE dipole lineation of the eastern Alboran Sea have roughly similar features to those of the NE-SW dipole lineation of the central Alboran Sea and those that continue along the Algerian coast (Fig. 4.2). Euler deconvolution depths are shallower and more scattered in the case of the NW-SE dipole lineation (Fig. 4.3). These anomalies are roughly located along the Yusuf fault system, including the Yusuf basin (Fig. 4.1b), and increase their irregularity eastwards, up to the smaller dipoles close to the Algerian coast (Fig. 4.2). This geometry points to a discontinuous aspect of the causative bodies, in contrast to the NE-SW continuous elongated body identified in the central Alboran Sea.

AS maxima are related to magnetization contrasts suggesting that deep basic igneous bodies are located along the northern African continental crust boundary (Figs. 4.1, 4.2 and 4.9), at the contact with the East Alboran Basin thinned crust and the Algerian oceanic crust (Booth-Rea *et al.*, 2007; Do Couto *et al.*, 2016; Gómez de la Peña *et al.*, 2020a).

4.5.2 Geodynamics implications

The analysis of magnetic anomalies contributes to constrain the initial stages of the opening and evolution of the Alboran Sea (Fig. 4.9). The emplacement of the NE-SW and NW-SE dipole lineations must have occurred during the initial NNW-SSE extensional stages, based on their trend and disconnection from surface structures (Jolivet *et al.*, 2021 and references therein). In fact, the NE-SW dipole lineation (Fig. 4.2) has a direction similar to the rift axis proposed in paleogeographic reconstructions of the AlKaPeCa Domain (Do Couto *et al.*, 2016; Faccena *et al.*, 2014; Mauffret *et al.*, 2007; Schentino and Turco, 2011; Spakman *et al.*, 2018). These bodies may have been the relict of the westwards rifting axis of the AlKAPeCa Domain that remained into the crust of the Alboran Domain (Fig. 4.9a, Bouillin *et al.*, 1986; Mauffret *et al.*, 2007; Romagny *et al.*, 2020; Rosenbaum *et al.*, 2002). Therefore, the

age of emplacement of these deep basic bodies should be Oligocene to Lower Miocene. This extension was probably the result of the southward retreat of the slab attached

to the African margin (Chertova *et al.*, 2014; Do Couto *et al.*, 2016; Faccena *et al.*, 2014; Gueguen *et al.*, 1997; Mauffret *et al.*, 2007; Romagny *et al.*, 2020; Rosenbaum *et al.*, 2002; Schentino and Turco, 2011; Spakman *et al.*, 2018). The magnetic anomalies that continue along the Algerian continental slope (Fig. 4.2) may also be a remnant of that rift, in agreement with the rift location proposed by Yelles *et al.* (2009).

After the Early Miocene, the extension changed direction to E-W, in response to the westward displacement of the Alboran Domain with orthogonal compression (Comas *et al.*, 1992; Do Couto *et al.*, 2016; Faccena *et al.*, 2014, Mauffret *et al.*, 2007; Rosenbaum *et al.*, 2002; Royden *et al.*, 1993). Magnetic, gravity and seismic reflection studies in the East Algerian basin show these two extensional stages (a NW-SE directed extension, followed by an E-W directed one) marked by an oceanic crust generation (Driussi *et al.*, 2015).

In this scenario (Fig. 4.9b), the igneous bodies formed during the first extensional stage, along the rift and transfer fault axis, could have moved westward within the southern part of the Alboran Domain. During this period, the southern boundary of the Alboran Domain acted as a STEP fault that accommodated the westward displacement (Fig. 4.9b, d'Acremont *et al.*, 2020). This period was marked by the generation of calk-alkaline magmatism (Middle Miocene to Late Pliocene) related to subduction processes and crustal contamination (Duggen *et al.*, 2004, 2008; Fernández-Soler *et al.*, 2000; Turner *et al.*, 1999).

During post-Tortonian times, the westward retreat of the Gibraltar slab decreased its influence in this region, so the STEP fault activity also declined and the NW-SE compression increased its influence (d'Acremont *et al.*, 2020; Gómez de la Peña *et al.*, 2020b). The STEP fault was displaced northwards and deformed, which generated some of the modern faults of the Alboran Sea, such as the Yusuf fault (Fig. 4.9c, d'Acremont *et al.*, 2020). The eastward change of orientation of the dipoles lineation to NW-SE and their heterogeneity may be due to the initial emplacement along a transform fault of the AlKaPeCa Domain rifting axis (Fig. 4.9a) and to a later fragmentation and disruption of the main body by the Yusuf fault (Figs. 4.9c, 4.9d). In

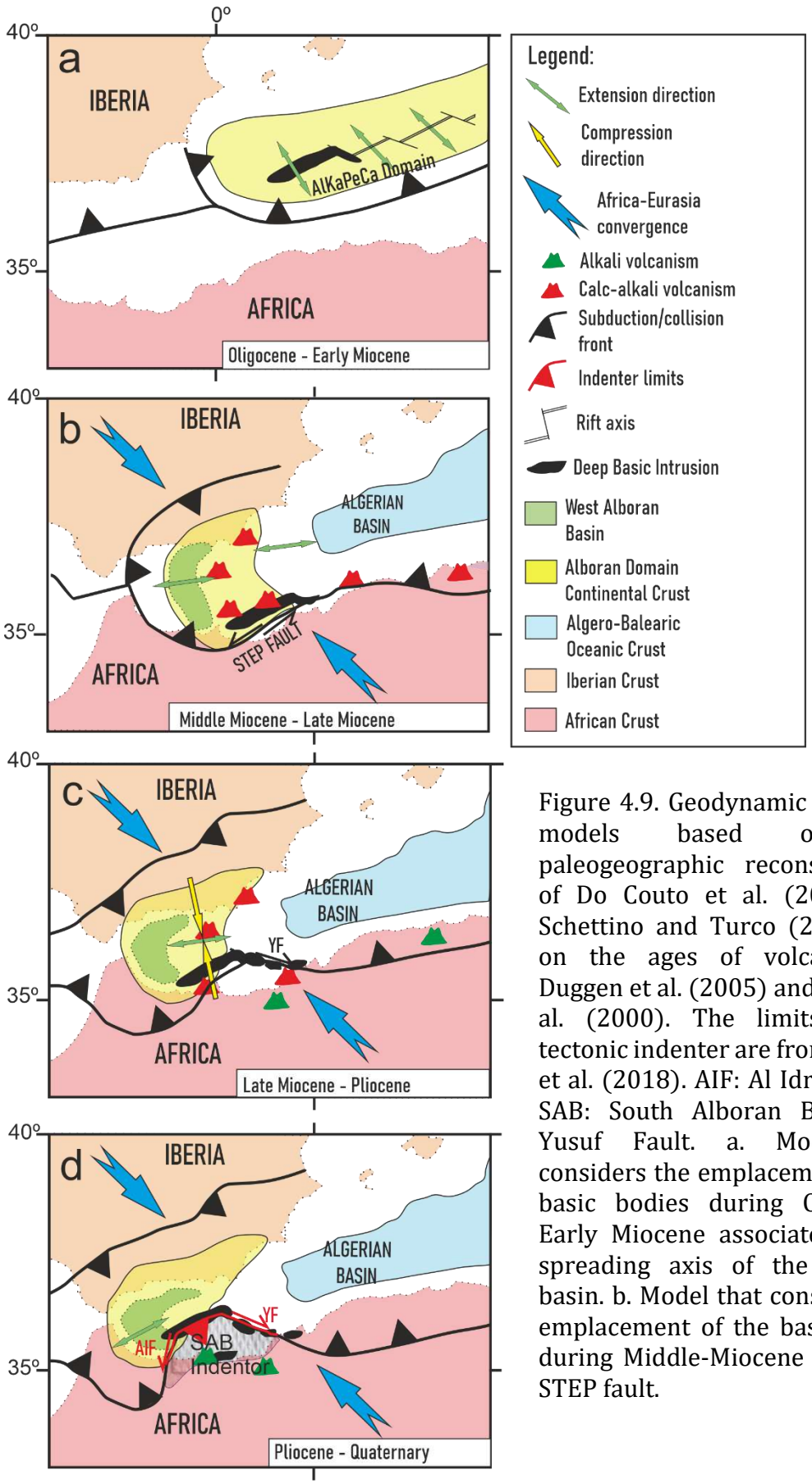

Figure 4.9. Geodynamic evolution models based on the paleogeographic reconstructions of Do Couto et al. (2016) and Schettino and Turco (2011) and on the ages of volcanism of Duggen et al. (2005) and Maury et al. (2000). The limits of the tectonic indenter are from Estrada et al. (2018). AIF: Al Idrissi Fault, SAB: South Alboran Block, YF: Yusuf Fault. a. Model that considers the emplacement of the basic bodies during Oligocene-Early Miocene associated to the spreading axis of the Algerian basin. b. Model that considers the emplacement of the basic bodies during Middle-Miocene along the STEP fault.

addition, transtensional areas like the pull-apart Yusuf basin (Fig. 4.1b) may have favored the emplacement of new magmas (*e.g.*, Cocchi *et al.*, 2017; Gómez de la Peña *et al.*, 2020b; Jolivet *et al.*, 2021) that generated small dipoles into the main ones (Fig. 4.2, Fig. 4.7 SONOTRACH_S1 model). The emplacement of these igneous bodies could have determined the late evolution of the basins (Martínez-García *et al.*, 2011). Later, this fault may have evolved into a boundary between the African continental crust and the Algerian oceanic crusts (Fig. 4.9d).

In recent times (Plio-Quaternary), the NE-SW elongated body acted as a rigid backstop block where the South Alboran Block collides (Fig. 4.9d). This contributed to the elevation of the Alboran Ridge (Estrada *et al.*, 2018) and the development of conjugate strike-slip fault sets in the northern Alboran Sea. The indenter of the South Alboran Block is bounded by the Al Idrissi fault zone to the west (Estrada *et al.*, 2018), which must be a very recent development (Pleistocene in age, Lafosse *et al.*, 2020), since the western tip of the NW-SE anomaly lineation shows little displacement between the main dipoles (Fig. 4.2). To the east, the boundary of the indenter is the Yusuf fault, which forms a contact between the continental crust of the indenter and the magmatic crust of the East Alboran Basin (Figs. 4.1 and 4.9). Thus, the current northern position of the anomalies is conditioned by the NNW push of the indenter. The deep igneous intrusions condition the limit of the indenter and the deformation of the northern Alboran Sea.

Recent magmatism: the Nador dipole

The E-W orientation of the Nador dipole (Fig. 4.2) is not in line with the other major structures of the area and, consequently, it should be explained by the lithospheric evolution. We tentatively suggest that it may be connected to the emplacement of recent magmas related to the westward progression of the slab tear along the African margin (Fig. 4.9, Duggen *et al.*, 2005; Hidas *et al.*, 2019). While the Alboran Sea structures reached their current positions during the westward displacement of the Alboran domain, the subducted slab that generated the back-arc opening of the Algerian Basin was being decoupled from the African margin (Carminati *et al.*, 1998; Chertova *et al.*, 2014; Hidas et a., 2019; Jolivet *et al.*, 2021). This process has also been proposed to explain the progression of the alkaline volcanism of the eastern Morocco and northern Algeria, as in the case of the Gourougou volcano (Duggen *et al.*, 2005;

Maury *et al.*, 2000). Therefore, our hypothesis considers that the E-W elongate causative body of the Nador dipole is an intrusion generated by the last alkaline magmatism episode that affected eastern Morocco (Fig. 4.9d).

Implications for other marine basins

The analysis of the magnetic anomalies helps to explain the complex history of magmatism and deformations in the Alboran Sea. The results highlight the utility of potential field methods to improve the knowledge of deep igneous intrusions in marine basins. They also show the interaction between rifting intrusions with a STEP fault and the later tectonic indentation. Furthermore, they evidence that these rigid bodies condition the subsequent geodynamic evolution of marine basins. Literature shows examples of deep igneous intrusions in basins of other seas and oceans developed on thinned continental and transitional crust, such as the South China Sea (Li *et al.*, 2008; Sun *et al.*, 2014), the southern Norwegian Sea (Planke *et al.*, 2005), or the Bight basin, in southern Australia (Reynolds *et al.*, 2017). Nevertheless, these igneous intrusions have frequently been considered as local features into the overall geodynamic of the basin. Our findings demonstrate that the interaction between magmatism and tectonic structures must be seriously considered, in order to fully understand the different geodynamic scenarios. This approach establishes a new framework for future studies that aim to decode the onset and tectonic evolution of marine basins.

4.6 Conclusions

The magnetic anomalies of the Alboran Sea reveal the location and structure of the main basic and intermediate igneous rock bodies that contribute to decipher the origin and evolution of the Alboran Sea basin.

The most relevant NE-SW and NW-SE dipole lineations that cross the Alboran Sea toward the Algerian basin are related to elongate basic or intermediate igneous intrusions with 4-6 km of thickness, and that are located at ~12 km of depth. These deep basic intrusions can represent the westward tip of the Oligocene-Miocene rifting of the AlKaPeCa Domain, related to the Algerian basin (Fig. 4.9a). These bodies were westward displaced, together with the Alboran Domain, and accommodated by a STEP fault in its southern boundary (Fig. 4.9b). The development, since the Late

Miocene, of a tectonic indentation deformed the STEP fault which led to the development of the Yusuf fault. Then, transtensional processes occurring at the time when the STEP and Yusuf faults were active segmented the eastern part of the magmatic body (Fig. 4.9c). This development would have favored the emplacement of new magmas and contributed to the formation of the discontinuous NW-SE anomalies. During the post-Miocene compression (Fig. 4.9d), the former deep, rigid, basic rock bodies facilitated the development of the Alboran Ridge and the conspicuous strike-slip fault system associated to the tectonic indentation. Moreover, they reveal the scarce recent displacement of the left-lateral Al Idrissi fault and the reactivation of former crustal heterogeneities, such as the Yusuf fault.

The other major dipoles are associated with most of the volcanic edifices since the Middle-Late Miocene (*e.g.*, Cabo de Gata, Djibouti Bank, Figs. 4.1 and 4.2). The most remarkable is the Nador dipole that connects the Gourougou and Chafarinas volcanoes offshore. Magnetic forward modeling of this dipole shows a 4 km thick, 60 km long E-W elongated body close to the coast line, at 5-9 km of depth. The E-W elongated crustal Nador dipole intrusion may be the consequence of the tearing of a subducting slab attached to the African margin.

Altogether, this makes the Alboran Sea an interesting example of tectonic inversion in oblique continental convergence and development of STEP faults, where the analysis of the magnetic anomalies helps to explain the complex history of magmatism and deformations. These results highlight the usefulness of potential field methods to improve the knowledge of deep igneous intrusions in other marine basins with thinned continental crusts.

Data Availability

Magnetic dataset used in this article were obtained from the second version of the World Digital Magnetic Anomaly Map Project (http://wdmam.org/). Seismic profiles used in this article can be found at http://www.icm.csic.es/geo/gma/SurveyMaps, a dataset hosted at the Instituto de Ciencias del Mar, ICM-CSIC.

Acknowledgements

The comments of two anonymous reviewers have improved the quality of this manuscript. This study was supported by projects CGL2016-80687-R AEI/FEDER,

P18-RT-3275, B-RNM-301-UGR18 and RNM148 (Junta de Andalucía/FEDER). Y.M.M was supported by NASA under award number 80GSFC17M0002. V.T.S. was supported by the FPU PhD grant (16/04038). ICM-CSIC author acknowledges the Severo Ochoa funding from the Spanish government through the "Severo Ochoa Centre of Excellence" accreditation (CEX2019-000928-S).

References

Amar, N., Khattach, D., Azdimousa, A., Chourak, M., Jabaloy, A., Manar, A., & Amar, M. (2015). Structure and peridotite of Gibraltar arc southern bloc: gravimetric and aeromagnetic evidences. *Arabian Journal of Geosciences*, *8*(11), 9801-9813.

Andrés, J., Marzán, I., Ayarza, P., Martí, D., Palomeras, I., Torné, M., ... & Carbonell, R. (2018). Curie point depth of the Iberian Peninsula and surrounding margins. A thermal and tectonic perspective of its evolution. *Journal of Geophysical Research: Solid Earth*, *123*(3), 2049-2068.

Anahnah, F., Galindo-Zaldívar, J., Azzouz, O., Ruano, P., Chalouan, A., Pedrera, A., ... & Bouregba, N. (2009). The Nador dipole: one of the main magnetic anomalies of the NE Rif. *Trabajos de Geología*, (29).

Balanya, J. C., Crespo-Blanc, A., Díaz-Azpiroz, M., Expósito, I., Torcal, F., Pérez-Peña, V., & Booth-Rea, G. (2012). Arc-parallel vs back-arc extension in the Western Gibraltar arc: Is the Gibraltar forearc still active? *Geologica Acta, 10*(3), 249-263.

Baratin, L. M., Mazzotti, S., Chéry, J., Vernant, P., Tahayt, A., & Mourabit, T. (2016). Incipient mantle delamination, active tectonics and crustal thickening in Northern Morocco: Insights from gravity data and numerical modelling. *Earth and Planetary Science Letters, 454,* 113-120.

Blanco, M. J., & Spakman, W. (1993). The P-wave velocity structure of the mantle below the Iberian Peninsula: Evidence for subducted lithosphere below southern spain. *Tectonophysics, 221*(1), 13-34. https://doi.org//10.1016/0040-1951(93)90025-F

Bohoyo, F., Galindo-Zaldívar, J., Maldonado, A., Schreider, A. A., & Suriñach, E. (2002). Basin development subsequent to ridge-trench collision: the Jane Basin, Antarctica. *Marine Geophysical Researches*, *23*(5), 413-421.

Booth-Rea, G., Ranero, C. R., Martínez-Martínez, J. M., & Grevemeyer, I. (2007). Crustal types and Tertiary tectonic evolution of the Alborán Sea, western Mediterranean. *Geochemistry, Geophysics, Geosystems, 8*(10).

Bouillin, J. P., Durand-Delga, M., & Olivier, P. (1986). Betic-Rifian and Tyrrhenian arcs: distinctive features, genesis and development stages. In *Developments in Geotectonics* (Vol. 21, pp. 281-304). Elsevier.

Carminati, E., Wortel, M. J. R., Meijer, P. T., & Sabadini, R. (1998). The two-stage opening of the western–central Mediterranean basins: a forward modeling test to a new evolutionary model. *Earth and Planetary Science Letters*, *160*(3-4), 667-679.

Catalán, M., Galindo-Zaldivar, J., Davila, J. M., Martos, Y. M., Maldonado, A., Gambôa, L., & Schreider, A. A. (2013). Initial stages of oceanic spreading in the Bransfield Rift from magnetic and gravity data analysis. *Tectonophysics*, *585*, 102-112.

Catalán, M., Dyment, J., Choi, Y., Hamoudi, M., Lesur, V., Thebault, E., de Santis, A., Ishihara, T., Korhonen, J., Litvinova, T. , Luis, J., Meyer, B., Milligan,P., Nakanishi, M., Okuma, S., Pilkington, M., Purucker, M., Ravat, D., Gaina, C., Maus, S., Quesnel, Y., Saltus,R., & Taylor, P. (2016). Making a better magnetic map. *Eos, 97*. doi:10.1029/2016EO054645.

Chertova, M. V., Spakman, W., Van den Berg, A. P., & Van Hinsbergen, D. J. J. (2014). Absolute plate motions and regional subduction evolution. *Geochemistry, Geophysics, Geosystems, 15*(10), 3780-3792.

Cocchi, L., Passaro, S., Tontini, F. C., & Ventura, G. (2017). Volcanism in slab tear faults is larger than in island-arcs and back-arcs. *Nature communications*, *8*(1), 1-12.

Comas, M.C., García-Dueñas, V., and Jurado, M.J., (1992).Neogene tectonic evolution of the Alboran Sea from MCS data. *Geo-Marine Lett., 12*, 157-164.

Comas, M. C., Platt, J. P., Soto, J. I., & Watts, A. B. (1999). 44. The origin and tectonic history of the Alboran Basin: insights from Leg 161 results. In *Proceedings of the Ocean Drilling Program Scientific Results* (Vol. 161, pp. 555-580).

Corsini, M., Chalouan, A., & Galindo-Zaldivar, J. (2014). Geodynamics of the Gibraltar Arc and the Alboran Sea region. *Journal of Geodynamics, 77,* 1-3. https://doi.org/10.1016/j.jog.2014.04.005

Coulon, C., Megartsi, M. H., Fourcade, S., Maury, R. C., Bellon, H., Louni-Hacini, A., ... & Hermitte, D. (2002). Post-collisional transition from calc-alkaline to alkaline volcanism during the Neogene in Oranie (Algeria): magmatic expression of a slab breakoff. *Lithos, 62*(3-4), 87-110.

d'Acremont, E., Lafosse, M., Rabaute, A., Teurquety, G., Do Couto, D., Ercilla, G., Juan, C., Lépinay, M. B., Lafuerza, S., Galindo-Zaldivar, J., Estrada F., Vazquez, J. T., Leroy, S., Poort, J., Ammar, A., & Gorini, C. (2020). Polyphase tectonic evolution of fore-arc basin related to STEP fault as revealed by seismic reflection data from the Alboran Sea (W-Mediterranean). *Tectonics*, *39*(3), e2019TC005885. https://doi.org/10.1029/2019TC005885

Davies, J. H. (2013). Global map of solid Earth surface heat flow. *Geochemistry, Geophysics, Geosystems*, *14*(10), 4608-4622.

DeMets, C., Gordon, R. G., & Argus, D. F. (2010). Geologically current plate motions. *Geophysical Journal International, 181*(1), 1-80. https://doi.org//10.1111/j.1365-246X.2009.04491.x

Do Couto, D., Gorini, C., Jolivet, L., Lebret, N., Augier, R., Gumiaux, C., d'Acremont, E., Ammar, A., Jabour, H., & Auxietre, J. L. (2016). Tectonic and stratigraphic evolution of the Western Alboran Sea Basin in the last 25 Myrs. *Tectonophysics, 677-678*, 280-311.

Doglioni, C. (1991). A proposal of kinematic modeling for W-dipping subduction possible application to the TyrrhenianeApennine system. *Terra Nova, 3,* 423-434. http://dx.doi.org/10.1111/j.1365-3121.1991. tb00172.x.

Driussi, O., Briais, A., & Maillard, A. (2015). Evidence for transform motion along the South Balearic margin and implications for the kinematics of opening of the Algerian basin. *Bulletin de la Société Géologique de France*, *186*(4-5), 353-370.

Duggen, S., Hoernle, K., Bogaard, P., & Harris, C. (2004). Magmatic evolution of the Alboran Region: the role of subduction in forming the western Mediterranean and causing the Messinian Salinity Crisis. *Earth Planet Sci Lett, 218,* 91–108.

Duggen, S., Hoernle, K., van den Bogaard, P., & Garbe-Schönberg, D. (2005). Post-collisional transition from subduction-to intraplate-type magmatism in the westernmost Mediterranean: evidence for continental-edge delamination of subcontinental lithosphere. *Journal of Petrology*, *46*(6), 1155-1201.

Duggen, S., Hoernle, K., Klügel, A., Geldmacher, J., Thirlwall, M., Hauff, F., ... & Oates, N. (2008). Geochemical zonation of the Miocene Alborán Basin volcanism (westernmost Mediterranean): geodynamic implications. *Contributions to Mineralogy and Petrology, 156*(5), 577.

El Bakkali, S., Gourgaud, A., Bourdier, J. L., Bellon, H., & Gundogdu, N. (1998). Post-collision neogene volcanism of the Eastern Rif (Morocco): magmatic evolution through time. *Lithos*, *45*(1-4), 523-543.

Estrada, F., Galindo-Zaldivar, J., Vázquez, J. T., Ercilla, G., D'Acremont, E., Alonso, B., & Gorini, C. (2018). Tectonic indentation in the central Alboran Sea (westernmost Mediterranean). *Terra Nova, 30*(1), 24-33. https://doi.org//10.1111/ter.12304

Faccena, C., Becker, T. W., Auer, L., Billi, A., Boschi, L., Brun, J. P., Capitanio, F. A., Funiciello, F., Horvàth, F., Jolivet, L., Piromallo, C., Royden, L., Rossetti, F. & Serpelloni, E. (2014). Mantle dynamics in the Mediterranean. *Rev. Gephys., 52,* 283-332. doi:10.1002/2013RG000444

Fernández-Soler, J., Martínez-Ruíz, F., Akhmanov, G., Akhmetzhanov, A., Stadnitskaya, A., Kozlova, E., Sautkin, A., Mazurenko, L., Ovsyannikov, D., Sadekov, A., Belenkaya, I., Suslova, E. & Goncharov, D. (2000). Bottom sampling. In: Multidisciplinary Study of Geological Processes on the North East Atlantic and Western Mediterranean Margins, Preliminary results of geological and geophysical investigations during the TTR-9 of R/V Professor Logachev, June-July, 1999 (Ed. by N. H. Kenyon, M. K. Ivanov, A. M. Azhmetzhanov & G. G. Akhmanov), 56, 85–91, IOC Technical Series, UNESCO.

Galdeano, A., Courtillot; V., Le Borgne, E., Le Mouel, J. L., & Rossignol, J. C. (1974). An aeromagnetic survey of the southwest of the western Mediterranean: Description and tectonic implications. *Earth and Planetary Science Letters, 23,* 323-336.

Galindo-Zaldivar, J., González-Lodeiro, F., Jabaloy, A., Maldonado, A., & Schreider, A.A. (1998). Models of magnetic and Bouguer gravity anomalies for the deep structure of the central Alboran Sea basin. *Geo-Mar. Lett., 18*, 10-18.

Garrido, C. J. (1995). Estudio geoquimico de las capas maficas del macizo ultramafico de Ronda (Cordillera Betica, Espana). Doctoral dissertation, Universidad de Granada.

Garcia-Castellanos, D., & Villaseñor, A. (2011). Messinian salinity crisis regulated by competing tectonics and erosion at the Gibraltar arc. *Nature*, *480*(7377), 359-363.

García-Dueñas, V., Balanyá, J.C., & Martínez-Martínez, J.M., (1992). Miocene extensional detachments in the outcropping basement of the Northern Alboran Basin (Betics) and their tectonic implications. *Geo-Mar. Lett.* 12, 88–95.

Gill, R. C. O., Aparicio, A., El Azzouzi, M., Hernandez, J., Thirlwall, M. F., Bourgois, J., & Marriner, G. F. (2004). Depleted arc volcanism in the Alboran Sea and shoshonitic volcanism in Morocco: geochemical and isotopic constraints on Neogene tectonic processes. *Lithos, 78*(4), 363-388.

Gómez de la Peña, L., Grevemeyer, I., Kopp, H., Díaz, J., Gallart, J., Booth-Rea, G., ... & R. Ranero, C. (2020) a. The lithospheric structure of the Gibraltar Arc System from wide-angle seismic data. *Journal of Geophysical Research: Solid Earth*, *125*(9), e2020JB019854.

Gómez de la Peña, L., Ranero, C. R., Gràcia, E., & Booth-Rea, G. (2020)b. The evolution of the westernmost Mediterranean basins. *Earth-Science Reviews, 103445*.https://doi.org/10.1016/j.earscirev.2020.103445

González-Castillo, L., Galindo-Zaldivar, J., de Lacy, M. C., Borque, M. J., Martinez-Moreno, F. J., García-Armenteros, J. A., & Gil, A. J. (2015) a. Active rollback in the Gibraltar Arc: Evidences from CGPS data in the western Betic Cordillera. *Tectonophysics, 663*, 310-321.

González-Castillo, L., Galindo-Zaldívar, J., Junge, A., Martínez-Moreno, F. J., Löwer, A., de Galdeano, C. S., ... & Martínez-Martos, M. (2015) b. Evidence of a large deep conductive body within the basement of the Guadalquivir foreland Basin (Betic Cordillera, S-Spain) from tipper vector modelling: Tectonic implications. *Tectonophysics*, *663*, 354-363.

Govers, R., & Wortel, M. J. R. (2005). Lithosphere tearing at STEP faults: Response to edges of subduction zones. *Earth and Planetary Science Letters*, *236*(1-2), 505-523.

Gueguen, E., Doglioni, C., & Fernandez, M. (1997). Lithospheric boudinage in the Western Mediterranean back-arc basin. *Terra Nova, 9*(4), 184-187.

Gueguen, E., Doglioni, C., & Fernandez, M. (1998). On the post-25 Ma geodynamic evolution of the western Mediterranean. *Tectonophysics, 298*(1-3), 259-269. http://dx.doi.org/10.1016/S0040-1951(98)00189-9.

Gutscher, M. A., Dominguez, S., Westbrook, G. K., Le Roy, P., Rosas, F., Duarte, J. C., ... & Sallarès, V. (2012). The Gibraltar subduction: A decade of new geophysical data. *Tectonophysics, 574*, 72-91.

Hatzfeld, D. (1976). Étude sismologique et gravimétrique de la estructure profonde de la mer d'Alborán: Mise en évidence d'un manteau anormal. *C. R. Acad. Sci., Ser. IIA Earth Planet. Sci., 5,* 483-500.

Heuret, A., & Lallemand, S. (2005). Plate motions, slab dynamics and back-arc deformation. *Physics of the Earth and Planetary Interiors*, *149*(1-2), 31-51.

Hidas, K., Garrido, C. J., Booth-Rea, G., Marchesi, C., Bodinier, J. L., Dautria, J. M., ... & Azzouni-Sekkal, A. (2019). Lithosphere tearing along STEP faults and synkinematic formation of lherzolite and wehrlite in the shallow subcontinental mantle. *Solid Earth*, *10*(4), 1099-1121.

Hoernle, K., Bogaard, P., Duggen, S., Mocek, B., & Garbe-Schönberg, D. (1999). Evidence for Miocene subduction beneath the Alboran Sea: $^{40}Ar/^{39}Ar$ dating and geochemistry of volcanic rocks from Holes 977A and 978A. In: Zahn R, Comas MC, Klaus A (eds) Proceedings of the ocean drilling program 161, Scientific Results, vol 161, pp 357–373.

Jolivet, L., Menant, A., Roche, V., Le Pourhiet, L., Maillard, A., Augier, R., ... & Canva, A. (2021). Transfer zones in Mediterranean back-arc regions and tear faults. *BSGF-Earth Sciences Bulletin*, *192*(1), 11.

Juan, C., Ercilla, G., Hernández-Molina, J. F., Estrada, F., Alonso, B., Casas, D., García, M., Farrán, M., Llave, E., Palomino, D., Vázquez, J. T., Medialdea, T., Gorini, C., d'Acremont, E., El Moumni, B., & Ammar, A. (2016). Seismic evidence of current-controlled sedimentation in the Alboran Sea during the Pliocene and Quaternary: Palaeoceanographic implications. *Marine Geology, 378*, 292–311. https://doi.org/10.1016/j.margeo.2016.01.006

Keating, P., & Sailhac, P. (2004). Use of the analytical signal to identify magnetic anomalies due to kimberlite pipes. *Geophysics, 69,* 180-190.

Lafosse, M., d'Acremont, E., Rabaute, A., Estrada, F., Jollivet-Castelot, M., Vazquez, J. T., Galindo-Zaldivar, J., Ercilla, G., Alonso, B., Smit, J., Ammar, A., & Gorini, C. (2020). Plio-Quaternary tectonic evolution of the southern margin of the Alboran Basin (Western Mediterranean). *Solid Earth, 11*(2), 741-765. https://doi.org/10.5194/se-11-741-2020

Lawver, L. A., & Hawkins, J. W. (1978). Diffuse magnetic anomalies in marginal basins: Their possible tectonic and petrologic significance. *Tectonophysics*, *45*(4), 323-339.

Lesur, V., Hamoudi, M., Choi, Y., Dyment, J., & Thébault, E. (2016). Building the second version of the world digital magnetic anomaly map (WDMAM). *Earth, Planets and Space*, *68*(1), 1-13.

Li, C. F., Zhou, Z., Li, J., Chen, B., & Geng, J. (2008). Magnetic zoning and seismic structure of the South China Sea ocean basin. *Marine Geophysical Researches, 29*(4), 223-238.

Li, C. F., Lu, Y., & Wang, J. (2017). A global reference model of Curie-point depths based on EMAG2. *Scientific reports*, *7*, 45129.

Malinverno, A., & Ryan, W. B. (1986). Extension in the Tyrrhenian Sea and shortening in the Apennines as result of arc migration driven by sinking of the lithosphere. *Tectonics*, *5*(2), 227-245.

Mancilla, F. d. L., Stich, D., Berrocoso, M., Martín, R., Morales, J., Fernandez-Ros, A., Páez, R., & Pérez-Peña, A. (2013). Delamination in the Betic Range: Deep structure, seismicity, and GPS motion. *Geology, 41*(3), 307-310. https://doi.org//10.1130/G33733.1

Martínez-García, P., Soto, J. I., & Comas, M. (2011). Recent structures in the Alboran Ridge and Yusuf fault zones based on swath bathymetry and sub-bottom profiling: evidence of active tectonics. *Geo-Marine Letters*, *31*(1), 19-36.

Mauffret, A., Ammar, A., Gorini, C., & Jabour, H. (2007). The Alboran Sea (Western Mediterranean) revisited with a view from the Moroccan margin. *Terra Nova*, *19*(3), 195-203.

Maury, R. C., Fourcade, S., Coulon, C., Bellon, H., Coutelle, A., Ouabadi, A., ... & Réhault, J. P. (2000). Post-collisional Neogene magmatism of the Mediterranean Maghreb margin: a consequence of slab breakoff. *Comptes Rendus de l'Académie des Sciences-Series IIA-Earth and Planetary Science*, *331*(3), 159-173.

Nabighian, M. N. (1984). Toward a three-dimensional automatic interpretation of potential field data via generalized Hilbert transforms: fundamental relations. *Geophysics, 49*(6), 780-786.

Neres, M., Carafa, M. M. C., Fernandes, R. M. S., Matias, L., Duarte, J. C., Barba, S., & Terrinha, P. (2016). Lithospheric deformation in the Africa-Iberia plate boundary: Improved neotectonic modeling testing a basal-driven Alboran plate. *Journal of Geophysical Research: Solid Earth*, *121*(9), 6566-6596. https://doi.org/10.1002/2016JB013012

Pedley, R. C., Busby, J. P., & Dabek, Z. K., (1993). GRAVMAG user manual–interactive 2.5 D gravity and magnetic modelling. British Geological Survey, Technical Report WK/93/26/R. 73.

Planke, S., Rasmussen, T., Rey, S. S., & Myklebust, R. (2005, January). Seismic characteristics and distribution of volcanic intrusions and hydrothermal vent complexes in the Vøring and Møre basins. In *Geological Society, London, Petroleum Geology Conference series* (Vol. 6, No. 1, pp. 833-844). Geological Society of London.

Polyak, B.G., Fernàndez, M., Khutorskoy, M.D., Soto, J.I., Basov, I.A., Comas, m.C., Khain, V.Ye., Alonso, B., Agapova, G.V., Mazurova, I.S., Negredo, A., Tochitsky, V.O., de la Linde, J., Bogdanov, N.A., &

Banda, E. (1996). Heat flow in the Alboran Sea, westrn Mediterranean. *Tectonophysics, 263,* 191-218.

Quesnel, Y., Catalán, M., & Ishihara, T. (2009). A new global marine magnetic anomaly data set. *Journal of Geophysical Research: Solid Earth*, *114*(B4).

Ravat, D. (1996). Analysis of the Euler method and its applicability in environmental magnetic investigations. *Journal of Environmental and Engineering Geophysics,* 229-238.

Reid, A.B., Allsop, J.M., Granser, H., Millet, A.J., & Somerton, L.W. (1990). Magnetic interpretation in three dimensions using the Euler deconvolution. *Geophysics, 55*(1), 80-91.

Reynolds, P., Holford, S., Schofield, N., & Ross, A. (2017). The shallow depth emplacement of mafic intrusions on a magma-poor rifted margin: an example from the Bight Basin, southern Australia. *Marine and Petroleum Geology*, *88*, 605-616.

Roest, W. R., Verhoef, J., & Pilkington, M. (1992). Magnetic interpretation using the 3-D analytical signal. *Geophysics, 57,* 116-125.

Roest, W.R. & Pilkington, M. (1993). Identifying remanent magnetization effects in magnetic data. *Geophysics, 58,* 653-659.

Romagny, A., Jolivet, L., Menant, A., Bessière, E., Maillard, A., Canva, A., ... & Augier, R. (2020). Detailed tectonic reconstructions of the Western Mediterranean region for the last 35 Ma, insights on driving mechanismsReconstructions détaillées de la Méditerranée occidentale depuis 35 Ma, implications en terme de mécanismes moteur. *Bulletin de la Société Géologique de France*, *191*(1).

Rosenbaum, G., Lister, G. S., & Duboz, C. (2002). Reconstruction of the tectonic evolution of the western Mediterranean since the Oligocene. *Journal of the Virtual Explorer*, *8*, 107-130.

Royden, L. H. (1993). Evolution of retreating subduction boundaries formed during continental collision. *Tectonics*, *12*(3), 629-638.

Salem, A., Ravat, D., Gamey, T.J., & Ushjima, K., (2002). Analytical signal approach and its applicability in environmental magnetic investigations. *J. App. Geophys., 49,* 231-244.

Schettino, A., & Turco, E. (2011). Tectonic history of the western Tethys since the Late Triassic. *Bulletin*, *123*(1-2), 89-105.

Seber, D., Barazangi, M., Ibenbrahim, A., & Demnati, A. (1996). Geophysical evidence for lithospheric delamination beneath the Alboran Sea and Rif–Betic mountains. *Nature, 379*(6568), 785–790.

Spakman, W., & Wortel, R. (2004). A tomographic view on western Mediterranean geodynamics. In *The TRANSMED atlas. The Mediterranean region from crust to mantle* (pp. 31-52). Springer, Berlin, Heidelberg.

Spakman, W., Chertova, M. V., van den Berg, A., & van Hinsbergen, D. J. (2018). Puzzling features of western Mediterranean tectonics explained by slab dragging. *Nature Geoscience*, *11*(3), 211-216. https://doi.org/10.1038/s41561-018-0066-z

Sun, Q., Wu, S., Cartwright, J., Wang, S., Lu, Y., Chen, D., & Dong, D. (2014). Neogene igneous intrusions in the northern South China Sea: Evidence from high-resolution three dimensional seismic data. *Marine and Petroleum Geology*, *54*, 83-95.

Suriñach, E., & Vegas, R. (1993) Estructura general de la corteza en una transversal del Mar de Alborán a partir de datos de sísmica de refracción-reflexión de gran ángulo. Interpretación geodinámica. *Geogaceta, 14,* 126-128.

Taylor, B. (Ed.). (2013). *Backarc basins: Tectonics and magmatism*. Springer Science & Business Media.

Taylor, B., Zellmer, K., Martinez, F., & Goodliffe, A. (1996). Sea-floor spreading in the Lau back-arc basin. *Earth and Planetary Science Letters*, *144*(1), 35-40.

Telford, W. M., Geldart, L. P., Sheriff, R. E., & Sheriff, R. E. (1990). *Applied geophysics*. Cambridge university press.

Thomson, D. T. (1982.) EULDPH: A new technique for making computer-assisted depth estimates from magnetic data. *Geophysics; 55*, 80-91.

Torres-Ruiz, J. (2006). Geochemical constraints on the genesis of the Marquesado iron ore deposits, Betic Cordillera, Spain: REE, C, O, and Sr isotope data. *Economic Geology*, *101*(3), 667-677.

Turner, S. P., Platt, J. P., George, R. M. M., Kelley, S. P., Pearson, D. G., & Nowell, G. M. (1999). Magmatism associated with orogenic collapse of the Betic–Alboran domain, SE Spain. *Journal of Petrology, 40*(6), 1011-1036.

Valera, J. L., Negredo, A. M., & Villaseñor, A. (2008). Asymmetric delamination and convective removal numerical modeling: comparison with evolutionary models for the Alboran Sea region. In *Earth Sciences and Mathematics* (pp. 1683-1706). Birkhäuser Basel.

Watts, A.B., Platt, J.P., & Buhl, P. (1993). Tectonic evolution of the Alboran Sea basin. *Basin Research, 5,* 153-177.

Weissel, J. K. (1981). Magnetic lineations in marginal basins of the western Pacific. *Philosophical Transactions of the Royal Society of London. Series A, Mathematical and Physical Sciences*, *300*(1454), 223-247.

Yelles, A., Domzig, A., Déverchère, J., Bracène, R., de Lépinay, B. M., Strzerzynski, P., ... & Djellit, H. (2009). Plio-Quaternary reactivation of the Neogene margin off NW Algiers, Algeria: the Khayr al Din bank. *Tectonophysics*, *475*(1), 98-116.

Zeck, H. P., Kristensen, A. B., & Williams, I. S. (1998). Post-collisional volcanism in a sinking slab setting—crustal anatectic origin of pyroxene–andesite magma, Caldear volcanic province, southeastern Spain. *Lithos, 45,* 499–522.

CHAPTER 5

Application of Automated Throw Backstripping Method to Characterize Recent Faulting Activity Migration in the Al Hoceima Bay (Northeast Morocco): Geodynamic Implications.

Víctor Tendero-Salmerón[1*], Manfred Lafosse[2,3], Elia d' Acremont[2], Alain Rabaute[2], Omar Azzouz[4], Gemma Ercilla[5], Mohamed Makkaoui[4], Jesus Galindo-Zaldivar[1,6]

[1]Instituto Andaluz de Ciencias de la Tierra (CSIC-UGR), 18100 Armilla (Granada), Spain

[2]Institut des Sciences de la Terre Paris, ISTeP UMR 7193, INSU-CNRS, Sorbonne Université, 75252 Paris Cedex 05, France

[3]Tectonic and Structural Geology groups, Department of Earth Sciences, Utrecht University, 3584 CS Utrecht, the Netherlands

[4]Laboratoire de Géologie Appliquée, Faculté des Sciences, Université Mohammed Ier, BP 717 Oujda 60000, Morocco

[5]Instituto de Ciencias del Mar, Continental Margins Group, CSIC, 08003 Barcelona, Spain

[6]Departamento de Geodinámica, Universidad de Granada, 18071 Granada, Spain

Published on:

Frontiers in Earth Science, 9:645942. (April 2021)

https://doi.org/10.3389/feart.2021.645942

(Received 24 December 2020, Accepted 19 March 2021, Published 13 April 2021)

JCR(2020): 3.498 (Q2)

Abstract

Automation of the throw backstripping method has proven to be an effective tool for the determination of the evolution of tectonic activity in wide fault zones. This method has been applied to the Al Hoceima Bay (southwesternmost Mediterranean, Alboran Sea) for a time period covering the last 280 kyr on 672 faults imaged on 265 high-resolution seismic reflection profiles. This area was affected by major earthquakes and corresponds to a transtensional basin deformed by growth faults. The automated application of throw backstripping allowed for a faster deciphering of the migration of tectonic activity. Results show a westward migration of the deformation with quickly increasing deformation rates in the most recent time frames near the Al Hoceima City, the most populated area. This migration is in agreement with the current seismicity, the GPS data and recent brittle deformation data. Vertical throw rates of up to 0.47 mm/yr have been calculated, for the most recent time periods, in segments of the Bokkoya fault zone. The westward migration of the deformation fits with the reconstruction suggested by westernmost Mediterranean geodynamic models during the Pleistocene, and it may be the consequence of interaction between the NW movement of the South Alboran indenter and the back Rif south-westwards displacement. The highly accurate constraints of evolution of tectonic activity offered by this automation will substantially improve the seismic hazard assessment.

Keywords: active tectonics, throw backstripping, faulting migration, marine faulting, Alboran Sea

5.1 Introduction

Active faults associated with earthquakes are generally characterized by deformation of very recent deposits and geomorphological signatures such as continuous scarps, linear valleys, or low sinuosity mountain fronts (*e.g.*, Keller and Pinter, 1996; Wesnousky, 1986). These geomorphological features are not very marked in young and small scale faults because of the minor accumulated deformation, even when very active. Moreover, smaller faults can remain generally undetected as blind structures that do not reach the surface. Consequently, recent small-scale and blind faults are not usually the target of palaeoseismic studies which generally focus on faults with a well-preserved record of major earthquakes, even if their most recent activity is decreasing (Cornell, 1968; McCalpin, 2009 and references therein). Another issue is the importance of differentiating between neotectonics and active tectonic activity, and between recent faults and newly formed faults. In faulted submarine basins with considerable sedimentation rates, growth faults are the best candidates for study. Their activity creates significant vertical movement affecting deposits that can be quantified using deformed regional reference markers in both fault blocks (*e.g.*, Mansfield and Cartwright, 1986; Worrall and Snelson, 1989; Childs *et al.*, 1995; Cartwright *et al.*, 1998; Back *et al.*, 2006; Baudon and Cartwright, 2008). The best method for determining the incremental throw of syn-sedimentary faults such as growth faults (Carver, 1968) through time is the throw backstripping (Petersen *et al.*, 1992; Childs *et al.*, 1993, 1995) method. In the study of the evolution of fault systems, the latter has been employed as a useful tool in many geological settings (Jackson *et al.*, 2017, and references therein). The throw backstripping have been applied over long periods of time (several millions of years) in fault systems (Nicol *et al.*, 1997; Meyer *et al.*, 2002; Walsh *et al.*, 2003; Giba *et al.*, 2010; Phillips *et al.*, 2018) and over short periods of time (Nicol *et al.*, 2005, 2006).

In contexts of fast migration of deformation, such as those of orogenic wedges (*e.g.*, Davis *et al.*, 1983; Carrapa, 2009) or back-arc basins (Milia *et al.*, 2018), a quick rise and abandonment of faults generally occurs. Small faults may experience an acceleration in the deformation rate, with the increase of the associated seismic hazard (Goldsworhty and Jackson, 2000; Galadini and Messina, 2003). Since the distance to earthquakes sources is a key factor to evaluate seismic hazard (*e.g.*,

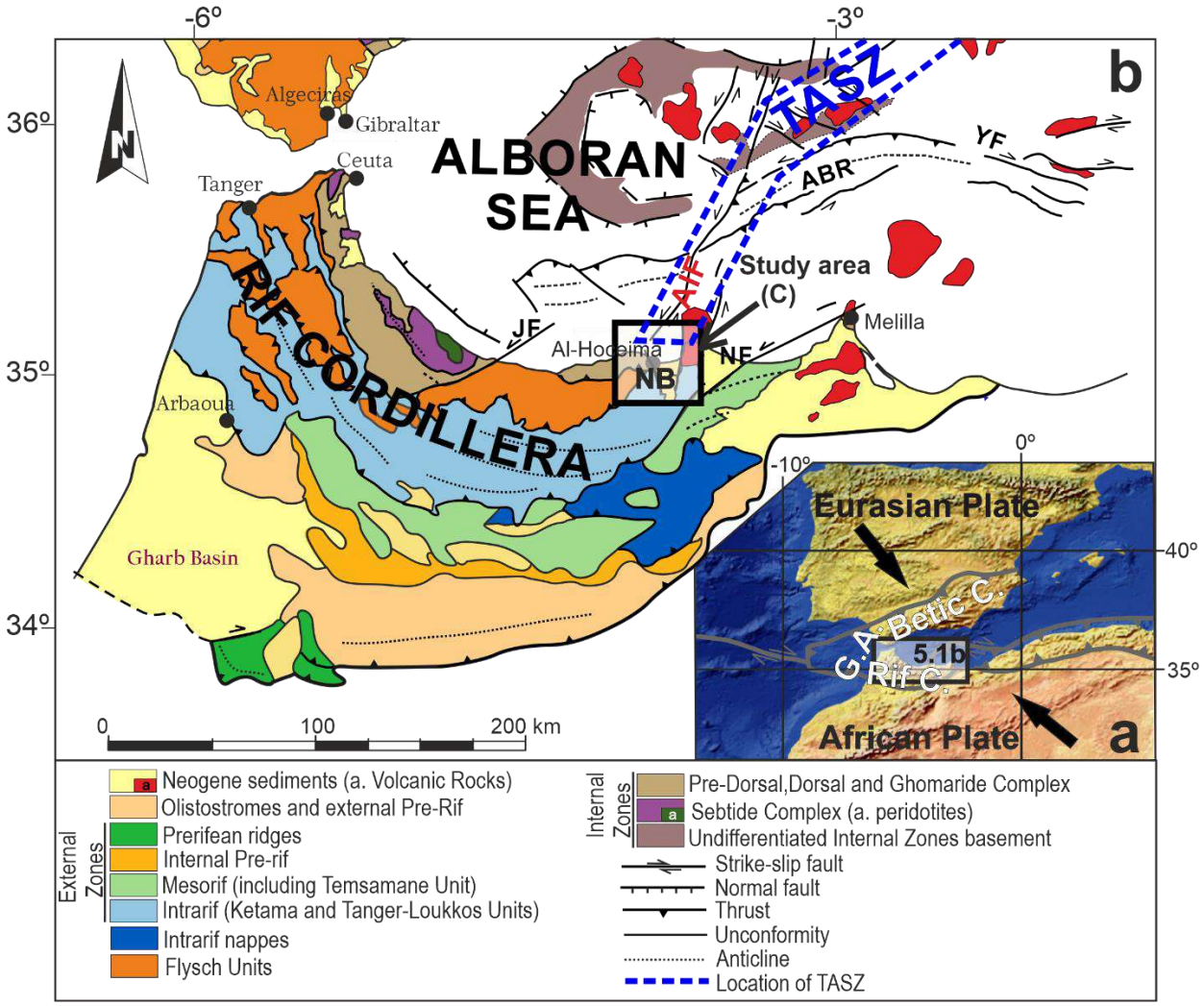

Figure 5.1. Location of the study area. a) Regional setting. Plate boundaries from Do Couto *et al.* (2016). G. A.: Gibraltar Arc; b) Geological map of Southern Alboran Sea and Rif Cordillera (modified from Galindo-Zaldivar *et al.*, 2015). ABR: Alboran Ridge, AIF: Al Idrissi Fault, JF: Jebha Fault, NB: Nekor basin, NF: Nekor Fault, YF: Yusuf fault.

Cornell, 1968; Wang, 2011, and references therein), it is important to understand the evolution of the fault systems and where the active deformation migrates to. Moreover, in complex and slowly deforming continental crusts that are affected by wide fault zones, the identification and evolution of recent active deformation may be a complex subject. This is the case of the Nekor basin, in northeastern Morocco (Fig. 5.1). This Neogene basin, located in the southern Alboran Sea (Westernmost Mediterranean), is surrounded by the Gibraltar Arc which is formed by the Betic-Rif cordilleras (Comas *et al.*, 1992) (Fig. 5.1). This basin is considered a key area as it is located at the plate boundary between Africa and Eurasia (*e.g.*, Vernant *et al.*, 2010; Lafosse *et al.*, 2020). It constitutes the tip of a strike-slip zone (Al Idrissi fault

system)that has become incipient since 1.8 Ma (Lafosse *et al.*, 2020), and where the active left-lateral displacement recorded along the major Al Idrissi fault system is transmitted to the Rif Cordillera in Morocco, accompanied by the development of new faults (Galindo-Zaldívar *et al.*, 2018). In the context of the convergence between the Eurasian and African plates, the Alboran Domain extending up to the Al Hoceima region is undergoing a westward displacement (Balanya *et al.*, 2007; Corsini *et al.*, 2014; González-Castillo *et al.*, 2015). The recent geodynamic evolution has been related to different lithospheric processes, with two groups of hypotheses: on one side those related to a slab roll-back of the retreating subduction zone starting from the Miocene (Blanco and Spakman, 1993; Ruiz-Constán *et al.*, 2011; Spakman *et al.*, 2018, and references therein), and on the other those related to lithospheric delamination (*e.g.*, Seber *et al.*, 1996; Mancilla *et al.*, 2013; Baratin *et al.*, 2016). At a local scale, several points are under discussion such as (i) the position of seismicity and its origin, which includes the biggest onshore and offshore earthquakes in the region for the last few decades (Mw 6.0 in 1994, Mw 6.4 in 2004 and Mw 6.3 in 2016, Fig. 5.2, El Alami *et al.*, 1998; Stich *et al.*, 2005; Galindo-Zaldivar *et al.*, 2009; Van der Woerd *et al.*, 2014; Galindo-Zaldivar *et al.*, 2018; Gràcia *et al.*, 2019), and (ii) the driving force and chronology of the westward movement of the Rifian block (Koulali *et al.*, 2011; Petit *et al.*, 2015).

This study of Pleistocene to present day offshore faults in the Al Hoceima area aims to quantify their deformation rates through time. For that purpose, we automated the throw backstripping method (Petersen *et al.*, 1992) in order to analyze a high number of faults efficiently. Al Hoceima bay constitutes a key area of the Eurasian-African plate boundary, and the results bring new data enhancing regional tectonic modeling and allowing for better estimations of coastal seismic hazard.

5.2 Geological setting

The Gibraltar Arc is composed by the Betic Cordillera in the north and the Rif in the south, connected though the Gibraltar Arc (Fig. 5.1). Both cordilleras are composed of stacked nappes divided into the Internal Zone (Alboran Domain) and the External Zones (sediments from the Iberian and African palemargins) separated by the Flysch Units. In the Rif, the Internal Zone is mainly formed by allochthonous metamorphic complexes that include Paleozoic rocks emplaced during the Eocene-Oligocene Alpine

tectonic phase. These complexes are, from bottom to top, the Sebtide and the Ghomaride (Chalouan, 1986; Chalouan *et al.*, 2008). Moreover, the Dorsal and Predorsal Complexes (Andrieux, 1971; Frizon de Lamotte, 1985), which are mostly made up of carbonates, also belongs to the Internal Zone. The Flysch Units are characterized by detrital sediments deposited in the trench between Internal and External Zones from the Cretaceous to the Oligocene (Frizon de Lamotte, 1985). The External Zones are parautochthonous rocks composed by carbonate and pelitic Mesozoic and Cenozoic sequences, some of them with low to medium grade of metamorphism (Andrieux, 1971).

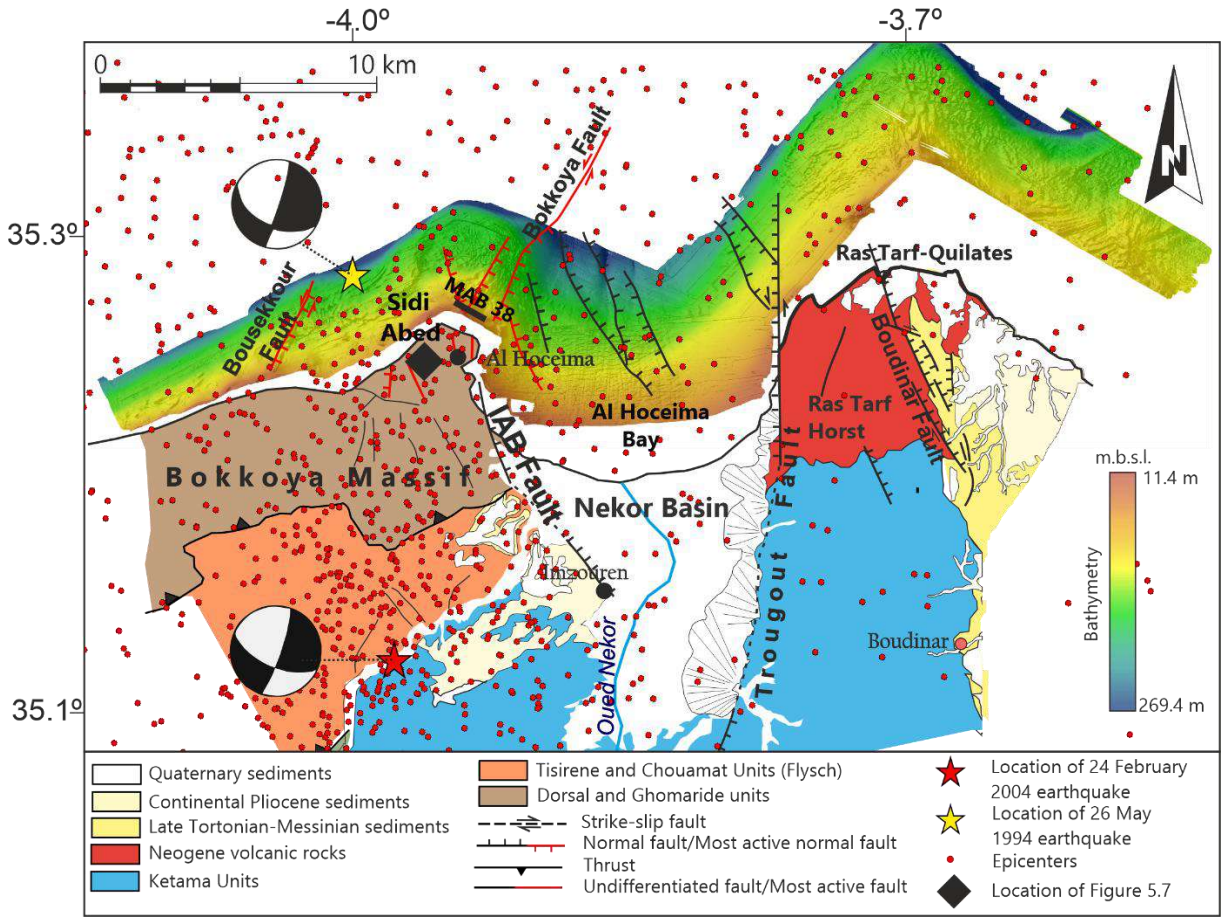

Figure 5.2. Geological map of Nekor Basin and swath-bathymetry of the Al Hoceima margin from Marlboro-2 Survey (modified from Galindo-Zaldivar *et al.*, 2015 and d'Acremont *et al.*, 2014). Seismicity from IGN catalog 2000–2020; earthquakes with Mw > 1.5, and the position of the main shocks of the seismic series of 2004 and 1994 from Calvert *et al.* (1997) and Van der Woerd *et al.* (2014). The focal mechanism of both earthquakes are from Van der Woerd *et al.* (2014). The location of the outcrop of Sidi Abed presented in Figure 5.7 and MAB 38 profile is also displayed.

The Alboran Sea is a Neogene basin that is surrounded by the Gibraltar Arc (Fig. 5.1; Comas *et al.*, 1992). The thinned continental crust that constitutes its basement is

made up of alpine metamorphic rocks of the Alboran Domain (Internal Zones) (Comas *et al.*, 1992; García-Dueñas *et al.*, 1992; Gomez de la Peña *et al.*, 2018), and above it the Miocene to Quaternary sedimentary infill is mainly detritic (Comas *et al.*, 1992; Juan *et al.*, 2016). The westward displacement of the Alboran Domain is well-known since Andrieux *et al.* (1971) and has been corroborated with GPS data (Koulali *et al.*, 2011; Palano *et al.*, 2015). During the Miocene, crustal thinning took place followed by a compression in the Late Tortonian (Comas *et al.*, 1992; Do Couto *et al.*, 2016). Both the westward displacement and the crustal extension has been explained by two groups of lithospheric models: slab roll-back of the retreating subduction zone that thinned a previous orogen (Blanco and Spakman, 1993; Ruiz-Constán *et al.*, 2011; Spakman *et al.*, 2018, and references therein) and mantle delamination of the thickened lithosphere of that orogen (*e.g.*, Seber *et al.*, 1996; Mancilla *et al.*, 2013; Baratin *et al.*, 2016).

The current compression is combined with an orthogonal extension that continues nowadays (Comas *et al.*, 1992; Vissers *et al.*, 1995; Sanz de Galdeano and Alfaro, 2004; DeMets *et al.*, 2010; Neres *et al.*, 2016). Active strike-slip faults are widely distributed and most of them are grouped in NE-SW left lateral faults (*e.g.*, Al-Idrissi fault zone) and NW-SE dextral faults (*e.g.*, Yusuf fault) (Fig. 5.1). The en échelon NE-SW left lateral strike-slip faults that crosses the Alboran Sea and continues in the eastern Betic Cordillera is called the Trans-Alboran Shear Zone (TASZ, Fig. 5.1b; De Larouzière *et al.*, 1988). Recent indentation and block rotation processes (Perea *et al.*, 2018) in the Alboran Sea deform the TASZ and explain the conjugate sets of present day right lateral faults (Estrada *et al.*, 2018) and the initiation of the Al Idrissi fault zone (Gràcia *et al.*, 2019; Lafosse *et al.*, 2020).

The southern termination of the Al Idrissi fault zone is a transtensional basin that acts as a horsetail splay, the Nekor basin (Figs. 5.1b and 5.2; d'Acremont *et al.*, 2014; Lafosse *et al.*, 2016). The study area covers the offshore continental margin of Al Hoceima Bay (Fig. 5.2) and the northeasternmost part of the onshore Bokkoya Massif margin belonging to the internal zone (Fig. 5.2). This carbonate massif is made up of a thrust-sheet stack of Dorsal and Ghomaride units (Andrieux, 1971; Chalouan, 1986). South of the Nekor basin, the major Nekor fault is located (Fig. 5.1b), which accommodates the SW-wards emplacement of the Rif Internal Zones during the

Miocene (Leblanc and Olivier, 1984). The western Nekor basin boundary corresponds to the Imzouren-Ajdir-Boujibar normal faults (Fig. 5.2; Aït Brahim *et al.*, 1990; d'Acremont *et al.*, 2014) that separate the Plio-Quaternary sedimentary Nekor basin infill from the Internal Zones (Bokkoya Massif), the nappes of Flysch, and the Ketama Unit of the External Zones (Azdimousa *et al.*, 1998). The eastern boundary of the Nekor basin corresponds to the Trougout fault (Fig. 5.2), an oblique normal left lateral fault whose slip decreases southwards and that makes the Al Hoceima Bay an asymmetric graben (Aït Brahim and Chotin, 1990; Galindo-Zaldivar *et al.*, 2009; Lafosse *et al.*, 2016; Lafosse *et al.*, 2020). Trougout fault separates the basin from the Ketama Unit and the Upper Miocene volcanic rocks of Ras Tarf cape (Fig. 5.2; El Azzouzi *et al.*, 1999). The Nekor basin is filled by a 400 to 500 m thick Plio-Quaternary sequence overlying undated marls (Aït Brahim, 1985; Galindo-Zaldivar *et al.*, 2009). This basin is considered as a transtensional basin with a rhombohedral shape (Lafosse *et al.*, 2016).

Offshore, the whole bay presents a set of NW-SE normal faults that cross the bay between the Bokkoya and the Trougout faults (Fig. 5.2; Calvert *et al.*, 1997; Lafosse *et al.*, 2016). This network of normal NW-SE to N-S faults located in the bay has a syn-sedimentary character (Lafosse *et al.*, 2016; Lafosse *et al.*, 2018) similar to that of growth faults: most of them are normal and are quickly buried by sedimentation. The Bokkoya fault is considered a normal NE-SW left lateral fault (Calvert et al, 1997; d'Acremont *et al.*, 2014; Lafosse *et al.*, 2016). The Bokkoya fault and the offshore prolongation of the Trougout fault can connect to the southern termination of the Al Idrissi fault and other parallel faults (d'Acremont *et al.*, 2014; Lafosse *et al.*, 2016; Galindo-Zaldivar *et al.*, 2018; Gràcia *et al.*, 2019). Westward, outside of the Nekor basin, the Bousekkour fault is interpreted as a left-lateral normal fault parallel to the Bokkoya fault (Fig. 5.2, d'Acremont *et al.*, 2014).

While offshore displacements are significant (d'Acremont *et al.*, 2014; Lafosse *et al.*, 2016; Gràcia *et al.*, 2019), it is difficult to observe any clear displacement onshore (Fig. 5.2, Galindo-Zaldivar *et al.* 2009). The earthquake epicenters reveal the deep tectonic activity and are mainly distributed west of the Imzouren-Ajdir-Boujibar normal faults, with the biggest earthquakes recorded in the last few decades (Fig. 5.2; 1994 and 2004 main shocks; El Alami *et al.*, 1998; Biggs *et al.*, 2006; Van der Woerd *et al.*, 2014).

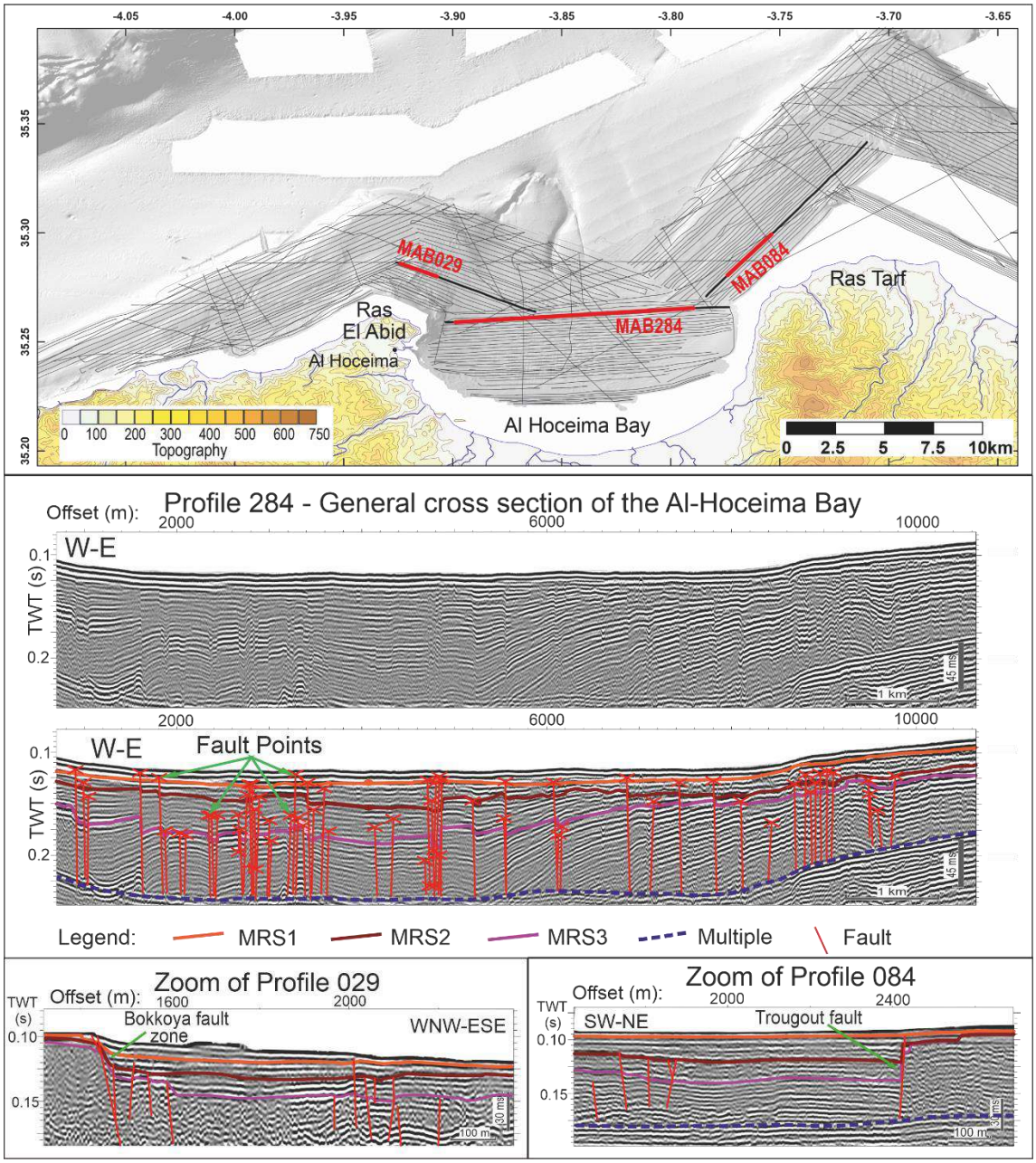

Figure 5.3. Seismic images of Al Hoceima Bay cross section and details of Bokkoya and Trougout faults on multibeam bathymetric map, including the location of the high-resolution seismic reflection profiles used for this study (Marlboro-2 survey). The profile 284 has been displayed with and without interpretation as a general overview of the bay. The red "X" represents the fault points displayed in a seismic profile. Profiles 29 and 84 magnifications are intended to present the Bokkoya fault and the Trougout fault.

The easternmost part of the Bokkoya Massif provides field observations on recent and active faults in the region (Stich *et al.*, 2005; Galindo-Zaldivar *et al.*, 2009; Van der Woerd *et al.*, 2014; Galindo-Zaldivar *et al.*, 2015). This region is deformed by recent or active minor fractures (Galindo-Zaldivar *et al.*, 2009). These brittle deformations are evidence of a present day roughly E-W extension orthogonal to the coast line. This

appears to be in contrast with the occurrence of strike-slip focal mechanisms at depth, which could be due to the existence of a crustal detachment decoupling some deeper deformation zones from more shallow ones (Galindo-Zaldivar *et al.*, 2009; Galindo-Zaldivar *et al.*, 2015). In contrast, the Trougout fault in the eastern part of Al Hoceima Bay presents a straight relief of 13 km length, but there is no significant seismicity and only local outcrops show some evidence of recent fault activity (Poujol *et al.*, 2014).

5.3 Data and methods

5.3.1 Data

Multichannel high-resolution seismic reflection and multibeam bathymetry were acquired during Malboro-2 survey along 265 profiles, which cover 190 km2 from the eastern limits of Al Hoceima Bay to 14 km westward of Ras El Abid Promontory continental shelf (Fig. 5.3). These data were acquired using a 250-500 J SPARKER source and a six-channel streamer, with a vertical resolution of 1 m. The swath bathymetry was acquired in Marlboro-2 survey by means of a shallow-water Reson 8101 system. It has a horizontal definition of 5 m/pi and a vertical resolution of 0.5 m at depths of above -100 mbsl (d'Acremont *et al.*, 2014; Lafosse *et al.*, 2016).

5.3.2 Methods

To quantify the fault throw, a methodology based on the displacement/throw backstripping developed by Petersen *et al.* (1992) was used. This method makes no assumptions about the patterns of throw accumulation or the style of fault growth (Jackson *et al.*, 2017), and consists of measuring the vertical throw at regular intervals along the fault and across multiple stratigraphic horizons. Each throw is calculated by removing the throw accumulated on the youngest horizons, starting with the youngest. This allows for the determination of the activity of the fault through time (Petersen *et al.*, 1992; Childs *et al.*, 1993; Nicol *et al.*, 1997). This method was applied on 672 faults determined by Lafosse *et al.* (2016). Although most of the fault inside the Al Hoceima Bay are normal, some of them have strike-slip components (Lafosse *et al.*, 2016, 2020). Onshore, the normal faults located at Sidi Abed (Figs. 5.2 and 5.7) present striae with pitch >70º. In the Trougout fault, which outcrops onshore, estimations of the horizontal and vertical components has been done for the last 7190

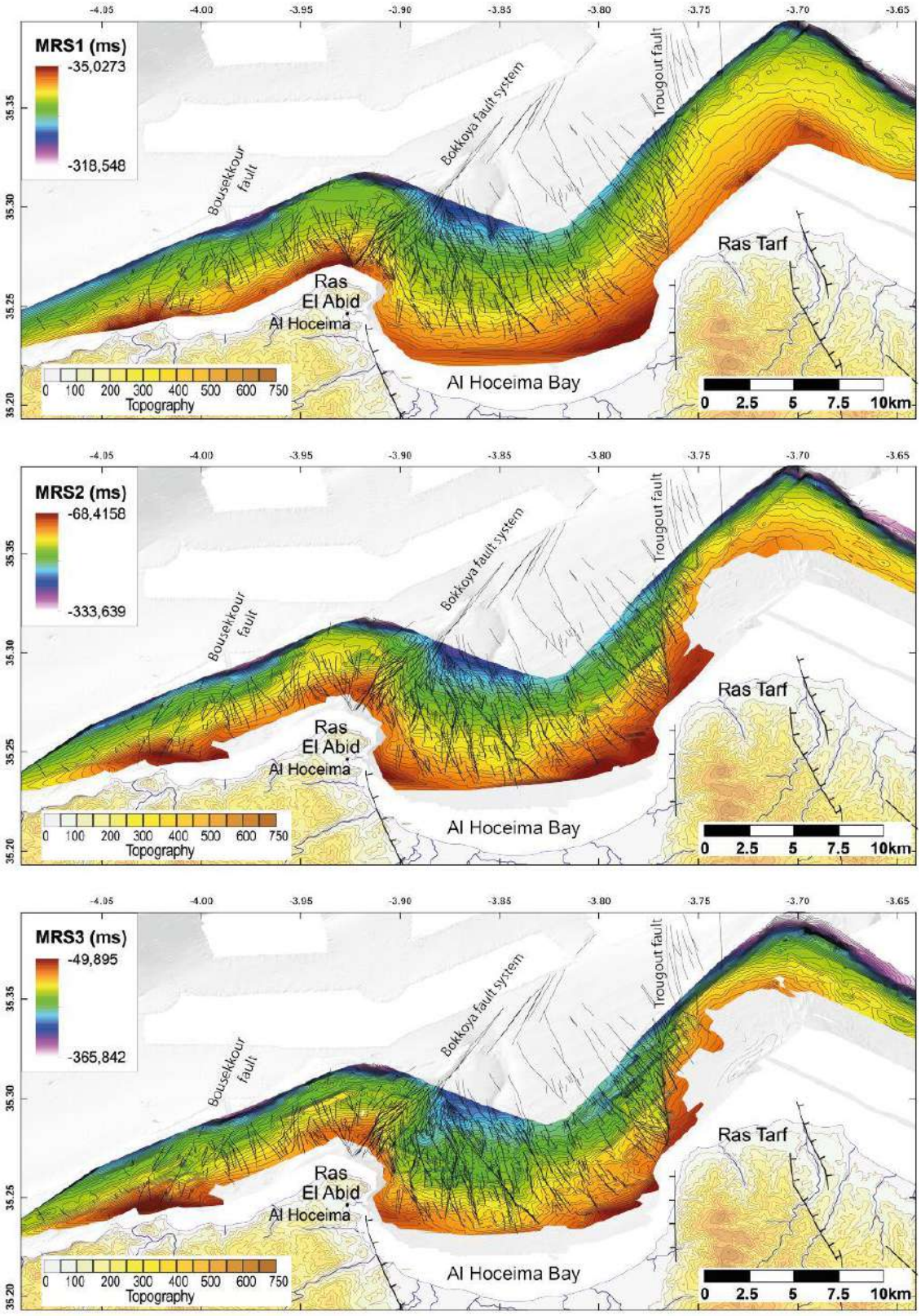

Figrue 5.4. Maximum regressive surfaces used for the throw analysis. The fault traces considered are also depicted.

years (Poujol *et al.*, 2014), which provide a ratio vertical/horizontal of ~1.75. The vertical throw of the faults that border the basin, like Bokkoya and Trougout (Lafosse

et al., 2020), is big enough to affect the seafloor (Lafosse et al, 2016). Thus, the analysis of the vertical component can be used as an indicator of the fault activity.

In order to determine their age, basin scale stratigraphic surfaces of very low dipping angles have been selected (Figs. 5.3 and 5.4). In the study area, these surfaces represent Marine Regressive Surfaces (MRS) reworked during fast marine transgressions (Lafosse *et al.*, 2018). These surfaces correspond to major sea level drops during the Late and Middle Pleistocene, related to the 100 kyr glacio-eustatic cycles. The three most recent regressive surfaces (here named MRS1, 25 kyr; MRS2, 150 kyr; and MRS3, 280 kyr; according to sea level variations of Frigola *et al.*, 2012, and Grant *et al.*, 2014 and identified by Lafosse *et al.*, 2018) have been used to analyze the fault activity since 280 kyr. The vertical displacement of these very low dipping surfaces is attributed to fault activity and was measured in ms TWT (two-way-time). A rough estimation of the vertical throws in meters has been calculated using an average value of propagation velocity for the Quaternary sediments (1576 m/sec) obtained from Martínez-García *et al.* (2017) and sedimentation rates have been considered constant (Martínez-García *et al.*, 2013, Lafosse *et al.*, 2016).

The throw of all the faults of every seismic profile, for the three most recent MRS, were measured. Then, maps of the throw values for each period ranging between each MRS until the present have been generated. Initially, four groups of data were exported from the IHS Kingdom Suite© software to the ArcGis© software: a shapefile layer with the traces of the profiles, three raster layers that correspond to the isopach map for each MRS containing the depth value in TWT expressed in ms, a shapefile layer with the fault traces, and a shapefile layer called “fault points”. These “fault points” represent each crossing's location between a fault and a seismic profile (Fig. 5.3). These fault points were obtained from IHS Kingdom Suite by extracting the upper tip of each fault drawn in each seismic profile. Then, work-flows were created using the model builder tool of ArcGIS as follows:

i) Extraction of the depth range at each MRS, for each fault point. First, the pixels located inside an area of 60 m around the trace of the profiles were extracted for each MRS raster layer (Fig. 5.4) with the buffer tool. With the newly extracted rasters of MRS1, MRS2, and MRS3, the focal statistics tool was applied in a radius of 60 m and the range parameter. The tool calculates the difference between the

maximum and minimum depth values using every pixel's values inside a 60m radius and assigns that value to a central pixel in a new raster layer. The radius of 60 m was chosen after testing different distances. This radius is adequate since the faults are high-angle normal faults (most of them with dip >65º) and some of them are vertical faults. It also minimizes local errors likes bending associated to faulting. Thus, the application of this method is optimal in high dipping faults. Since the values of the pixels are the depth of the MRS, the range is proportional to the paleo-topographic vertical displacement. The maximum difference corresponds to the throw generated by the fault in locations close to a fault (considering the slope is gentle on all the surfaces, see below). After that, the range was extracted at each fault point.

ii) Determination of whether a fault cuts each MRS at each fault point. Part of the fault points belong to faults that do not cut any MRS used in this study. The depth value of each MRS was extracted using the "extract multi values to points" tool. In the layer's attribute table, three new fields were created to flag the position of fault tips relative to each MRS. When the faults do not cut any MRS, a throw value of 0 is assigned.

iii) Calculation of the throw of each fault point and each interval following the throw backstripping method. For the oldest intervals, the throw accumulated at the youngest horizons was removed.

iv) Making raster layers of the throw of the area for each MRS interval. The attribute table of the fault points layer has all the throw data calculated in the previous steps.

Finally, once the throw maps were obtained, throw rate maps were created by transforming TWT into depth and then dividing by the period of time between MRS. These throw rates only consider the vertical deformation associated to the faults.

During the process, negative values of fault throw were produced. In the results, negative values are not considered in the throw backstripping method, since throw values related to fault activity are supposed to be positive except in cases where inversion tectonics might have occurred. Inversion is considered to be an uncommon process in the context of short time periods and a homogeneous regional pattern is expected in most of the faults, therefore it is assumed that the tectonic regime

remained constant since 280 kyr. Negative values with irregular patterns are related to sedimentary and erosion processes like the shelf edges, talwegs and canyons (*e.g.*, the canyon located NE of Al Hoceima, Fig. 5.5), where younger MRS locally can show high slopes and, consequently, higher depth ranges with respect to the older ones. For example, in the canyon submarine erosion increases the local slope through time, and when throw backstripping was applied, negative values were obtained in the MRS2 and MRS3. Other example related to sediment process is the uncompacted sedimentary wedges in the central part of the basin, where fluvial sediments are deposited, can lead to locally increase the throws of MRS1 or MRS2, which leads to negative values. Some situations lead to poor vertical resolutions, which causes negative values, like low vertical offsets or thickness variations from either part of the fault zones. Other negative values may be related to errors in the fault locations, irregularities in the reference surfaces (MRS) or artefacts generated during the interpolation of these surfaces. In most of the cases, negative values are between -4 and 0 ms because are related with small faults with small throws. TWT shifts between seismic lines are minimum because the data were recorded during the same survey in similar and good sea conditions. Nevertheless, since the aim of this work is to consider the tectonic activity data and then to analyze the positive throw values related to the tectonic activity, the maps only show the neighborhood of the faults to avoid noise interferences (Figs. 5.5 and 5.8).

5.4 Results

Faults in Al Hoceima bay are high angle and reach sometimes vertical dip. The distribution of fault throws in the study area through time highlights the variation of fault activity, and it is represented by the timing throw maps. Taking into consideration the time period comprised by each map, and a constant sedimentation rate, the data presented here have been used to estimate the average throw rates. The faulting throw rate maps provide a tool to analyze the acceleration and slowing of tectonic activity in each sector affected by the migration of the deformation.

5.4.1 Deformation distribution through time

Three timing maps of the vertical displacement have been established (Fig. 5.5) in TWT (ms), since 280 kyr. These detailed vertical displacement maps allowed us to identify high throw values focused along faults. The high values that were instead

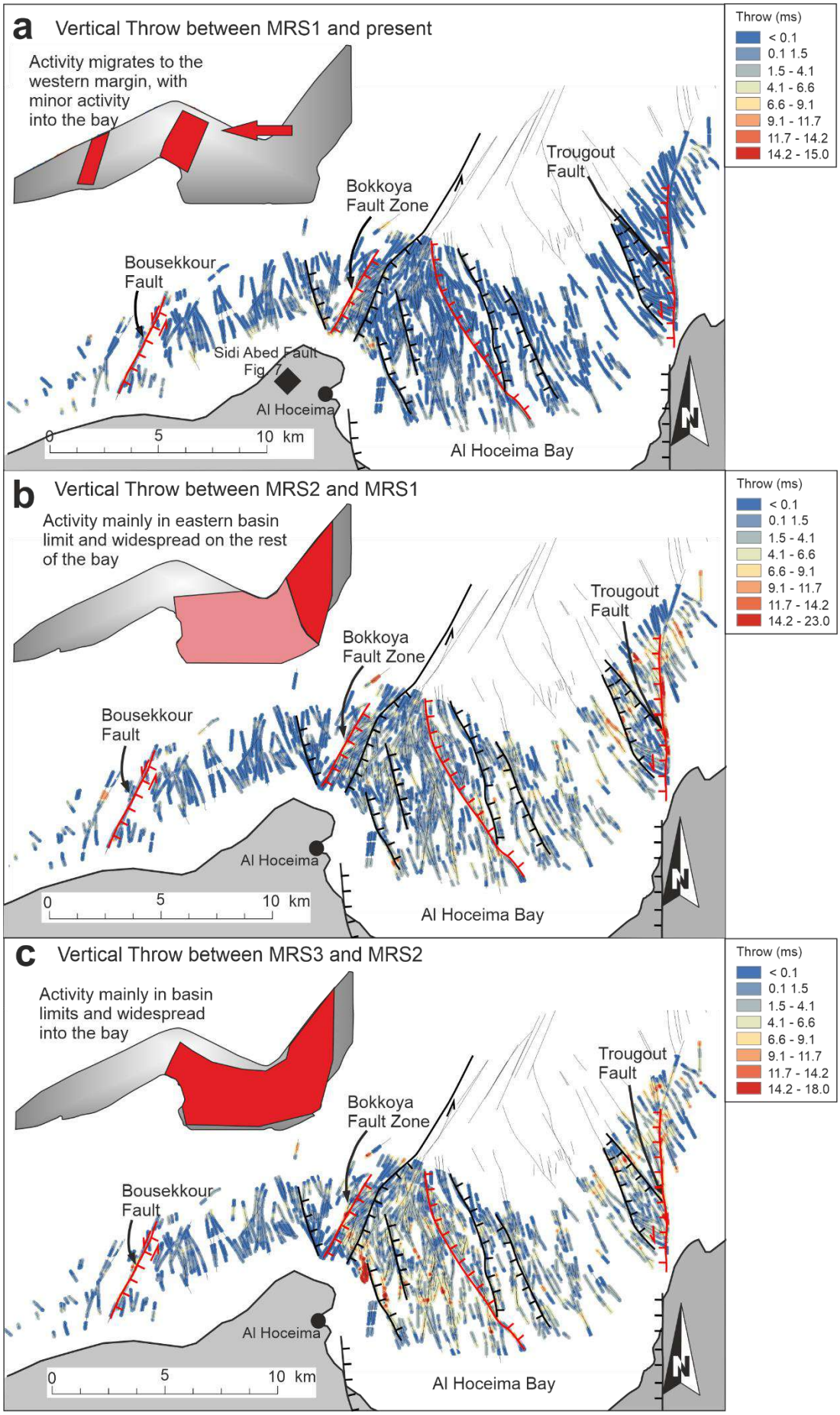
a
Vertical Throw between MRS1 and present
Activity migrates to the western margin, with minor activity into the bay
Bokkoya Fault Zone
Trougout Fault
Bousekkour Fault
Sidi Abed Fault
Fig. 7
Al Hoceima
0 5 10 km
Al Hoceima Bay
Throw (ms)
< 0.1
0.1 1.5
1.5 - 4.1
4.1 - 6.6
6.6 - 9.1
9.1 - 11.7
11.7 - 14.2
14.2 - 15.0
b
Vertical Throw between MRS2 and MRS1
Activity mainly in eastern basin limit and widespread on the rest of the bay
Bokkoya Fault Zone
Trougout Fault
Bousekkour Fault
Al Hoceima
0 5 10 km
Al Hoceima Bay
Throw (ms)
< 0.1
0.1 1.5
1.5 - 4.1
4.1 - 6.6
6.6 - 9.1
9.1 - 11.7
11.7 - 14.2
14.2 - 23.0
c
Vertical Throw between MRS3 and MRS2
Activity mainly in basin limits and widespread into the bay
Bokkoya Fault Zone
Trougout Fault
Bousekkour Fault
Al Hoceima
0 5 10 km
Al Hoceima Bay
Throw (ms)
< 0.1
0.1 1.5
1.5 - 4.1
4.1 - 6.6
6.6 - 9.1
9.1 - 11.7
11.7 - 14.2
14.2 - 18.0

Figure 5.5. Throw maps in milliseconds (ms), including the traces of faults from Lafosse *et al.*, 2017; 2018. a) Between MRS1 and present days; b) Between MRS2 and MRS1; and c) Between MRS3 and MRS2. The maps in the top left corner are outlines of broad areas with major tectonic activity for each period. These areas have been simplified from the detailed throw maps. The main faults traces are also depicted; those in red are the fault traces used for the throw-length profiles of Figure 5.6.

observed in a distributed pattern over broad sectors will not be considered as these are not related to fault activity, but to the presence of high slopes at the edge of the shelf and are to be attributed to canyon and platform edge processes (north of Al Hoceima city and north-west of Trougout fault).

The vertical displacement between MRS3 (280 kyr) and MRS2 (150 kyr) (Fig. 5.5c) shows that deformation is distributed throughout the Al Hoceima Bay, since most of the faults have significant values (average of 4.1-11.7 ms, Fig. 5.6, 4-9 m, peak values over 15 ms, 11.8 m, Fig. 5.5c). The high values are concentrated along lines which roughly match the fault zones; values up to 21 ms occur at the Trougout fault zone (16.5 m), up to 18 ms at the Bokkoya fault zone (14.2 m) and at the normal NW-SE fault set in the western part of the Bay (Figs. 5.5c and 5.6).

The throw value obtained between MRS2 (150 kyr) and MRS1 (25 kyr) (Fig. 5.5b) shows that deformation is also distributed throughout the Al Hoceima Bay, but with lower values to the MRS3-MRS2 period (most of them returned values below 11.7 ms, some faults reach up to 12 ms, 9.5 m; Figs. 5.5b and 5.6). The maximum values (23 ms, 18.2 m) are clearly focused at the Trougout fault zone (Figs. 5.5b and 5.6).

The throw value obtained between MRS1 (25 kyr) and the present (Fig. 5.5a), displays that the relatively high values are concentrated at the Bokkoya fault zone (15 ms maximum, 11.8 m, Figs. 5.5a and 5.6) and nearby area, and at the Bousekkour fault zone (close to 10 ms, 7.9 m, Fig. 5.6). On the contrary, the Trougout fault zone shows the lower values, with only a short segment of the fault still showing tectonic activity (5 ms, roughly 3.9 m), (Figs. 5.5a and 5.6).

The onshore field study has identified the Sidi Abed fault west of Al Hoceima city, close to the offshore faults (Figs. 5.5a and 5.7). This fault, which displaces a limestone formation (Dorsal Complex), has a very high dip (80º), and the fault surface includes dip-slip striations attesting to its normal component. This N-S high angle normal fault

is the most outstanding recent deformation recorded onshore (Fig. 5.7). The onshore normal fault of Sidi Abed (Figs. 5.2 and 5.7) can be considered as belonging to the same onshore-offshore fault system that joins the Bokkoya fault zone and the NW-SE normal fault network (Figs. 5.2, 5.5a and 5.7c).

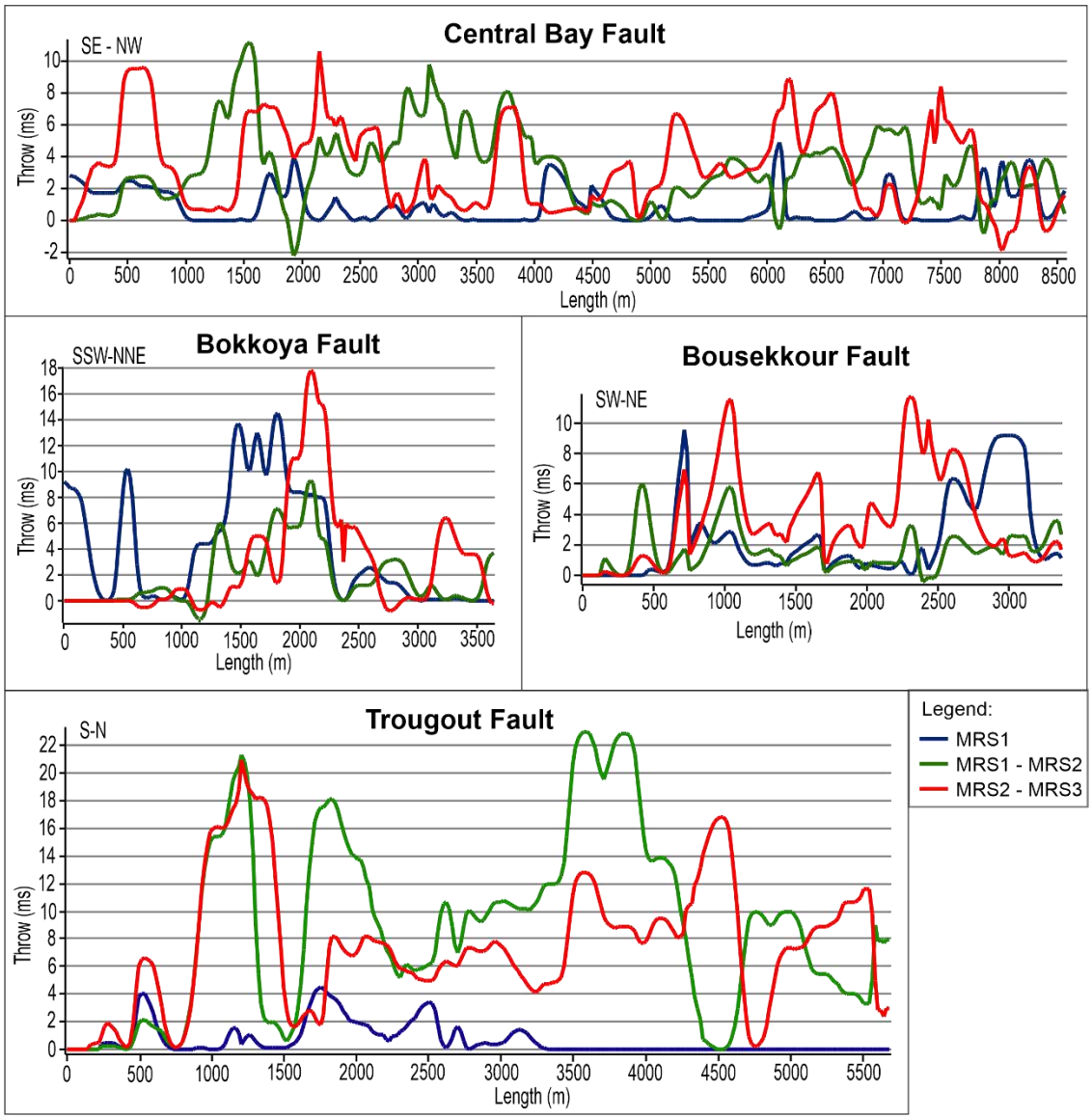

Figure 5.6. Throw- length profiles obtained from throw maps corresponding to the main faults depicted in Figure 5. Central Bay Fault profile constitutes a representative example of the normal faults located into the bay and corresponds to a group of aligned fault traces.

5.4.2 Deformation rate on the main fault zones

Since the MRS1 to present period is shorter than the others, the throw rate maps are useful to compare the activity between time periods. Periods MRS3-MRS2 and MRS2-MRS1 are similar: rates of 0.05-0.07 mm/yr in the faults of the bay, with some peaks

close to 0.10 mm/yr in some segments (Fig. 5.8). The Trougout fault shows rates of 0.11 mm/yr in the MRS3-MRS2 period and of 0.15 mm/yr in the MRS2-MRS1, where the rates are higher along the whole fault (Fig. 5.8). The Bokkoya fault shows a rate of 0.07 mm/yr at the MRS3-MRS2 period and of 0.06 mm/yr at the MRS2-MRS1 period (Fig. 5.8).

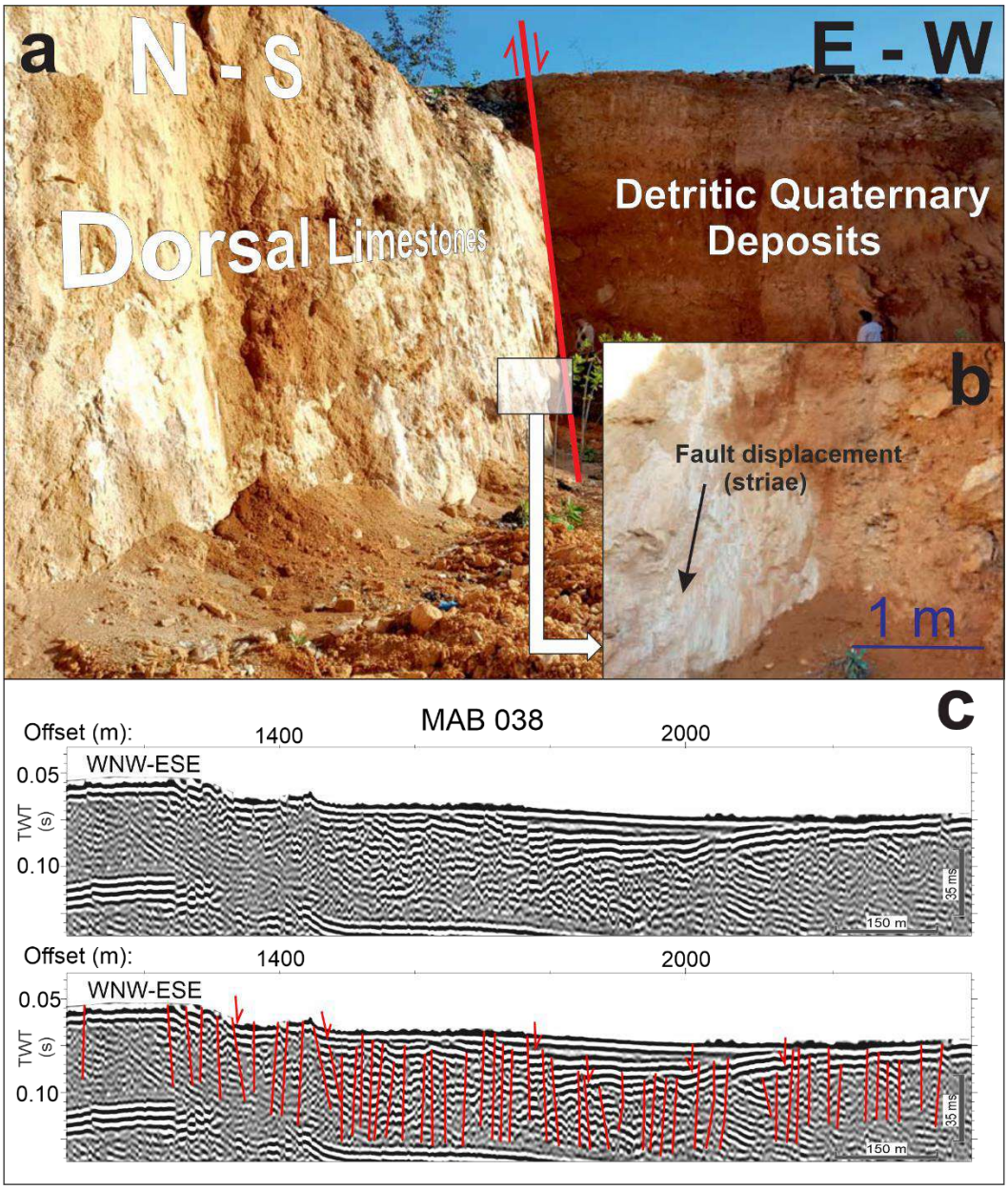

Figure 5.7. Onshore-offshore link in the Al Hoceima region with the illustration of the onshore Sidi Abed normal fault and the offshore Bokkoya normal faults. a) Normal fault in the Sidi Abed area that affects to local Quaternary deposits. Fault orientation and dipping are N000ºE /80ºW. b) Detail of the fault plane; the black arrow marks the orientation and sense of the striae. c) Uninterpreted and interpreted seismic reflection profile MAB 038 showing normal faults (lines in red) that are associated to the onshore faults of Sidi Abed and to the offshore NE-SW Bokkoya normal faults.

The throw rates of the period MRS1 to present contain higher values of throw rate that can go as high as 0.48 mm/yr (Fig. 5.8a). An increase in the values of the Bokkoya fault are observed as it reaches values of 0.47 mm/yr (Fig. 5.8). In contrast, the Trougout fault shows maximum values of 0.15 mm/yr, which are similar to the previous period.

5.5 Discussion

5.5.1 Migration deformation in Al Hoceima Bay

The positive throw values in Al Hoceima Bay can be interpreted as an indicator of tectonic activity. Some faults in the study area show mainly strike-slip kinematics (Lafosse *et al.*, 2016), but they have also recorded a vertical throw that reveals their activity. If we consider a roughly constant sedimentary rate during this period, then we may obtain an estimation of the variation of vertical throw rates. In the earliest time windows (periods MRS3-MRS2, 280-150 kyr, and MRS2-MRS1, 150-25 kyr; Figs. 5.5b,c; and 5.8b,c), the highest vertical throw and slip rates are located in the Nekor basin: in particular at the N-S Trougout fault and in the NNW-SSE faults of the western Al Hoceima Bay. The maximum average throw rates in fault zones are comprised between 0.10 and 0.15 mm/yr with extreme values reaching up to 0.19 mm/yr. Eastwards, the longest syn-sedimentary NW-SE normal faults in the Al Hoceima Bay also show activity in these periods. The results clearly evidence that during the Middle Pleistocene the extension through the Al Hoceima bay was active and distributed between the Bokkoya fault and the Trougout fault. There is a slight regional decrease of the throw values and activity in the period MRS2-MRS1 (150-25 kyr), when only the Trougout fault showed throws higher than 7.9 m (Fig. 5.5b) and some faults in the bay area.

In contrast, in the youngest period (25 kyr to Present) the maximum average throw rates are located along the western margin faults and westwards of the bay (Fig. 55.a, 8). The Trougout fault has very low throw values (Fig. 5.5a). The maximum rates are similar to previous periods (0.15 mm/yr) but these high values are mainly located in the Bousekkour and Bokkoya fault segments. Although a long recurrence interval could be considered for the Trougout fault, the decrease in the activity of this fault in the onshore segment has been indicated in Poujol *et al.* (2014) from geochronological

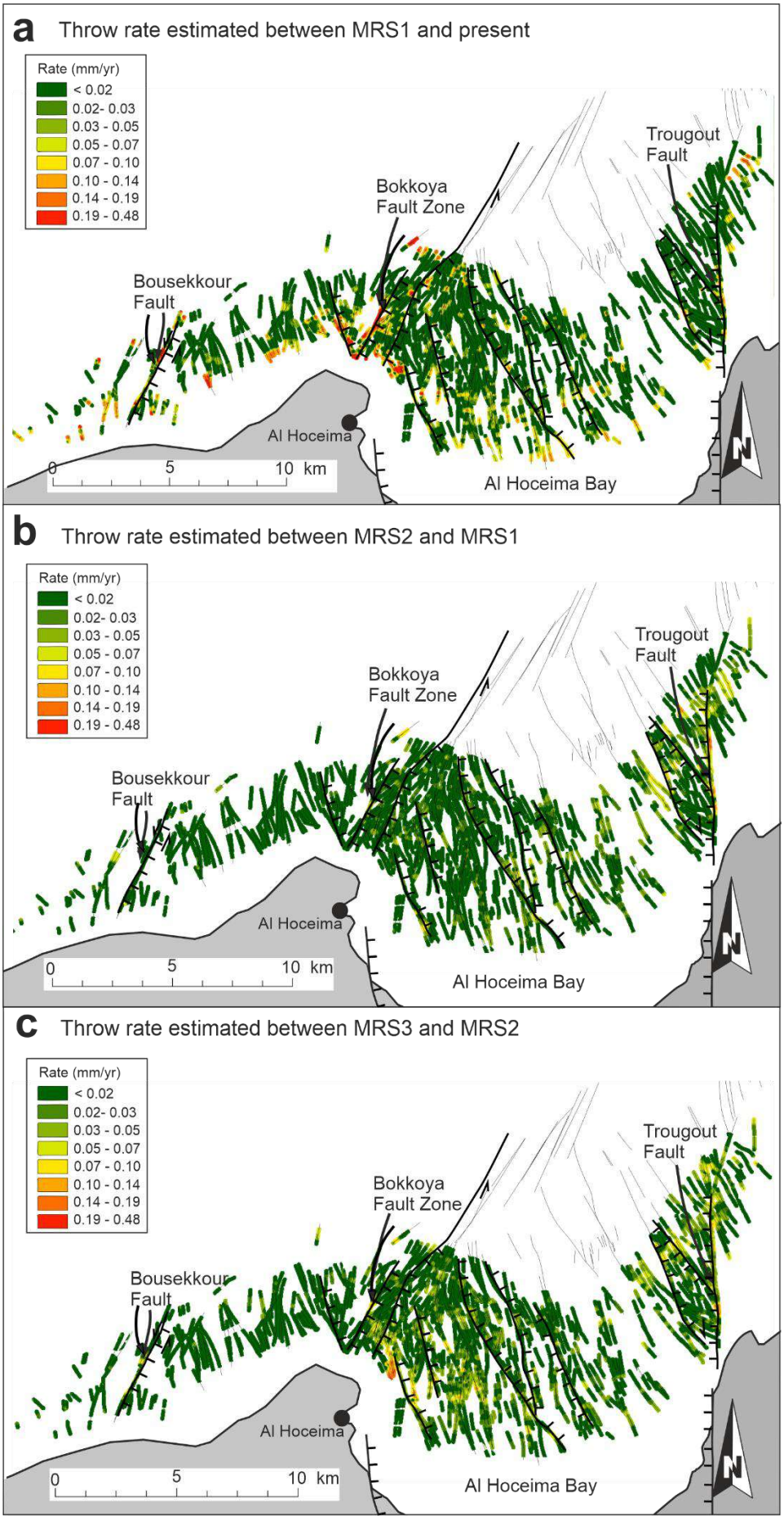
a
Throw rate estimated between MRS1 and present
Rate (mm/yr)
< 0.02
0.02- 0.03
0.03 - 0.05
0.05 - 0.07
0.07 - 0.10
0.10 - 0.14
0.14 - 0.19
0.19 - 0.48
Trougout Fault
Bokkoya Fault Zone
Bousekkour Fault
Al Hoceima
0 5 10 km
Al Hoceima Bay
N
b
Throw rate estimated between MRS2 and MRS1
Rate (mm/yr)
< 0.02
0.02- 0.03
0.03 - 0.05
0.05 - 0.07
0.07 - 0.10
0.10 - 0.14
0.14 - 0.19
0.19 - 0.48
Trougout Fault
Bokkoya Fault Zone
Bousekkour Fault
Al Hoceima
0 5 10 km
Al Hoceima Bay
N
c
Throw rate estimated between MRS3 and MRS2
Rate (mm/yr)
< 0.02
0.02- 0.03
0.03 - 0.05
0.05 - 0.07
0.07 - 0.10
0.10 - 0.14
0.14 - 0.19
0.19 - 0.48
Trougout Fault
Bokkoya Fault Zone
Bousekkour Fault
Al Hoceima
0 5 10 km
Al Hoceima Bay
N

Figure 5.8. Throw rate maps, including the traces of faults from Lafosse *et al.*, 2017; 2018, with the main faults traces highlighted. a) Deformation rates between MRS1 and present day; b) Between MRS2 and MRS1; and c) Between MRS3 and MRS2. Note that the scale of deformation rates between MRS1 and present day is different due to the high values obtained.

data, where a return period of 3.1 kyr is proposed. This estimation make us to consider that a period of 25 kyr is enough to study the fault activity evolution. Moreover, the absence of recent continuous fault scarps onshore (Galindo-Zaldivar *et al.*, 2009) and of sediments that overlap the fault offshore (Fig. 5.3, profile 84) suggests a very recent inactivation of the structure, which may remain with a residual activity. Unlike the Trougout Fault, the Bokkoya fault reaches highest throw rate values in the most recent period (0.48 mm/yr) which indicates a clear acceleration with respect to the previous periods (maximum of 0.06 mm/yr) and that deformation is focused in this structure. Similar behavior is observed in the Bousekkour fault with previous rates of up to 0.10 mm/yr and the most recent rates of 0.33 mm/yr. This suggests an acceleration of the deformation speed in these faults. In fact, if we consider a general overestimation of throw rates at the MRS1-present period due to the high slope of the MRS1 related to the margins and sedimentary processes, the throw rate of the Trougout fault would be lower than in the previous period. On the other hand, even taking into account the possible overestimation, a change from 0.07 to 0.48 would imply an acceleration of the deformation rate in the Bokkoya fault zone. This deformation could be related to recent coseismic deformation, since the western area of the bay is where the seismicity is concentrated (Fig. 25.).

These results show that fault activity during the Late Pleistocene has increased and migrated westward in Al Hoceima Bay. The sum of the data presented indicates an evolution from an initial stage of distributed transtensional extension affecting the whole bay to a localized deformation stage characterized by a concentrated fault activity in the westward part of the Bay, and in the Bokkoya and Bousekkour faults. This activity is also simultaneous to a progressive inactivation of the eastern bay faults, including the Trougout fault.

The westward migration implies that the most active faults are now closer to the most populated areas nearby Al Hoceima city, and thus have strong implications in terms of hazard assessment. Some of the faults that are very close to Al Hoceima port may

have tsunamigenic effects during coseismic deformation events and may have incidence in this infrastructure.

Westward migration of shallow deformation is in coherence with the major earthquake epicenter locations westward of the Al-Idrissi and Trougout fault zones, under the Bokkoya Massif and Bokkoya fault zones (Fig. 5.2; El Alami *et al.*, 1998; Stich *et al.*, 2005; Galindo-Zaldivar *et al.*, 2009; Van der Woerd *et al.*, 2014; Galindo-Zaldivar *et al.*, 2018). Onshore, the activity of recent normal faults has been only clearly observed in the Sidi Abed to Sabadia beach coastal area (Figs. 5.2 and 5.7), suggesting that the most recent offshore fault activity is in clear continuity with onshore faulting and seismicity near Al Hoceima city (Fig. 5.2). The Sidi Abed fault provides the best opportunity to have a direct observation of fault features that belong to the same fault system as that of the offshore faults. It is also remarkable that the very high dip value (80º) of the Sidi Abed fault surface showed dip-slip striations instead of just strike-slip ones, as would be expected according to focal mechanisms of the earthquakes of the area (Figs. 5.2 and 5.7). Similar faults have been observed in the Campo de Dalias, North of Alboran Sea (Marín-Lechado *et al.*, 2004), and are the result of fault reactivation of early extensional hybrid or strike-slip joints characterized by vertical fracture surfaces that are reactivated as extensional faults during the most recent extensional stage. Another zone with a similar evolution and propagationof its faulting pattern is located in the Taranaki Basin and the Taupo Rift (New Zealand) (Gibat *et al.*, 2010, 2012, 2013; Seebeck *et al.*, 2014).

5.5.2 Local deformation into the westernmost Mediterranean geodynamics

The Al Hoceima Bay is located in a key area of the plate boundary affected simultaneously by the tectonic indentation in the central Alboran Sea and the subducted slab delamination processes related with the westward migration of the Gibraltar Arc (Fig. 5.9). The deformation of recent deposits constitutes an opportunity to improve the knowledge on the evolution of deformation in this plate boundary.

The rigid South Alboran Block (Fig. 5.9b) attached to the African Plate moves NW causing indentation in the Alboran Domain (Estrada *et al.*, 2018). The western limit of the South Alboran Block is the left lateral Al Idrissi Fault Zone, formed by the former Al Idrissi fault (Gràcia *et al.*, 2019) and new faults that develop westwards (Galindo-

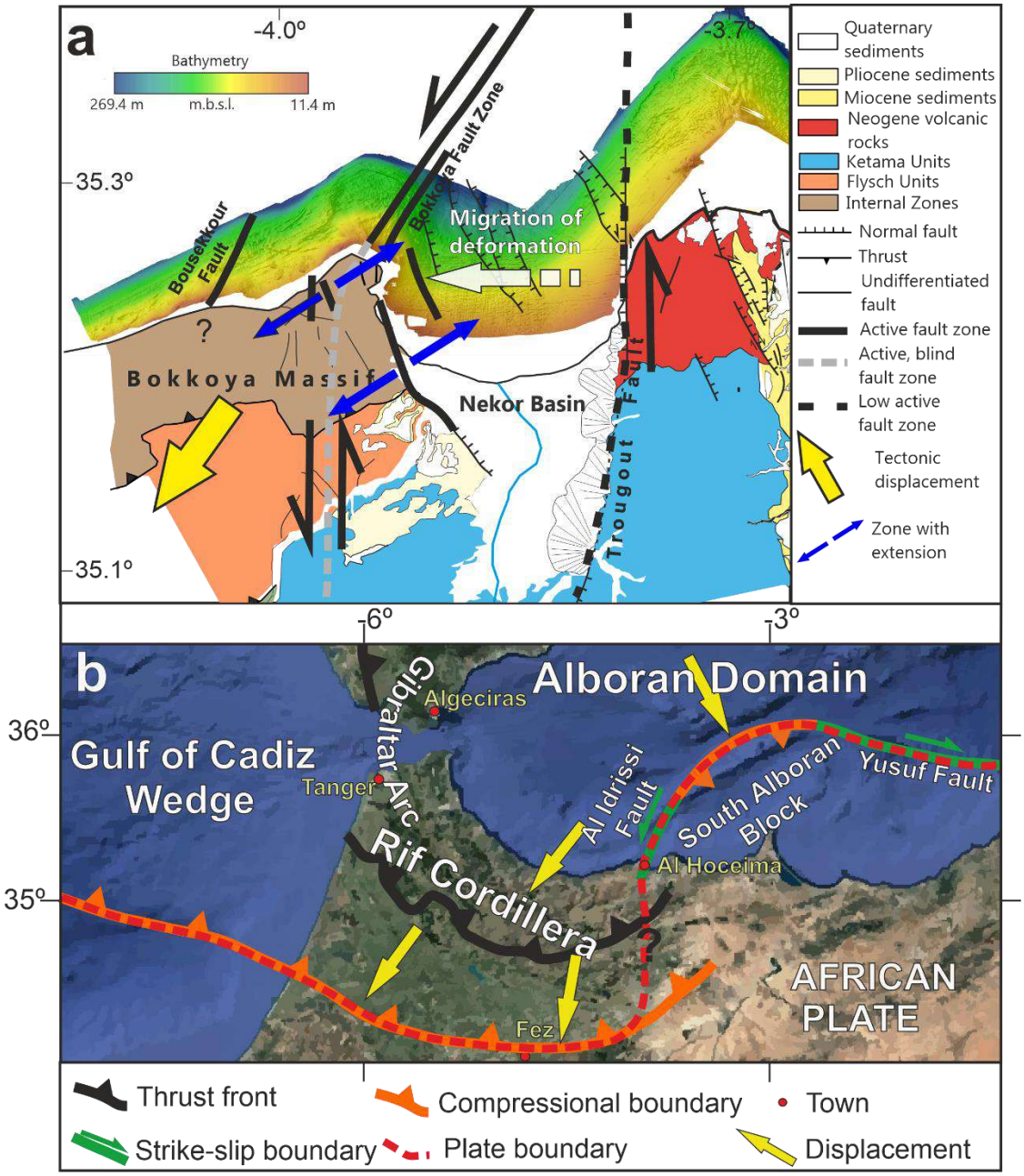

Figure 5.9. Geodynamic sketch at the local scale (a) and regional scale (b). Displacements directions with respect to Africa, based on Galindo-Zaldivar *et al.* (2018) and GPS studies (Koulali *et al.*, 2011; Palano *et al.*, 2015). Geological map modified from Galindo-Zaldivar *et al.* (2015) and swath-bathymetry of the Al Hoceima margin from Marlboro-2 Survey (d'Acremont *et al.*, 2014).

Zaldívar *et al.*, 2018). This fault zone extends towards the NW-SE normal fault splay in the Al Hoceima Bay (Lafosse *et al.*, 2020) and produced the Nekor transtensional basin (d'Acremont *et al.*, 2014) facilitating the SW-ward motion of the Rif (Fig. 5.9). The Bokkoya Massif, which belongs to the Rif, underwent ENE-WSW extension and a westward displacement with respect to Africa (Fig. 5.9). The westward migration of the tectonic activity has already been proposed for the whole region and for the

Gibraltar Arc (Fig. 5.9; *e.g.*, Galindo-Zaldivar *et al.*, 2009; Koulali *et al.*, 2011; d'Acremont *et al.*, 2014; Palano *et al.*, 2015; Crespo-Blanc *et al.*, 2016; Galindo-Zaldivar *et al.*, 2018). The driving mechanism responsible for this migration is still being discussed. Most proposals consider mantle delamination (*e.g.*, Seber *et al.*, 1996; Mancilla *et al.*, 2013; Petit *et al.*, 2015; Hidas *et al.*, 2019) or subduction with or without slab roll-back (*e.g.*, Blanco and Spakman, 1993; Ruiz-Constán *et al.*, 2011; González-Castillo *et al.*, 2015; Do Couto *et al.*, 2016; Spakman *et al.*, 2018). GPS studies (Koulali *et al.*, 2011; Palano *et al.*, 2015) show a southward movement of the Rif Cordillera, possibly due to the drag of a subducted slab according to mantle tomographies (*e.g.*, Faccena *et al.*, 2014 and references therein) or subduction following mantle delamination (Baratin *et al.*, 2016). This work demonstrated for the first time that the westward migration of the deformation can also be observed in the shallow sedimentary record at a local scale. However, the development of the fault systems as part of a transtensional basin related with the Al Idrissi fault zone southern termination as a horsetail splay (d'Acremont *et al.*, 2014; Lafosse *et al.*, 2020) does not fully justify this westward migration. The continuous Al Idrissi fault zone activity may increase the brittle deformation at the fault tip and the enlargement of the Al Hoceima Bay system, but it does not explain why the eastern faults decrease their activity while the western ones increase it. In order to fully support this migration model, other regional processes need to be taken into account. For the purposes of this paper, the progressive inactivation of the Trougout (relayed over by western faults) and eastern bay faults is proposed to be an indication of the NW movement of the South Alboran indenter described in Estrada *et al.* (2018) interacting with the deformation of the Rif that moves towards the SW (Fig. 5.9).

Overall, our results fit with the proposal of Fadil *et al.* (2006) that the central Alboran Sea and the Rif front should represent two segments of the Africa-Eurasia collisional plate boundary zone in the westernmost Mediterranean. These compressional boundaries are linked by the Al-Idrissi-Bokkoya left lateral fault system and continue eastwards through the right lateral Yusuf fault system (Fig. 5.9). This hypothesis is in coherence with crustal velocity models which shows a strong thinning of the crust in the Nekor basin (e. g., Koulali *et al.*, 2011; Palano *et al.*, 2015) in a setting with NW-SE compression and orthogonal NE-SW extension (*e.g.*, Stich *et al.*, 2005; Stich *et al.*, 2006; Neres *et al.*, 2016).

This automation of throw backstripping has been successful in the analysis of a large number syn-sedimentary faults in Al Hoceima Bay at the same time and provided throw maps in a zone densely faulted, so the migration of the activity inside the system can be seen without analyzing fault by fault. It may be also applied to growth fault systems like that of the Gulf of Mexico (Worrall and Snelson, 1989), Eastern Mediterranean (Baudon and Cartwright, 2008) or Niger Delta (Back *et al.*, 2006). The method could also be useful in transtensional fault zones like the Southern Dead Sea Fault (Smit *et al.*, 2010) and the western tip of Enriquillo-Plantain Garden Fault Zone in Haiti (Leroy *et al.*, 2015), and may improve the analysis of major changes in the style of deformation of complex regions like the Aegean (Sakellariou and Tsamppouraki-Kraounaki, 2019).

5.6 Conclusion

Faulting throw analysis in the Al Hoceima Bay reveals a westward increase and migration of the deformation. The automation of the throw backstripping method applied on 672 faults has resulted to be an effective and quickly tool to decipher the distribution of tectonic activity during the last 280 kyr, considering the deformation of the recent and widespread marine regressive surfaces by high dipping faults. The detailed analysis of the fault throws, their distribution through time and their quantification was achieved for the first time in the zone, which demonstrates a westward increase and migration of the deformation towards the western part of the Al Hoceima Bay and offshore Bokkoya Massif. Our data indicate a present day highest deformation rate in the faults next to the most populated city, Al Hoceima, reaching values of throw up to 0.47 mm/yr. Therefore, this automation of the throw backstripping method may be adopted as a basis for reliable and accurate seismic (and potential tsunami) hazard assessments by detecting the zones where further and detailed studies should be carried out.

The westward migration of deformation in the Al Hoceima Bay is framed into the Westernmost Mediterranean geodynamic model, and it may be the result of the interaction between the NW movement of the South Alboran indenter and the back Rif south-westwards displacement due to subduction with roll-back, the sinking of the subducted continental slab, or mantle delamination.

The automation of the throw backstripping may also be applied to growth fault systems in similar contexts of the Eastern Mediterranean and western Atlantic in the Gulf of Mexico and Caribbean Sea. The high accuracy degree in constraining the timing and rate of fault activity will contribute to improve the seismic hazard assessment.

Acknowledgments

We acknowledge the Editor and the reviewers their future suggestions which will helpt to improve the final version of the manuscript. We also acknowledge the support of the different institutions that have funded this study.

Data Availability Statement

Seismic reflection and bathymetric data collected during the MARLBORO 2 cruise https://doi.org/10.17600/12450090.

References

Andrieux, J., (1971). La structure du Rif Central. Étude des relations entre la tectonique de compression et les nappes de glissement dans un tronçon de la chaîne alpine. Ed. Notes et Mém. Serv. Géol. Maroc.

Aït Brahim, L., and Chotin, P. (1990). Oriental Moroccan Neogene volcanism and strike-slip faulting. *Journal of African Earth Sciences,* 11(3), 273-280.

Azdimousa, A., Bourgois, J., Poupeau, G., and Montigny, R. (1998) : Histoire thermique du massif de Ketama (Maroc): sa place en Afrique du Nord et dans les Cordilleres Betiques. *C. R. Acad. Sci.,* 326, 847–853.

Back, S., Höcker, C., Brundiers, M. B., and Kukla, P. A. (2006). Three-dimensional-seismic coherency signature of Niger Delta growth faults: integrating sedimentology and tectonics. *Basin Research*, 18(3), 323-337.

Balanyá, J. C., Crespo-Blanc, A., Díaz Azpiroz, M., Expósito, I., and Luján, M. (2007). Structural trend line pattern and strain partitioning around the Gibraltar Arc accretionary wedge: insights as to the mode of orogenic arc building. *Tectonics,* 26(2). DOI: 10.1029/2005TC001932

Baratin, L. M., Mazzotti, S., Chéry, J., Vernant, P., Tahayt, A., and Mourabit, T. (2016). Incipient mantle delamination, active tectonics and crustal thickening in Northern Morocco: Insights from gravity data and numerical modelling. *Earth and Planetary Science Letters,* 454, 113-120.

Baudon, C., and Cartwright, J. (2008). Early stage evolution of growth faults: 3D seismic insights from the Levant Basin, Eastern Mediterranean. *Journal of Structural Geology,* 30(7), 888-898

Blanco, M. J., and Spakman, W. (1993). The P-wave velocity structure of the mantle below the Iberian Peninsula: Evidence for subducted lithosphere below southern spain. *Tectonophysics,* 221(1), 13-34. https://doi.org//10.1016/0040-1951(93)90025-F

Bourgois, J., Mauffret, A., Ammar, A., and Demnati, A. (1992). Multichannel seismic data imaging of inversion tectonics of the Alboran Ridge (western Mediterranean Sea). *Geo-Marine Letters,* 12(2-3), 117–122. https://doi.org/10.1007/BF02084921

Calvert, A., Gomez, F., Seber, D., Barazangi, M., Jabour, N., Ibenbrahim, A., and Demnati, A. (1997). An integrated geophysical investigation of recent seismicity in the Al-Hoceima region of North Morocco. *Bull. Seismol. Soc. Am.,* 87*,* 637–651.

Carrapa, B. (2009). Tracing exhumation and orogenic wedge dynamics in the European Alps with detrital thermochronology. *Geology,* 37(12), 1127-1130.

Cartwright, J., Bouroullec, R., James, D., and Johnson, H. (1998). Polycyclic motion history of some Gulf Coast growth faults from high-resolution displacement analysis. *Geology*, 26(9), 819-822.

Carver, R. E. (1968). Differential compaction as a cause of regional contemporaneous faults. *The American Association of Petroleum Geologists Bulletin,* 52(3), 414-419.

Chalouan, A., (1986). Les nappes Ghomarides (Rif Septentrional, Maroc), un terrain varisque dans la Chaine Alpine. [doctoral these],[Strasbourg, France]: Université Louis Pasteur

Chalouan, A., Michard, A., Kadiri, K., Negro, F., Lamotte, D., Soto, J.I., and Saddiqi, O. (2008). "The Rif belt," in Continental Evolution. The Geology of Morocco, ed. Springer (Berlin, Heidelberg), 203–302.

Childs, C., Easton, S. J., Vendeville, B. C., Jackson, M. P. A., Lin, S. T., Walsh, J. J., & Watterson, J. (1993). Kinematic analysis of faults in a physical model of growth faulting above a viscous salt analogue. *Tectonophysics*, *228*(3-4), 313-329.

Childs, C., Watterson, J., & Walsh, J. J. (1995). Fault overlap zones within developing normal fault systems. *Journal of the Geological Society*, *152*(3), 535-549. https://doi.org/10.1144/gsjgs.152.3.0535

Comas, M., García-Dueñas, V., and Jurado, M. (1992). Neogene tectonic evolution of the Alboran Sea from MCS data. *Geo-Marine Letters,* 12(2-3), 157–164. https://doi.org/10.1007/BF02084927

Cornell, C. A. (1968). Engineering seismic risk analysis. *Bulletin of the seismological society of America,* 58(5), 1583-1606.

Corsini, M., Chalouan, A., and Galindo-Zaldivar, J. (2014). Geodynamics of the Gibraltar Arc and the Alboran Sea region. *Editoria l /Journal of Geodynamics,* 77*,* 1-3. https://doi.org/10.1016/j.jog.2014.04.005

d'Acremont, E., Gutscher, M. A., Rabaute, A., Mercier de Lépinay, B., Lafosse, M., Poort, J., Ammar, A., Tahayt, A., Le Roy, P., Smit, J., Do Couto, D., Cancaouët, R., Prunier, C., Ercilla, G., and Gorini, C. (2014). High-resolution imagery of active faulting offshore Al Hoceima, Northern Morocco. Tectonophysics*,* 632, 160‑166. https://doi.org/10.1016/j.tecto.2014.06.008

d'Acremont, E., Lafosse, M., Rabaute, A., Teurquety, G., Do Couto, D., Ercilla, G., Juan, C., Mercier de Lépinay, B., Lafuerza, S., Galindo-Zaldívar, J., Estrada, F., Vazquez, J. T., Leroy, S., Poort, J., Ammar, A., and Gorini, C. (2020). Polyphase tectonic evolution of fore-arc basin related to STEP fault as revealed by seismic reflection data from the Alboran Sea (W-Mediterranean). Tectonics, 39(3), e2019TC005885. https://doi.org/10.1029/2019TC005885

Davis, D., Suppe, J., and Dahlen, F. A. (1983). Mechanics of fold-and-thrust belts and accretionary wedges. *Journal of Geophysical Research: Solid Earth,* 88(B2), 1153-1172.

DeMets, C., Gordon, R. G., and Argus, D. F. (2010). Geologically current plate motions. *Geophysical Journal International,* 181(1), 1-80. https://doi.org//10.1111/j.1365-246X.2009.04491.x

Do Couto, D., Gorini, C., Jolivet, L., Lebret, N., Augier, R., Gumiaux, C., Acremont, E., Ammar, A., Jabour, H, and Auxietre, J. L. (2016). Tectonic and stratigraphic evolution of the Western Alboran Sea Basin in the last 25 Myrs. *Tectonophysics,* 667-668*,* 208-311. http://dx.doi.org/10.1016/j.tecto.2016.03.020

El Alami, S. O., Tadili, B. A., Cherkaoui, T. E., Medina, F., Ramdani, M., Brahim, L. A., and Harnafi, M. (1998) The Al Hoceima Earthquake of May 26, 1994 and its aftershocks: A seismotectonic study. *Anali di Geofisica,* 41, 519–537.

El Azzouzi, M., Bernard-Griffiths, J., Bellon, H., Maury, R.C., Pique, A., Fourcade, S., Cotten, J., and Hernandez, J., (1999). Evolution des sources du volcanisme marocain au cours du Neogene. *C. R. Acad. Sci. París,* 329*,* 95–102.

Estrada, F., Galindo-Zaldivar, J., Vázquez, J. T., Ercilla, G., D'Acremont, E., Alonso, B., and Gorini, C. (2018). Tectonic indentation in the central Alboran Sea (westernmost Mediterranean). *Terra Nova,* 30(1), 24-33. https://doi.org//10.1111/ter.12304

Faccena, C., Becker, T. W., Auer, L., Billi, A., Boschi, L., Brun, J. P., Capitanio, F. A., Funiciello, F., Horvàth, F., Jolivet, L., Piromallo, C., Royden, L., Rossetti, F. and Serpelloni, E. (2014). Mantle dynamics in the Mediterranean. *Rev. Gephys.,* 52*,* 283-332. doi:10.1002/2013RG000444

Fadil, A., Vernant, P., McClusky, S., Reilinger, R., Gomez, F., Sari, D. B., Mourabit, T., Feigl, K., and Barazangi, M. (2006). Active tectonics of the western Mediterranean: Geodetic evidence for rollback of a delaminated subcontinental lithospheric slab beneath the Rif Mountains, Morocco. *Geology*, 34(7), 529-532. https://doi.org/10.1130/G22291.1

Frigola, J., Canals, M., Cacho, I., Moreno Caballud, A., Sierro, F. J., Flores, J. A., Berné, S., Jouet, G., Dennielou, B., Herrera, G., Pasqual, C., Grimalt, J. O., Galavazi, M., and Schneider, R. (2012). A 500 kyr record of global sea level oscillations in the Gulf of Lion, Mediterranean Sea: new insights into MIS 3 sea level variability. *Clim. Past,* 8, 1067-1077. DOI: 10.5194/cp-8-1067-2012

Frizon de Lamotte, D., (1985). La structure du Rif Oriental (Maroc). Rôle de la tectonique longitudinale et importance des fluides. [doctoral these]. [Paris, France]: Université Pierre et Marie Curie

Galadini, F., and Messina, P. (2004). Early–Middle Pleistocene eastward migration of the Abruzzi Apennine (central Italy) extensional domain. *Journal of Geodynamics*, 37(1), 57-81.

Galindo-Zaldivar, J., Chalouan, A., Azzouz, O., Sanz de Galdeano, C., Anahnah, F., Ameza, L., Ruano, P., Pedrera, A., Ruiz-Constán, A., Marín-Lechado, C., Benmakhlouf, M., López-Garrido, A.C., Ahmamou, M., Saji, R., Roldán-García, F.J., Akil, M., and Chabli, A. (2009). Are the seismological and geological observations of the Al Hoceima (Morocco, Rif) 2004 earthquake (M = 6.3) contradictory? *Tectonophysics,* 475, 59‐67.

Galindo-Zaldívar, J., Azzouz, O., Chalouan, A., Pedrera, A., Ruano, P., Ruiz-Constán, A., Sanz de Galdeano, C., Marín-Lechado, C., López-Garrido, A. C., Anahnah, F., and Benmakhlouf, M. (2015). Extensional tectonics, graben development and fault terminations in the eastern Rif (Bokoya–Ras Afraou area). *Tectonophysics*, 663, 140-149. https://doi.org/10.1016/j.tecto.2015.08.029

Galindo-Zaldivar, J., Ercilla, G., Estrada, F., Catalán, M., d' Acremont, E., Azzouz, O., Casas, D., Chourak, M., Vazquez, J. T., Chalouan, A., Sanz de Galdeano, C., Benmakhlouf, M., Gorini, C., Alonso, B., Palomino, D., Rengel, J. A., and Gil, A. J. (2018). Imaging the growth of recent faults: The case of 2016–2017 seismic sequence sea bottom deformation in the Alboran Sea (western Mediterranean). *Tectonics,* 37, 2513–2530. https://doi.org/10.1029/2017TC004941

García-Dueñas, V., Balanyá, J.C., and Martínez-Martínez, J.M., (1992). Miocene extensional detachments in the outcropping basement of the Northern Alboran Basin (Betics) and their tectonic implications. *Geo-Mar. Lett.* 12, 88–95.

Giba, M., Nicol, A., & Walsh, J. J. (2010). Evolution of faulting and volcanism in a back-arc basin and its implications for subduction processes. *Tectonics*, *29*(4).

Giba, M., Walsh, J. J., & Nicol, A. (2012). Segmentation and growth of an obliquely reactivated normal fault. *Journal of Structural Geology*, *39*, 253-267.

Giba, M., Walsh, J. J., Nicol, A., Mouslopoulou, V., & Seebeck, H. (2013). Investigation of the spatio-temporal relationship between normal faulting and arc volcanism on million-year time scales. *Journal of the Geological Society*, *170*(6), 951-962.

Goldsworthy, M., and Jackson, J. (2001). Migration of activity within normal fault systems: examples from the Quaternary of mainland Greece. *Journal of Structural Geology*, 23(2-3), 489-506.

Gomez de la Pena, L., Ranero, C. R., & Gràcia, E. (2018). The crustal domains of the Alboran Basin (western Mediterranean). *Tectonics*, *37*(10), 3352-3377.

González-Castillo, L., Galindo-Zaldivar, J., de Lacy, M. C., Borque, M. J., Martinez-Moreno, F. J., García-Armenteros, J. A., and Gil, A. J. (2015). Active rollback in the Gibraltar Arc: Evidences from CGPS data in the western Betic Cordillera. *Tectonophysics,* 663, 310-321.

Gràcia, E., Grevemeyer, I., Bartolomé, R., Perea, H., Martínez-Loriente, S., de la Peña, L. G., ... & Ranero, C. R. (2019). Earthquake crisis unveils the growth of an incipient continental fault system. *Nature communications*, *10*(1), 1-12.

Grant, K. M., Rohling, E. J., Ramsey, C. B., Cheng, H., Edwards, R. L., Florindo, F., Heslop, D., Marra, F, Roberts, A. P., Tamisiea, M. E., and Williams, F. (2014). Sea-level variability over five glacial cycles. *Nature communications,* 5(1), 1-9.

Hidas, K., Garrido, C. J., Booth-Rea, G., Marchesi, C., Bodinier, J. L., Dautria, J. M., Louni-Hacini, A., and Azzouni-Sekkal, A. (2019). Lithosphere tearing along STEP faults and synkinematic formation of lherzolite and wehrlite in the shallow subcontinental mantle. *Solid Earth*, 10(4), 1099-1121. https://doi.org/10.5194/se-10-1099-2019

Jackson, C. A.-L., Bell, R. E., Rotevatn, A., and Tvedt, A. B. M. (2017). Techniques to determine the kinematics of synsedimentary normal faults and implications for fault growth models. *Geological Society, London, Special Publications,* 439. https://doi.org/10.1144/SP439.22

Juan, C., Ercilla, G., Hernández-Molina, J. F., Estrada, F., Alonso, B., Casas, D., García, M., Farrán, M., Llave, E., Palomino, D., Vázquez, J. T., Medialdea, T., Gorini, C., d'Acremont, E., El Moumni, B., and Ammar, A. (2016). Seismic evidence of current-controlled sedimentation in the Alboran Sea during the Pliocene and Quaternary: Palaeoceanographic implications. *Marine Geology,* 378, 292–311. https://doi.org/10.1016/j.margeo.2016.01.006

Keller, E. A., and Pinter, N. (1996). Active tectonics (Vol. 19). Upper Saddle River, NJ: Prentice Hall.

Koulali, A., Ouazar, D., Tahayt, A., King, R.W., Vernant, P., Reilinger, R.E., McClusky, S., Mourabit, T., Davila, J.M., and Amraoui, N. (2011). New GPS constraints on active deformation along the Africa–Iberia plate boundary. *Earth Planet. Sci. Lett. 308*, 211–217.

Lafosse, M., d'Acremont, E., Rabaute, A., Mercier de Lépinay, B., Tahayt, A., Ammar, A., and Gorini, C. (2016). Evidence of Quaternary transtensional tectonics in the Nekor basin (NE Morocco). *Basin Research,* 29(4), 470–489. https://doi.org/10.1111/bre.12185

Lafosse, M., Gorini, C., Le Roy, P., Alonso, B., d'Acremont, E., Ercilla, G., Rabineau, M., Vázquez, J. T., Rabaute, A., and Ammar, A. (2018). Late Pleistocene-Holocene history of a tectonically active segment of the continental margin (Nekor basin, Western Mediterranean, Morocco). *Marine and Petroleum Geology,* 97, 370-389. https://doi.org/10.1016/j.marpetgeo.2018.07.022

Lafosse, M., d'Acremont, E., Rabaute, A., Estrada, F., Jollivet-Castelot, M., Vazquez, J. T., Galindo-Zaldivar, J., Ercilla, G., Alonso, B., Smit, J., Ammar, A., and Gorini, C. (2020). Plio-Quaternary tectonic evolution of the southern margin of the Alboran Basin (Western Mediterranean). *Solid Earth*, 11(2), 741-765. https://doi.org/10.5194/se-11-741-2020

Leblanc, D., and Olivier, P. (1984). Role of strike-slip faults in the Betic-Rifian orogeny. *Tectonophysics* 101, 345–355.

Leroy, S., Ellouz-Zimmermann, N., Corbeau, J., Rolandone, F., de Lepinay, B. M., Meyer, B., Momplaisir, R., Granja-Bruna, J. L., Battani, A., Baurion, C., Burov, E., Clouard, V., Deschamps, R., Gorini, C., Hamon, Y., Lafosse, M., Leonel, J., Pourhiet, L., Llanes-Estrada, P., Loget, N., Lucazeau, F., Pillot, D., Poort, J., Tankoo, K. R., Cuevas, J. L., Alcaide, J. F., Poix, C. J., Muñoz-Martin, A., Mitton, S., Rodriguez, Y., Schmitz, J., Seeber, L., Carbo-Gorosabel, A., and Muñoz, S. (2015). Segmentation and kinematics of the North America-Caribbean plate boundary offshore Hispaniola. *Terra Nova*, 27(6), 467-478. https://doi.org/10.1111/ter.12181

Mancilla, F. d. L., Stich, D., Berrocoso, M., Martín, R., Morales, J., Fernandez-Ros, A., Páez, R., and Pérez-Peña, A. (2013). Delamination in the Betic Range: Deep structure, seismicity, and GPS motion. *Geology,* 41(3), 307-310. https://doi.org//10.1130/G33733.1

Mansfield, C. S., and Cartwright, J. A., 1996, High resolution displacement mapping from 3-D seismic data. *Journal of Structural Geology,* 18, 249–263.

Marín-Lechado, C., Galindo-Zaldívar, J., Rodríguez-Fernández, L. R., and González-Lodeiro, F. (2004). Faulted hybrid joints: an example from the Campo de Dalias (Betic Cordilleras, Spain). *Journal of Structural Geology,* 26, 2025-2037.

Martínez-García, P., Comas, M., Soto, J. I., Lonergan, L., & Watts, A. B. (2013). Strike-slip tectonics and basin inversion in the Western Mediterranean: the Post-Messinian evolution of the Alboran Sea. *Basin Research*, *25*(4), 361-387.

Martínez-García, P., Comas, M., Lonergan, L., and Watts, A. B. (2017). From extension to shortening: Tectonic inversion distributed in time and space in the Alboran Sea, western Mediterranean. *Tectonics,* 36, 2777–2805. https://doi.org/10.1002/2017TC004489

Mauffret, A., Ammar, A., Gorini, C., and Jabour, N. (2007). The Alboran Sea (Western Mediterranean) revisited with a view from the Moroccan Margin. *Terra Nova,* 19, 195–203.

McCalpin, J. P. (Ed.). (2009). *Paleoseismology*. Academic Press.

Meyer, V., Nicol, A., Childs, C., Walsh, J. J., & Watterson, J. (2002). Progressive localisation of strain during the evolution of a normal fault population. *Journal of Structural Geology*, *24*(8), 1215-1231.

Milia, A., and Torrente, M. M. (2018). Extensional Messinian basins in the Central Mediterranean (Calabria, Italy): new stratigraphic and tectonic insights. *Oil and Gas Science and Technology–Revue d'IFP Energies nouvelles*, 73, 45. https://doi.org/10.2516/ogst/2018040

Neres, M., Carafa, M. M. C., Fernandes, R. M. S., Matias, L., Duarte, J. C., Barba, S., and Terrinha, P. (2016). Lithospheric deformation in the Africa-Iberia plate boundary: Improved neotectonic modeling testing a basal-driven Alboran plate. *Journal of Geophysical Research: Solid Earth*, 121(9), 6566-6596. https://doi.org/10.1002/2016JB013012

Nicol, A., Walsh, J. J., Watterson, J., & Underhill, J. R. (1997). Displacement rates of normal faults. *Nature*, *390*(6656), 157-159.

Nicol, A., Walsh, J., Berryman, K., & Nodder, S. (2005). Growth of a normal fault by the accumulation of slip over millions of years. *Journal of Structural Geology*, *27*(2), 327-342.

Nicol, A., Walsh, J., Berryman, K., & Villamor, P. (2006). Interdependence of fault displacement rates and paleoearthquakes in an active rift. *Geology*, *34*(10), 865-868.

Palano, M., González, P. J., and Fernández, J. (2015). The Diffuse Plate boundary of Nubia and Iberia in the Western Mediterranean: Crustal deformation evidence for viscous coupling and

fragmented lithosphere. *Earth and Planetary Science Letters,* 430, 439-447. http://dx.doi.org/10.1016/j.epsl.2015.08.040

Perea, H., Gràcia, E., Martínez-Loriente, S., Bartolome, R., de la Peña, L. G., de Mol, B., ... & Dañobeitia, J. J. (2018). Kinematic analysis of secondary faults within a distributed shear-zone reveals fault linkage and increased seismic hazard. *Marine Geology*, *399*, 23-33.

Petersen, K., Clausen, O. R., & Korstgård, J. A. (1992). Evolution of a salt-related listric growth fault near the D-1 well, block 5605, Danish North Sea: displacement history and salt kinematics. *Journal of Structural Geology*, *14*(5), 565-577.

Petit, C., Le Pourhiet, L., Scalabrino, B., Corsini, M., Bonnin, M., and Romagny, A. (2015). Crustal structure and gravity anomalies beneath the Rif, northern Morocco: implications for the current tectonics of the Alboran region. *Geophysical Journal International*, 202(1), 640-652. https://doi.org/10.1093/gji/ggv169

Phillips, T. B., Jackson, C. A. L., Bell, R. E., and Duffy, O. B. (2018). Oblique reactivation of lithosphere-scale lineaments controls rift physiography – the upper-crustal expression of the Sorgenfrei-Tornquist Zone, offshore southern Norway. *Solid Earth,* 9, 403-429. https://doi.org/10.5194/se-9-403-2018

Poujol, A., Ritz, J. F., Tahayt, A., Vernant, P., Condomines, M., Blard, P. H., Billant, J., Vacher, L., Tibari, B., Hni, L., and Idrissi, A. K. (2014). Active tectonics of the Northern Rif (Morocco) from geomorphic and geochronological data. *Journal of Geodynamics,* 77, 70-88.

Ruiz-Constán, A., Galindo-Zaldivar, J., Pedrera, A., Célérier, B., and Marín-Lechado, C. (2011). Stress distribution at the transition from subduction to continental collision (northwestern and central Betic Cordillera). *Geochemistry, Geophysics, Geosyst-ems,* 12(12) https://doi.org////doi.org/10.1029/2011GC003824

Sakellariou, D., and Tsampouraki-Kraounaki, K. (2019). "Plio-Quaternary extension and strike-slip tectonics in the Aegean," in Transform Plate Boundaries and Fracture Zones, Elsevier, 339-374. https://doi.org/10.1016/B978-0-12-812064-4.00014-1

Sanz de Galdeano, C., and Alfaro, P. (2004). Tectonic significance of the present relief of the Betic Cordillera. *Geomorphology,* 63*,* 175–190. https://doi.org/10.1016/j.geomorph.2004.04.002

Seber, D., Barazangi, M., Ibenbrahim, A., and Demnati, A. (1996). Geophysical evidence for lithospheric delamination beneath the Alboran Sea and Rif–Betic mountains. *Nature,* 379(6568), 785–790.

Seebeck, H., Nicol, A., Villamor, P., Ristau, J., & Pettinga, J. (2014). Structure and kinematics of the Taupo Rift, New Zealand. *Tectonics*, *33*(6), 1178-1199.

Smit, J., Brun, J. P., Cloetingh, S., and Ben-Avraham, Z. (2010). The rift-like structure and asymmetry of the Dead Sea Fault. *Earth and Planetary Science Letters*, 290(1-2), 74-82. https://doi.org/10.1016/j.epsl.2009.11.060

Spakman, W., Chertova, M. V., van den Berg, A., and van Hinsbergen, D. J. (2018). Puzzling features of western Mediterranean tectonics explained by slab dragging. *Nature Geoscience*, 11(3), 211-216. https://doi.org/10.1038/s41561-018-0066-z

Stich, D., Mancilla, F., Baumont, D., and Morales, J. (2005). Source analysis of the Mw 6.3 2004 Al Hoceima Earthquake (Morocco) using regional apparent source time functions. *J. Geophys. Res.,* 110, B06306. doi: 10.1029/2004JB003366

Stich, D., Serpelloni, E., Mancilla, F., and Morales, J. (2006). Kinematics of the Iberia-Maghreb plate contact from seismic moment tensors and GPS observations. *Tectonophysics,* 426(3-4)*,* 295-317. doi: 10.1016/j.tecto.2006.08.004

Van der Woerd, J., Dorbath, C., Ousadou, F., Dorbath, L., Delouis, B., Jacques, E., Tapponier, P., Hahou, Y., Menzhi, M., Frogneux, M., and Haessler, H. (2014). The Al Hoceima Mw 6.4 earthquake of 24 February 2004 and its aftershocks sequence. *Journal of Geodynamics,* 77, 89–109. https://doi.org/10.1016/j.jog.2013.12.004

Vernant, P., Fadil, A., Mourabit, T., Ouazar, D., Koulali, A., Davila, J. M., Garate, J., McClusky, S., and Reilinger, R. (2010). Geodetic constraints on active tectonics of the Wester Mediterranean: Implications for the kinematics and dynamics of the Nubia-Eurasia plate boundary zone. *Journal of Geodynamics,* 49, 123-129.

Vissers, R.L.M., Platt, J.P., and van der Wal, D. (1995). Late orogenic extension of the Betic Cordillera and the Alboran Domain: a lithospheric view. *Tectonics,* 14, 786–803.

Walsh, J. J., Childs, C., Imber, J., Manzocchi, T., Watterson, J., & Nell, P. A. R. (2003). Strain localisation and population changes during fault system growth within the Inner Moray Firth, Northern North Sea. *Journal of Structural Geology*, *25*(2), 307-315.

Wang, Z. (2011). Seismic Hazard Assessment: Issues and Alternatives. *Pure Appl. Geophys.,* 168*,* 11-25. DOI: 10.1007/s00024-010-0148-3

Wesnousky, S. G. (1986). Earthquakes, Quaternary faults, and seismic hazard in California. *Journal of Geophysical Research: Solid Earth*, 91(B12), 12587-12631.

Worrall, D. M., and Snelson, S. (1989). Evolution of the northern Gulf of Mexico. The geology of North America; an overview: Geological Society of America, v. A, 97-138.

CHAPTER 6

The Campo de Dalías GNSS Network Unveils the Interaction between Roll-Back and Indentation Tectonics in the Gibraltar Arc.

J. Galindo-Zaldívar [1,2,*], A.J. Gil [3,4], V. Tendero [2], M.J. Borque [3,4], G. Ercilla [5], L. Gonzalez-Castillo [1], A. Sánchez-Alzola [6], M.C. Lacy [3,4], F. Estrada [5], M. Avilés [3,4], P. Alfaro [7], A. Madarieta-Txurruka [1] and F. Chacón [3,4]

[1]Departamento de Geodinámica, Universidad de Granada, 18071 Granada, Spain

[2]Instituto Andaluz de Ciencias de la Tierra (CSIC-UGR), 18071 Granada, Spain

[3]Departamento Ing. Cartográfica, Geodésica y Fotogrametría, Universidad de Jaén, Campus de Las Lagunillas, 23071 Jaén, Spain

[4]Centro de Estudios Avanzados en Ciencias de la Tierra, Energía y Medio Ambiente (CEACTEMA), Universidad de Jaén, Campus de Las Lagunillas, 23071 Jaén, Spain

[5]Instituto de Ciencias del Mar, CSIC, Continental Margins Group, 08003 Barcelona, Spain

[6]Departamento de Estadística e Investigación Operativa, Universidad de Cádiz, 11510 Puerto Real, Spain

[7]Departamento de Ciencias de la Tierra y del Medio Ambiente, Facultad de Ciencias, Universidad de Alicante, 03080 Alicante, Spain

Published on:

Sensors, Volume 22 (6). (March 2022)

https://doi.org/10.3390/s22062128

(Received 4 February 2022, Accepted 7 March 2022, Published 9 March 2022)

JCR(2020): 3.576 (Q1)

Abstract

The Gibraltar Arc includes the Betic and Rif Cordilleras surrounding the Alboran Sea; it is formed at the northwest–southeast Eurasia–Nubia convergent plate boundary in the westernmost Mediterranean. Since 2006, the Campo de Dalias GNSS network has monitored active tectonic deformation of the most seismically active area on the north coast of the Alboran Sea. Our results show that the residual deformation rates with respect to Eurasia range from 1.7 to 3.0 mm/year; roughly homogenous west-southwestward displacements of the northern sites occur, while the southern sites evidence irregular displacements towards the west and northwest. This deformation pattern supports simultaneous east-northeast–west-southwest extension, accommodated by normal and oblique faults, and north-northwest–south-southeast shortening that develops east-northeast–west-southwest folds. Moreover, the GNSS results point to dextral creep of the main northwest–southeast Balanegra Fault. These GNNS results thus reveal, for the first time, present-day interaction of the roll-back tectonics of the Rif–Gibraltar–Betic slab in the western part of the Gibraltar Arc with the indentation tectonics affecting the eastern and southern areas, providing new insights for improving tectonic models of arcuate orogens.

Keywords: GNSS network, active fold and fault interaction, roll-back, indentation tectonics, Gibraltar Arc

6.1 Introduction

GNSS networks make it possible to determine the present-day strain field, thereby contributing to our overall understanding of active tectonic processes (Elliot *et al.*, 2016). Regional networks provide valuable new data on plate motion (Kreemer *et al.*, 2014), whereas local networks focus on the most active tectonic structures, mainly

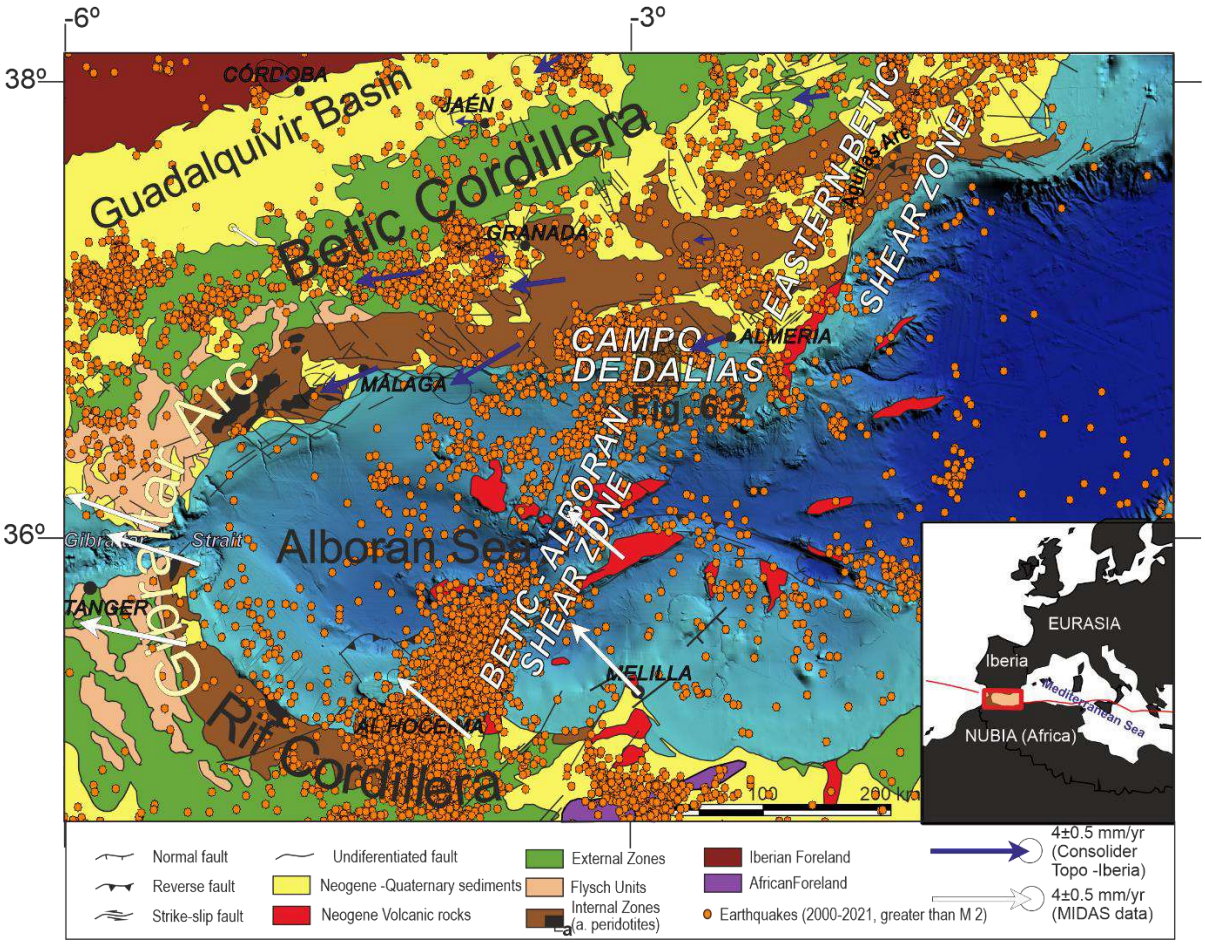

Figure 6.1. Regional geological setting and seismicity of the Gibraltar Arc: Major geological units are included onshore. Offshore, the main tectonic structures are indicated with detailed bathymetry. Earthquake data from IGN (www.ign.es, accessed on 1 February 2022); GNSS displacement in the central and eastern Betic Cordillera from the Consolider Topo-Iberia network (Garate *et al.*, 2015; Galindo-Zaldivar *et al.*, 2015; Gonzalez-Castillo *et al.*, 2015), and in the Rif Cordillera, Gibraltar Strait, and central Alboran Sea from MIDAS velocity fields, Nevada Geodetic Laboratory (http://geodesy.unr.edu/velocities/midas.IGS14.txt, accessed on 20 February 2022). The location of the Campo de Dalias study area (Fig. 2) is indicated.

formed at plate boundaries. The networks may characterize the fold (Tsukahara and Takada, 2018) or fault activity as having creep or seismic behavior (Azzaro *et al.*, 2020). Recent geological evolution derived from field geological and geophysical studies is completed through analysis of the active tectonic deformation provided by

geodetic data (Allmendinger *et al.*, 2009). Moreover, in coastal areas, the seaward continuity of tectonic structures offers a stage to integrate complementary—offshore and onshore—geological observations (Vardar *et al.*, 2021).

The Gibraltar Arc (Fig. 6.1) is an Alpine arched tectonic belt developed since the Cenozoic at the Eurasia–Nubia (Africa) plate boundary (Platt and Vissers, 1989), currently undergoing a regional northwest–southeast convergence rate of 4.5 to 5 mm/year (Argus *et al.*, 1989; DeMets *et al.*, 1990; 1994; Nocquet, 2012; Sparacino *et al.*, 2020); it formed as a result of the Betic Cordillera's connection through the Strait of Gibraltar to the Rif Cordillera, surrounding the Alboran Sea, in the westernmost Mediterranean Sea.

In 2006, we installed a non-permanent GNSS network in the western Campo de Dalias (Marín-Lechado *et al.*, 2010). The network was initially intended to quantify the activity of the northwest–southeast normal Balanegra Fault—one of the most active faults in the area—related to the 1993–94 seismic series. The throw of the Balanegra Fault determined the straight orientation of the coastline, separating the northeast uplifted Campo de Dalias block from the southwest downthrown block, located below sea level. Vertical deformation rates obtained from high-precision leveling lines were analyzed by (Galindo-Zaldivar *et al.*, 2013).

The aim of this paper is to present the quantitative results of the western Campo de Dalias GNSS network (Figs. 6.1 and 6.2) in order to discuss the local interaction of folds and faults. This key area is located at the northern tip of the Betic–Alboran shear zone (Martín *et al.*, 2015; Stich *et al.*, 2006), where the wide fault zone affecting the Alboran Sea reaches the southern boundary of the Betic Cordillera (Fig. 6.1). New GNSS data provide relevant findings about the present-day activity of the roll-back and indentation mechanisms proposed for the Gibraltar Arc's development.

6.2 Geological setting

The internal zones of the Betic and Rif Cordilleras comprise overprinted Alpine metamorphic complexes in the central part of the tectonic arc, including the Alboran Sea; they are separated by a flysch belt from the external zones that would correspond to the former Mesozoic South Iberian and African paleomargins. The Neogene–Quaternary sedimentary basins—including the Guadalquivir foreland basin, the

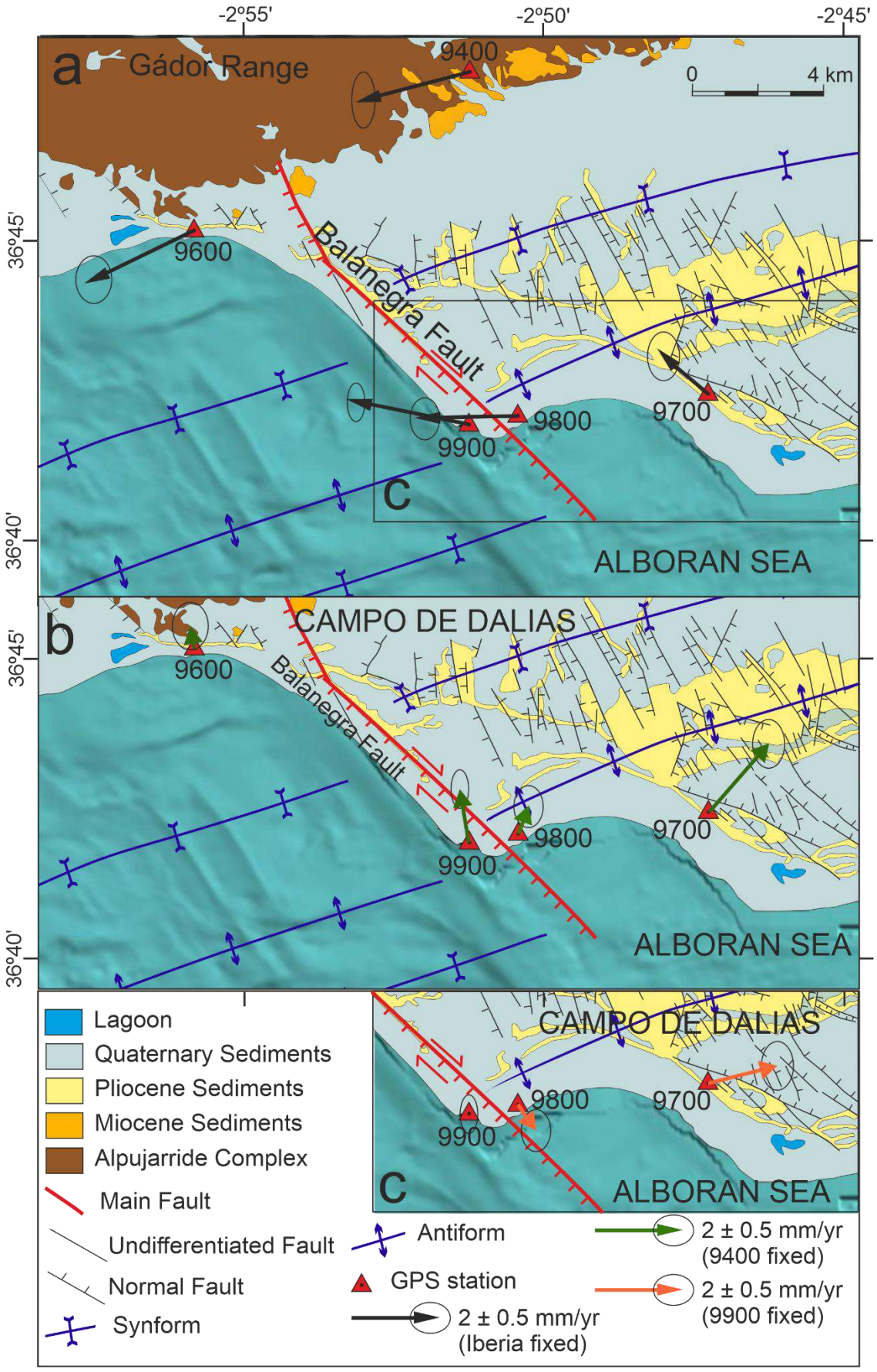
-2°55'
-2°50'
-2°45'
36°45'
36°40'
a
Gádor Range
9400
0
4 km
9600
Balanegra Fault
9800
9900
9700
c
ALBORAN SEA
b
CAMPO DE DALIAS
9600
Balanegra Fault
9800
9900
9700
ALBORAN SEA
CAMPO DE DALIAS
9800
9700
9900
c
ALBORAN SEA
Lagoon
Quaternary Sediments
Pliocene Sediments
Miocene Sediments
Alpujarride Complex
Main Fault
Undifferentiated Fault
Normal Fault
Synform
Antiform
GPS station
2 ± 0.5 mm/yr
(Iberia fixed)
2 ± 0.5 mm/yr
(9400 fixed)
2 ± 0.5 mm/yr
(9900 fixed)

Figure 6.2. Geological sketch of the western Campo de Dalias, including residual GNSS velocities; error ellipses of 95% confidence: (a) Velocities with respect to stable Eurasia. (b) Velocities with respect to the relatively stable Site 9400 (Gador Range). (c) Velocities with respect to the relatively stable Site 9900 (southwest block of the Balanegra Fault).

intramontane basins, and the Alboran Sea—are filled by sediments and, locally, volcanic rocks. The main present-day reliefs, formed since the Tortonian (Braga *et al.*, 2003; Sanz de Galdeano and Alfaro, 2004), are a consequence of the interaction of folds and faults (Galindo-Zaldivar *et al.*, 2003) whose activity continues and is related to present-day seismicity.

Seismic activity in the Eurasia–Africa plate boundary setting occurs along a section over 300 km wide, affecting the Betic and Rif Cordilleras, although the most intense activity can be linked to some specific sectors (Fig. 6.1). One relevant seismic sector is that of a strip from the Al Hoceima area, crossing the Alboran Sea up to the Campo de Dalias, and formerly designated as the Trans-Alboran shear zone (Bousquet, 1979; De Larouzière *et al.*, 1988; Leblanc and Olivier, 1984; Sanz de Galdeano, 1990). More precisely, according to the structures that remained active, the Betic–Alboran shear zone should be underlined (Fig. 6.1, Martín *et al.*, 2015; Stich *et al.*, 2006). This fault zone was responsible for the seismicity in 1992 to 1994 that affected the Al Hoceima area and the Campo de Dalias, the catastrophic earthquake of Al Hoceima in 2004, and the seismic series of the southern Alboran Sea in 2016 (Galindo-Zaldivar *et al.*, 2018). The zone, including Al Idrissi and new faults, constitutes the western boundary of the crustal indenter that is recognized in the Alboran Sea (Estrada *et al.*, 2018), and continues eastward to join the Eastern Betic shear zone (Silva *et al.*, 1993).

The controversial geological and geophysical data for this complex region have led to different tectonic concepts of the development of the Gibraltar Arc since Cenozoic times. Discussion remains alive, offering models mainly based on delamination (Heit *et al.*, 2017; Mandilla *et al.*, 2015) or subduction (Bessière *et al.*, 2021; Gutscher *et al.*, 2002); some include roll-back (Blanco and Spakman, 1993; Fadil *et al.*, 2006; Galindo-Zaldivar *et al.*, 2015; Gonzalez-Castillo *et al.*, 2015; Pérouse *et al.*, 2010), or can be understood as hybrid models (Civiero *et al.*, 2020). Moreover, the central Alboran Sea (Estrada *et al.*, 2018) and the eastern Betics (Coppier *et al.*, 1989; Tendero-Salmerón *et al.*, 2020) are affected by indentation tectonics that might contribute to the escape

tectonics affecting the westernmost Gibraltar Arc (Chalouan *et al.*, 2006). Recent GNSS regional data (Fig. 6.1, Garate *et al.*, 2015; Galindo-Zaldivar *et al.*, 2015; Gonzalez-Castillo *et al.*, 2015) provide a new framework for interpreting present-day tectonic movements and discussing their possible underlying processes. GNSS data on the central and western Betic Cordillera, for example, demonstrate that subduction with roll-back may be active at present in the western Gibraltar Arc (Fadil *et al.*, 2006; Gonzalez-Castillo *et al.*, 2015; Pérouse *et al.*, 2010). In contrast, the kinematics of recent deformations along the eastern Betic Cordillera—*i.e.*, affected by the Eastern Betic shear zone (Borque *et al.*, 2019)—could be attributed to indenter tectonics. To date, however, we lack evidence of the interaction of these two active tectonic mechanisms proposed in the boundary regions.

The Campo de Dalias is a coastal area marking the transition from the southern Betic Cordillera, with a thickened crust, to the Alboran Sea, floored by a thinned continental crust (Galindo-Zaldivar *et al.*, 1997). This region of the internal zones of the Betic Cordillera has an Alpujarride metamorphic basement (marbles, phyllites, and schists) covered by late-Tortonian to Quaternary shallow marine and continental sediments (Marín-Lechado *et al.*, 2005). The area is deformed by a fracture system comprising north–south- to northwest–southeast-faulted extensional and reactivated hybrid joints that accommodate the east-northeast–west-southwest extension (Marín-Lechado *et al.*, 2005). Moreover, east-northeast–west-southwest folds developed since the Tortonian (Marín-Lechado *et al.*, 2007; Pedrera *et al.*, 2015) accommodate the north-northwest–south-southeast shortening related to Eurasia–Nubia convergence.

6.3 GNSS Equipment and Data Processing

The western Campo de Dalias GNSS local network includes five sites (9400, 9600, 9700, 9800, and 9900; Fig. 6.2, Table 6.1), and belongs to a wide regional network (Galindo-Zaldivar *et al.*, 2015) built in 2006 and adequately conserved up to now. The network features self-centering mounting devices anchored to rocks; up to 2010 the measurement equipment comprised LEIAX1202 antennas and Leica Geosystem GX1230 receivers, yet since then LEIAR10 antennas and LEICA Geosystem AR10 receivers have been used. Records reflect at least 96 h for each observation, divided into 24 h and 30 s RINEX file sampling intervals.

Site ID	Velocity (mm yr^{-1})		Uncertainty (mm yr^{-1})		Residual Velocity (mm yr^{-1})	
	East	**North**	East	North	East	North
940	17.5	15.6	±0.3	±0.7	−2.7	−0.9
960	17.6	15.0	±0.4	±0.6	−2.5	−1.6
970	19.0	17.7	±0.4	±0.6	−1.2	1.2
980	17.8	16.4	±0.4	±0.5	−2.4	−0.1
990	17.3	17.2	±0.3	±0.5	−2.9	0.7

Table 6.1. Absolute velocity field in IGS14 reference frame and residual velocity field with respect to stable Eurasia based on the ITRF2014 PMM.

Data processing was done with GIPSY-OASIS software using JPL's orbit and clock products for the GPS constellation (Bertiger *et al.*, 2010). Antenna calibration file, GMF troposphere mapping function, ionosphere TEC values, FES2004 ocean tide loading model (Lyard *et al.*, 2006), and WahrK1 terrestrial tide model were taken into account. Positions were computed according to 300 s sampling of the RINEX observations for the coordinate estimation in the IGS14 reference frame. The linear trend on the position time series (Fig. 6.3) was computed using CATS time series analysis software (Williams, 2008). The model applied to the original time series consists of an intercept, a site rate, and an offset to account for the change of antenna and receiver between the 2011 and 2016 campaigns. Finally, the residual velocity field was calculated with respect to stable Eurasia by subtracting the rigid motion of Eurasia from the ITRF2014 plate motion model (Fig. 6.2a, Altamimi *et al.*, 2017). The plate velocity v_i of a site at position R_i on a plate with rotation described by the angular velocity vector of the plate Ω is given by the vector cross-product $v_i = \Omega \times R_i$. To highlight the activity of local structures, we also determined relative velocities with respect to Sites 9400 (Fig. 6.2b) and 9900 (Fig. 6.2c).

6.4 GNSS Network Results

The GNSS network and position time series (Figs. 6.2 6.3) reveal a displacement pattern evidencing present-day progressive deformation of the region. All of the sites

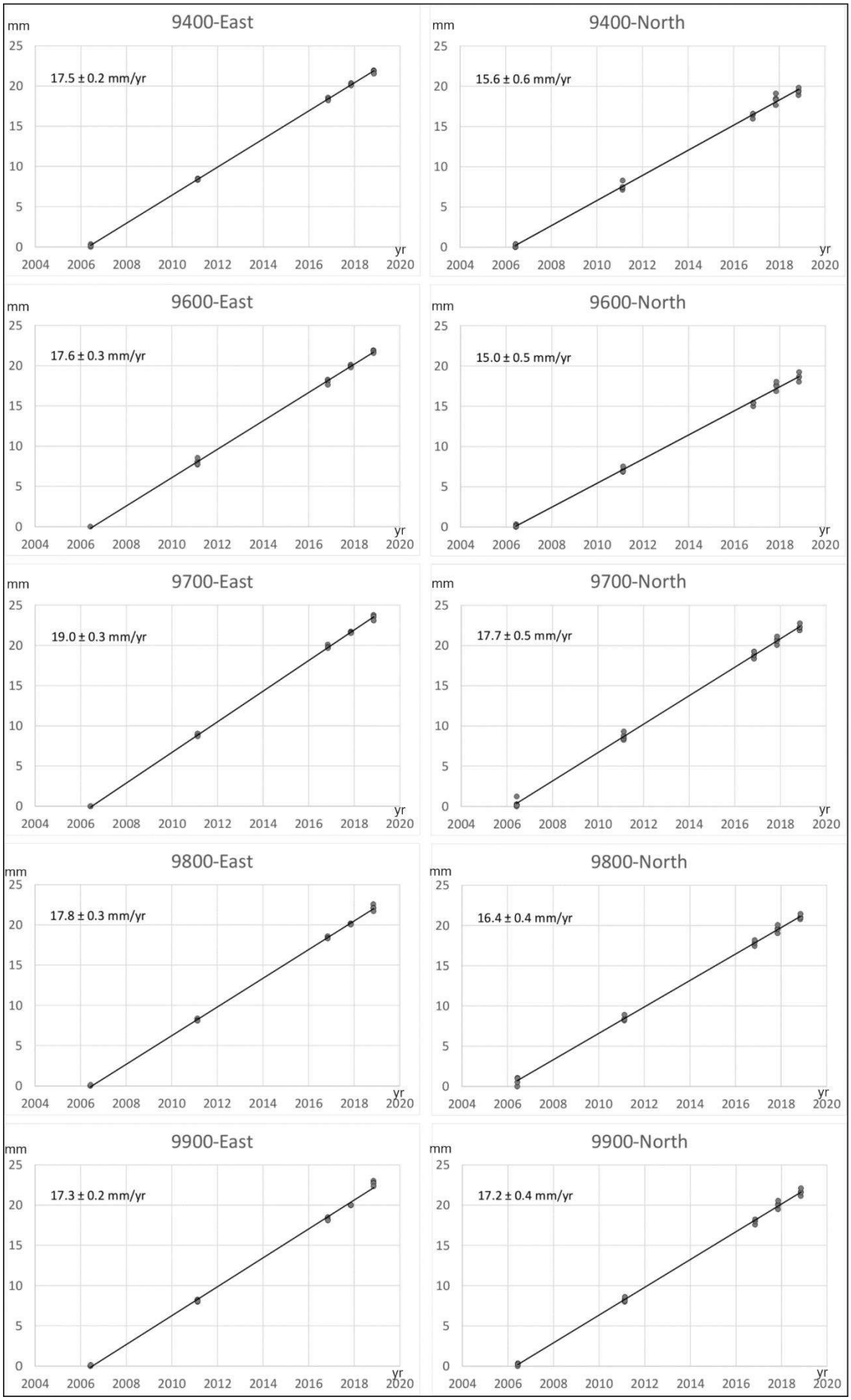
9400-East
17.5 ± 0.2 mm/yr
9400-North
15.6 ± 0.6 mm/yr
9600-East
17.6 ± 0.3 mm/yr
9600-North
15.0 ± 0.5 mm/yr
9700-East
19.0 ± 0.3 mm/yr
9700-North
17.7 ± 0.5 mm/yr
9800-East
17.8 ± 0.3 mm/yr
9800-North
16.4 ± 0.4 mm/yr
9900-East
17.3 ± 0.2 mm/yr
9900-North
17.2 ± 0.4 mm/yr
mm
yr

Figure 6.3. Position time series of the Campo de Dalias network stations (north and east components in millimeters). Absolute velocities are included in Table 6.1.

have a westward component of displacement with respect to stable Eurasia, in agreement with the regional GPS results (Fig. 6.1, Garate *et al.*, 2015). At a local scale, the approximately similar behavior of the two northern sites (9400 and 9600; Figure 2a) would suggest that they should be considered as being located roughly in the same tectonic block, practically unaffected by the present-day activity of the Balanegra Fault, and determinant of its northern tip.

When Site 9400 is taken as a stable reference for the northern region (Fig. 6.2b), Site 9600 shows a short displacement towards the north-northwest, while Site 9900 shows marked displacements towards the north-northwest and Site 9800 is displaced towards the north-northeast. This displacement pattern evidences shortening related to east-northeast–west-southwest fold activity. In turn, Site 9700 displays a relative northeastward displacement, whose northward component could also be compatible with the shortening related to folds.

Finally, in order to analyze the horizontal deformation related to the Balanegra Fault near the coastline, the relative displacement of the network fixing Site 9900 may be considered (Fig. 6.2c). In this framework, Site 9800 has a relative displacement to the southeast, evidencing the dextral activity of the Balanegra Fault close to the coastline. Moreover, the east-northeastward relative displacement of Site 9700 is consistent with east-northeast–west-southwest active extension related to the north-northwest–south-southeast normal fault set and the northwest–southeast Balanegra Fault, over an area probably affected by active fractures not yet identified at the surface.

6.5 Recent Offshore Active Tectonics Deformations West of the Campo de Dalías

Seismic reflection data offshore of the western Campo de Dalias (Figs. 6.4 and 6.5) were analyzed to determine the main features of the active faults and folds. Multichannel and high-resolution seismic reflection profiles from the database of the Instituto de Ciencias del Mar (ICM-CSIC, http://gma.icm.csic.es/sites/default/files/geowebs/OLsurveys/index.htm, accessed on 1 February 2022) were obtained following standard procedures of

acquisition and processing. The southeastward offshore continuity of the Balanegra Fault zone (Fig. 6.4a) is intersected orthogonally by profile 82 ABA-4 (Fig. 6.4b), imaging a roughly vertical deformation zone, with a downthrown eastern block covered by unfaulted sediments with an eastward upraised bathymetric elevation. This geometry may be compatible with an early strike-slip motion that became inactive in this section. Profile AM-139 (Fig. 6.4c), orthogonal to the east-northeast–west-southwest fold system, shows that folds are open and irregular, reaching kilometric sizes, yet deformation increases in depth, supporting the progressive activity. High-resolution profiles to the west of the Balanegra Fault (Fig. 6.5) show that both folds and faults also affect the most recent sediments, even displacing the topography, and should therefore be considered to be active structures.

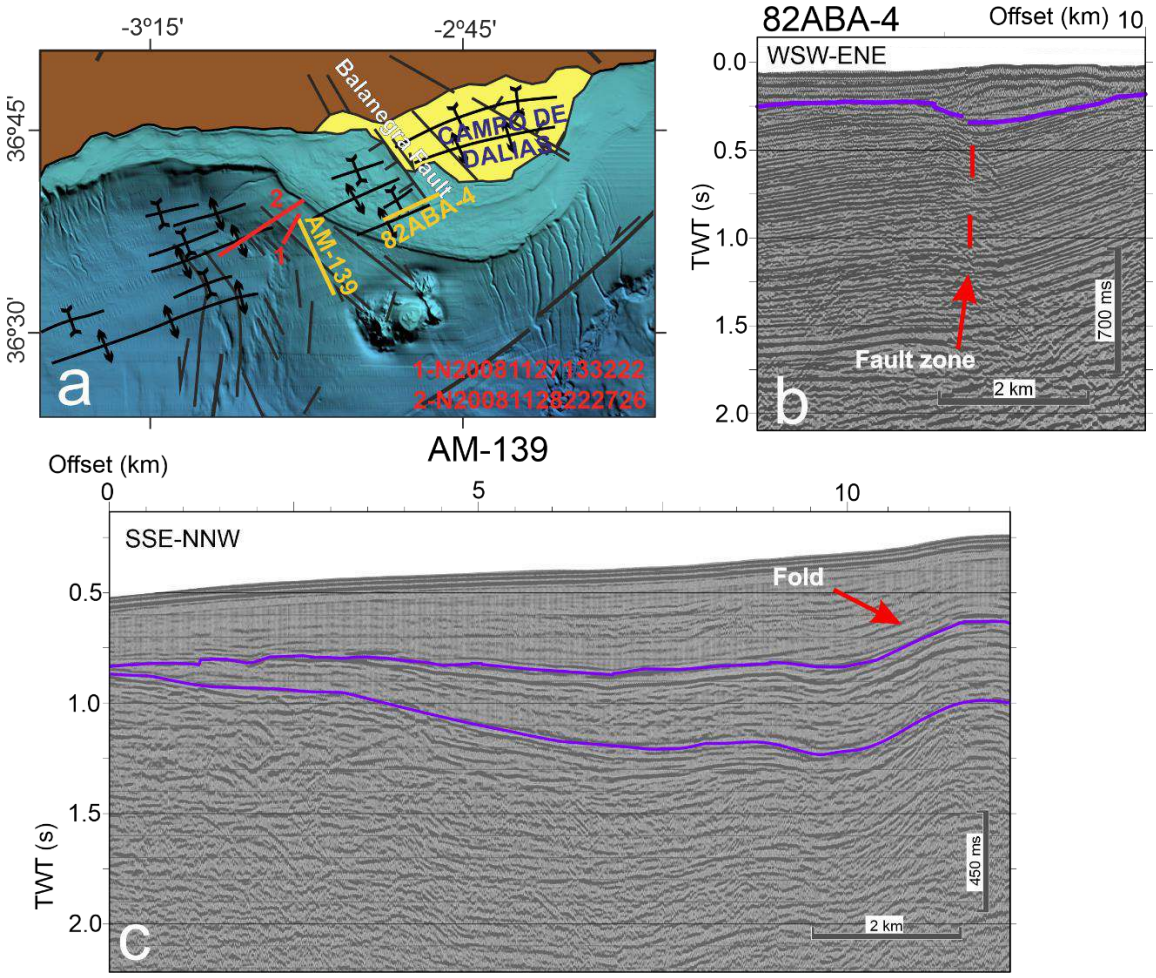

Figure 6.4. Seismic reflection profiles offshore of the Campo de Dalias: (a) Location of the profiles on the regional sketch of the main tectonic structures. (b) Profile 82 ABA-4, at the southern tip of the Balanegra Fault. (c) Profile AM-139, orthogonal to the east-northeast–west-southwest folds.

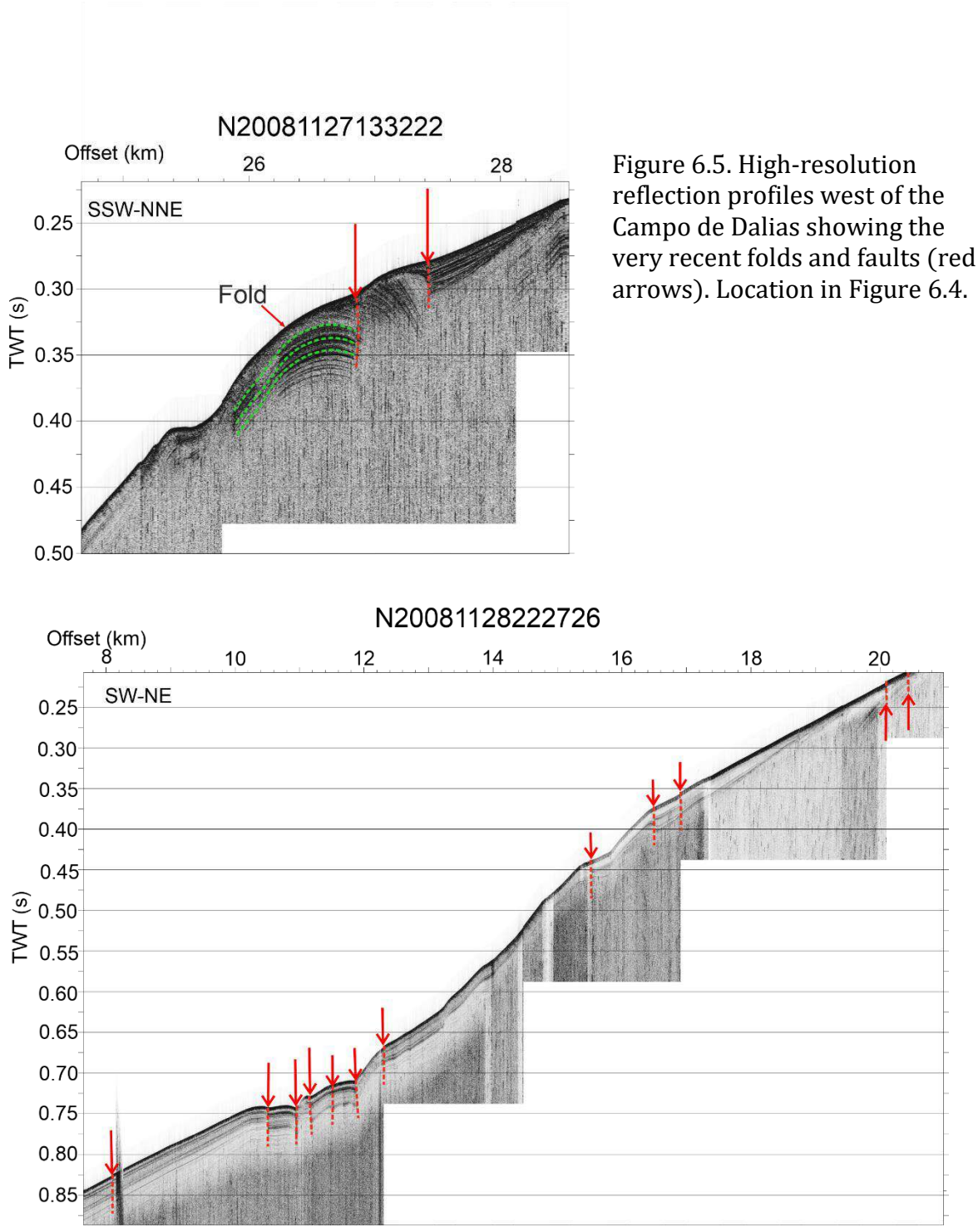

Figure 6.5. High-resolution reflection profiles west of the Campo de Dalias showing the very recent folds and faults (red arrows). Location in Figure 6.4.

6.6 Discussion

GNSS observations shed new light on active tectonics at a local scale in the western Campo de Dalias, and at a regional scale in the westernmost Mediterranean (Figs. 6.1, 6.2 and 6.6). Detailed analysis of the Balanegra Fault, considered to be a simple normal fault, proves its complexity; it is a 10 km long fault, whose northwest tip lies near the Gádor Range boundary, while the southeast tip lies offshore (Fig. 6.2).

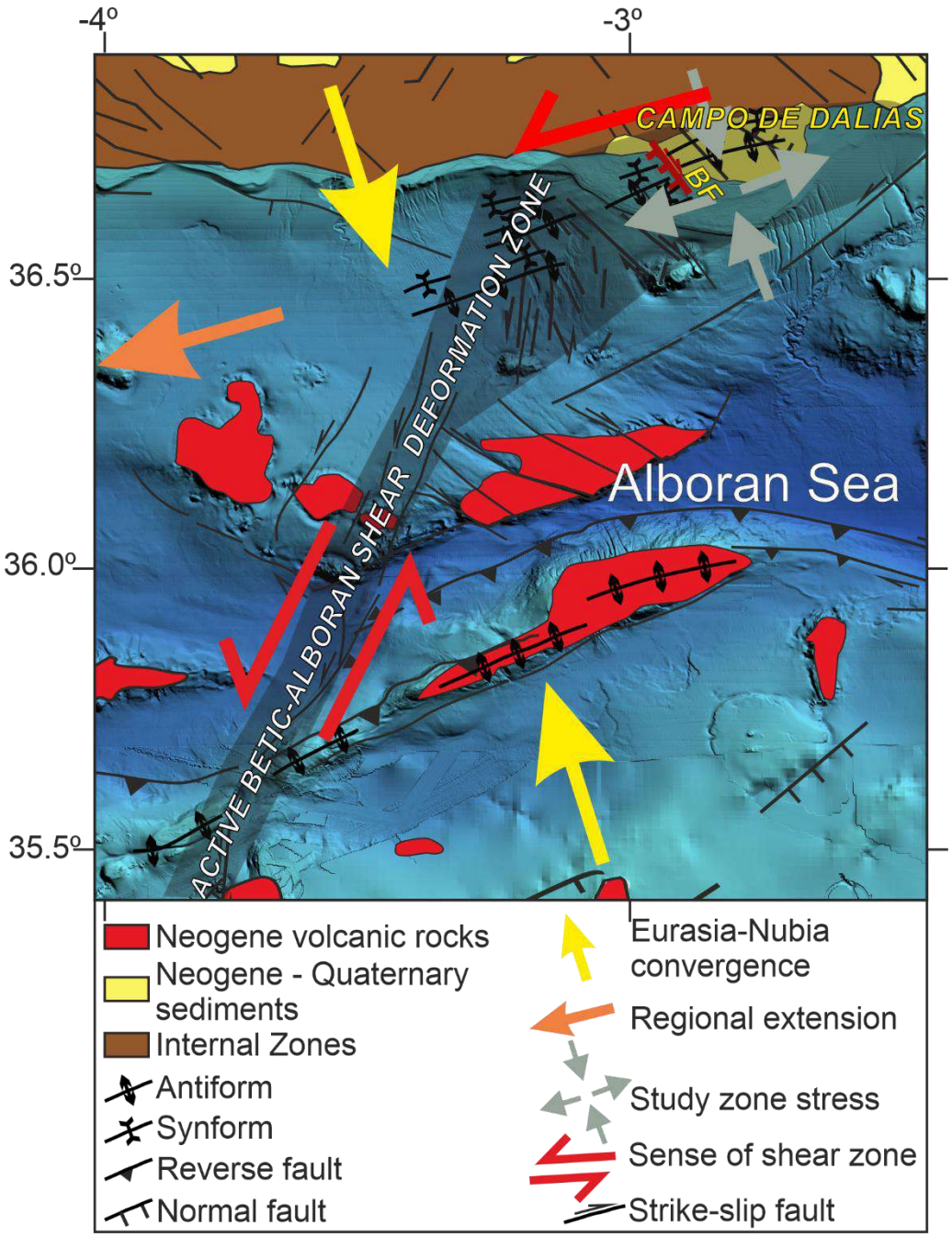

Figure 6.6. Tectonic sketch of the central Alboran Sea, relating deformation of the Campo de Dalias to the northeast tip of the active Betic-Alboran shear zone. BF: Balanegra Fault.

Seismic data on the activity of the Balanegra Fault are apparently controversial, pointing to dextral strike-slip earthquake focal mechanisms for northwest–southeast faults in the region (Stich *et al.*, 2003), but normal slip during the 1993–94 seismic crisis (Stich *et al.*, 2001). In addition, previous high-precision leveling data and field geological research support the hypothesis that this fault has a vertical component with a westward downthrown block (Galindo-Zaldivar *et al.*, 2013). The present-day

displacement, based on GNSS data, links these results, indicating that the Balanegra Fault is active, with a dextral creep displacement of close to 1 mm/year at the surface. This dextral displacement for the northwest–southeast fault is consistent with a

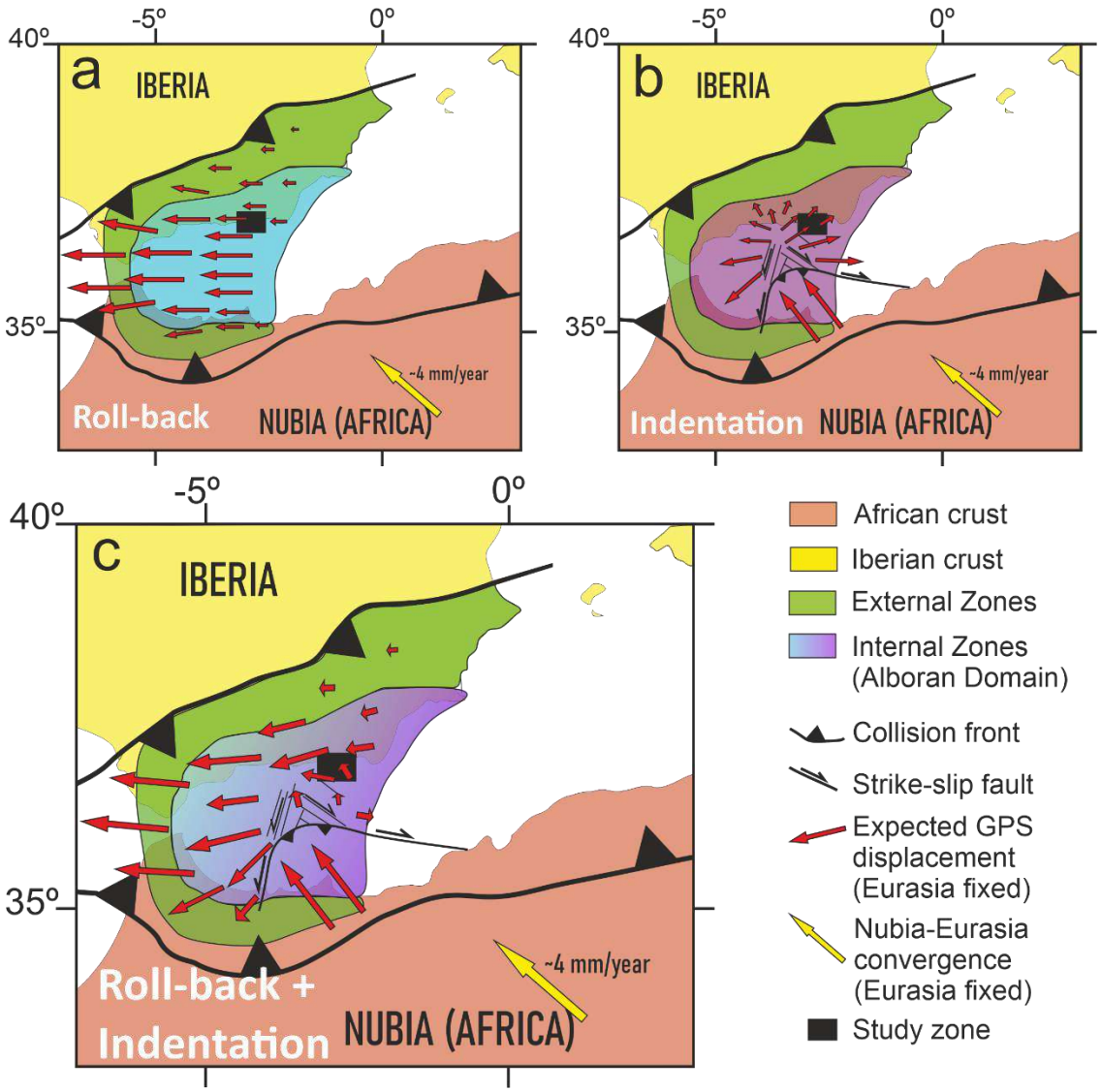

Figure 6.7. Expected displacement patterns during the development of the Gibraltar Arc with respect to stable Eurasia by (a) roll-back tectonics, with a regional westward displacement increasing toward the central and western parts of the tectonic arc; (b) indentation tectonics, with a radial pattern; and (c) the interaction of roll-back and indentation tectonics—in agreement with the Campo de Dalias GNSS network's present results, the residual velocity field decreases and rotates clockwise from the north towards the south of the study area.

deformation field determined by the north-northwest–south-southeast shortening simultaneous with east-northeast–west-southwest extension. Such kinematics can be found in other northwest–southeast faults outcropping in the Campo de Dalias (Marín-Lechado *et al.*, 2005), interpreted as shear or hybrid joints reactivated as

faults under east-northeast–west-southwest extension. These results suggest that the fault has a behavior including creep at shallow levels, decreasing the seismic hazard, while its activity at depth represents moderate seismicity.

Furthermore, the southwestward motion of the northern sites (9400 and 9600), in contrast to the remarkable northwestward displacements of the southern sites (9700 and 9900) (Fig. 6.2a), indicates regional north-northwest–south-southeast shortening, in agreement with the development of east-northeast–west-southwest folds that are still active. This small region—located above a sharp boundary between the Betic Cordillera's thick continental crust and the Alboran Sea's thin continental crust (Galindo-Zaldivar *et al.*, 1997)—accommodates approximately 1 mm/year of the total 4.5–5 mm/year shortening of the Eurasian and Nubian plates. These folds have progressively developed since the Tortonian (Marín-Lechado *et al.*, 2007; Pedrera *et al.* 2015), owing to the north-northwest–south-southeast plate convergence. In this context, the Campo de Dalias, undergoing simultaneous northwest–southeast compression and northeast–southwest extension, may constitute an accommodation zone of the main north-northeast–south-southwest sinistral active fault zone that crosses the Alboran Sea—the Betic–Alboran shear zone, in the frontal part of the Alboran Sea indenter (Fig. 6.6).

Although the entire region undergoes westward displacements (Fig. 6.2a)—most likely a consequence of roll-back tectonics (Fig. 6.7, Fadil *et al.*, 2006; Pérouse *et al.*, 2010) —the decreasing westward displacement towards the southern sites (Fig. 6.2a) offers clues as to the tectonic mechanisms active in the westernmost Mediterranean (Fig. 6.7). If a simple roll-back model is considered for the development of the Alboran Sea, increasing westward displacement towards the central Alboran Sea (Fig. 6.7a) should be expected (Fadil *et al.*, 2006; Pérouse *et al.*, 2010), but this is not observed. If simple indentation tectonics are envisaged for the central Alboran Sea, similar to the eastern Betic Cordillera indenters (Borque *et al.*, 2019), a radial pattern of displacements should occur which, again, is not observed (Fig. 6.7b). Thus, a model involving roll-back in the western Alboran Sea and indentation in the central and eastern areas would be needed to fit the observed displacement pattern, where the Campo de Dalias constitutes a boundary region (Fig. 6.7c).

6.7 Conclusions

Despite the long periods necessary to yield suitable results in regions with slow deformation, GNSS network observations provide independent data that improve our geological and geophysical understanding of active tectonic structures. The GNSS Campo de Dalias network shows that the entire region is affected by continuous deformation, including north-northwest–south-southeast convergence accommodated by east-northeast–west-southwest folds, and orthogonal east-northeast–west-southwest extension accommodated by normal faults.

The GNSS results highlight the activity of the north-northwest–south-southeast normal Balanegra Fault, which constitutes a complex structure of 10 km in length, south of the Gádor Range, with a shallow dextral creep displacement of up to 1 mm/year, and a deep seismic character.

At a regional scale, the study area accommodated deformation of the north-northeast tip of the sinistral Betic–Alboran shear zone, crossing the Alboran Sea. The pattern of active deformation, with westward displacement decreasing toward the south, is consistent with the coexistence in this region of roll-back tectonics—a driving process well developed in the western Gibraltar Arc—and indentation tectonics, dominant farther east and south. These results point to the coexistence of different tectonic mechanisms during the development in the westernmost Mediterranean, leading to the development of the Gibraltar Arc.

Funding

Junta de Andalucia; European Regional Development Fund; grant numbers: AGORA P18-RT-3275, PAPEL B-RNM-301-UGR18. Programa Operativo FEDER-Andalucia 2014–2020 Project ref. 1263446; University of Jaén; CEACTEMA; grant number: POAIUJA 21/22. Junta de Andalucía (Andalusian Board); grant numbers: RNM-148, RNM-282, RNM-370. V.T.S. was supported by the FPU PhD grant (16/04038).

References

Allmendinger, R.W., Loveless, J.P., Pritchard, M.E., & Meade, B. (2009). From decades to epochs: Spanning the gap between geodesy and structural geology of active mountain belts. *J. Struct. Geol., 31,* 1409–1422.

Altamimi, Z., Métivier, L., Rebischung P., Rouby, H., & Collilieux, X. (2017). ITRF2014 plate motion model. *Geophys. J. Int.*, *209*, 1906–1912.

Argus, D.F., Gordon, R.G., DeMets, C., & Stein, S. (1989). Closure of the Africa-Eurasia-North America plate motion circuit and tectonics of the Gloria fault. *J. Geophys. Res. Solid Earth*, *94*, 5585–5602.

Azzaro, R., Bonforte, A., D'Amico, S., Guglielmino, F., & Scarfì, L. (2020). Stick-slip vs. stable sliding fault behaviour: A case-study using a multidisciplinary approach in the volcanic region of Mt. Etna (Italy). *Tectonophysics*, *790*, 228554.

Bertiger, W., Desai, S.D., Haines, B., Harvey, N., Moore, A., Owen, S., & Weiss, J.P. (2010). Single receiver phase ambiguity resolution with GPS data. *J. Geod.*, *84*, 327‑337.

Bessière, E., Jolivet, L., Augier, R., Scaillet, S., Précigout, J., Azañon, J. M., ... & Do Couto, D. (2021). Lateral variations of pressure-temperature evolution in non-cylindrical orogens and 3-D subduction dynamics: the Betic-Rif Cordillera example. *BSGF-Earth Sciences Bulletin*, *192*(1), 8.

Blanco, M.J., & Spakman, W. (1993). The P-wave velocity structure of the mantle below the Iberian Peninsula: Evidence for subducted lithosphere below southern Spain. *Tectonophysics*, *221*, 13–34.

Borque, M. J., Sánchez-Alzola, A., Martin-Rojas, I., Alfaro, P., Molina, S., Rosa-Cintas, S., ... & Gil, A. J. (2019). How much Nubia-Eurasia convergence is accommodated by the NE end of the Eastern Betic Shear Zone (SE Spain)? Constraints from GPS velocities. *Tectonics*, *38*(5), 1824-1839.

Bousquet, J.C. (1979). Quaternary strike-slip faults in southeastern Spain. *Tectonophysics*, *52*, 277–286.

Braga, J.C., Martín, J.M., & Quesada, C. (2003). Patterns and average rates of late Neogene–Recent uplift of the Betic Cordillera, SE Spain. *Geomorphology*, *50*, 3–26.

Chalouan, A., Galindo-Zaldívar, J., Akil, M., Marín, C., Chabli, A., Ruano, P., ... & Gourari, L. (2006). Tectonic wedge escape in the southwestern front of the Rif Cordillera (Morocco). *Geological Society, London, Special Publications*, *262*(1), 101-118.

Civiero, C., Custódio, S., Duarte, J. C., Mendes, V. B., & Faccenna, C. (2020). Dynamics of the Gibraltar arc system: a complex interaction between plate convergence, slab pull, and mantle flow. *Journal of Geophysical Research: Solid Earth*, *125*(7), e2019JB018873.

Coppier, G., Griveaud, P., de Larouziere, F. D., Montenat, C., & Ott d'Estevou, P. (1989). Example of Neogene tectonic indentation in the Eastern Betic Cordilleras: the Arc of Águilas (southeastern Spain). *Geodinamica Acta*, *3*(1), 37-51.

De Larouzière, F. D., Bolze, J., Bordet, P., Hernandez, J., Montenat, C., & Ott d'Estevou, P. (1988). The Betic segment of the lithospheric Trans-Alboran shear zone during the Late Miocene. *Tectonophysics*, *152*(1-2), 41-52.

DeMets, C., Gordon, R. G., Argus, D. F., & Stein, S. (1990). Current plate motions. *Geophysical journal international*, *101*(2), 425-478.

DeMets, C., Gordon, R. G., Argus, D. F., & Stein, S. (1994). Effect of recent revisions to the geomagnetic reversal time scale on estimates of current plate motions. *Geophysical research letters*, *21*(20), 2191-2194.

Elliott, J. R., Walters, R. J., & Wright, T. J. (2016). The role of space-based observation in understanding and responding to active tectonics and earthquakes. *Nature communications*, *7*(1), 1-16.

Estrada, F., Galindo-Zaldívar, J., Vázquez, J. T., Ercilla, G., d'Acremont, E., Alonso, B., & Gorini, C. (2018). Tectonic indentation in the central Alboran Sea (westernmost Mediterranean). *Terra Nova*, *30*(1), 24-33.

Fadil, A., Vernant, P., McClusky, S., Reilinger, R., Gomez, F., Ben Sari, D., ... & Barazangi, M. (2006). Active tectonics of the western Mediterranean: Geodetic evidence for rollback of a delaminated subcontinental lithospheric slab beneath the Rif Mountains, Morocco. *Geology*, *34*(7), 529-532.

Galindo-Zaldívar, J., Jabaloy, A., González-Lodeiro, F., & Aldaya, F. (1997). Crustal structure of the central sector of the Betic Cordillera (SE Spain). *Tectonics*, *16*(1), 18-37.

Galindo-Zaldıvar, J., Gil, A. J., Borque, M. J., González-Lodeiro, F., Jabaloy, A., Marın-Lechado, C., ... & Sanz de Galdeano, C. (2003). Active faulting in the internal zones of the central Betic Cordilleras (SE, Spain). *Journal of Geodynamics*, *36*(1-2), 239-250.

Galindo-Zaldívar, J., Borque, M. J., Pedrera, A., Marín-Lechado, C., Gil, A. J., & López-Garrido, A. C. (2013). Deformation behaviour of the low-rate active Balanegra Fault Zone from high-precision levelling (Betic Cordillera, SE Spain). *Journal of Geodynamics*, *71*, 43-51.

Galindo-Zaldivar, J., Gil, A. J., Sanz de Galdeano, C., Lacy, M. C., García-Armenteros, J. A., Ruano, P., ... & Alfaro, P. (2015). Active shallow extension in central and eastern Betic Cordillera from CGPS data. *Tectonophysics*, *663*, 290-301.

Galindo-Zaldivar, J., Ercilla, G., Estrada, F., Catalán, M., d'Acremont, E., Azzouz, O., ... & Gil, A. J. (2018). Imaging the growth of recent faults: the case of 2016–2017 seismic sequence sea bottom deformation in the Alboran Sea (Western Mediterranean). *Tectonics*, *37*(8), 2513-2530.

Garate, J., Martin-Davila, J., Khazaradze, G., Echeverria, A., Asensio, E., Gil, A. J., ... & Harnafi, M. (2015). Topo-Iberia project: CGPS crustal velocity field in the Iberian Peninsula and Morocco. *GPS Solutions*, *19*(2), 287-295.

Gonzalez-Castillo, L., Galindo-Zaldivar, J., de Lacy, M. C., Borque, M. J., Martinez-Moreno, F. J., García-Armenteros, J. A., & Gil, A. J. (2015). Active rollback in the Gibraltar Arc: Evidences from CGPS data in the western Betic Cordillera. *Tectonophysics*, *663*, 310-321.

Gutscher, M. A., Malod, J., Rehault, J. P., Contrucci, I., Klingelhoefer, F., Mendes-Victor, L., & Spakman, W. (2002). Evidence for active subduction beneath Gibraltar. *Geology*, *30*(12), 1071-1074.

Heit, B., Mancilla, F. D. L., Yuan, X., Morales, J., Stich, D., Martín, R., & Molina-Aguilera, A. (2017). Tearing of the mantle lithosphere along the intermediate-depth seismicity zone beneath the Gibraltar Arc: The onset of lithospheric delamination. *Geophysical Research Letters*, *44*(9), 4027-4035.

Kreemer, C., Blewitt, G., & Klein, E. C. (2014). A geodetic plate motion and Global Strain Rate Model. *Geochemistry, Geophysics, Geosystems*, *15*(10), 3849-3889.

Leblanc, D., & Olivier, P. (1984). Role of strike-slip faults in the Betic-Rifian orogeny. *Tectonophysics*, *101*(3-4), 345-355.

Lyard, F., Lefevre, F., Letellier, T., & Francis, O. (2006). Modelling the global ocean tides: modern insights from FES2004. *Ocean dynamics*, *56*(5), 394-415.

Mancilla, F. L., Booth-Rea, G., Stich, D., Pérez-Peña, J. V., Morales, J., Azañón, J. M., ... & Giaconia, F. (2015). Slab rupture and delamination under the Betics and Rif constrained from receiver functions. *Tectonophysics*, *663*, 225-237.

Marín-Lechado, C., Galindo-Zaldívar, J., Rodríguez-Fernández, L. R., Serrano, I., & Pedrera, A. (2005). Active faults, seismicity and stresses in an internal boundary of a tectonic arc (Campo de Dalías and Níjar, southeastern Betic Cordilleras, Spain). *Tectonophysics*, *396*(1-2), 81-96.

Marín-Lechado, C., Galindo-Zaldívar, J., Rodríguez-Fernández, L. R., & Pedrera, A. (2007). Mountain front development by folding and crustal thickening in the Internal Zone of the Betic Cordillera-Alboran Sea boundary. *Pure and Applied Geophysics*, *164*(1), 1-21.

Marín-Lechado, C., Galindo-Zaldívar, J., Gil, A. J., Borque, M. J., De Lacy, M. C., Pedrera, A., ... & Sanz de Galdeano, C. (2010). Levelling profiles and a GPS network to monitor the active folding and faulting deformation in the Campo de Dalias (Betic Cordillera, Southeastern Spain). *Sensors*, *10*(4), 3504-3518.

Martín, R., Stich, D., Morales, J., & Mancilla, F. (2015). Moment tensor solutions for the Iberian-Maghreb region during the IberArray deployment (2009–2013). *Tectonophysics*, *663*, 261-274.

Nocquet, J. M. (2012). Present-day kinematics of the Mediterranean: A comprehensive overview of GPS results. *Tectonophysics*, *579*, 220-242.

Pedrera, A., Marín-Lechado, C., Galindo-Zaldívar, J., & Lobo, F. J. (2015). Smooth folds favoring gypsum precipitation in the Messinian Poniente marginal basin (Western Mediterranean). *Tectonophysics*, *663*, 48-61.

Pérouse, E., Vernant, P., Chéry, J., Reilinger, R., & McClusky, S. (2010). Active surface deformation and sub-lithospheric processes in the western Mediterranean constrained by numerical models. *Geology*, *38*(9), 823-826.

Platt, J. P., & Vissers, R. L. M. (1989). Extensional collapse of thickened continental lithosphere: A working hypothesis for the Alboran Sea and Gibraltar arc. *Geology*, *17*(6), 540-543.

Sanz de Galdeano, C. (1990). Geologic evolution of the Betic Cordilleras in the Western Mediterranean, Miocene to the present. *Tectonophysics*, *172*(1-2), 107-119.

Sanz de Galdeano, C., & Alfaro, P. (2004). Tectonic significance of the present relief of the Betic Cordillera. *Geomorphology*, *63*(3-4), 175-190.

Silva, P. G., Goy, J. L., Somoza, L., Zazo, C., & Bardají, T. (1993). Landscape response to strike-slip faulting linked to collisional settings: Quaternary tectonics and basin formation in the Eastern Betics, southeastern Spain. *Tectonophysics*, *224*(4), 289-303.

Sparacino, F., Palano, M., Peláez, J. A., & Fernández, J. (2020). Geodetic deformation versus seismic crustal moment-rates: insights from the Ibero-Maghrebian region. *Remote Sensing*, *12*(6), 952.

Stich, D., Alguacil, G., & Morales, J. (2001). The relative locations of multiplets in the vicinity of the Western Almería (southern Spain) earthquake series of 1993–1994. *Geophysical Journal International*, *146*(3), 801-812.

Stich, D., Ammon, C. J., & Morales, J. (2003). Moment tensor solutions for small and moderate earthquakes in the Ibero-Maghreb region. *Journal of Geophysical Research: Solid Earth*, *108*(B3).

Stich, D., Serpelloni, E., Mancilla, F. L., & Morales, J. (2006). Kinematics of the Iberia–Maghreb plate contact from seismic moment tensors and GPS observations. *Tectonophysics*, *426*(3-4), 295-317.

Tendero-Salmerón, V., Galindo-Zaldivar, J., Peláez, J. A., Martínez-Martos, M., Henares, J., Marín-Lechado, C., ... & López-Garrido, Á. C. (2020). Seismicity in strike-slip foreland faults (central Betic cordillera front): Evidence of indentation tectonics. *Tectonics*, *39*(7), e2020TC006143.

Tsukahara, K., & Takada, Y. (2018). Aseismic fold growth in southwestern Taiwan detected by InSAR and GNSS. *Earth, Planets and Space*, *70*(1), 1-7.

Vardar, D., Alp, H., Demirel, S., Aykurt Vardar, H., & Alpar, B. (2021). Offshore/onshore correlation of the North-Anatolian fault deformations in the Western Sea of Marmara. *Natural Hazards*, *107*(2), 1905-1923.

Williams, S. D. (2008). CATS: GPS coordinate time series analysis software. *GPS solutions*, *12*(2), 147-153.

CHAPTER 7

Shearing in an indenter boundary: the evolution of the Águilas Arc and its accommodation along the PFZ (Betic Cordillera, Spain).

Tendero-Salmerón, V.[1], Ercilla, G.[2], González-Castillo, L.[3], Madarieta-Txurruka, A.[3], Martínez-Moreno F.J.[4], Estrada, F.[2], Sanz de Galdeano, C.[1], Galindo-Zaldivar, J.[1,3]

[1]Instituto Andaluz de Ciencias de la Tierra (CSIC-UGR), 18100 Armilla (Granada), Spain

[2]Instituto de Ciencias del Mar, CSIC, Continental Margins Group, 08003 Barcelona, Spain

[3]Departamento de Geodinámica, Universidad de Granada, 18071 Granada, Spain

[4]Instituto Dom Luiz (IDL), Facultade de Ciências, Universidade de Lisboa, Campo Grande, 1749-016, Lisboa, Portugal

Submmited to: Tectonophysics (JCR in 2020; 3.933, Q1)

Abstract

This research provides new geophysical data (magnetic and gravimetric) that improves the knowledge of the Águilas Arc tectonic indentation (Betic Cordillera, Spain), in the frame of Eurasia-Africa convergence. Its accommodation along the Palomares fault zone (PFZ) is analyzed, as well as the interplay of this fault with the sedimentary infill geometry of the Vera and Pulpí basins and the western Guadalentín corridor, which are located along the western boundary of the Arc. The gravity anomaly models show the geometries of the basins' depocenters, which are the result of the interaction of synforms fragmented and rotated by the PFZ. Furthermore, the gravity anomaly and gravity models show that the PFZ extends from Sierra Cabrera to Sierra Almagrera and ends northwards in the Pulpí basin, where the basin infill has only a gentle symmetrical synform. This means that the Palomares fault zone is (i) confined to the zone of strongest fold flexure and fragmentation associated with the western indenter boundary and (ii) disconnected from the front of the Águilas Arc and the Alhama de Murcia fault (part of the Eastern Betic Shear Zone, EBSZ). Therefore, this structure segmented the EBSZ and reduced the expected geological hazard. The study of the PFZ enhances the understanding of tectonic indentation and accommodation along the indentation boundaries of the deformation through the interaction of fold bending and local faulting.

Keywords: tectonic indentation, strike-slip faults, Palomares fault, gravity models, Vera basin

7.1 Introduction

The accommodation of displacements during indenter tectonics results in large transcurrent fault zones separating continental blocks along indenter block sides and also either in the hinterland or foreland (Davy and Cobbold, 1988; Mann, 2007; Sylvester, 1988; Tapponnier *et al.*, 1982; Zweigel, 1998). These strike-slip systems have been studied worldwide, with remarkable results in the India-Asia collision (*e.g.*, Cobbold and Davy, 1988; Tapponnier *et al.*, 1982), in Taiwan (*e.g.*, Lu and Malavieille, 1994; Zweigel, 1998), in the Zagros Cordillera in the context of the Arabian indentation (*e.g.*, Azad *et al.*, 2019 and references therein) or in the Alpine Cordillera (*e.g.*, Lickorish *et al.*, 2002; Rosenberg *et al.*, 2004). On the other hand, fault zones located at the lateral margins of the indenter strongly condition the relief and delineate the indented block by deforming and dissecting pre-existing structures (*e.g.*, Coppier *et al.*, 1989; Davy and Cobbold, 1988; Estrada *et al.*, 2018; Tapponnier *et al.*, 1982). The latest ones are typically strike-slip fault zones with associated structures as restraining and releasing bends (Mann, 2007), such as the Chaman fault zone in Pakistan (*e.g.*, Crupa *et al.*, 2017, Davy and Cobbold, 1988). However, the boundaries of the indenter can also produce transfer faults caused by fragmentation of the mountain front due to an irregular shape of the indenter or by the progression of the indentation, as in the case of the Zagros Mountains (Azad *et al.*, 2019; Tavakoli *et al.*, 2008). In the event of rotations of the indenter or corner indentations, the lateral boundary faults of the indenter may be transpressive or even overshooting (Lickorish *et al.*, 2002; Zweigel, 1998). In addition, some of these faults may become inactive as a result of changes in the shape of the intrusion, which may lead to accretion of material, as the Vuache fault in the Jura Mountains (Homberg *et al.*, 1999). These fault zones can therefore be tectonically complex and have a wide variety of geometries that still remain unresolved. That is the case of the Palomares fault zone (hereinafter, PFZ), located at the western boundary of the Águilas Arc in the eastern Betic Cordillera (SE Spain, Fig. 7.1). In the Águilas Arc, the indenter rigid block is part of the Neogene Algerian oceanic crust that is rigid, and pushes into the thin and deformed Internal Zones of the Betic Cordillera, which supposes an interesting case of study to improve the knowledge of tectonic indentation processes (Fig. 7.1a, Borque *et al.*, 2019; Gómez de la Peña *et al.*, 2016; Gueguen *et al.*, 1998; Palano *et al.*, 2015; Rehault *et al.*, 1985; Silva *et al.*, 1993).

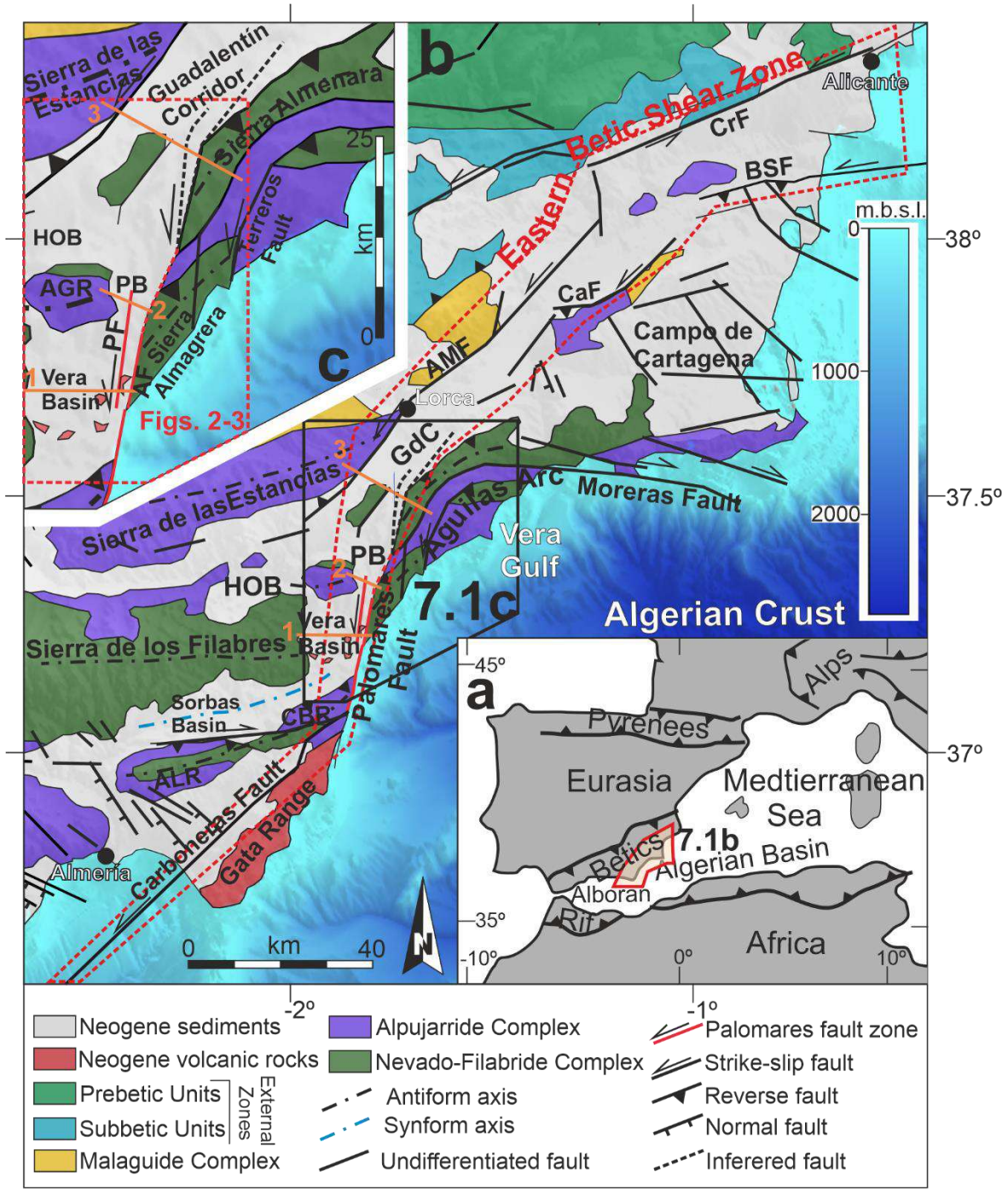

Figure 7.1. Geological context of the study zone based on Ercilla *et al.* (2022). a. Tectonic plate sketch showing the location of the zone. b. Simplified geological map of Eastern Betic Shear Zone and the Águilas Arc. The modeled profiles are also depicted. c. Zoom of the study zone. The area of Figures 2 and 3 is depicted. AF: Arteal fault; AGR: Sierra de Almagro; AL: Sierra de Alhamilla; AMF: Alhama de Murcia fault; BSF: Bajo Segura fault; CaF: Carrascoy fault; CBR: Sierra Cabrera; CrF: Crevillente fault; GdC: Guadalentín corridor; HOB: Huércal Overa basin; PB: Pulpí basin; PF: Palomares fault.

The PFZ is a NNE-SSW sinistral strike-slip fault that accommodates the displacement of the tectonic indenter of the Águilas Arc (Coppier *et al.*, 1989; Ercilla *et al.*, 2022;

Silva *et al.*, 1993). This tectonic indentation was formed as part of the NNW-SSE convergence of the Eurasian and African plates in the western Mediterranean, which has uplifted the Betic Cordillera since the Late Tortonian (*e.g.*, Comas *et al.*, 1992; Braga *et al.*, 2003; De Mets *et al.*, 2010; Sanz de Galdeano, 1990). The PFZ disrupts the antiforms and thrusts of Sierra Cabrera and those of the Águilas Arc, such as Sierra Almagrera (Fig. 7.1b), so it is also considered a transfer fault (Booth-Rea *et al.*, 2004; Giaconia *et al.*, 2015; Weijermars, 1987). The PFZ is considered part of the Eastern Betic Shear Zone (EBSZ, Fig. 7.1), a system of NE-SW to N-S, sinistral strike-slip faults that crosses the eastern Betic region and is connected to the Alboran Sea faults via the Carboneras fault (the Trans-Alboran Shear Zone) (Fig. 7.1, De Larouzière *et al.*, 1988; Silva *et al.*, 1993). Along the EBSZ, several basins are considered the result of strike-slip faults activity, such as the Vera, Pulpí and Guadalentín basins that are related to the PFZ; while others are the result of major fold and fault interactions, like the Huércal Overa basin or the Campo de Cartagena (Fig. 7.1, Barragán, 1997; Booth-Rea *et al.*, 2003; Montenat and Ott d'Estevou, 1999; Pedrera *et al.*, 2010; Silva *et al.*, 1993; Wenzens and Wenzens, 1997).

The aim of this study is to understand the evolution of the Águilas Arc tectonic indentation and its accommodation along the PFZ. To this aim, the main features of the sedimentary infill geometry of the basins along the western boundary of the Águilas Arc are analyzed using gravity and magnetic prospecting and to discuss the implications on the PFZ evolution.

7.2 Geological setting

The Águilas Arc and the PFZ are located in the Betic Cordillera, the northern branch of the Gibraltar Arc (Fig. 7.1), formed by the oblique convergence of the Eurasian and African plates (*e.g.*, DeMets *et al.*, 2010; Sanz de Galdeano, 1990). In the Miocene, the Alboran Domain (forming the Internal Zones of the orogen and the basement of the Alboran Sea) collided with the Iberian and African margins (External Zones) and thrust over them, forming the Gibraltar Arc (García-Dueñas and Balanyá, 1986; Platt *et al.*, 2003). The Alboran Domain consists on continental crust that was part of a domain whose fragmentation since the Early Miocene gave rise to the oceanic Algerian Basin (Gueguen *et al.*, 1998; Mauffret *et al.*, 2007; Spakman *et al.*, 2018). The Internal Zones of the Betic Cordillera are formed by three superimposed

metamorphic complexes formed by Palaeozoic and Mesozoic rocks, which are from bottom to top: Nevado-Filábride, Alpujárride and Maláguide (Jabaloy-Sánchez *et al.*, 2019; Platt and Vissers, 1989; Sanz de Galdeano, 1990). The Nevado-Filábride and Alpujárride complexes are made up of metapelites (phyllites, schists), marbles, some metabasites (diabases, serpentinites) and mineralizations of Fe, Pb, Ag or Zn (Jabaloy-Sánchez *et al.*, 2019 and references therein). These complexes were initially affected by thrust-sheet stacking and later by extension with low-angle normal faults (Galindo-Zaldívar *et al.*, 1989; 2003; Jabaloy-Sánchez *et al.*, 2019; Platt and Vissers, 1989).

The NNW-SSE continental collision occurred simultaneously with the westward movement of the Alboran Domain, which was associated with the ENE-WSW continental extension since the Late Tortonian (Comas *et al.*, 1992; Corsini *et al.*, 2014; Galindo-Zaldivar *et al.*, 2003; Sanz de Galdeano, 1990). This stress state led to the formation of intra-mountain basins in the Betic Cordillera, which were located in the synforms, sometimes faulted, between E-W and NE-SW antiforms that formed the major ranges of the Cordillera (Fig. 7.1, Braga *et al.*, 2003; Galindo-Zaldívar *et al.*, 2003; 2019; Sanz de Galdeano, 1990). The filling of these basins, such as the Huércal Overa or Vera basins, is characterized by a succession of Miocene marls, turbidites, sandstones and calcarenites with Messinian gypsum, followed by Plio-Quaternary, fluvial-alluvial conglomerates and sands (Barragán, 1997; Booth-Rea *et al.*, 2003; Braga *et al.*, 2003; Montenat and Ott d'Estevou, 1999; Völk, 1966; Weijermars, 1987). In addition, the area was affected by Neogene volcanism, as the Sierra de Cabo de Gata evidenced, and small volcanic outcrops in the Vera Basin (*e.g.*, Duggen *et al.*, 2008).

The stress field has formed E-W oriented dextral and reverse faults, NW-SE normal faults and NE-SW sinistral and normal faults with dextral conjugate faults since the Late Miocene (Sanz de Galdeano, 1990). The eastern Betic is also crossed by the Eastern Betic Shear Zone (EBSZ), which includes the Carboneras, Palomares and Alhama de Murcia sinistral fault zones (Fig. 7.1, Bousquet, 1979; Borque *et al.*, 2019; Silva *et al.*, 1993). Some studies also suggest a rotation of the palaeostress during the Messinian from NW-SE to N-S, which rotated again during the Pliocene and has the present orientation NNW-SSE (Huibregtse *et al.*, 1998; Jonk and Biermann, 2002).

In addition, some areas such as the central Alboran Sea (Estrada *et al.*, 2018; Galindo-Zaldivar *et al.*, 2022; Tendero-Salmerón *et al.*, 2022) and the Águilas Arc (Ercilla *et al.*, 2022; Silva *et al.*, 1993) were affected by tectonic indentation. This geodynamic setting led to the bending of the former structures (Coppier *et al.*, 1989) and the development of faults (*e.g.*, the PFZ) and the deformation of sedimentary basins like Vera (Fig. 1b, Barragán, 1997; Booth-Rea *et al.*, 2003; Montenat and Ott d'Estevou, 1999; Weijermars, 1987). The transition between the Internal Zones of the Betic Cordillera and the indenter made of Algerian oceanic crust (Gueguen *et al.*, 1998; Palano *et al.*, 2015; Rehault *et al.*, 1985; Silva *et al.*, 1993) is characterised by strong crustal thinning (Diaz *et al.*, 2016; Medaouri *et al.*, 2014). The northward displacement of the indenter was mainly accommodated by the Palomares sinistral fault zone (including the Arteal fault) and the Moreras dextral fault (Fig. 7.1, Ercilla *et al.*, 2022; Silva *et al.*, 1993). The onset of the indentation is probably before Middle Miocene or Tortonianaccording to the beginning of Palomares faulting (Coppier *et al.*, 1989; Weijermars, 1987). Huibregtse *et al.* (1998) considered as first evidence the intrusion of volcanic rocks along the fault zone during Tortonian.

In the eastern block of the PFZ, the mountain ranges such as the Sierra Almagrera are NNE-SSW oriented and turns towards E-W forming the Águilas Arc itself (Fig. 7.1). Offshore, the deformation also extends to the Palomares margin and E-W and NE-SW ridges can be observed, as well as sedimentary instabilities affecting most of the Gulf of Vera due to the progressive, southeastward tectonic tilting of the whole land-sea region (Ercilla *et al.*, 2022). Although the PFZ is formed by fault segments 10-15 km long, it has been commonly extended from the eastern boundary of Sierra Cabrera to the frontal thrusts of the Águilas Arc, considering the low sinuosity of Sierra Almenara and Sierra Almagrera (García-Mayordomo, 2005 and references therein).

Recent and active tectonics

The tectonic indentation is still active, as evidenced by seismicity, GPS data and the uplift of the Vera and Pulpí basins (Echeverria *et al.*, 2013; García-Mayordomo, 2005; García-Mayordomo *et al.*, 2017; Palano *et al.*, 2015; Stich *et al.*, 2010; Stokes, 2008). GPS data show active NW-SE shortening that affects the entire EBSZ (Borque *et al.*, 2019), with a radial pattern of the displacements around the Águilas Arc and greater shortening at the western boundary of the Guadalentín corridor (Alhama de Murcia

fault), but not at the Águilas Arc front (Echeverria *et al.*, 2013; Palano *et al.*, 2015). The Vera and Pulpí basins and the Águilas Arc have been uplifted during the Plio-Quaternary and their drainage net are conditioned by PFZ activity and the southwards tilting of the region (Booth-Rea *et al.*, 2004; Giménez *et al.*, 2000; Stokes, 2008; Sotkes and Mather, 2003). Uplift is also observed along the coast and sea margins of the Águilas Arc and Palomares (Bajardí *et al.*, 2015; Durán *et al.*, 2018; Ercilla *et al.*, 2022). However, the uplift of the Vera Basin is lower than that of surrounding basins such as the Sorbas or Pulpí basins (Braga *et al.*, 2003; García-Mayordomo, 2005; Stokes, 2008; Stokes and Mather, 2003).

Regarding recent tectonic activity in the area, fault slip rates range from values of 1 mm/yr (*e.g.*, Alhama de Murcia and Carrascoy faults) to values of less than 0.1 mm/yr (*e.g.*, the PFZ, including the Arteal fault and the eastern flank of Sierra Almenara) (Alfaro *et al.*, 2012; Booth-Rea *et al.*, 2004; Borque *et al.*, 2019; Ferrater *et al.*, 2017; García Mayordomo *et al.*, 2017; Herrero-Barbero *et al.*, 2021; Martín-Banda *et al.*, 2016; Silva *et al.*, 2003). Notwithstanding, some simulations consider seismic rupture of entire sections of the EBSZ (or propagation of the rupture through multiple faults), which would generate earthquakes with magnitudes greater than $M_W > 6.7$ (Herrero-Barbero *et al.*, 2021). South of the PFZ, the Carboneras fault shows disperse seismic activity with some historical, major earthquakes. It has been active since the Serravalian, with sinistral strike-slip kinematics during the Miocene and transpression during the Plio-Quaternary (Echverria *et al.*, 2015; Giaconia *et al.*, 2015; Rutter *et al.*, 2012). Compared to other areas like the Alhama de Murcia fault or the Huércal Overa basin, where the southern termination of this fault is located, earthquakes in the Vera basin are also rare (Alfaro *et al.*, 2012; Echeverria *et al.*, 2013; Sánchez-Roldán *et al.*, 2021; Stich *et al.*, 2010). The M_W 5.2 Lorca earthquake of 2011 (Martínez-Díaz *et al.*, 2012) shows that the Alhama de Murcia fault is transpressive. On the opposite edge of the Guadalentín corridor, paleoseismic sutdies have detected earthquakes with magnitudes above $M_W > 5$ in the frontal fault zone of Sierra Almenara, which is considered part of the PFZ (Roquero *et al.*, 2019).

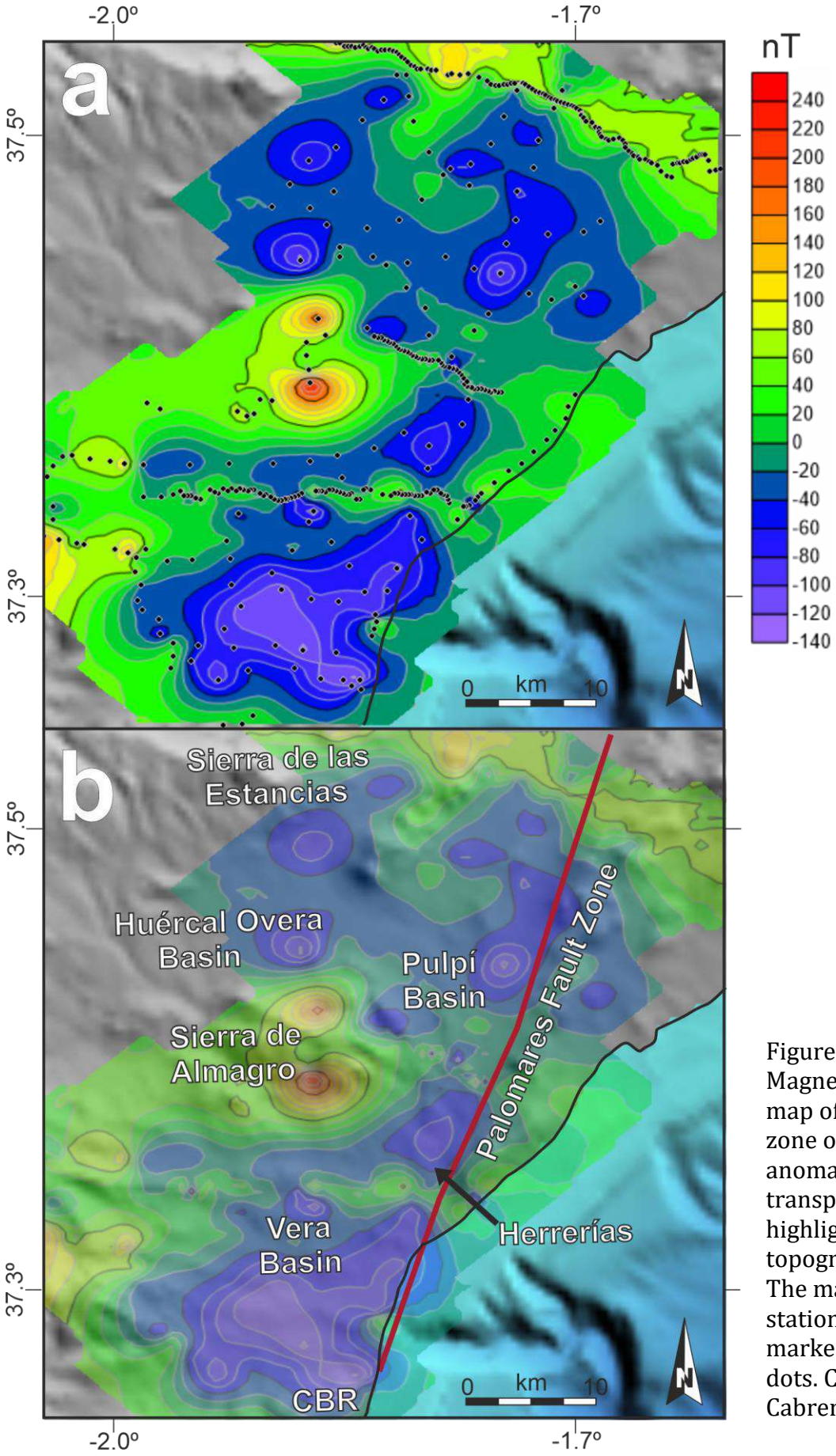

Figure 7.2. Magnetic anomaly map of the study zone over (a) and anomaly map with transparency to highlight topography (b). The magnetic stations are marked as black dots. CBR; Sierra Cabrera.

7.3 Data and methods

Field campaigns were carried out in the zone to make geological recognitions and obtain accurate gravity and magnetic field measurements, both along profiles orthogonal to the PFZ and to cover the adjacent Vera and Pulpí basins. There were 392 measurements of both gravity and magnetic total field (measured simultaneously at each point), of which 231 points belong to the three main profiles (Figs. 7.2 and 7.3) and other points to fulfill the grid. For the profiles, the distance between points is about 200 m in average. Profile 1 (south) includes 77 stations, profile 2 (centre) includes 44 stations and profile 3 (north) includes 110 stations (Fig. 7.3).

Magnetic total field measurements were acquired with a GSM-8 proton precession magnetometer with an accuracy of 1 nT. Each measurement point was located far away from anthropogenic interference sources such as metallic objects or power lines. To calculate the magnetic anomalies, the diurnal variations of the magnetic field were removed. These variations are due to external sources of the geomagnetic field and were corrected with data from the nearest permanent magnetic station of Intermagnet in San Fernando, Cádiz (Royal Institute and Observatory of the Spanish Navy). Finally, a reduction to the 2020 IGRF (International Geomagnetic Reference Field, Alken *et al.*, 2021) was made using the Oasis Montaj software and the results were used to calculate a map of the magnetic anomaly (Fig. 7.2). In this work, only a qualitative interpretation of the magnetic anomaly results was considered.

Gravity measurements were acquired using a Scintrex Autograv CG -5 gravimeter with an accuracy of 1 μGal. The measurements were referenced to the Granada absolute gravity station (National Geographic Institute, IGN) by calibrating a field base near the town of Garrucha (Fig. 7.1). For each point, the Free-Air, Bouguer and Terrain corrections were applied to calculate the Complete Bouguer anomaly by means of Oasis Montaj software and considering a standard background density of 2.67 g/cm^3. For the calculation of the Terrain correction based on the methods of Kane (1962) and Nagy (1966), a digital terrain model (DTM) with a pixel accuracy of 5 m provided by IGN was used, combined with bathymetry of the Gulf of Vera from the GEBCO database (https://www.gebco.net/data_and_products/gridded_bathymetry_data/).

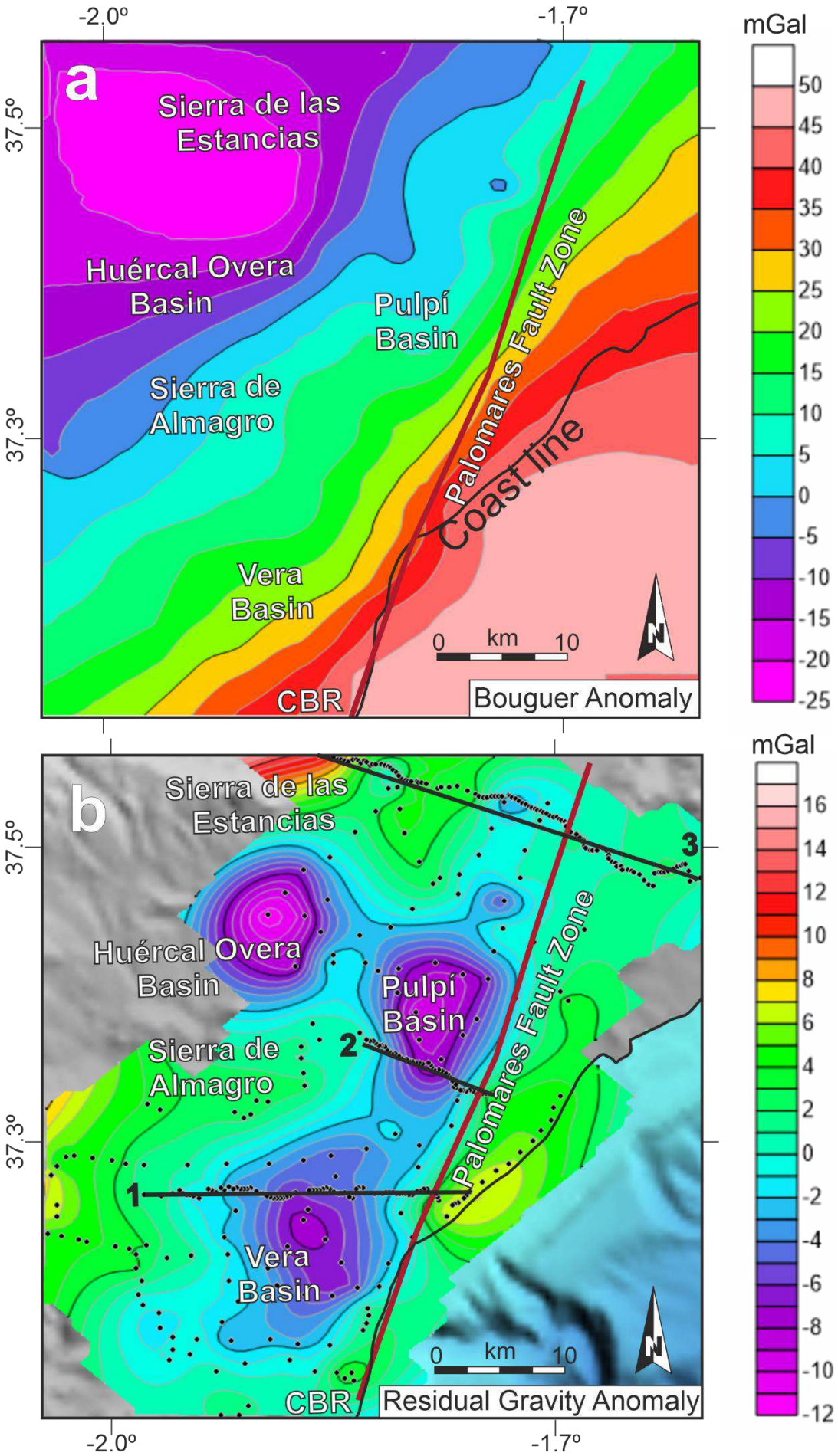
-2.0º
-1.7º
37.5º
37.3º
a
Sierra de las Estancias
Huércal Overa Basin
Pulpí Basin
Sierra de Almagro
Vera Basin
Palomares Fault Zone
Coast line
CBR
0 km 10
N
Bouguer Anomaly
mGal
50
45
40
35
30
25
20
15
10
5
0
-5
-10
-15
-20
-25
b
Sierra de las Estancias
Huércal Overa Basin
Pulpí Basin
Sierra de Almagro
Vera Basin
Palomares Fault Zone
1
2
3
CBR
0 km 10
N
Residual Gravity Anomaly
mGal
16
14
12
10
8
6
4
2
0
-2
-4
-6
-8
-10
-12

Figure 7.3. Maps of the complete Bouguer anomaly (a) and residual anomaly (b) of the study zone. The gravity stations are marked as black dots and the modeled profiles are depicted. CBR: Sierra Cabrera.

The residual gravity anomaly map (Fig. 7.3b) was created by subtracting the regional anomaly map from the Bouguer anomaly map (Fig. 7.3a) to remove basement variations effects and preserve sedimentary basin impacts. The regional anomaly map was calculated by a first-order polynomial fit —as the Bouguer anomaly has a linear trend— in the Oasis Montaj software, resulting in a residual anomaly where the 0 mGal isoline almost coincides with the basin boundaries. Subsequently, profiles 1, 2 and 3 were modelled taking into account the residual gravity anomaly using GRAVMAG v1.7 software from the British Geological Survey (Pedley *et al.*, 1993). The density values were estimated after testing a range of values based on the predominant lithologies of the region (Fig. 7.1) and standard averages (Telford *et al.*, 1990). The models show the final chosen value. The value of the background corresponding to the undifferentiated basement is 2.67 g/cm^3, a standard value for continental crust (Telford *et al.*, 1990). Some basement polygons with higher densities (2.8-2.9 g/cm^3) were added to compensate some positive anomalies. The density value used for the sediments in the residual anomaly models is 2.4 g/cm^3, which is an average value for the basin sediments. Only in profile 1 another sediment polygon, with a density of 2.55 g/cm^3, was added at the intersection with the Almanzora River (Fig. 7.4) near its mouth.

7.4 Results

7.4.1 Anomaly maps

The map of magnetic anomalies (Fig. 7.2) shows that the maximum values are measured over the bedrock (like the maximum of 110 nT on profile 3, Fig. 7.2), while the basins are generally characterized by minima. The eastern Huércal Overa basin has two minima of -101 nT and -73 nT, the Pulpí basin has one of -103 nT and the Vera basin has another with an irregular shape that extends to Sierra Cabrera (Fig. 7.2). This anomaly has two lowest values, of -124 nT in the southern and of -118 nT in the north-eastern, next to Sierra Cabrera (-118 nT). In contrast, Sierra de Almagro has two maxima of 172 nT (north) and 218 nT (south).

Regarding to gravity anomalies, the Complete Bouguer anomaly (Fig. 7.3a) shows a SE-ward decreasing trend with some irregularities, most of which coincide with the Vera and Pulpí basins. The map of the residual anomaly (Fig. 7.3b) is almost aligned with the basin boundaries and shows three main depocenters located in the Vera, Pulpí and eastern Huércal Overa basins. The lowest values are -7.5 mGal in the Vera basin, -9.6 mGal in the Pulpí basin and -11.4 mGal in the eastern Huércal Overa basin (Fig. 7.3b).

7.4.2 Residual gravity anomaly models

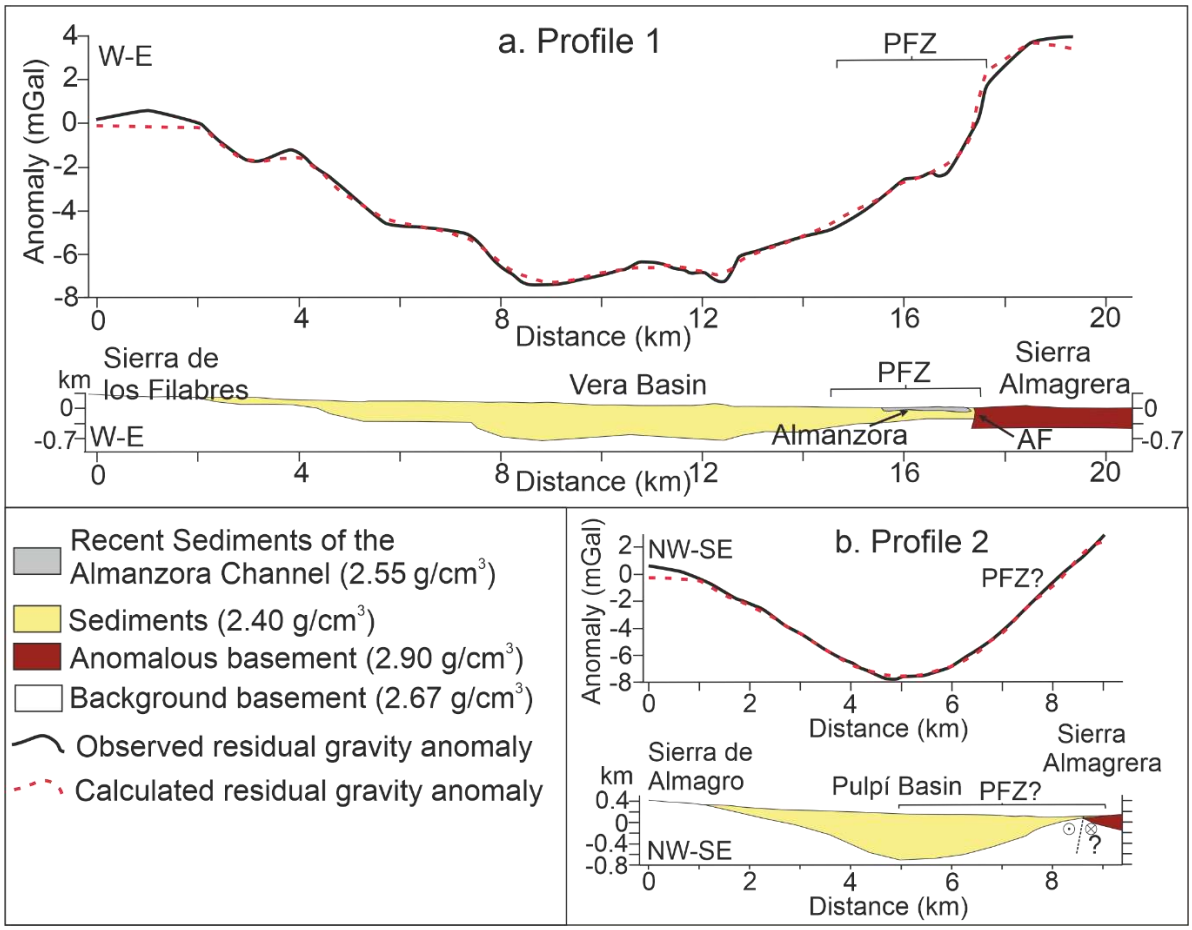

Figure 7.4. Gravity models of profile 1 (a) and 2 (b). The locations of the profiles is indicated in Figs. 7.1b, c and 7.3b. AF: Arteal fault; PFZ: Palomares fault zone.

Profile 1 (Fig. 7.4a) runs from the end of Sierra de Filabres (W) to the southern end of Sierra Almagrera (E), crossing the northern part of the Vera Basin and the PFZ (Fig. 7.3). The residual anomaly has a shape with the lowest values in the central part of the basin and two relevant minima of -7.5 mGal at ~9 km and ~12.5 km from the beginning of the profile (Fig. 7.4a). There are also some steps along the shape (at ~4

km, ~6 km and ~16.5 km) and an abrupt increase of the anomaly of 4 mGal that matches with the Arteal fault; in fact, the biggest step (> 200 m) occurs in this fault (Fig. 7.4a). These steps are reflected in the modelled sediment polygon, with a change of the sediments thickness of 300 m at 1.5-2 km (Fig. 7.4a). There is also a polygon of 2.55 g/cm^3 with a thickness of 50-80 m coincident with the Almanzora River, probably related to conglomerates recently deposited in the river channel.

Profile 2 (Figs. 7.3 and 7.4b) crosses the Pulpí Basin from Sierra de Almagro (NW) to Sierra Almagrera (SE). The curve of the residual anomaly is smooth and has no significant steps, with a minimum value of -8 mGal in the center of the basin (~5km). Thus, the sediment polygon of the model has an approximately symmetrical shape with a depocenter that reaches a maximum thickness of 850 m (Fig. 7.4b).

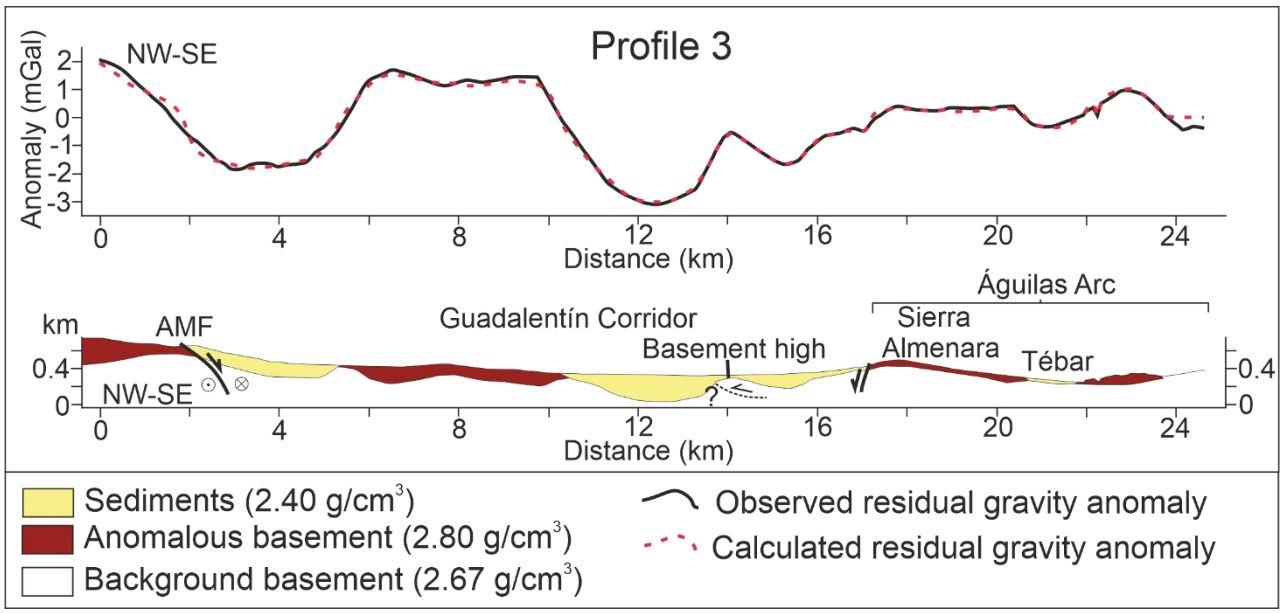

Figure 7.5. Gravity model of profile 3 with a vertical exaggeration (VE x2). The location of the profile is indicated in Figs. 1b, c and 3b. The proposed blind thrust below the Guadalentín Corridor is depicted. AMF: Alhama de Murcia fault.

Profile 3 (Figs. 7.3 and 7.5) is located in the Guadalentín corridor and runs from the Sierra de las Estancias (NW) to the Águilas Arc (Sierra Almenara). The profile of the residual anomaly has several minima and maxima corresponding to the sub-basins and basement outcrops respectively. The westernmost sub-basin has a sediment thickness of 200 m, corresponding to a minimum of -2 mGal. Coincident with the trace of the Alhama de Murcia fault, a step of 1.5 mGal occurs, which is related to a downfall of the basement of > 250 m. In the central sub-basin (from kms 10 to 17, Fig. 7.5),

only highlights a central high (-0.5 mGal, 50 m of sediment thickness polygon) covered with sediments between two lows of -3 mGal (300 m of thickness) and - 1.5 mGal (180 m of thickness). In the eastern part (Fig. 7.5), a minimum value of - 0.4 mGal and 40 m of estimated sediment thickness occurs. It is linked to the small Tébar basin within the Águilas Arc.

7.5 Discussion

7.5.1 The Palomares fault zone

The magnetic anomalies are due to the presence of metabasites in the metamorphic complexes of the Internal Zones (mountain ranges of Filabres and Almagro) and to the presence of Neogene volcanic rocks or mineralizations as found in the fault zone in Herrerías (Fig. 7.2). It appears that no significant igneous bodies have been intruded along the PFZ, unlike other strike-slip faults in the eastern Alboran Domain (*e.g.*, Carboneras Fault, Rutter *et al.*, 2012; Yusuf Fault, Tendero-Salmerón *et al.*, 2022). Gravity anomalies show that the major depocenters of the Vera and Pulpí basins are centered suggesting, therefore, that they are not primarily conditioned by the PFZ, as it is expected in wrench fault basins, where subsidence is mainly controlled by faulting (*e.g.*, Jonk and Biermann, 2002; Montenat and Ott d'Estevou, 1999; Weijermars, 1987). Only in the Vera basin, the PFZ has generated significant subsidence, with a step up to 200 m in the eastern boundary (Fig. 7.4a), which can be related to the oblique movement of the Arteal fault (Booth-Rea *et al.*, 2003) and the displacement of the Sierra Almagrera antiform (Coppier *et al.*, 1989; Silva *et al.*, 1993). Notwithstanding, the Vera depocenter is located up to 4 km west of the PFZ (Figs. 7.3b and 7.4a) and sediments are up to 350 m thicker than in the fault zone.

Northwards, the influence of the fault on the development of the basin decreases, as evidenced by the profile 2 (Fig. 7.4b) that shows a smooth filled synform, without any step associated with the fault (Fig. 7.4b). This is not in agreement with a fault zone that could be 3.5 km wide, from the northern tip of the Palomares fault to the Arteal fault, the western boundary of Sierra Almagrera (*e.g.*, Booth-Rea *et al.*, 2003; Silva *et al.*, 2003). Thus, it is likely that the PFZ does not reach this part of the Pulpí basin. In profile 3, the Alhama de Murcia fault (Fig. 7.5, km ~2) is located at the boundary of the sedimentary basin. However, along the profile, the alternation of basins and

basement outcrops is more similar to a succession of antiforms and sediment-filled synforms. This could be the origin of the basement high located at the km ~14 in profile 3 (Fig. 7.5). Alternatively, it could be interpreted as a blind thrust due to its asymmetry. The frontal fault of the Águilas Arc could be related to a step of 0.5 mGal at km ~17 on profile 3.

Although pure strike-slip faults may not exhibit significant vertical displacements, field researches suggests that the PFZ acted as a normal fault in the Pliocene (García-Mayordomo, 2005; Huibregtse *et al.*, 1998; Jonk and Biermann, 2002) and vertical displacements are to be expected from fault activity. Moreover, the Vera basin may have undergone less recent uplift than surrounding basins due to subsidence of the Palomares fault (Booth-Rea *et al.*, 2003; Braga *et al.*, 2003; García-Mayordomo, 2005; Stokes, 2008; Stokes and Mather, 2003). However, the lack of significant changes in the thickness of the sedimentary infill in profiles 2 (Fig. 7.4b) and 3 (Fig. 7.5) points out that the PFZ is disconnected from the northern sector, the western boundary of Sierra Almenara, contrary to what has been interpreted (*e.g.*, Bousquet *et al.*, 1979; García-Mayordomo, 2005; García-Mayordomo *et al.*, 2017; Weijermars, 1987). The PFZ is shorter than expected by the continuity of the western mountain fronts of the Sierra Almagrera and Sierra Almenara, and is mainly related to antiform structures. Then, the uplift of the Pulpí basin (Wenzens and Wenzens, 1997) could be more conditioned by other processes, such as folding, rather than recent PFZ activity (less than 0.1 mm/yr, Herrero-Barbero *et al.*, 2021).

In this area, estimates and simulations of earthquakes of magnitude $M_W > 6.7$ due to ruptures longer than 15 km have been considered (*e.g.*, Herrero-Barbero *et al.*, 2021; García-Mayordomo *et al.*, 2017). These assessments assume fault propagation along the EBSZ and/or include the entire PFZ with a single rupture encompassing the presumed total length of the fault from the northern Sierra Almenara to Sierra Cabrera. However, based on the gravity modelling results, the EBSZ cannot be assumed to be continuous because PFZ and Alhama de Murcia fault are not connected nor parallel, as it is not connected to the Sierra Almenara. Thus, these earthquake estimates might be overestimated.

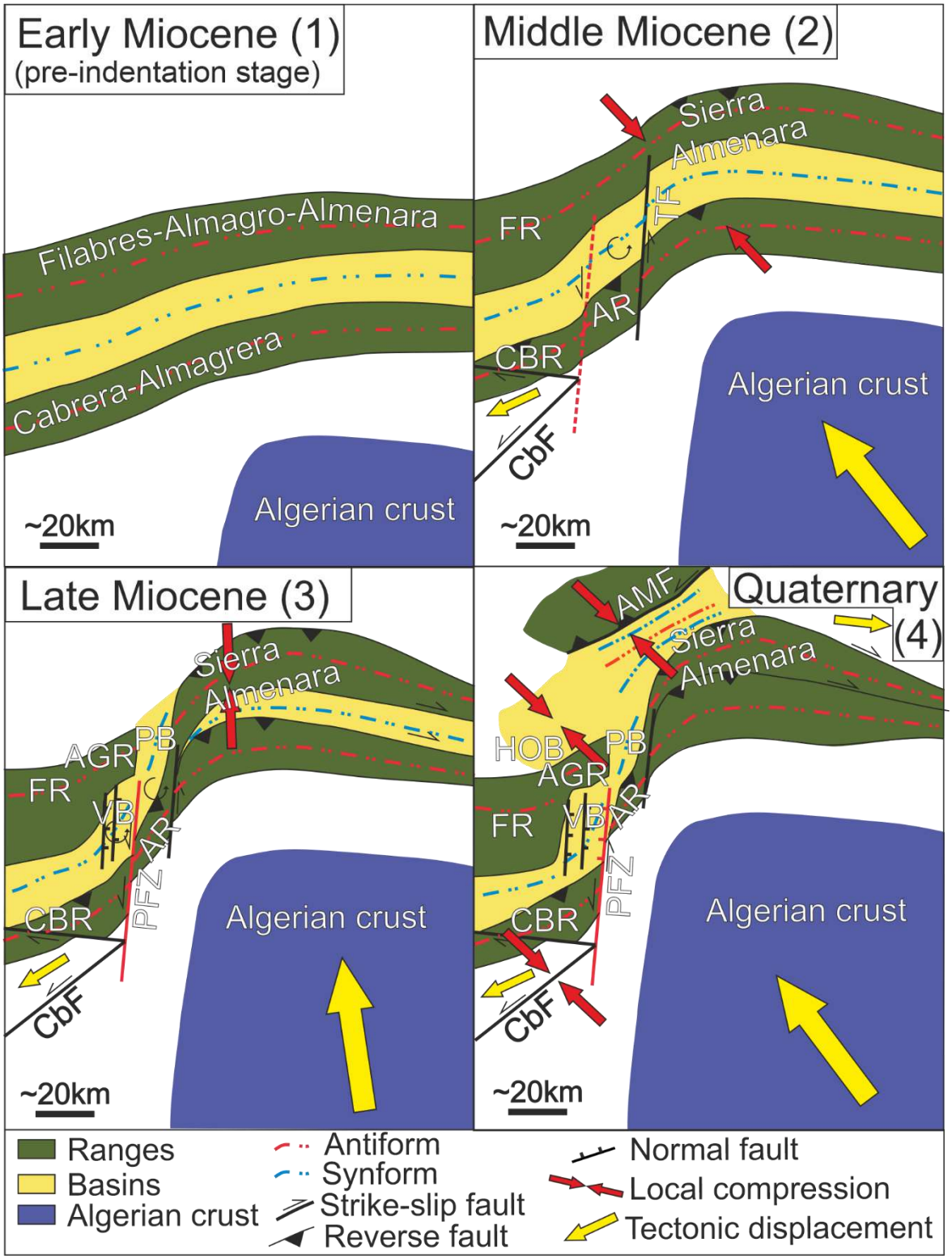

Figure 7.6. Tectonic sketch of the evolution of the Águilas Arc based on Coppier *et al.* (1989) and the activity of the Palomares fault zone. The yellow arrow indicates the regional convergence of Eurasia and Africa. The traces of sinforms and antiforms represent the main trend of the real folds. AGR: Sierra de Almagro; AMF: Alhama de Murcia fault; ALR: Sierra Almagrera; CBR: Sierra Cabrera; FR: Sierra de los Filabres; HOB: Huércal Overa basin; PFZ: Palomares fault zone; PB: Pulpí basin; TF: Terreros fault; VB: Vera basin.

7.5.2 Geodynamics implications

The PFZ can be interpreted as a strike-slip fault that has accommodated the indentation of the Águilas Arc (*e.g.*, Ercilla *et al.*, 2022; Silva *et al.*, 1993) and is the result of a shear zone that has fragmented and rotated the folds of the Betic Internal Zones (*e.g.*, Coppier *et al.*, 1989; Jonk and Biermann, 2002). In the second case, the fault can be considered as a transfer fault bounded by Sierra Cabrera and Sierra Almagrera (*e.g.*, Booth-Rea *et al.*, 2004; Giaconia *et al.*, 2015). Then, a first stage before indentation (Fig. 7.6) may be considered during Early Miocene to Middle Miocene, when folding took place due to the collision of the Betic Cordillera. Once the northwards displacement of part Algerian crust started, the indentation tectonics began and a second stage can be distinguished (Fig. 7.6) characterized by the formation of the PFZ as a shear zone that bent the earlier and active folding and thrusts of the Internal Zones, as noted by Coppier *et al.* (1989) and Weijermars (1987). However, the fold deformation and rotation seems to be the main process, so the PFZ began to form when this process led to their fragmentation (Fig. 7.6). During the Messinian (third stage, Fig. 7.6), the rotation of the compression to N-S trend could have favored the action of the PFZ (Coppier *et al.*, 1989; Huibregtse *et al.*, 1998; Jonk and Biermann, 2002) and the fragmentation of the rotated folds, which better separates the Pulpí and Vera basins. According to the gravity results, the faulting would have affected the synform located under the Vera basin, while in the Pulpí basin the rotation would have been the main process leading to the synform to have N-S trend. Thus, rotation of earlier folds would have been the main mechanism controlling the configuration of the Pulpí and Vera basins, rather than faulting along the PFZ.

In contrast, the current NW-SE compression (last stage, Fig. 7.6) that has started during Plio-Quaternary (*e.g.*, Borque *et al.*, 2019; DeMets *et al.*, 2010; Palano *et al.*, 2015) implies a corner indentation more in line with the model described by Zweigel (1998) than with the model of Tapponier *et al.* (1982) applied to the Águilas Arc by Silva *et al.* (1993). This better explains the transpression and GPS motion radial across the Águilas Arc (Borque *et al.*, 2019; Echeverria *et al.*, 2013; Palano *et al.*, 2015) and the transpression on the Carboneras fault (Echeverria *et al.*, 2015; Rutter *et al.*, 2012). The low seismicity in the Vera and Pulpí basins compared to the Huércal Overa basin and the Alhama de Murcia fault (Alfaro *et al.*, 2012; Echeverria *et al.*, 2013; Herrero-

Barbero *et al.*, 2021; Sánchez-Roldán *et al.*, 2021; Silva *et al.*, 2003) could indicate a northwesterly displacement of the deformation front of the indentation, while compression in Vera and Pulpí basins could be accommodated by folding. Then, the transpressional earthquakes such as the 2011 Lorca earthquake (Martínez-Díaz *et al.*, 2012; Sánchez-Roldán *et al.*, 2021) would be caused by compression of the northwest-trending indentation in combination with lateral uplift (Fig. 7.6). In addition, Roquero *et al.* (2019) found faults in the Guadalentín corridor that were active during the Pleistocene, but sealed by a mature calcrete, so this area may have experienced compression by folding at least until recent times (last stage, Fig. 7.6), as shown by Profile 3 (Fig. 7.5). This could indicate a progressive inactivation of the frontal faults of the Sierra Almenara.

The development of the Águilas Arc indentation into a corner indentation and the transfer of deformation to the northwest could lead to the PFZ inactivation or being blocked in the future. This is supported by recent estimates of low slip rates (Herrero-Barbero *et al.*, 2021, and references therein), GPS data (*e.g.*, Echeverria *et al.*, 2013; Borque *et al.*, 2019) and earthquake distribution (García-Mayordomo, 2005; Herrero-Barbero *et al.*, 2021; Silva *et al.*, 2003). The PFZ could develop in a similar way to the Vauche fault in the Jura Mountains (Homberg *et al.*, 1999) and the Pulpí, Vera and part of the Guadalentín corridor basins could be included in the indenter in the future if indentation progresses. This process has already occurred on the Terreros fault and in the sub-basins of the Águilas Arc (such as the Tébar basin, profile 3, Fig. 7.5), as suggested by Coppier *et al.* (1989). The lower uplift of the Vera basin (Braga *et al.*, 2003; Stokes, 2008) may also be related to its location south of the indentation front, which implies less compression than on the Águilas Arc front.

7.6 Conclusions

This research provides new geophysical data (magnetic and gravimetric) that enhances the understanding of the evolution and configuration of the Vera and Pulpí basins, as well as on the evolution of the PFZ, in the context of the tectonic indentation of the Águilas Arc. The results show that, contrary to previous studies, the depocenters of the Vera and Pulpí basins are located in the central parts of the basins associated with synforms rather than the expected geometry of a wrench fault basin. Only the Vera Basin has a shape clearly influenced by the fault zone, with a stepped

synform and a vertical, eastern boundary (the Arteal fault, which is part of the PFZ). In the north, the Pulpí Basin has a symmetrical synform with no evidence of major faults. The northern sector, along the western part of the Guadalentín corridor, shows a sequence of folds and the effects of the Alhama de Murcia fault are visible. Thus, the PFZ is probably separated from the frontal faults of Sierra Almenara and the EBSZ.

The length of the PFZ is constrained by the deformation, fragmentation and rotation of the folds of the Betic Internal Zones, specifically the antiforms of the Almagrera and Cabrera ranges. The adjacent Vera and Pulpí basins are the result of the corresponding rotated and fragmented synform. These fold rotations are caused by the tectonic indentation of a rigid fragment of the Algerian crust into the eastern Betic. The present-day deformation field from the GPS data and seismicity indicate NW migration of the indentation front, with consequent folding of the western Guadalentín corridor and propagation to the Alhama de Murcia fault. In this context, the activity of the Palomares fault decreases and the Vera Basin experiences a low rate of uplift. The current Eurasia-Africa convergence has led to corner indentation with transpression at the margins, as proposed in the model of Zweigel (1998) for the Carpathian region or the model of Lickorish *et al.* (2002) for the western Alps. However, in contrast to the well-known models of indentation tectonics, the Águilas Arc indentation developed by folds fracture and rotation rather than by the development of large, strike-slip systems that accommodate the indenter displacement. Moreover, the lateral strike-slip faults of the indenter are disconnected from the strike-slip systems developed in the indented block.

References

Alfaro, P., Bartolomé, R., Borque Arancón, M. J., Estévez, A., García Mayordomo, J., García-Tortosa, F. J., ... & Lo Iacono, C. (2012). The Bajo Segura fault zone: active blind thrusting in the eastern betic cordillera (SE Spain). *Journal of Iberian Geology, 38*(1), 271-284. http://dx.doi.org/10.5209/rev_JIGE.2012.v38.n1.39217

Alken, P., Thébault, E., Beggan, C. D., Amit, H., Aubert, J., Baerenzung, J., ... & Zhou, B. (2021). International geomagnetic reference field: the thirteenth generation. *Earth, Planets and Space*, *73*(1), 1-25.

Azad, S. S., Nemati, M., Abbassi, M. R., Foroutan, M., Hessami, K., Dominguez, S., ... & Shahpasandzadeh, M. (2019). Active-couple indentation in geodynamics of NNW Iran: Evidence from synchronous left-and right-lateral co-linear seismogenic faults in western Alborz and Iranian Azerbaijan domains. *Tectonophysics*, *754*, 1-17.

Bardají, T., Cabero, A., Lario, J., Zazo, C., Silva, P. G., Goy, J. L., & Dabrio, C. J. (2015). Coseismic vs. climatic factors in the record of relative sea level changes: An example from the Last Interglacials in SE Spain. *Quaternary Science Reviews*, *113*, 60-77.

Barragán, G. (1997). *Evolución geodinámica de la depresión de Vera: provincia de Vera*. (Doctoral dissertation). Universidad de Granada.

Booth-Rea, G., Azañón, J. M., García-Dueñas, V., & Augier, R. (2003). Uppermost Tortonian to Quaternary depocentre migration related with segmentation of the strike-slip Palomares Fault Zone, Vera Basin (SE Spain). *Comptes Rendus Geoscience*, *335*(9), 751-761.

Booth-Rea, G., Azañón, J. M., Azor, A., & García-Dueñas, V. (2004). Influence of strike-slip fault segmentation on drainage evolution and topography. A case study: the Palomares Fault Zone (southeastern Betics, Spain). *Journal of Structural Geology*, *26*(9), 1615-1632.

Borque, M. J., Sánchez-Alzola, A., Martin-Rojas, I., Alfaro, P., Molina, S., Rosa-Cintas, S., ... & Gil, A. J. (2019). How much Nubia-Eurasia convergence is accommodated by the NE end of the Eastern Betic Shear Zone (SE Spain)? Constraints from GPS velocities. *Tectonics*, *38*(5), 1824-1839.

Bousquet, J. C. (1979). Quaternary strike-slip faults in southeastern Spain. *Tectonophysics*, *52*(1-4), 277-286.

Braga, J. C., Martín, J. M., & Quesada, C. (2003). Patterns and average rates of late Neogene–Recent uplift of the Betic Cordillera, SE Spain. *Geomorphology*, *50*(1-3), 3-26.

Cobbold, P. R., & Davy, P. H. (1988). Indentation tectonics in nature and experiment. II: Central Asia. *Bulletin of the Geological Institution of the University of Upsala*, *14*, 143-162.

Comas, M. C., García-Dueñas, V., & Jurado, M. J. (1992). Neogene tectonic evolution of the Alboran Sea from MCS data. *Geo-Marine Letters*, *12*(2), 157-164.

Coppier, G., Griveaud, P., de Larouziere, F. D., Montenat, C., & Ott d' Estevou, P. (1989). Example of Neogene tectonic indentation in the Eastern Betic Cordilleras: the Arc of Águilas (southeastern Spain). *Geodinamica Acta*, *3*(1), 37-51.

Corsini, M., Chalouan, A., & Galindo-Zaldivar, J. (2014). Geodynamics of the Gibraltar Arc and the Alboran Sea region. *J. Geodyn., 77*, 1–3. https://doi.org/10.1016/j. jog.2014.04.005

Crupa, W. E., Khan, S. D., Huang, J., Khan, A. S., & Kasi, A. (2017). Active tectonic deformation of the western Indian plate boundary: A case study from the Chaman Fault System. *Journal of Asian Earth Sciences*, *147*, 452-468.

Davy, P., & Cobbold, P. R. (1988). Indentation tectonics in nature and experiment. 1. Experiments scaled for gravity. Bull. Geol. Inst. Univ. Uppsala, 14, 129-141.

De Larouzière, F. D., Bolze, J., Bordet, P., Hernandez, J., Montenat, C., & d'Estevou, P. O. (1988). The Betic segment of the lithospheric Trans-Alboran shear zone during the Late Miocene. *Tectonophysics*, *152*(1-2), 41-52.

DeMets, C., Gordon, R. G., & Argus, D. F. (2010). Geologically current plate motions. *Geophysical Journal International*, *181*(1), 1–80. https://doi.org/10.1111/j.1365-246X.2009.04491.x

Diaz, J., Gallart, J., & Carbonell, R. (2016). Moho topography beneath the Iberian-Western Mediterranean region mapped from controlled-source and natural seismicity surveys. *Tectonophysics*, *692*, 74-85.

Duggen, S., Hoernle, K., Klügel, A., Geldmacher, J., Thirlwall, M., Hauff, F., ... & Oates, N. (2008). Geochemical zonation of the Miocene Alborán Basin volcanism (westernmost

Mediterranean): geodynamic implications. *Contributions to Mineralogy and Petrology, 156*(5), 577.

Durán, R., Lobo, F. J., Ribó, M., García, M., & Somoza, L. (2018). Variability of shelf growth patterns along the Iberian Mediterranean margin: sediment supply and tectonic influences. *Geosciences*, *8*(5), 168.

Echeverria, A., Khazaradze, G., Asensio, E., Gárate, J., Dávila, J. M., & Suriñach, E. (2013). Crustal deformation in eastern Betics from CuaTeNeo GPS network. *Tectonophysics*, *608*, 600-612.

Echeverria, A., Khazaradze, G., Asensio, E., & Masana, E. (2015). Geodetic evidence for continuing tectonic activity of the Carboneras fault (SE Spain). *Tectonophysics*, *663*, 302-309.

Ercilla, G., Galindo-Zaldívar, J., Estrada, F., Valencia, J., Juan, C., Casas, D., ... & Yenes, M. (2022). Understanding the complex geomorphology of a deep sea area affected by continental tectonic indentation: The case of the Gulf of Vera (Western Mediterranean). *Geomorphology*, 108126.

Estrada, F., Galindo-Zaldivar, J., Vázquez, J. T., Ercilla, G., D'Acremont, E., Alonso, B., & Gorini, C. (2018). Tectonic indentation in the central Alboran Sea (westernmost Mediterranean). *Terra Nova, 30*(1), 24-33. https://doi.org//10.1111/ter.12304

Ferrater, M., Ortuño, M., Masana, E., Martínez-Díaz, J. J., Pallàs, R., Perea, H., ... & Arrowsmith, R. (2017). Lateral slip rate of Alhama de Murcia fault (SE Iberian Peninsula) based on a morphotectonic analysis: Comparison with paleoseismological data. *Quaternary International*, *451*, 87-100.

Galindo-Zaldivar, J., Gonzalez-Lodeiro, F., & Jabaloy, A. (1989). Progressive extensional shear structures in a detachment contact in the western Sierra Nevada, (Betic Cordilleras, Spain). *Geodinamica Acta, 3*(1), 73-85.

Galindo-Zaldıvar, J., Gil, A. J., Borque, M. J., González-Lodeiro, F., Jabaloy, A., Marın-Lechado, C., ... & De Galdeano, C. S. (2003). Active faulting in the internal zones of the central Betic Cordilleras (SE, Spain). *Journal of Geodynamics*, *36*(1-2), 239-250. https://doi.org/10.1016/S0264-3707(03)00049-8

Galindo-Zaldívar, J., Braga, J. C., Marín-Lechado, C., Ercilla, G., Martín, J. M., Pedrera, A., ... & Alonso, B. (2019). Extension in the Western Mediterranean. In *The geology of Iberia: a geodynamic approach* (pp. 61-103). Springer, Cham.

García-Dueñas, V., & Balanyá, J. C. (1986). Estructura y naturaleza del Arco de Gibraltar. *Maleo Bolletin. Societa Geologica del Portugal*, *2*, 23.

García-Mayordomo, J. (2005). *Caracterización y Análisis de la Peligrosidad Sísmica en el Sureste de España.* Doctoral dissertation. Universidad Complutense de Madrid.

García-Mayordomo, J., Martín-Banda, R., Insua-Arévalo, J. M., Álvarez-Gómez, J. A., Martínez-Díaz, J. J., & Cabral, J. (2017). Active fault databases: building a bridge between earthquake geologists and seismic hazard practitioners, the case of the QAFI v. 3 database. *Natural Hazards and Earth System Sciences*, *17*(8), 1447-1459.

Giaconia, F., Booth-Rea, G., Martínez-Martínez, J. M., Azañón, J. M., & Pérez-Peña, J. V. (2012). Geomorphic analysis of the Sierra Cabrera, an active pop-up in the constrictional domain of conjugate strike-slip faults: The Palomares and Polopos fault zones (eastern Betics, SE Spain). *Tectonophysics*, *580*, 27-42.

Giaconia, F., Booth-Rea, G., Ranero, C. R., Gràcia, E., Bartolome, R., Calahorrano, A., ... & Viñas, M. (2015). Compressional tectonic inversion of the Algero-Balearic basin: Latemost Miocene to

present oblique convergence at the Palomares margin (Western Mediterranean). *Tectonics*, *34*(7), 1516-1543.

Giménez, J., Suriñach, E., & Goula, X. (2000). Quantification of vertical movements in the eastern Betics (Spain) by comparing levelling data. *Tectonophysics*, *317*(3-4), 237-258.

Gómez de la Peña, L., Gràcia, E., Muñoz, A., Acosta, J., Gómez-Ballesteros, M., Ranero, C. R., & Uchupi, E. (2016). Geomorphology and Neogene tectonic evolution of the Palomares continental margin (Western Mediterranean). *Tectonophysics*, *689*, 25-39.

Gueguen, E., Doglioni, C., & Fernandez, M. (1998). On the post-25 Ma geodynamic evolution of the western Mediterranean. *Tectonophysics, 298*(1-3), 259–269. https://doi.org/10.1016/S0040-1951(98)00189-9.

Herrero-Barbero, P., Álvarez-Gómez, J. A., Williams, C., Villamor, P., Insua-Arévalo, J. M., Alonso-Henar, J., & Martínez-Díaz, J. J. (2021). Physics-Based Earthquake Simulations in Slow-Moving Faults: A Case Study From the Eastern Betic Shear Zone (SE Iberian Peninsula). *Journal of Geophysical Research: Solid Earth*, *126*(5), e2020JB021133.

Homberg, C., Lacombe, O., Angelier, J., & Bergerat, F. (1999). New constraints for indentation mechanisms in arcuate belts from the Jura Mountains, France. *Geology*, *27*(9), 827-830.

Huibregtse, P., van Alebeek, H., Zaal, M., & Biermann, C. (1998). Palaeostress analysis of the northern Nijar and southern Vera basins: constraints for the Neogene displacement history of major strike-slip faults in the Betic Cordilleras, SE Spain. *Tectonophysics*, *300*(1-4), 79-101.

Jabaloy-Sánchez, A., Martín-Algarra, A., Padrón-Navarta, J. A., Martín-Martín, M., Gómez-Pugnaire, M. T., Sánchez-Vizcaíno, V. L., & Garrido, C. J. (2019). Lithological successions of the Internal Zones and Flysch Trough units of the Betic Chain. In *The Geology of Iberia: A Geodynamic Approach* (pp. 377-432). Springer, Cham. https://doi.org/10.1007/978-3-030-11295-0_8

Jonk, R., & Biermann, C. (2002). Deformation in Neogene sediments of the Sorbas and Vera Basins (SE Spain): constraints on simple-shear deformation and rigid body rotation along major strike-slip faults. *Journal of Structural Geology*, *24*(5), 963-977.

Kane, M. (1962). A comprehensive system of terrain corrections using a digital computer. *Geophysics*, *27*(4), 455–462. https://doi.org/ 10.1190/1.1439044

Lickorish, W. H., Ford, M., Burgisser, J., & Cobbold, P. R. (2002). Arcuate thrust systems in sandbox experiments: A comparison to the external arcs of the Western Alps. *Geological Society of America Bulletin*, *114*(9), 1089-1107.

Lu, C. Y., & Malavieille, J. (1994). Oblique convergence, indentation and rotation tectonics in the Taiwan Mountain Belt: Insights from experimental modelling. *Earth and Planetary Science Letters*, *121*(3-4), 477-494.

Mann, P. (2007). Global catalogue, classification and tectonic origins of restraining-and releasing bends on active and ancient strike-slip fault systems. *Geological Society, London, Special Publications*, *290*(1), 13-142.

Martín-Banda, R., García-Mayordomo, J., Insua-Arévalo, J. M., Salazar, Á. E., Rodríguez-Escudero, E., Álvarez-Gómez, J. A., ... & Herrero, M. J. (2016). New insights on the seismogenic potential of the Eastern Betic Shear Zone (SE Iberia): Quaternary activity and paleoseismicity of the SW segment of the Carrascoy Fault Zone. *Tectonics*, *35*(1), 55-75.

Martínez-Díaz, J. J., Bejar-Pizarro, M., Álvarez-Gómez, J. A., de Lis Mancilla, F., Stich, D., Herrera, G., & Morales, J. (2012). Tectonic and seismic implications of an intersegment rupture: The damaging May 11th 2011 Mw 5.2 Lorca, Spain, earthquake. *Tectonophysics*, *546*, 28-37.

Medaouri, M., Déverchère, J., Graindorge, D., Bracene, R., Badji, R., Ouabadi, A., ... & Bendiab, F. (2014). The transition from Alboran to Algerian basins (Western Mediterranean Sea): chronostratigraphy, deep crustal structure and tectonic evolution at the rear of a narrow slab rollback system. *Journal of Geodynamics*, *77*, 186-205.

Montenat, C., & Ott d'Estevou, P. (1999). The diversity of late Neogene sedimentary basins generated by wrench faulting in the Eastern Betic Cordillera, SE Spain. *Journal of Petroleum Geology*, *22*(1), 61-80.

Nagy, D. (1966). The gravitational attraction of a right rectangular prism. *Geophysics*, *31*(2), 362–371. https://doi.org/10.1190/1.1439779

Palano, M., González, P. J., & Fernández, J. (2015). The Diffuse Plate boundary of Nubia and Iberia in the Western Mediterranean: Crustal deformation evidence for viscous coupling and fragmented lithosphere. *Earth and Planetary Science Letters*, *430*, 439-447.

Pedley, R. C., Busby, J. P., & Dabek, Z. K. (1993). *GRAVMAG user manual-interactive 2.5 D gravity and magnetic modelling* (technical report WK/93/26/R.73). British Geological Survey.

Pedrera, A., Galindo-Zaldívar, J., Tello, A., & Marín-Lechado, C. (2010). Intramontane basin development related to contractional and extensional structure interaction at the termination of a major sinistral fault: The Huércal-Overa Basin (Eastern Betic Cordillera). *Journal of Geodynamics*, *49*(5), 271-286.

Platt, J. P., & Vissers, R. L. M. (1989). Extensional collapse of thickened continental lithosphere: A working hypothesis for the Alboran Sea and Gibraltar arc. *Geology*, *17*(6), 540–543.

Platt, J. P., Allerton, S., Kirker, A., Mandeville, C., Mayfield, A., Platzman, E. S., & Rimi, A. (2003). The ultimate arc: Differential displacement, oroclinal bending, and vertical axis rotation in the External Betic-Rif arc. *Tectonics*, *22*(3).

Rehault, J.P., Boillot, G., & Mauffret, A. (1985). *The Western Mediterranean Basin.* In: Stanley, D.J., Wezel, F.-C. (Eds.), *Geological Evolution of the Mediterranean Basin: Raimondo Selli Commemorative Volume.* Springer New York, New York, NY, pp. 101–129.

Roquero, E., Silva, P. G., Rodríguez-Pascua, M. A., Bardají, T., Elez, J., Carrasco-García, P., & Giner-Robles, J. L. (2019). Analysis of faulted fan surfaces and paleosols in the Palomares Fault Zone (Betic Cordillera, SE Spain): Paleoclimatic and paleoseismic implications. *Geomorphology*, *342*, 88-102.

Rosenberg, C. L., Brun, J. P., & Gapais, D. (2004). Indentation model of the Eastern Alps and the origin of the Tauern Window. *Geology*, *32*(11), 997-1000.

Rutter, E. H., Faulkner, D. R., & Burgess, R. (2012). Structure and geological history of the Carboneras Fault Zone, SE Spain: Part of a stretching transform fault system. *Journal of Structural Geology*, *45*, 68-86.

Sánchez-Roldán, J. L., Martínez-Díaz, J. J., Cantavella, J. V., Álvarez-Gómez, J. A., & Morales, J. (2021). Relocation of Seismicity in the Guadalentín Tectonic Valley, Eastern Betics Shear Zone (Southeast Iberia). *Seismological Society of America*, *92*(5), 3046-3064.

Sanz De Galdeano, C. (1990). Geologic evolution of the Betic Cordilleras in the Western Mediterranean, Miocene to the present. *Tectonophysics*, *172*(1-2), 107–119. https://doi.org/10.1016/0040-1951(90)90062-D

Silva, P. G., Goy, J. L., Somoza, L., Zazo, C., & Bardají, T. (1993). Landscape response to strike-slip faulting linked to collisional settings: Quaternary tectonics and basin formation in the Eastern Betics, southeastern Spain. *Tectonophysics*, *224*(4), 289-303.

Silva, P. G., Goy, J. L., Zazo, C., & Bardajı, T. (2003). Fault-generated mountain fronts in southeast Spain: geomorphologic assessment of tectonic and seismic activity. *Geomorphology*, *50*(1-3), 203-225.

Spakman, W., Chertova, M.V., van den Berg, A., & van Hinsbergen, D. J. (2018). Puzzling features of western Mediterranean tectonics explained by slab dragging. *Nat. Geosci., 11*(3), 211–216. https://doi.org/10.1038/s41561-018-0066-z.

Stokes, M. (2008). Plio-Pleistocene drainage development in an inverted sedimentary basin: Vera basin, Betic Cordillera, SE Spain. *Geomorphology*, *100*(1-2), 193-211.

Stokes, M., & Mather, A. E. (2003). Tectonic origin and evolution of a transverse drainage: the Río Almanzora, Betic Cordillera, Southeast Spain. *Geomorphology*, *50*(1-3), 59-81.

Stich, D., Martín, R., & Morales, J. (2010). Moment tensor inversion for Iberia–Maghreb earthquakes 2005–2008. *Tectonophysics*, *483*(3-4), 390-398.

Sylvester, A. G. (1988). Strike-slip faults. *Geological Society of America Bulletin*, *100*(11), 1666-1703.

Tapponnier, P., Peltzer, Le Dain, A. Y., Armijo, R., & Cobbold, P. (1982). Propagating extrusion tectonics in Asia: New insights from simple experiments with plasticine. *Geology*, *10*(12), 611-616.

Tavakoli, F., Walpersdorf, A., Authemayou, C., Nankali, H. R., Hatzfeld, D., Tatar, M., ... & Cotte, N. (2008). Distribution of the right-lateral strike–slip motion from the Main Recent Fault to the Kazerun Fault System (Zagros, Iran): Evidence from present-day GPS velocities. *Earth and Planetary Science Letters*, *275*(3-4), 342-347.

Telford, W. M., Geldart, L. P., & Sheriff, R. E. (1990). *Applied Geophysics*. Cambridge, UK. Cambridge University Press.

Tendero-Salmerón, V., Galindo-Zaldivar, J., d'Acremont, E., Catalán, M., Martos, Y. M., Ammar, A., & Ercilla, G. (2022). New insights on the Alboran Sea basin extension and continental collision from magnetic anomalies related to magmatism (western Mediterranean). *Marine Geology*, *443*, 106696.

Völk, H. R. (1966). *Geologie et stratigraphie du Bassin Neogene de Vera*. Doctoral dissertation. University of Amsterdam.

Weijermars, R. (1987). The Palomares brittle—ductile Shear Zone of southern Spain. *Journal of Structural Geology*, *9*(2), 139-157.

Wenzens, E., & Wenzens, G. (1997). The influence of tectonics, sea-level fluctuations and river capture on the Quaternary morphogenesis of the semi-arid Pulpi Basin (southeast Spain). *Catena*, *30*(4), 283-293.

Zweigel, P. (1998). Arcuate accretionary wedge formation at convex plate margin corners: results of sandbox analogue experiments. *Journal of Structural Geology*, *20*(12), 1597-1609.

CHAPTER 8

Seismicity in Strike-Slip Foreland Faults (Central Betic Cordillera Front): Evidence of Indentation Tectonics.

Víctor Tendero-Salmerón[1], Jesus Galindo-Zaldivar[1,2], José A. Peláez[3], Manuel Martínez-Martos[2], Jesús Henares[3], Carlos Marín-Lechado[4], Antonio J. Gil[5,6], Ángel Carlos López-Garrido[1]

[1]Instituto Andaluz de Ciencias de la Tierra (CSIC-UGR), 18100 Armilla (Granada), Spain.

[2]Departamento de Geodinámica, Universidad de Granada, 18071 Granada, Spain.

[3]Departamento de Física, Universidad de Jaén, Campus de Las Lagunillas, 23071 Jaén, Spain.

[4]Instituto Geológico-Minero de España, Madrid, Spain.

[5]Departamento de Ingeniería Cartográfica, Geodésica y Fotogrametría, Universidad de Jaén, Campus de Las Lagunillas, 23071 Jaén, Spain

[6]Centro de Estudios Avanzados en Ciencias de la Tierra, Energía y Medio Ambiente (CEACTEMA), Universidad de Jaén, Campus de Las Lagunillas, 23071 Jaén, Spain

Published on:

Tectonics, Volume 39 (7) (May 2020)
https://doi.org/10.1029/2020TC006143

(Received 11 February 2020, Accepted 25 May 2020, Published 27 May 2020)

JCR (2020): 4.851 (Q1)

Abstract

Unexpected seismicity has been detected in the past few years along the northern Guadiana Menor River (Guadalquivir foreland basin), at the northern boundary of the Betic Cordillera. Earthquake focal mechanisms evidence the activity of N-S to NNE-SSW sinistral faults in the basement. Yet continuous GPS (CGPS) data show a westward movement in both the Prebetic Arc and the eastern Guadalquivir basin infill, which disagrees with the strike-slip faults. To more precisely describe the structure and evolution of the area, new Bouguer anomaly data from the southeastern basin combined with seismicity data, electric resistivity tomography profiles (ERT) and surface studies are provided. Given the soft consistency of the sedimentary infill in the area, surface evidence of faulting is scarce, limited to elongated channel and minor vertical faults affecting Quaternary sediments, where ERT profiles suggested the presence of faults. These results suggest that the Guadalquivir basin infill, the Prebetic Arc and the central Betic Cordillera move towards the west, independent from the Iberian crust, but indicating to some extent an upward propagation of the basement deformation. However, the basement is coupled with the Alboran Domain and undergoes NNW-SSE Eurasia-Nubia convergence and orthogonal extension. This scenario is suggestive of the initial stages of indentation tectonics, better developed in the eastern Betic Cordillera and the central Alboran Sea.

Plain Language Summary

Earthquakes in Guadalquivir valley were not thought to be important until the last decade. In the eastern part, some of these earthquakes have even been felt by population and some groups of them have attracted attention. We study the origin (a fault or a group of faults) of the last group that occurred in the Guadiana Menor valley and that have reached magnitude 4. The main problem is some data are apparently contradictory. The analysis of the earthquakes allows us to figure out how is the movement of the fault, but it contradicts the movement we observed at surface with other techniques, such as GPS measurements. In addition, the fault(s) we propose must have an explanation together with the evolution of the region. Thus, we suggest that the lower part of the terrain (the basement) is moving different from the upper part (the sediments) and it is experimenting deformation derived from the convergence of Europe and Africa. Thus, a new fault is growing in the lower part,

meaning a change of the tectonic pattern in this area. These results provide information useful in the study of the region evolution and how, why and where we can expect forthcoming earthquakes.

Key Words: seismicity, seismic series, strike-slip faults, foreland basin, gravity anomalies

8.1 Introduction

Fold and thrust belts develop a deformation front with related foreland basins (Flemings and Jordan, 1990) separating the orogenic belts from the undeformed regions. Their most predominant features are thrust faults, caused by shortening as a consequence of compression during the advance of the belts (Dahlen *et al.*, 1984), while the development of a bulge and tilting in the foreland basin may be related to normal faults (Flemings and Jordan, 1990) and it is due to flexure caused by the subduction of the downgoing plate (*e.g.*, Bradley and Kidd, 1991; Granado *et al.*, 2016). In a simple scenario of plate convergence, the growth of strike-slip faults is secondary depending on the regional geological setting; they are tear faults, consequence of the accommodation of the different rates of the thrusted units. Deformation and seismicity largely decrease in the mountain front, and the foreland is considered more stable than the hinterland. Only when end-stage irregular continental collision takes place, and coupling between the two continents is high, do strike-slip faults appear in the foreland block at the back of the initial protrusion that indents into the foreland (Sengör, 1976; Tapponnier *et al.*, 1982). The presence of large strike-slip fault sets has been interpreted as resulting from indentation tectonics, especially when taking place in the hinterland portions of orogenic systems; examples of this have been reported for the Himalaya orogeny (Tapponnier *et al.*, 1982), the Arabian region (Regard *et al.*, 2005), or the eastern Alps (Rosenberg *et al.*, 2004).

In contrast, in oblique plate convergence, strike-slip faulting can take the form of primary structures. Strain partitioning generates a combination of dipping faults and strike-slip faults, as can be seen in the Gulf of Cadiz (*e.g.*, Rosas *et al.*, 2012; Terrinha *et al.*, 2009), in subduction zones such as Sumatra (*e.g.*, MacCaffrey *et al.*, 2000) and in transpressive plate boundaries (e.g,. Braun and Beaumont, 1995). Arc-shaped

orogens are common in oblique convergence and are associated with lithospheric processes such as delamination (*e.g.*, central and western Mediterranean, Channel and Mareschal, 1989; Platt and Vissers, 1989) and subduction with related roll-back. Subduction with roll-back has been evoked in various tectonic contexts: the eastern and central Mediterranean region (Wortel and Spakman, 2000); the southwest Pacific region (Schellart *et al.*, 2006); or the Banda subduction zone (Hall and Spakman, 2010).

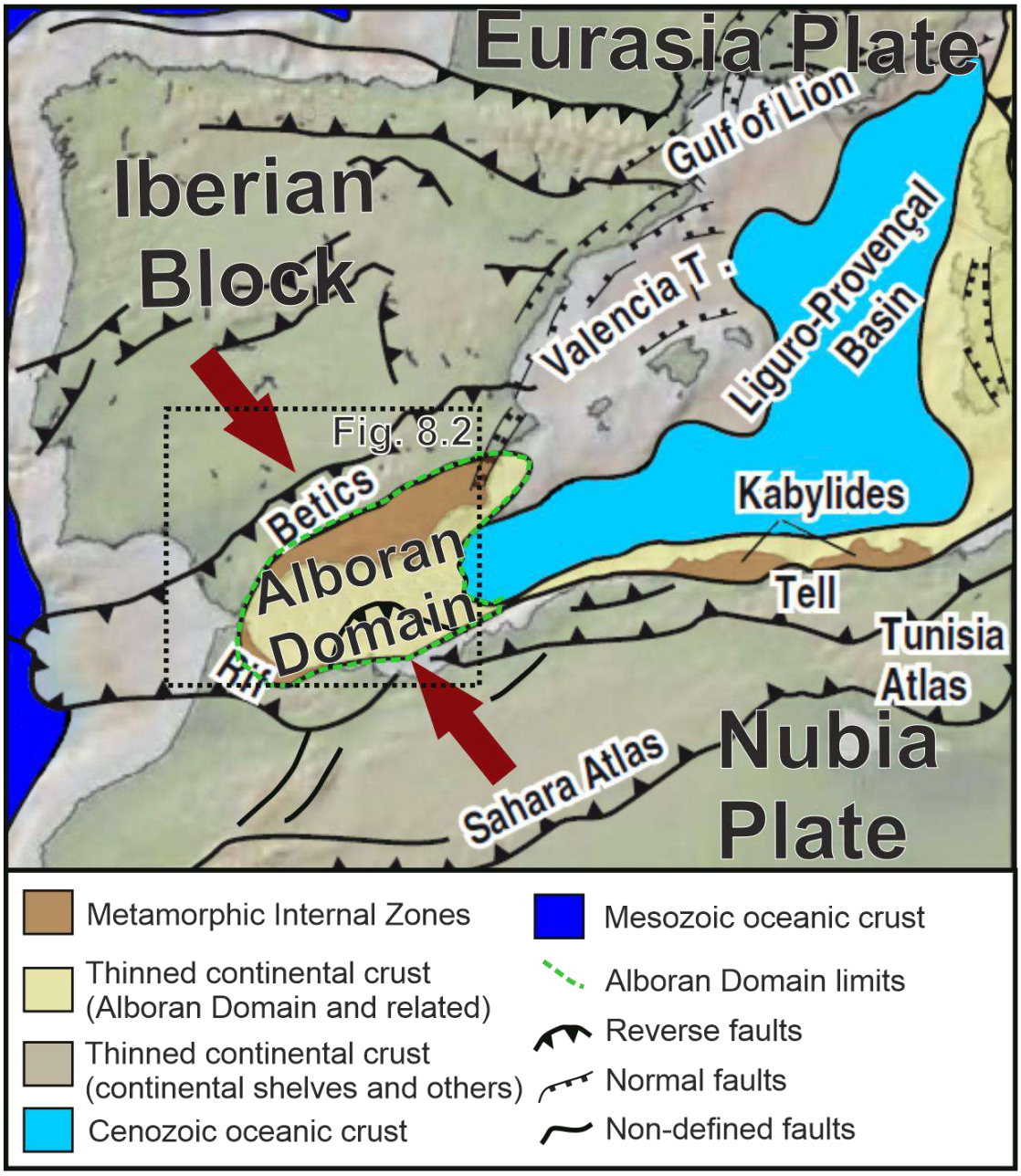

Figure 8.1. Tectonic map of westernmost Mediterranean Sea. The location of Figure 8.2 is despicted. Modified from Do Couto *et al.* (2016). Red arrows indicate present-day direction of shortening.

The Gibraltar Arc (Figs. 8.1 and 8.2) is an example of arc-shaped orogen in oblique plate convergence. It is formed by the Betic and Rif cordilleras in the westernmost Mediterranean, is affected by extensional and compressional deformations in the context of the oblique Eurasia-Nubia (Africa) convergence and the westward motion of the Alboran Domain (DeMets *et al.*, 2010; Galindo-Zaldivar *et al.*, 2003; Sanz de Galdeano, 1990). To explain its evolution, several geodynamic models based on lithospheric delamination (Platt and Vissers, 1989) and roll-back subduction (Blanco and Spakman, 1993) have been proposed. Furthermore, indentation tectonic models have been suggested for some areas in the region, such as the central Alboran Sea (Estrada *et al.*, 2018) and eastern areas, in the Águilas Arc (Silva *et al.*, 1993). Its arc-shaped geometry attests to vertical axis rotations of crustal tectonic units during its development (Crespo-Blanc *et al.*, 2016; Platt *et al.*, 2003). Consequently, strike-slip earthquakes are more common and significant in these areas rather than in the Central Betics, where extension is predominant (Stich *et al.*, 2006). However, some strike-slip seismic swarms have affected to the Guadalquivir foreland basin (Fig. 8.2), where there are not outcrops of significant strike-slip faults. A seismic series rooted in the area of Torreperogil between 2012 and 2013 has been related with N-S faults (Serrano *et al.*, 2015), with N-S faults that turn E-W in Torreperogil (Morales *et al.*, 2015), and with a combination of E-W transpressive faults related to NE-SW faults (Marín-Lechado *et al.*, 2017; Pedrera *et al.*, 2013). Since 2016, a prolonged seismic sequence has been recorded in the northern Guadiana Menor valley near the village of Peal de Becerro, about 20 km southeast of Torreperogil. Though the earthquakes are characterized by strike-slip moment tensors (www.ign.es) (Fig. 8.2), at surface there are no clear signs of strike-slip tectonics. Moreover, CGPS data (Galindo-Zaldivar *et al.*, 2015) show WSW-ward movement with respect to Iberia, which implies homogenous displacement, yet there is no evidence of active deformation in the eastern Guadalquivir foreland basin (Fig. 8.2a).

The aim of this research is to propose a geodynamic model that integrate***s*** the strike-slip seismicity in the foreland basin. To this end we have determined the structures in the eastern Guadalquivir foreland basin that cause the seismicity of the North Guadiana Menor river. Our results point to a propagation of the indentation tectonics in eastern Betics towards the eastern Guadalquivir foreland basin.

8.2 Geological and Seismic Setting

The Betic Cordillera constitutes the northern branch of the Gibraltar Arc, an alpine orogen. It comprises the Alboran Domain (Internal Zones) and the South Iberian Domain (External Zones), separated by Flysch units (García-Dueñas and Balanyá, 1986; Sanz De Galdeano, 1990). During the Neogene and Quaternary, several sedimentary basins developed along the cordillera (Sanz De Galdeano, 1990). The Gibraltar Arc (Figs. 8.1 and 8.2) is the result of westward displacement of the Alboran Domain because of Eurasia-Nubia convergence —still active at a rate of 4 mm/year (DeMets *et al.*, 2010) — and slab roll-back (Blanco & Spakman, 1993). Subduction-related roll-back in the Western Mediterranean is considered one of the main mechanisms to explain the displacement of the Alboran Domain and the evolution of the Gibraltar Arc, but geodynamic models are still being developed (*e.g.*, Chertova *et al.*, 2014; Spakman *et al.*, 2018). In this setting, a deformed region of about 300 km wide constitutes the plate boundary, with heterogeneously widespread seismicity (Galindo-Zaldivar *et al.*, 2015).

The Internal Zones comprise overlapped metamorphic complexes of Palaeozoic to Mesozoic age (Fontboté, 1966; Platt and Vissers, 1989; Sanz De Galdeano, 1990). The Flysch units are a group of siliciclastic rocks deposited between the External and Internal zones during the Oligocene and the Miocene. The External Zones constitute a Mesozoic and Cenozoic marine carbonate platform that developed on the southern border of the Iberian Massif (García-Dueñas and Balanyá, 1986; García-Hernández *et al.*, 1980) and are divided into the Subbetic and Prebetic domains. Whereas the Subbetic corresponds to the outermost platform, the Prebetic harbors the shallow platform close to the continent, containing some continental facies (García-Dueñas and Balanyá, 1986). At present, the External Zones constitute a fold-and-thrust belt with large olistostromic deposits in the frontal area (García-Hernández *et al.*, 1980), where Triassic rocks of Keuper facies, which constitutes a layered clay-evaporitic sequence, act as a detachment level (García-Hernández *et al.*, 1980; Platt *et al.*, 2003; Rodríguez-Fernández *et al.*, 2015). The Guadalquivir foreland basin (Fig. 8.2) contains these olistostromic units together with Miocene marine sediments and Quaternary continental sediments (García-Castellanos *et al.*, 2002; García-Hernández *et al.*, 1980). The basement of the Guadalquivir basin is the crust of the Iberian Massif, made of

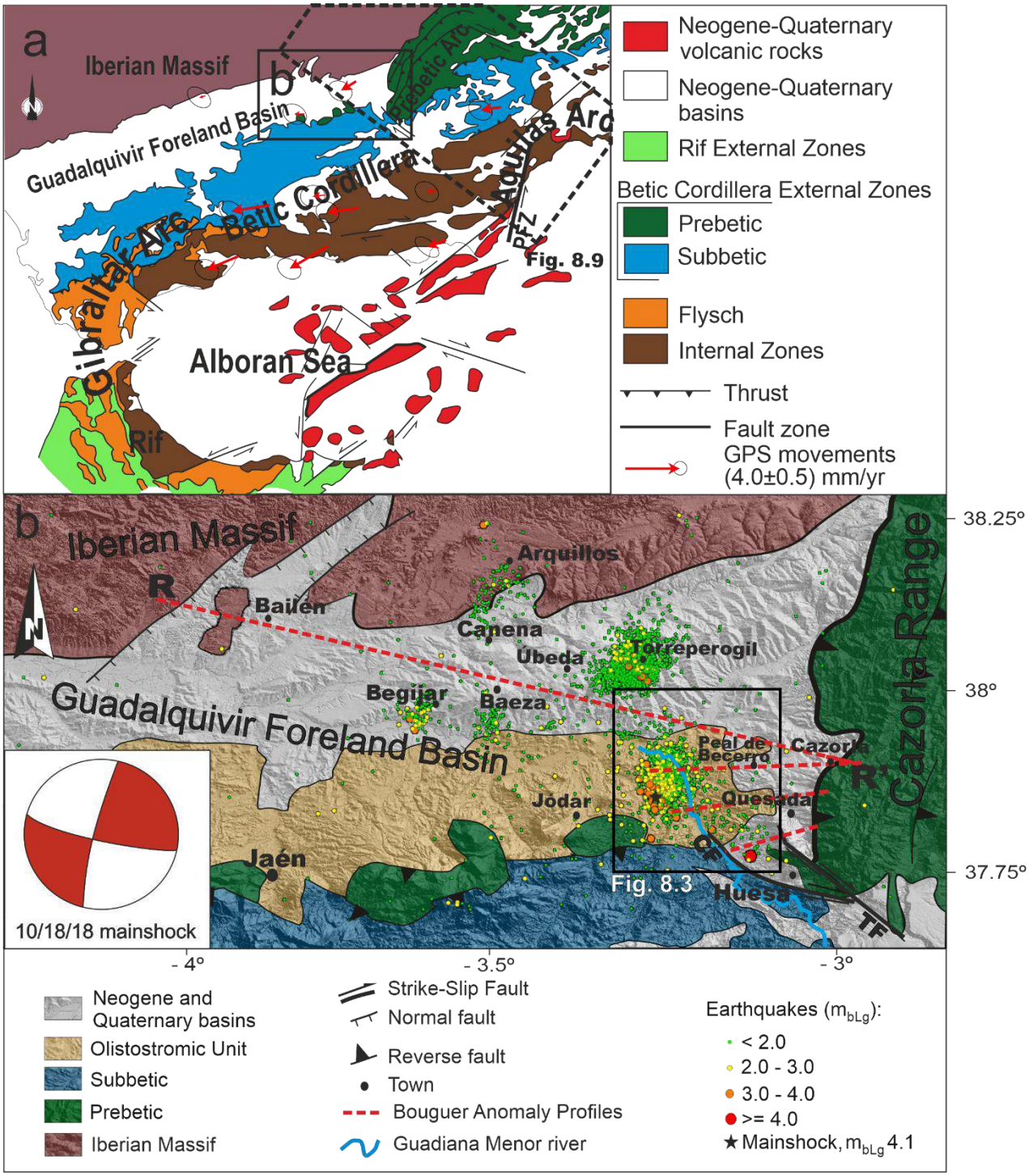

Figure 8.2. Geological setting of eastern Guadalquivir foreland basin seismicity in the central Betic Cordillera. a. Geologic map of the Gibraltar Arc with CGPS residual velocity field, with respect to the Eurasia fixed reference frame and 95% confidence ellipses of Galindo-Zaldívar *et al.* (2015). b. Geologic location of the study zone with seismicity and an example of the characteristic focal mechanism of those earthquakes. CF = Collejares fault, PFZ = Palomares Fault Zone, TF = Tíscar Fault. The locations of Figures 3, 4 (R-R') and 9 are also depicted. Both this figure and the following ones use WGS84 datum and geographic coordinates as projection system for all maps.

Variscan igneous and metamorphic rocks below a Mesozoic sedimentary cover (Julivert and Fontboté, 1977). The eastern limit of the Guadalquivir basin is the Prebetic Arc, being the Cazorla Range its southern part (Fig. 8.2). The Tíscar dextral fault constitutes the southern termination of the Prebetic Arc (Fig. 8.2). The area of study (Fig. 8.2b) comprises the Cazorla Range front, including the Tíscar fault, and the easternmost part of the Guadalquivir basin.

Compressional and extensional deformations have taken place in the Betic Cordillera since the Cretaceous (Galindo-Zaldıvar *et al.*, 2003; Jabaloy *et al.*, 2002; Platt and Vissers, 1989; Sanz De Galdeano, 1990). These deformations have affected even distant areas of the Iberian Peninsula, generating fault reactivation and folds (De Vicente and Vegas, 2009; Jabaloy *et al.*, 2002). Present-day stresses determined from seismic moment tensors, structural data and velocities from CGPS data vary throughout the cordillera (Fernández-Ibáñez *et al.*, 2007; Galindo-Zaldivar *et al.*, 2015; Garate *et al.*, 2015; Henares *et al.*, 2003; Stich *et al.*, 2006). In some areas the stresses deduced from seismic data do not fit calculations from outcropping structures, pointing to a vertical variation of present-day stress (Marín-Lechado *et al.*, 2005). Many studies describe important detachments affecting the crust (Galindo-Zaldivar *et al.*, 1989; Jabaloy *et al.*, 2002; Platt and Vissers, 1989; Silva *et al.*, 1993). Some authors propose mainly high-dipping shear zones crossing the Betic Cordillera and extending to the Alboran Sea to separate domains with different features (Andeweg and Cloetingh, 2001; De Larouzière *et al.*, 1988; Sanz De Galdeano, 1990; Stich *et al.*, 2006).

Local seismicity includes shallow widespread low-magnitude and low-to-moderate-magnitude earthquakes, as well as shallow and intermediate events in the western Alboran Sea, and scarce deep events (up to 650 km) south of Granada (Morales *et al.*, 1999). In the easternmost Guadalquivir foreland basin, a region holding low seismic hazard (Peláez and López-Casado, 2002), two significant swarms have been recorded in this decade: the 2012-2013 Torreperogil sequence, and the current northern Guadiana Menor seismic sequence (Fig. 8.2b), with most earthquakes located 9-13 km deep. The Torreperogil seismic swarm was clearly related to strike-slip basement tectonics, supported by some focal mechanisms, although seismicity data alone do not explain the basement´s active fault (Marín-Lechado *et al.*, 2017; Morales *et al.*, 2015;

Pedrera *et al.*, 2013; Roldán *et al.*, 2013). The characteristics of the Guadiana Menor seismicity are discussed for the first time in this study. Another minor seismic sequences that occurred in this region, near the study area, involved Arquillos in 2010-2011 (59 events, the biggest a m_{bLg} 3.2 earthquake), Baeza in 2011 (71 events, m_{bLg} 2.7), Canena, 2012-2013 (23 events, m_{bLg} 2.3), and Lupión-Begíjar in 2014 (46 events, m_{bLg} 3.8), the latter described in Marín Lechado *et al.* (2017) (Fig. 8.2b). In sum, recent years have witnessed regional seismicity of mainly low magnitude, reliably detected by the Spanish seismic network.

Deserving special mention here is the seismic series of Huesa, 2012, likewise in the Guadiana Menor area. It included 24 earthquakes, in which the largest event recorded was one of m_{bLg} 4.4. Unlike other seismic swarms, its behaviour followed the typical main event-foreshock sequence. In this case, no clear alignment of relocated epicentres was discerned, though an E-W direction prevails. The seismicity was initially linked to the Collejares Fault System (Fig. 8.2b), at the southern end of the Cazorla Range (Pérez-Valera *et al.*, 2017; Sánchez-Gómez *et al.*, 2014).

8.3 Methods

In order to highlight the origin and significance of Guadiana Menor seismicity, seismological reprocessed data were combined with new geophysical (gravimetry, electrical resistivity tomography) and geological data. These data were integrated with previous seismic reflection profiles (Marín-Lechado *et al.*, 2017; Roldán *et al.*, 2013) and with gravity data from the TopoIberia project (Ayala *et al.*, 2016; http://info.igme.es/SIGEOF/).

8.3.1 Seismicity analysis

The Guadiana Menor seismic swarm, including events from April 2016 until now, was relocated using HypoDD software (Waldhauser, 2001; Waldhauser and Ellsworth, 2000). This code uses the so-called double-difference (DD) earthquake location algorithm to improve relative locations of earthquakes, although it cannot precisely establish absolute locations (Waldhauser & Richards, 2004) because it depends on the reliability of the velocity model used.

We used the P and S phases provided by the Spanish National Geographic Institute (IGN, www.ign.es). Only earthquakes recorded in more than eight seismic stations

were considered in the relocation process. In addition to the regular data recorded by the national seismic network, two non-permanent seismic stations were deployed in the area by the IGN at different periods of the seismic series, providing supplementary data. This helped improve assessment of the event depths in particular.

Model used		IGN model		Palomeras *et al.* (2014) model	
Depth (km)	Vs (km/s)	Depth (km)	Vs (km/s)	Depth (km)	Vs (km/s)
				0 - 5	3.10
0 - 2	2.57			5 - 15	3.40
2 - 12	3.09	0 - 11	3.49	15 - 25	3.65
12 - 15	3.49	11 - 24	3.66	25 - 30	3.85
15 - 24	3.94	24 - 31	3.94	30 - 35	4.10
24 - 31	4.17	> 31	4.57	35 - 45	4.30
> 31	4.54			45 - 50	4.42
				50 - 75	4.45

Table 8.1. Shear velocity models used in the relocation process.

The velocity model was derived from two familiar velocity models: the Roldan *et al.* (2013) model for the upper and intermediate crust, used previously in the same region by Serrano *et al.* (2015) and Morales *et al.* (2015), and the Corchete *et al.* (1995) model for the lower crust and below (Table 8.1). Roldan *et al.* (2013) velocity model was developed in the context of hydrocarbon research, while Corchete *et al.* (1995) model was developed under the Iberian Lithosphere Heterogeneity and Anisotropy (ILIHA) project. The employment of a new velocity model integrating the two previous ones provides the smallest errors for relocated events. Moreover, the relocation process was performed using the velocity models by IGN and Palomeras *et al.* (2014) (Table 8.1) in order to detect differences in the depth pattern, and avoid artificial levels related to contrast in the boundary of velocity layers. The obtained solutions and clusters do not differ significantly when applying the different models (see supporting information, Appendix B).

In addition, five focal mechanism solutions computed by the IGN were used to interpret the seismic sequence. They were computed by means of the Rueda and Mezcua (2005) approach. From these solutions, and applying the inversion method

developed by Delvaux and Sperner (2003) and Delvaux and Barth (2010), the reduced stress tensor of the series was obtained from the Win-Tensor code.

8.3.2 Gravity prospecting

Accurate gravity measurement allows for detection of bodies having horizontal density contrasts and determination of their geometry underground. This is a suitable technique to study basement relief and sedimentary infill geometry. In addition to the 796 available Bouguer anomaly data (Ayala *et al.*, 2016; http://info.igme.es/SIGEOF/), we acquired 267 new measurements carried out with a Scintrex Autograv CG-5 gravity meter with 0.001 mGal resolution; they were referred to Granada´s absolute gravity station (IGN, ww.ign.es). Free Air, Bouguer and Terrain corrections were calculated to obtain the Complete Bouguer Anomaly for each point related to a standard density of 2.67 g/cm^3. Terrain correction was calculated based on a combination of the Kane (1962) and Nagy (1966) methods, using a digital terrain model (DTM) of 5 m pixel accuracy provided by the IGN, up to a distance of 160 km from the measurement stations. As results, we obtained the Bouguer anomaly values along a 95 km regional profile (R-R', Fig. 8.2b) and a Bouguer anomaly map of the study zone (see section 8.5, Fig. 8.5) including three local profiles, 28, 21 and 9.5 km long. The residual anomaly was calculated taking into account that Bouguer anomaly values at the locations of the local profiles are constant in the Bouguer Anomaly map of Spain (Instituto Geográfico Nacional, 1976). We consider that residual anomalies in outcrops of Prebetic rocks of the Cazorla range have a value close to 0 mGal. Four 2D profile forward models for the gravity anomaly were calculated by means of GravMag 1.7 software (Pedley *et al.*, 1993). Densities of anomalous bodies were estimated for the dominant lithologies of the region (García-Cortés & Trío-Maseda, 1994) and their standard average values (Telford *et al.*, 1990) (Fig. 8.4).

8.3.3 Electric resistivity tomography

Two 160 m long ERT profiles were acquired in the Guadiana Menor valley, at a site showing signs of active tectonics (see section 6, Figs. 8.7 and 8.8). Tomography profiles were made with an ABEM Terrameter SAS 4000, with a four-channel multiple electrode array. The profiles were acquired by means of GRAD4LX8 and GRAD4S8

gradient electrode array protocols (ABEM, 2006; Loke, 2014), with an electrode separation of 2 m. A standard least-squares profile inversion was calculated using Res2Dinv software.

8.4 Seismicity

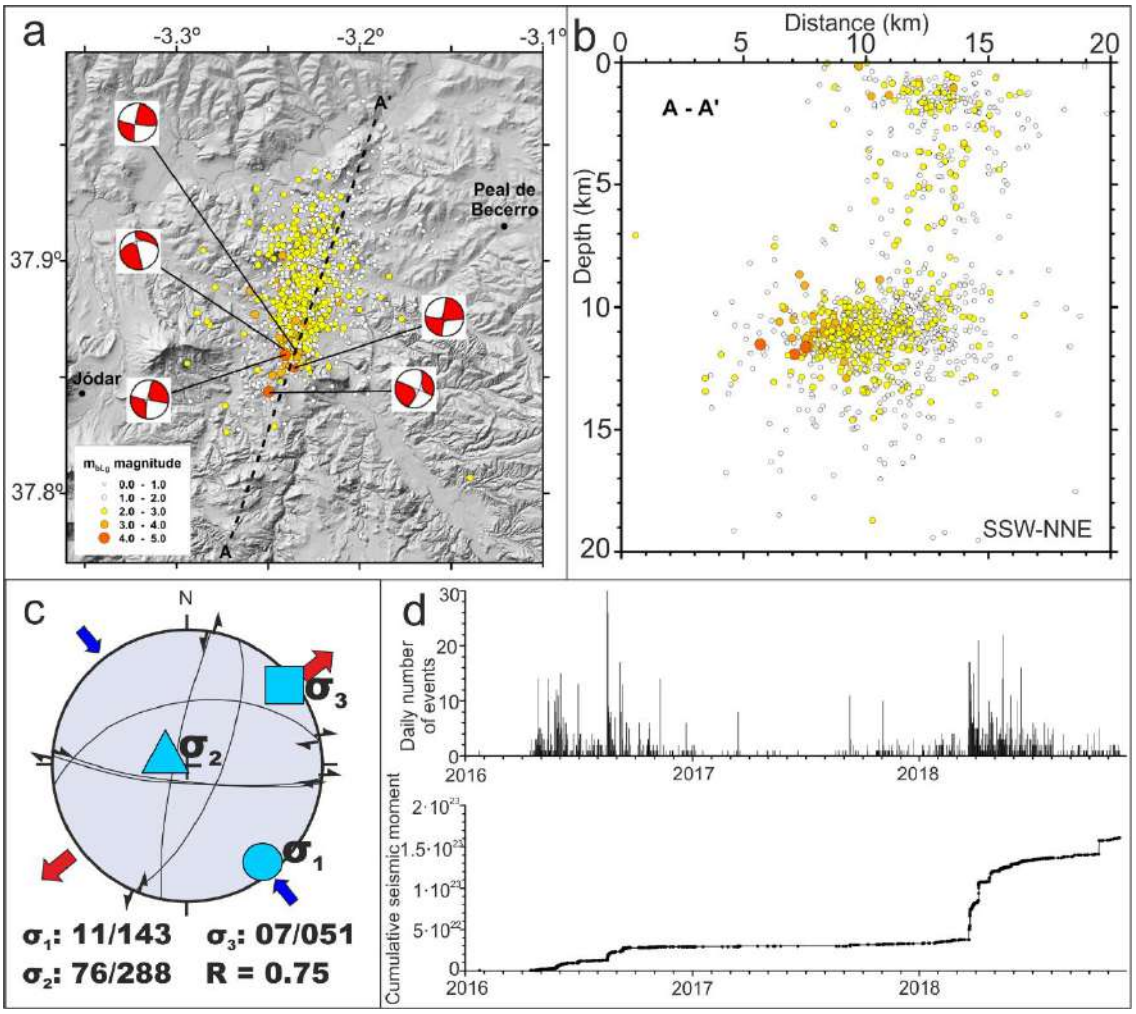

Figure 8.3. Seismic information of the Guadiana Menor seismic swarm. a. Relocated Guadiana Menor seismic swarm, including focal mechanism solutions determined by the IGN. b. SSW-NNE cross-section of the relocated seismic swarm. c. The reduced stress tensor. Orientation of the main stress components and the axial ratio are indicated. d. Temporal distribution of seismicity. Top: Daily number of earthquakes. Bottom: Cumulative seismic moment.

Although some events were previously recorded in the zone, the Guadiana Menor seismic swarm per se started in April 2016 (Fig. 8.3a) and some events are still recorded nowadays. During this time, more than 1200 events have been recorded by the IGN, three of them with a magnitude m_{bLg} 4.0, two of them in March 2018. The greatest magnitude recorded was m_{bLg} 4.1, in October 2018, while around 30 events

are in the range m_{bLg} 3.0-3.9. Altogether, the recorded events jointly released the same energy as a m_{bLg} 4.6 earthquake. Figure 3d shows the evolution of the seismic swarm, *i.e.*, the daily number of earthquakes and the cumulative seismic moment released. Two episodes stand out as the most energetic, one in 2016 and the other in 2018, separated by the overall calm stage of 2017.

Seismicity directly recorded and located by the IGN (Fig. 8.2b) has a spot-shaped distribution, showing a slight N-S elongation. Figure 3a depicts the relocated seismic swarm, in this case with a clearer NNE-SSW alignment. In addition, Figure 3a reflects the focal mechanism solutions as determined by the IGN, with almost purely strike-slip kinematics, whose nodal planes are N-S to NNE-SSW (sinistral) and E-W to WNW-ESE (dextral). The reduced stress tensor obtained from these solutions (Fig. 8.3c) shows nearly NE-SW horizontal extension combined with horizontal perpendicular compression, and σ_1 and σ_2 have close values, according to the axial ratio ($R = (\sigma_2-\sigma_3) / (\sigma_1-\sigma_3) = 0.75$). This solution is very similar to the regional stress field related to Eurasia-Nubia convergence (De Vicente and Vegas, 2009; DeMets *et al.*, 2010; Galindo-Zaldivar *et al.*, 2015).

Two clear clusters can be observed on the SSW-NNE plane (Fig. 8.3b) regardless of the velocity model used. The larger one, with depths approximately in the range 9-13 km and located to the SSW of the swarm, includes the three most energetic earthquakes, as well as a greater number of earthquakes in the range mbLg 3.0-4.0. This cluster clearly released greater seismic moment. The other cluster includes events at a depth less than 2 km and is located to the NNE of the seismic swarm, with just five earthquakes in the range mbLg 3.0-4.0. In view of the data at hand, two slipped regions are apparently separated by a 'barrier' (Aki, 1984) —that is a stressed region—between approximately 2 and 9 km depth. Alternatively, it may be acting as a zone of creeping.

8.5 Deep structures of the southeastern Guadalquivir Basin and the Cazorla mountain front

The Guadiana Menor seismic area is located in the Guadalquivir foreland basin, bounded eastwards by the Cazorla Range fold and thrust belt (Fig. 8.2). The Tíscar Fault is the main strike-slip fault cropping out in the region. It constitutes the southern

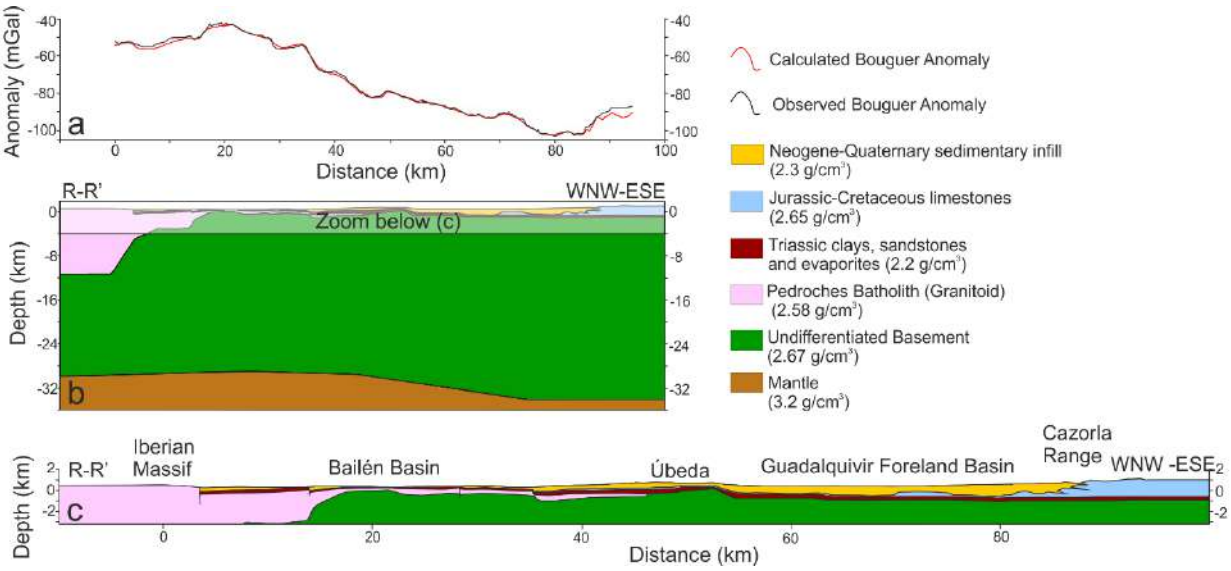

Figure 8.4. Deep structure of eastern Guadalquivir foreland basin from gravity data. a. Regional Bouguer Anomaly profile b. Density model c. Zoom of the shallow part. In this profile the density used for the background was 3.2 g/cm3, a typical density for the mantle; densities were taken from Telford *et al.* (1990). The dominant lithologies of the region were defined from field observations and geological maps (García-Cortés & Trío-Maseda, 1994). In this profile, no regional anomaly was considered, since we modelled the whole crust.

limit of the Prebetic Arc and is about 20 km long. The Iberian Massif forms the basement of the Guadalquivir foreland basin, and progressively deepens towards the Cazorla range (Fig. 8.4). In the regional gravimetric model (Fig. 8.4), the Moho discontinuity is 30 km deep in Bailén and reaches a depth of 34 km under the Cazorla range, in agreement with the increased Guadalquivir foreland basin infill. Within the Iberian crust, only the Pedroches batholith (thinning eastward) has been modelled (Fig. 8.4). The complex basin geometry includes highs and lows. The high located by 50 km (close to Úbeda) is noteworthy, with a difference in height of nearly 700 m (Fig. 8.4). There are also steps and changes in the sedimentary cover thickness, the sharper ones probably related to faults. A number of sedimentary depocenters can be distinguished: small basins related to normal faults in the W part of the profile, and the Guadalquivir basin itself, which becomes over 1 km thick close to Cazorla. Furthermore, near the Cazorla mountain front there are bodies of considerable thickness with density values in the range of limestones (Fig. 8.4).

The Bouguer anomaly map of the Guadalquivir Basin SE sector (Fig. 8.5) shows a significant westward 30 mGal decrease in anomaly values from the Cazorla range to the Guadalquivir basin, in concordance with expected changes in the crustal structure.

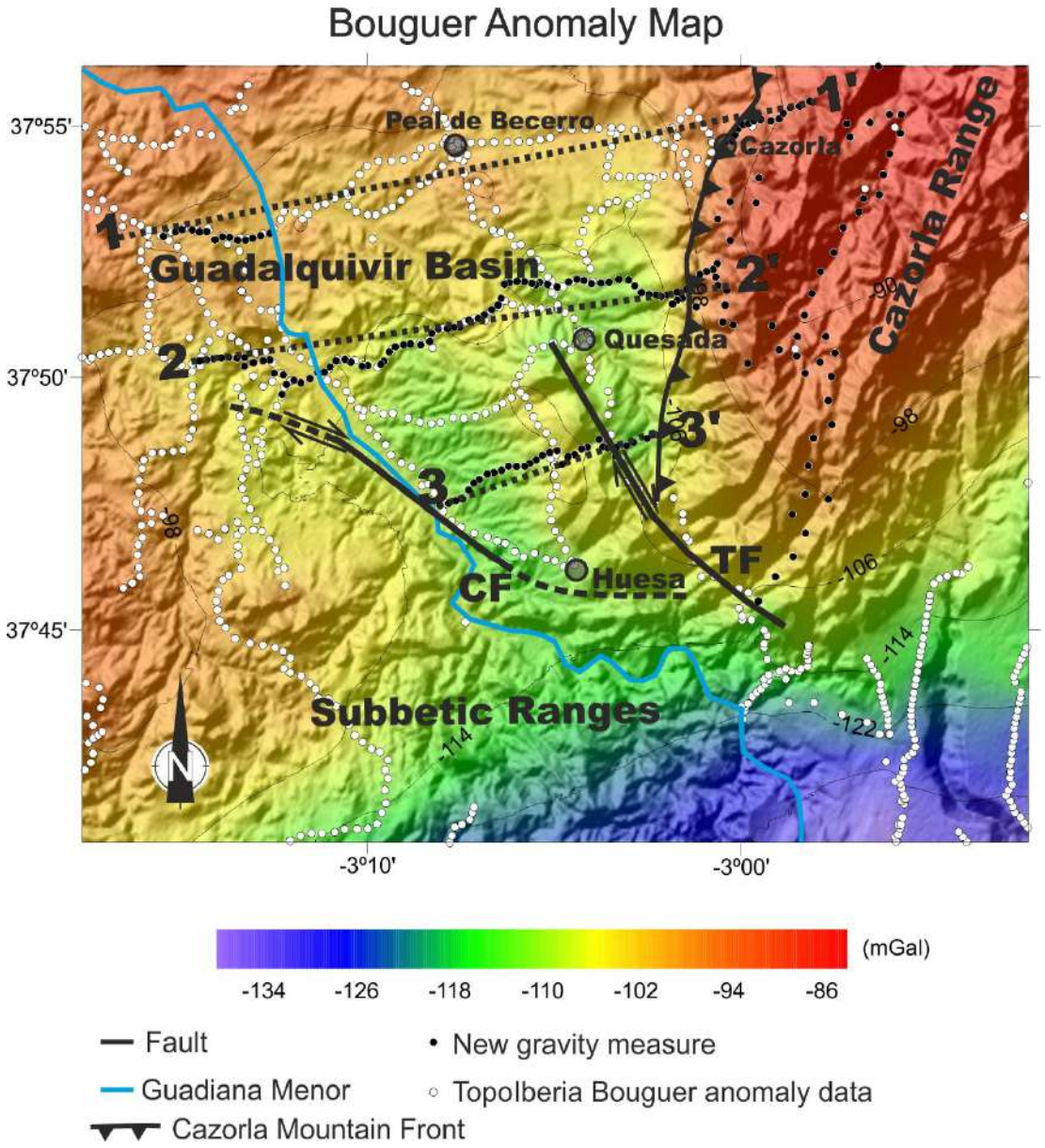

Figure 8.5. Bouguer anomaly map of the Cazorla front, Tíscar fault and Guadiana Menor valley. The residual gravity anomaly profiles are depicted. To derive this map, 675 Bouguer anomaly values were used, from our own measurements and based on previous data from the TopoIberia project (Ayala *et al.*, 2016; http://info.igme.es/SIGEOF/).

Gravity residual anomaly 2D models (Fig. 8.6) show a complex geometry of intercalations of low density (sedimentary infill type) and high density materials (External Zones type) under the Cazorla Range front. That may be interpreted as the fold and thrust structure observed at the mountain front, which continues westwards below the foreland basin. In detail, thickness variations and bodies with density values in the range of limestones can be seen in the sedimentary infill (Fig. 8.6). These bodies can be considered olistoliths, since profiles are located on an olistostromic

unit. Coinciding with some large cartographic carbonate olistoliths (or close to them), there are gravity anomaly maxima (Fig. 8.6). In addition, the Variscan basement is tilted eastward, with minor variations.

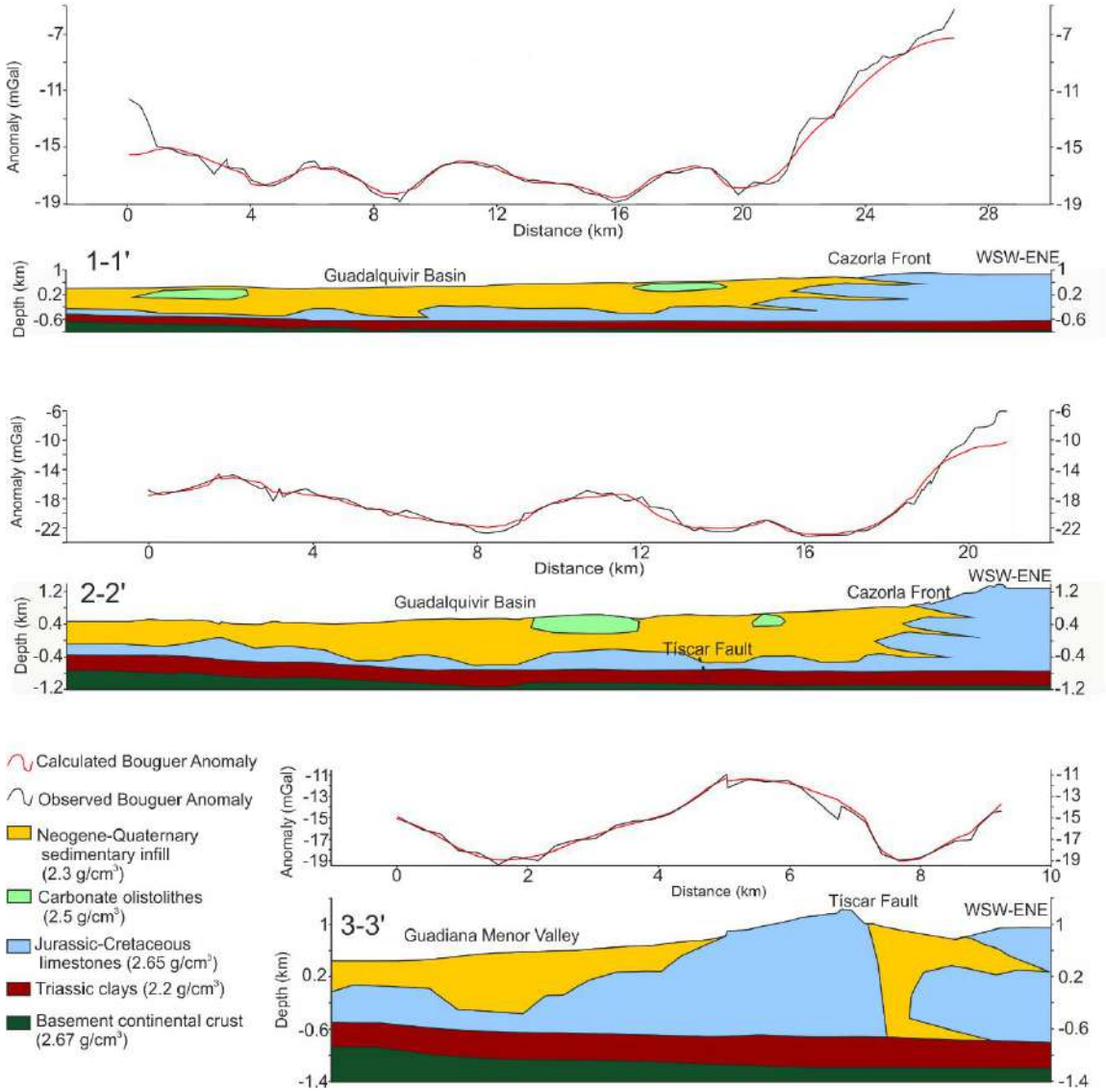

Figure 8.6. E-W residual gravity anomaly profiles cutting both the Guadiana Menor valley and the Cazorla mountain front. The density used for the background was 2.67 g/cm3, with average values for the continental crust and the dominant lithologies of the region, using the method and values expounded in Figure 4. A flat regional anomaly was added in each profile (82 mGal in profile 1, 86 mGal in profile 2 and 95.5 mGal in profile 3), in order to model just the basin infill and the Cazorla Front.

The Tíscar fault strikes N140°E-N150°E and is close to vertical. Striae point to mainly dextral kinematics and a secondary down-thrown of the eastern block (see supporting information, Appendix B, Fig. B8; Sanz de Galdeano *et al.*, 2006). Towards the north, the Tíscar fault trace and the Prebetic relief associated with its western

block progressively end, covered by the sediments. However, the gravimetric model in profile 2 (Fig. 8.6) suggests that the Tíscar fault may continue towards the Guadalquivir Basin.

8.6 Shallow recent tectonic structures of the Guadiana Menor seismic zone

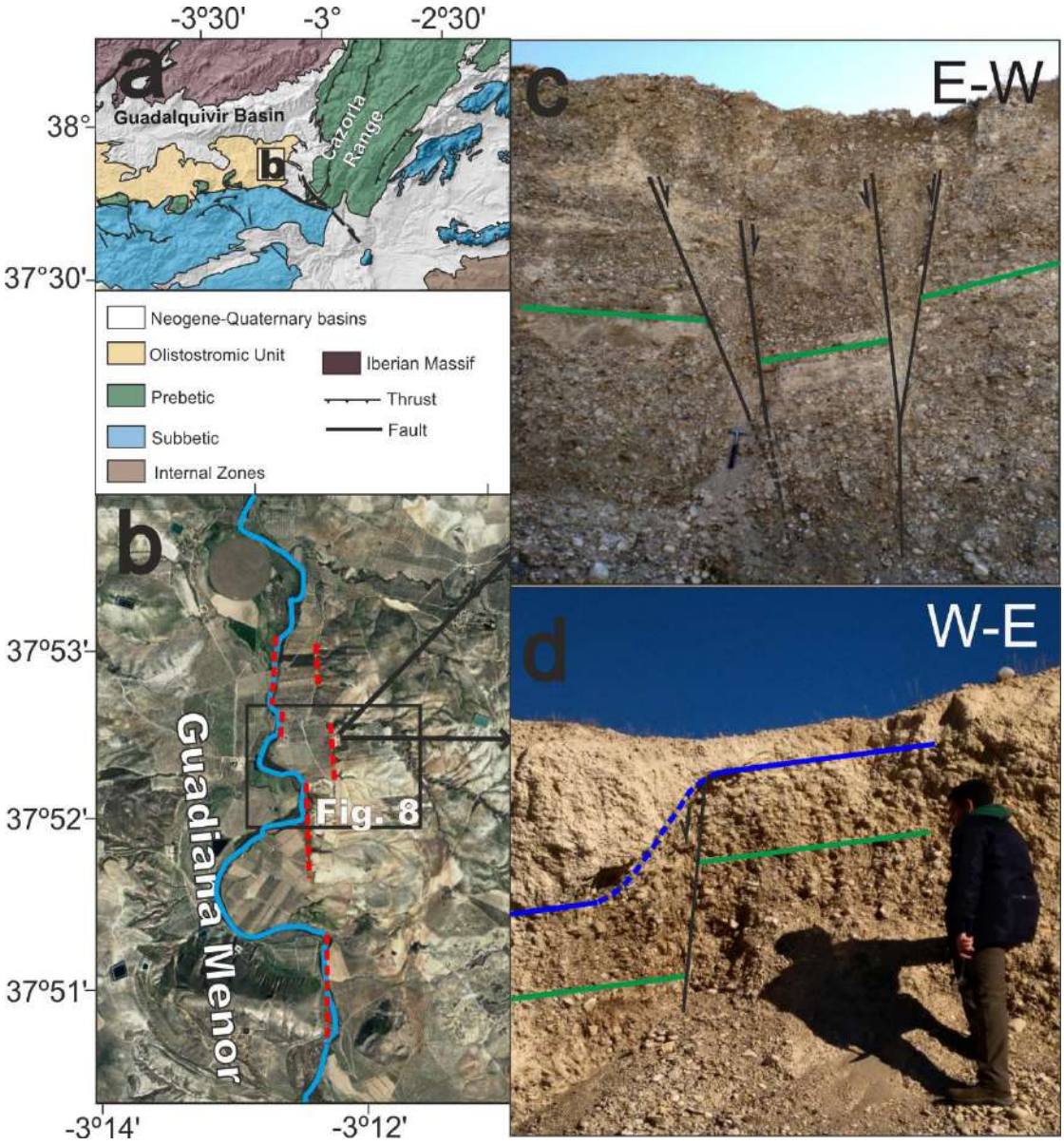

Figure 8.7. Quaternary faults in Guadiana Menor valley. a. Geologic location of the Guadiana Menor valley. b. Guadiana Menor valley, image modified from Google Earth. Note the straight segments between meanders marked with dashed lines, as well as straight slope changes parallel to them. Location of Figure 8.8 is also indicated. c, d. Photos taken in a quarry of Quaternary materials. Both photos show faults with a high dip down-throwing the western block.

There are some evidences of active tectonics in the Guadiana Menor valley's northern part (Fig. 8.7). The Guadiana Menor is a meandering river, but it also exhibits straight

segments (Figs. 8.5 and 8.7b) parallel to other straight topographic features (*e.g.*, terrain slope changes and surfaces), where several canyons end in alluvial fans. All these elements have a strike similar to one of the nodal planes of the seismic moment tensors (close to N-S).

Some quarries in alluvial Quaternary sediments (Roldán-García *et al.*, 1991) cut one straight slope change (Fig. 8.7). In fact, the deposit is affected by faults striking nearly N-S (N20°E and N170°E) with high dip (close to 80°) (Figs. 8.7c and 8.7d). Oxidized levels support that the western block is down-thrown with respect to the eastern one (Fig. 8.7c), with approximately 40 cm of vertical throw. Some of them are well exposed and have generally chaotic Quaternary fill (Fig. 8.7d). In some cases, a vertical orientation of clasts and deformation of the nearby layers are observed.

The electric resistivity tomography profiles cross, orthogonally, a straight slope change and image the shallow structure of the recent fault (Fig. 8.8). ERT profile 1 of Fig. 8.8 shows a sharp high-dipping boundary determined by the eastern end of a shallow, low resistivity layer, as well as the discontinuity and displacement affecting the underlying middle and high resistivity layers. This sharp boundary is aligned with the faults exposed in the quarries, and again the western block is down-thrown. ERT profile 2 (Fig. 8.8) cuts a sedimentary body situated at the end of a small canyon. A large low resistivity body is formed by the deposits of the canyon, with a triangular geometry and maximum thickness related to the straight slope change. The activity of a fault down-throwing the western block may have generated space, accommodating a wedge of conductive clay-rich sediments (Fig. 8.8). These structures evidence a recent N-S fault with a westward down-thrown block, along the linear slope of the eastern margin of the Guadiana Menor River.

8.7. Discussion

The seismic strike-slip faults in the foreland basin of the central Betic Cordillera have an unusual deformation pattern whose origin should be discussed in the framework of regional structural and seismicity data.

8.7.1 Cazorla mountain front and Tíscar fault

The most remarkable, recent major structures at the eastern Guadalquivir Basin are the Cazorla mountain front and the Tíscar fault. New gravity data clarify the geometry

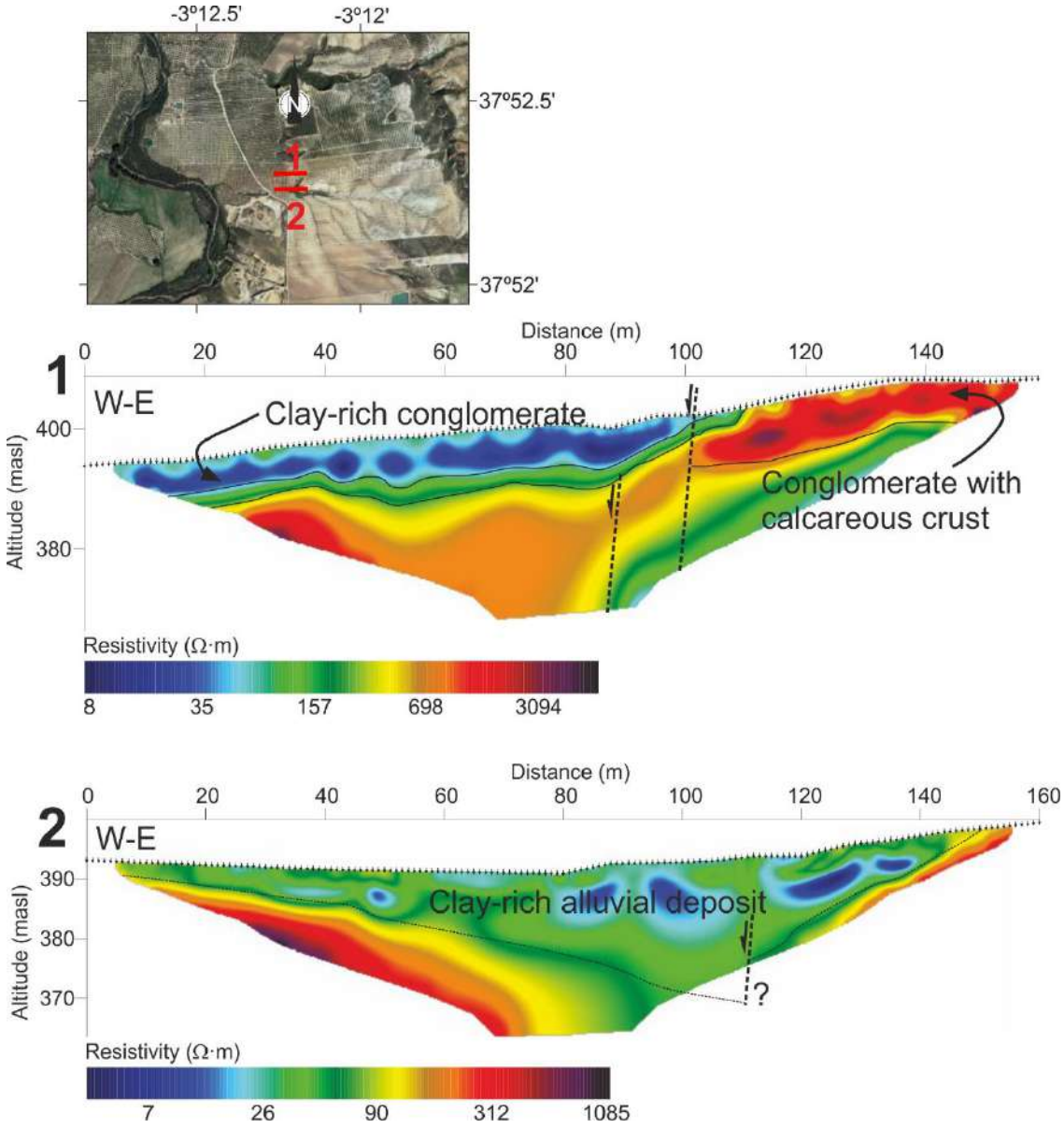

Figure 8.8. ERT profiles crossing a straight slope change parallel to the Guadiana Menor River. Their location is signed in the upper image, modified from Google Earth. Main inferred bodies are shown over the ERT values.

of the deep structure of the Cazorla mountain front and the possible continuity of the Tíscar fault. At regional scale, the profile R-R' (Fig. 8.4) indicates that the Moho depth varies due to the Betic Cordillera load. Thus, the asymmetry of the basin is consistent with flexural models of the Guadalquivir basin (García-Castellanos *et al.*, 2002; Van der Beek & Cloetingh, 1992). In turn, 2D residual anomaly models (Fig. 8.6) show high density bodies interpreted as Prebetic limestones that thrust the Guadalquivir basin infill below the basin surface and forward from the mountain front (Fig. 8.6). The geometry of some thick bodies in the Mesozoic basement cover could result from olistostromes, but also from thrusting. In fact, some studies propose the presence of

reverse faults in the basement (Marín-Lechado *et al.*, 2017). The Cazorla Range constitutes a prominent relief above the foreland basin, which suggests recent tectonic activity. Notwithstanding, there is no surface evidence of active tectonics near the Cazorla mountain front. Seismicity is located westward, where no earthquakes could be associated with Cazorla Range thrusts. Furthermore, CGPS data (Galindo-Zaldivar *et al.*, 2015) from west and east of the Cazorla range show similar westward movement, somewhat more intensive west of the Cazorla range (Fig. 8.2). Accordingly, the Cazorla range would not be active, although it might be affected by slight extension or westward spreading.

The basin basement below the Tíscar fault (Fig. 8.6) is not affected by vertical displacement, as supported by gravity models. Therefore, we deduce that the Tíscar fault is an important thin-skinned fault related with Prebetic unit movements during the development of the Prebetic Arc. Quaternary sediments are not affected by the fault. Moreover, the recorded seismicity does not overlap with its surface expression nor its projection in depth, and its dextral sense of movement is the opposite of that indicated by seismic moment tensors. Thus, the Tíscar fault must be inactive, supporting previous research findings (Sanz de Galdeano *et al.*, 2006). In summary, it is significant that the most remarkable tectonic structures of the zone are not related with the present day seismicity.

8.7.2 Guadiana Menor valley and related seismicity

Surface and geophysical research evidence active tectonic structures in the Guadiana Menor area. Field observations (Fig. 8.7) and ERT profiles (Fig. 8.8) support that the most remarkable shallow deformations consist of several N-S faults with related scarps that deform Quaternary sediments and down-throw the western block. These faults produced local W-E extension, at least during the Quaternary, possibly with some associated alluvial deposits in the eastern margin of the Guadiana Menor valley (Fig. 8.7). The geomorphological features of the valley (Fig. 8.7) and the regional CGPS residual velocities (Galindo-Zaldivar *et al.*, 2015) (Fig. 8.2) suggest that the extension is still active. This is also in coherence with the activity observed in other parts of the Betic Cordillera (Sanz de Galdeano *et al.*, 2012; Stich *et al.*, 2006). On the other hand, fault surfaces are generally close to vertical, which is coherent with strike-slip faulting, so they may also represent the upper horsetail splay of a deep fault. Most of

the seismicity in the area can be traced to the basement and the presence of faults in the Guadalquivir Basin basement has been proposed in previous work (Morales *et al.*, 2015; Roldán *et al.*, 2013). In terms of seismicity, the most important faults must be in the basement.

Gravity anomaly models do not show significant vertical steps in the area (Fig. 8.6). The anomaly values can be explained by variations in the thickness of the Iberian cover´s Jurassic and Triassic layers, or by small folds or monoclines detected in seismic profiles of the zone (Marín-Lechado *et al.*, 2017). Only some small basement steps could be considered as faults when sharp changes are observed (Figs. 8.4 and 8.6). The absence of faults with significant vertical displacements in the basement topography is consistent with almost purely strike-slip seismic moment tensors (Fig. 8.3a). In light of the NNE-SSW swarm elongation, geomorphological features and recent faults, NNE-SSW sinistral faulting is the most likely cause of the northern Guadiana Menor valley seismicity.

Regarding the seismic series in detail, though earthquakes are focused in two clusters, the most intensive events correspond to the southern, deeper one. This supports that the fracture could be growing southwards, because higher energy is released in each event during the propagation of the fault (southwards), rather than a reactivation of the fault (northwards), characterized by lower magnitude events. Meanwhile, the fact that two slipped regions are separated by a seismically inactive zone may fit with an initial faulting stage involving two regions that will eventually join through the breakage of this 'barrier' (Aki, 1984). We suggest that future earthquakes and fractures are very likely to occur in this sector, probably with magnitudes similar to those of the southernmost cluster. Alternatively, the two zones might be separated by a softer region deformed by creeping. The presence of two minor clusters at different depths also points to a heterogeneous basement. Since heterogeneities inside the basement have been described to the north, in Torreperogil (Serrano *et al.*, 2015), the Iberian crust in this region is probably heterogeneous as well.

Altogether, the seismic swarms of Torreperogil, northern Guadiana Menor and Huesa (Fig. 8.2b), and the computed focal mechanisms, point to a wide basement-linked sinistral strike-slip fault zone, where discontinuous segments are related to different seismic swarms (Fig. 8.9). This structure is now propagating toward the surface in

new vertical faults in the northern part of the Guadiana Menor valley. Such a setting indicates that the structure is in early stages of development (Hatem *et al.*, 2017; Yang *et al.*, 2017). Moreover, the new fracture is better developed in the basement, reaching over 12 km in length and propagating southwards.

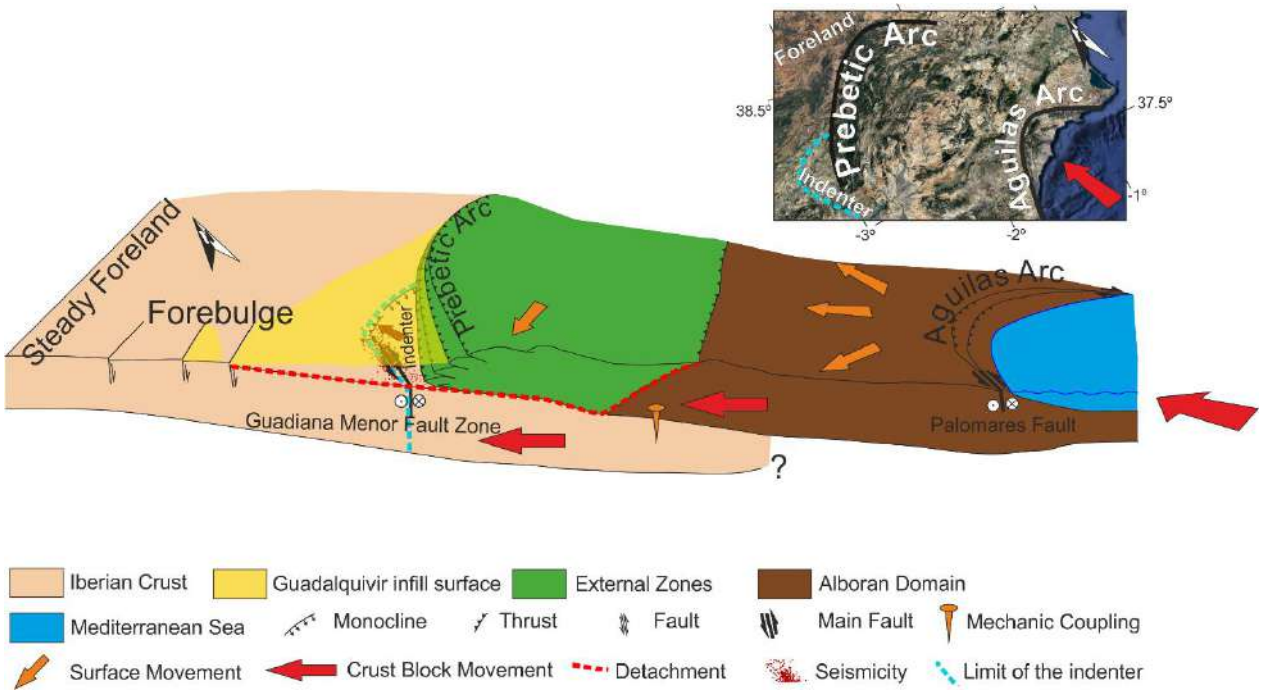

Figure 8.9. Geodynamic block diagram of the study region. The limit of the theoretical indenter in the study zone is signalled (it is coincident with the sinistral Guadiana Menor fault and the monocline). Note the detachment in between External Zones and Iberian Crust and the coupling of the Alboran Domain and the Iberian Crust. The geometry of the Iberian Crust where it ends under the Alboran Domain is uncertain. The regional image (upper right) was modified from Google Earth.

8.7.3 Geodynamic implications

The presence of a N-S to NE-SW sinistral strike-slip fault zone in the Iberian basement has important consequences for the geodynamics of the region and for the development of an arc-shaped orogen such as the Betic Cordillera. From the eastern to the central part of the Betic Cordillera, the brittle deformation changes from strike-slip to normal faulting (De Vicente and Vegas, 2009; Ruiz-Constán *et al.*, 2011; Stich *et al.*, 2006). As in our study area, westward surface motion is dominant in the central part of the Betic Cordillera (Galindo-Zaldivar *et al.*, 2015). Thus, normal faulting instead of strike-slip faulting could be expected in the area. The westward motion and normal component of the faults detected at the surface point to a control of WSW-ENE extension at the surface, while the basement presents different dynamics, according

to focal mechanisms. A similar scenario —main seismicity showing a strike-slip regime whereas surface data show an extensional regime— is observed in the Campo de Dalías (Betic Cordillera), and related to a vertical change in the stresses (Marín-Lechado *et al.*, 2005). In our study area, the axial ratio deduced from seismic moment tensors gives values of σ_1 close to σ_2 values. In the Guadalquivir Iberian basement, σ_1 is horizontal and parallel to the Eurasia-Nubia compression, with perpendicular extension or minor compression, probably because it is coupled with the Alboran Domain (Marín-Lechado *et al.*, 2017) (Fig. 8.9). This coupling can moreover be related with the attachment of Iberian crust to the Alboran Domain under the eastern Betic Cordillera and its detachment under the western part (*e.g.*, Chertova *et al.*, 2014; Mancilla *et al.*, 2013; Spakman *et al.*, 2018). These works consider the presence of a 'break zone' (usually a tear zone) under the central Betic Cordillera, where a slab detaches from the Iberian crust. Thus, in the eastern Betic Cordillera, Iberian crust lies below and attached to the Alboran Domain, which enables the transmission of compression to Iberia. In contrast, the Prebetic units and the Guadalquivir basin infill may be mainly affected by westward motion and extension associated with: (1) a spread of the compression caused by NW-SE active indentation along the Águilas Arc that pushes the eastern Betic Cordillera northwestward (Silva *et al.*, 1993); (2) subduction with roll-back affecting the central (Galindo-Zaldivar *et al.*, 2015) and western (González-Castillo *et al.*, 2015) Betic Cordillera; and/or (3) a slight spreading, whose origin may be gravitational forces (the eastern part of the basin is elevated). Given this setting, sedimentary cover rocks may be moving independently from the basement over plastic levels (Keuper facies, marls of Guadalquivir basin) (Fig. 8.9). On the other hand, if we consider the surface faults as an upper horsetail splay of the deep one, strike-slip faulting may be at an initial stage of development, propagating upwards; so the deformation at surface could mark a transition from the WSW-ENE extension to strike-slip tectonics.

Strike-slip kinematics in the Iberian basement can be tied to two findings. First, the Iberian basement is heterogeneous, as Serrano *et al.* (2015) found in the nearby Torreperogil zone and previous results indicate. The boundaries between areas of different mechanical properties may be zones of fault nucleation. Second, the regional stress of NNW-SSE compression with perpendicular, horizontal extension is adequate for strike-slip faulting. Regarding the geodynamic model associated with the fault,

there are several possibilities. Since we are in a context of compression in oblique convergence, it may be a case of transfer faulting or strain partitioning, as occurs near the region of the Gulf of Cadiz (Rosas *et al.*, 2012; Terrinha *et al.*, 2009). If we consider the transfer fault model, there should be two active structures located at the northern and southern tips, affecting the Iberian basement, but they have not yet been detected. In contrast to regions such as the Gulf of Cadiz, main seismicity has been located only in the strike-slip faults and there are not reverse (or normal) focal mechanisms. Another possible geodynamic model is that the fault forms part of a major system accommodating the westward displacement of the Betic Cordillera with respect to Iberia (Galindo-Zaldívar *et al.*, 2015). Nevertheless, this motion should affect the Betic Cordillera, not the Iberian crust under the cordillera. Furthermore, a dextral WSW-ENE fault would be the most probable structure to accommodate such displacement, but the elongation of the seismic swarm, the geomorphological features and recent faults in the surface point to a NNE-SSW sinistral fault.

The possibility we propose as the best explanation, given the available data, is a model of tectonic indentation. Large sets of sinistral faults with similar strikes are well-developed in the eastern Betic Cordillera and central Alboran Sea (*e.g.*, Andeweg and Cloetingh, 2001; De Larouzière *et al.*, 1988; De Vicente and Vegas, 2009; Sanz De Galdeano, 1990). In these parts of the Alboran Domain, NW-SE compression related to Eurasia-Nubia convergence generates tectonic indentation structures such as the central Alboran Sea (Estrada *et al.*, 2018) and the Águilas Arc (Silva *et al.*, 1993). In the central Alboran Sea, seismicity is mostly located in the sinistral NNE-SSW strike-slip fault zone that constitutes the western boundary of the indenter (Estrada *et al.*, 2018), as we observed in the Guadiana Menor area. A similar setting corresponds to the Palomares fault zone in the frame of the Aguilas Arc (Fig. 8.9). Below the Guadiana Menor valley, the compression transferred by the Alboran Domain to Iberian crust and combined with its internal heterogeneities may generate differential displacement between two parts of the Iberian crust. The eastern part is moving northward and generating the sinistral faults and compressional structures (Marín-Lechado *et al.*, 2017) under the easternmost Guadalquivir basin. Thus, the limits of this theoretical indenter would be the Guadiana Menor fault and the compressional structures located northward (Fig. 8.9).

The deformation propagated to the foreland shows that the orogeny is still active, but the nucleation of new seismic structures is taking place in the foreland basin basement —neither in the fold-and-thrust belt front nor in the sedimentary infill. Even more remarkable is the regional evolution from fold-and-thrust tectonics to strike-slip indentation tectonics. This change is linked to a high coupling between the foreland and hinterland of the orogeny, usually involving an irregular shaped continental collision (Sengör, 1976). The initial stage of the Guadiana Menor fault zone, which is still growing southwards, and possibly propagating to the infill, plus the different kinematics of the basement and the sedimentary cover may indicate the onset of indentation tectonics in the foreland; such a scenario is well developed in the eastern Alps (Sengör, 1976). Hence, we are speaking of a complex zone where extension associated with the westward displacement of an arc-shaped orogen interferes with the compression and indentation tectonics of two colliding and coupled continental domains.

8.8 Conclusions

The Betic foreland in the Guadiana Menor area has been affected by seismicity since 2016, which has resulted in a remarkable seismic swarm. This seismicity is related to a NNE-SSW sinistral fault zone affecting the Iberian basement. It may be propagating upwards to the sedimentary infill. Hypocenters configure two main clusters and support a minimum 12 km length of the fault. Most of them lie at a depth between 9 and 13 km. The fact that higher magnitudes occur in the southern one would support deformation propagation southwards. The very shallow earthquakes (< 5 km) are low magnitude events; they are more disperse and located to the north, where shallow sub-vertical faults affect Quaternary sediments and produce sharp linear surface slopes. The surface faults can be consequence of the upward propagation of the basement sinistral fault towards the sedimentary cover that undergone WSW-ENE regional extension.

Seismic swarms in the zone point to a sinistral discontinuous fault zone that affects the Guadalquivir foreland basin basement, and whose kinematics resembles those of the well-developed Palomares fault, located in the SE Betic Cordillera. In turn, CGPS velocities evidence moderate ENE-WSW extension in the region and support

uncoupling of the sedimentary infill with respect to the basement, as well as the inactivity of the Cazorla mountain front and the Tíscar fault.

In this setting, incipient sinistral faulting of the Guadalquivir foreland basement is probably related to the foreland propagation of indentation tectonics in the eastern Betic Cordillera. This area constitutes an excellent example of the propagation of active deformations related to indentation tectonics towards the foreland during continental collision disturbed by extension due to roll-back processes.

Acknowledgments

We acknowledge the comments of the editors Prof. Margaret Rusmore and Prof. Paola Vannucchi, the reviewers Dr. Pablo Granado, Dr. Federico Torcal Medina and two anonymous reviewers, which served to improve the quality of this paper. The geological data referenced in this paper are available in the text, the seismicity data are available on the IGN website at http://www.ign.es/web/ign/portal/sis-catalogo-terremotos, and the Bouguer anomaly data from the TopoIberia project are available on the IGME database SIGEOF, which is available on the website http://info.igme.es/SIGEOF/ (and select Gavimetria in data type, then select in the map the study area). This study was supported by the Spanish project DAMAGE (CGL2016-80687-R AEI/FEDER), by the Spanish project Evaluación de la Peligrosidad de Inestabilidades de Laderas Asociadas a Terremotos (CGL2015-65602-R AEI-FEDER), by the Andalusian research groups RNM-148, RNM-282, RNM-370, by PAIUJA 2019/20 from the University of Jaén, by the Programa Operativo FEDER Andalucía 2014-2020 (call made by the University of Jaén 2018), by projects B-RNM-301-UGR18 (call made by the University of Granada), project P18-RT-3275 and by the Spanish Ministry of Education, Culture and Sports, through a PhD grant (FPU program, reference 16/04038).

References

ABEM, (2006). *Instruction manual terrameter SAS 4000/SAS 1000.* Sundbyberg, Sweden: ABEM Instrument AB.

Aki, K. (1984). Asperities, barriers, characteristic earthquakes and strong motion prediction. *Journal of Geophysical Research 89*, 5867-5872.

Andeweg, B., & Cloetingh, S. (2001). Evidence for an active sinistral shear zone in the western Alboran region. *Terra Nova, 13*(1), 44-50. https://doi.org//10.1046/j.1365-3121.2001.00314.x

Ayala, C., Bohoyo, F., Maestro, A., Reguera, M. I., Torne, M., Rubio. F., Fernàndez, M., & García-Lobón, J. L. (2016). Updated Bouguer anomalies of the Iberian Peninsula: a new perspective to interpret the regional geology. *Journal of Maps, 12*(5), 1089-1092. https://doi.org//10.1080/17445647.2015.1126538

Blanco, M. J., & Spakman, W. (1993). The P-wave velocity structure of the mantle below the Iberian Peninsula: Evidence for subducted lithosphere below Southern Spain. *Tectonophysics, 221*(1), 13-34. https://doi.org//10.1016/0040-1951(93)90025-F

Bradley, D. C., & Kidd, W. S. F. 1991. Flexural extension of the upper continental crust in collisional foredeeps. *Bulletin of the Geological Society of America, 103*, 1416–1438.

Braun, J., & Beaumont, C. (1995). Three-dimensional numerical experiments of strain partitioning at oblique plate boundaries: Implications for contrasting tectonic styles in the southern Coast Ranges, California, and central South Island, New Zealand. *Journal of Geophysical Research, 100 (B9)*, 18059-18074.

Channell, J. E. T., & Mareschal, J. C. (1989). Delamination and asymetric lithospheric thickening in the development of the Tyrrhenian Rift. *Geological Society, Special Publications, 45*, 285-302. London. https://doi.org//10.1144/GSL.SP.1989.045.01.16

Chertova, M. V., Spakman, W., Geenen, T., van den Berg, A. P., & van Hinsbergen, D. J. J. (2014). Underpinning tectonic reconstructions of the western Mediterranean region with dynamic slab evolution from 3-D numerical modelling. *Journal of Geophysical Research: Solid Earth, 119*, 5876-5902. DOI: 10.1002/2014JB011150

Corchete, V., Badal, J., Serón, F.J., & Soria, A. (1995). Tomographic images of the Iberian subcrustal lithosphere and asthenosphere. *Journal of Geophysical Research, 100*, 24133-24146.

Crespo-Blanc, A., Comas, M., & Balanyá, J. C. (2016). Clues for a Tortonian reconstruction of the Gibraltar Arc: Structural pattern, deformation diachronism and block rotations. *Tectonophysics, 683*, 308-324. https://doi.org//10.1016/j.tecto.2016.05.045

Dahlen, F. A., Suppe, J., & Davis, D. (1984). Mechanics of fold-and-thrust belts and accretionary wedges: Cohesive Coulomb Theory. *Journal of Geophysical Research, 89,* 10087-10101. https://doi.org////doi.org/10.1029/JB089iB12p10087

De Larouzière, F. D., Bolze, J., Bordet, P., Hernandez, J., Montenat, C., & Ott d'Estevou, P. (1988). The Betic segment of the lithospheric Trans-Alboran ahear zone during the Late Miocene. *Tectonophysics, 152*(1), 41-52. https://doi.org//10.1016/0040-1951(88)90028-5

De Vicente, G., & Vegas, R. (2009). Large-scale distributed deformation controlled topography along the western Africa–Eurasia limit: Tectonic constraints. *Tectonophysics, 474*(1), 124-143. https://doi.org//10.1016/j.tecto.2008.11.026

Do Couto, D., Gorini, C., Jolivet, L., Lebret, N., Augier, R., Gumiaux, C., Acremont, E., Ammar, A., Jabour, H, & Auxietre, J. L. (2016). Tectonic and stratigraphic evolution of the Western Alboran Sea Basin in the last 25 Myrs. *Tectonophysics, 667-668*, 208-311. http://dx.doi.org/10.1016/j.tecto.2016.03.020

Delvaux, D., & Sperner, B. (2003). New aspects of tectonic stress inversion with reference to the TENSOR program. *Geological Society of London, Special Publication, 212*, 75-100.

Delvaux, D., & Barth, A. (2010). African stress pattern from formal inversion of focal mechanism data. *Tectonophysics, 482*, 105-128.

DeMets, C., Gordon, R. G., & Argus, D. F. (2010). Geologically current plate motions. *Geophysical Journal International, 181*(1), 1-80. https://doi.org//10.1111/j.1365-246X.2009.04491.x

Estrada, F., Galindo-Zaldivar, J., Vázquez, J. T., Ercilla, G., D'Acremont, E., Alonso, B., & Gorini, C. (2018). Tectonic indentation in the central Alboran Sea (westernmost Mediterranean). *Terra Nova, 30*(1), 24-33. https://doi.org//10.1111/ter.12304

Fernández-Ibáñez, F., Soto, J. I., Zoback, M. D., & Morales, J. (2007). Present-day stress field in the Gibraltar Arc (western Mediterranean). *Journal of Geophysical Research: Solid Earth, 112*(B8), B08404. https://doi.org//10.1029/2006JB004683

Flemings, P. B., & Jordan, T. E. (1990). Stratigraphic modeling of foreland basins: Interpreting thrust deformation and lithosphere rheology. *Geology, 18*(5), 430-434. https://doi.org//SMOFBI>2.3.CO;2

Fontboté, J. M. (1966*). Las Cordilleras Béticas. La depresión del Guadalquivir*. Madrid, Spain: Librería Paraninfo.

Galindo-Zaldivar, J., Gil, A. J., Sanz de Galdeano, C., Lacy, M. C., García-Armenteros, J. A., Ruano, P., Ruiz, A. M., Martínez-Martos, M., & Alfaro, P. (2015). Active shallow extension in central and eastern Betic Cordillera from CGPS data. *Tectonophysics, 663*, 290-301. https://doi.org//10.1016/j.tecto.2015.08.035

Galindo-Zaldivar, J., Gonzalez-Lodeiro, F., & Jabaloy, A. (1989). Progressive extensional shear structures in a detachment contact in the Western Sierra Nevada (Betic Cordilleras, Spain). *Geodinamica Acta, 3*(1), 73-85. https://doi.org//10.1080/09853111.1989.11105175

Galindo-Zaldıvar, J., Gil, A. J., Borque, M. J., González-Lodeiro, F., Jabaloy, A., Marín-Lechado, C., Ruano, P., & Sanz de Galdeano, C. (2003). Active faulting in the Internal Zones of the central Betic Cordilleras (SE, Spain). *Journal of Geodynamics, 36*(1), 239-250. https://doi.org//10.1016/S0264-3707(03)00049-8

García-Castellanos, D., Fernández, M., & Torné, M. (2002). Modeling the evolution of the Guadalquivir foreland basin (southern Spain). *Tectonics, 21*(3), 17. https://doi.org//10.1029/2001TC001339

García-Cortés, A., & Trío-Maseda, M. (1994). *Memoria del Mapa Geológico de España 1:50000 (MAGNA), Hoja de Cazorla (0928).* Madrid, Spain: IGME.

García-Dueñas, V., & Balanyá, J. C. (1986). Estructura y naturaleza del Arco de Gibraltar. *Maleo-Bol. Inf. Soc. Geol. (Portugal), 2*(23).

García-Hernández, M., López-Garrido, A. C., Rivas, P., Sanz de Galdeano, C., & Vera, J. A. (1980). Mesozoic palaeogeographic evolution of the External Zones of the Betic Cordillera. *Geologie en Mijnbouw, 59*(2), 155-168.

Granado, P., Thöny, W., Carrera, N., Gratzer, O., Strauss, P., & Muñoz, J. A. (2016). Basement-involved reactivation in foreland fold-and-thrust belts: the Alpine–Carpathian Junction (Austria). *Geol. Mag., 153*(5/6), 1110–1135.

Hall, R., & Spakman, W. (2010). Surface deformation and slab-mantle interaction during Banda arc subduction rollback. *Nature Geoscience, 3*(8), 562-566. https://doi.org//10.1038/ngeo917

Hatem, A. E., Cooke, M. L., & Toeneboehn, K. (2017). Strain localization and evolving kinematic efficiency of initiating strike-slip faults within wet kaolin experiments. *Journal of Structural Geology, 101*, 96-108. https://doi.org//10.1016/j.jsg.2017.06.011

Henares, J., López Casado, C., Sanz de Galdeano, C., Delgado, J., & Peláez, J.A. (2003). Stress fields in the Iberian-Maghrebi region. *Journal of Seismology 7,* 65-78.

Instituto Geográfico Nacional (IGN), (1976). *Mapa de anomalías de Bouguer.* Madrid, Spain: IGN.

Jabaloy, A., Galindo-Zaldivar, J., & González-Lodeiro, F. (2002). Palaeostress evolution of the Iberian Peninsula (Late Carboniferous to present-day). *Tectonophysics, 357*(1), 159-186. https://doi.org//10.1016/S0040-1951(02)00367-0

Julivert, M., & Fontboté, J. M. (1977). *Memoria Mapa Tectónico de la Península Ibérica y Baleares*. Madrid, Spain: IGME-Servicio de Publicaciones del Ministerio de Industria.

Kane, M. (1962). A comprehensive system of terrain corrections using a digital computer. *Geophysics, 27*(4), 455-462. https://doi.org//10.1190/1.1439044

Loke, M. H. (2014). *Tutorial: 2-D and 3-D electrical imaging surveys.* Geotomo Software Company (www.geotomosoft.com).

Mancilla, F. d. L., Stich, D., Berrocoso, M., Martín, R., Morales, J., Fernandez-Ros, A., Páez, R., & Pérez-Peña, A. (2013). Delamination in the Betic Range: Deep structure, seismicity, and GPS motion. *Geology, 41*(3), 307-310. https://doi.org//10.1130/G33733.1

Marín-Lechado, C., Galindo-Zaldivar, J., Rodríguez-Fernández, L. R., Serrano, I., & Pedrera, A. (2005). Active faults, seismicity and stresses in an internal boundary of a tectonic arc (Campo de Dalías and Níjar, southeastern Betic Cordilleras, Spain). *Tectonophysics, 396*(1), 81-96. https://doi.org//10.1016/j.tecto.2004.11.001

Marín-Lechado, C., Pedrera, A., Peláez, J. A., Ruiz-Constán, A., González-Ramón, A., & Henares, J. (2017). Deformation style and controlling geodynamic processes at the eastern Guadalquivir foreland basin (Southern Spain). *Tectonics, 36*(6), 1072-1089. https://doi.org//10.1002/2017TC004556

McCaffrey, R., Zwick, P. C., Vock, Y., Prawirodirdjo, L., Genrich, J. F., Stevens, C. W., Puntodewo, S. S. O., & Subarya, C. (2000). Strain partitioning during oblique plate convergence in northern Sumatra: Geodetic and seismologic constraints and numerical modeling. *Journal of Geophysical Research, 105(B12),* 28363-28376.

Morales, J., Azañón, J. M., Stich, D., Roldán, F. J., Pérez-Peña, J. V., Martín, R., Cantavella, J. V., Martín, J. B., Mancilla, F., & González-Ramón, A. (2015). The 2012–2013 earthquake swarm in the eastern Guadalquivir basin (South Spain): A case of heterogeneous faulting due to oroclinal bending. *Gondwana Research, 28*(4), 1566-1578. https://doi.org//10.1016/j.gr.2014.10.017

Morales, J., Serrano, I., Jabaloy, A., Galindo-Zaldivar, J., Zhao, D., Torcal, F., Vidal, F., & González-Lodeiro, F. (1999). Active continental subduction beneath the Betic Cordillera and the Alborán Sea. *Geology, 27*(8), 735-738. https://doi.org//ACSBTB>2.3.CO;2

Nagy, D. (1966). The gravitational attraction of a right rectangular prism. *Geophysics, 31*(2), 362-371. https://doi.org// 10.1190/1.1439779

Palomeras, I., Thurner, S., Levander, A., Liu, K., Villasenor, A., Carbonell, R., & Harnafi, M. (2014). Finite-frecuency Rayleigh wave tomography of the western Mediterranean: Mapping its lithospheric structure. *Geochemistry, Geophysics, Geosystems, 15,* 140-160.

Pedley, R. C., Busby, J. P., & Dabek, Z. K. (1993). *GRAVMAG user manual-interactive 2.5 D gravity and magnetic modelling* (Technical Report WK/93/26/R.73). British Geological Survey.

Pedrera, A., Ruiz-Constán, A., Marín-Lechado, C., Galindo-Zaldivar, J., González, A., & Peláez, J. A. (2013). Seismic transpressive basement faults and monocline development in a foreland basin (Eastern Guadalquivir, SE Spain). *Tectonics, 32*(6), 1571-1586. https://doi.org//10.1002/2013TC003397

Peláez, J.A., & López Casado, C. (2002). Seismic hazard estimate at the Iberian Peninsula. *Pure and Applied Geophysics, 159*, 2699-2713.

Pérez-Valera, F., Sánchez-Gómez, M., Pérez-López, A., & Pérez-Valera, L.A. (2017), An evaporite-bearing accretionary complex in the northern front of the Betic-Rif orogeny. *Tectonics, 36*, 1006-1036.

Platt, J. P., Allerton, S., Mandeville, C., Mayfield, A., Platzman, E. S., & Rimi, A. (2003). The ultimate arc: differential displacement, oroclinal bending, and vertical axis rotation in the External Betic-Rif Arc. *Tectonics, 22*(3), 1017.

Platt, J. P., & Vissers, R. L. M. (1989). Extensional collapse of thickened continental lithosphere: A working hypothesis for the Alboran Sea and Gibraltar Arc. *Geology, 17*(6), 540-543. https://doi.org//ECOTCL>2.3.CO;2

Regard, V., Faccenna, C., Martinod, J., & Bellier, O. (2005). Slab pull and indentation tectonics: Insights from 3D laboratory experiments. *Physics of the Earth and Planetary Interiors, 149*(1), 99-113. https://doi.org//10.1016/j.pepi.2004.08.011

Rodríguez-Fernández, J., Roldán, F. J., Azañón, J. M., & García-Cortés, A. (2015). El colapso gravitacional del frente orogénico alpino en el Dominio Subbético durante el Mioceno medio-superior: El Complejo Extensional Subbético. *Boletín Geológico y Minero, 124*(3), 477-504.

Roldán, F. J., Azañón, J. M., Rodríguez-Fernández, J., & Mateos, R. M. (2013). Fallas ciegas de carácter transtensivo en la Cuenca del Guadalquivir: posible origen del enjambre sísmico de Torreperogil (Octubre 2012-Enero 2013). *Geogaceta, 54*, 83-86.

Roldán-García, F. J., Lupiani-Moreno, E., Villalobos-Megía, M., & Jerez-Mir, L. (1991). *Memoria del Mapa Geológico de España 1:50000 (MAGNA), Hoja de Baeza (0927).* Madrid, Spain: IGME.

Rosas, F. M., Duarte, J. C., Neves, M. C., Terrinha, P., Silva, S., Matias, L., Gràcia, E., & Bartolomé, R. (2012). Thrust-wrench interference between major active faults in the Gulf of Cadiz (Africa-Eurasia plate boundary, offshore SW Iberia): tectonic implications from coupled analog and numerical modeling. *Tectonophysics, 548-549*, 1-21.

Rosenberg, C. L., Brun, J. P., & Gapais, D. (2004). Indentation model of the Eastern Alps and the origin of the Tauern Window. *Geology, 32*(11), 997-1000. https://doi.org//10.1130/G20793.1

Rueda, J., & Mezcua, J. (2005). Near-real-time seismic moment-tensor determination in Spain. *Seismological Research Letters, 76*, 455-465.

Ruiz-Constán, A., Galindo-Zaldivar, J., Pedrera, A., Célérier, B., & Marín-Lechado, C. (2011). Stress distribution at the transition from subduction to continental collision (northwestern and central Betic Cordillera). *Geochemistry, Geophysics, Geosystems, 12*(12) https://doi.org////doi.org/10.1029/2011GC003824

Sánchez-Alzola, A. (2014). *Monitorización geodésica de deformaciones en el archipiélago balear y en el sector oriental de la cordillera bética a partir de series temporales GNSS de estaciones permanentes por procesado PPP* (Doctoral Dissertetion). Retrieved from RUJA. (http://ruja.ujaen.es/handle/10953/695). Jaén, Spain: Jaén University.

Sánchez-Gómez, M., Pérez-Valera, F., Peláez, J.A., Henares, J., & Pérez-Valera, L.A. (2014). *Active faults at the southern end of the Cazorla Arc: the Collejares fault system.* Paper presented at 2nd Iberian Meeting on Active Faults and Paleoseismology, Lorca, Spain.

Sanz De Galdeano, C. (1990). Geologic evolution of the Betic Cordilleras in the Western Mediterranean, Miocene to the present. *Tectonophysics, 172*(1), 107-119. https://doi.org//10.1016/0040-1951(90)90062-D

Sanz de Galdeano, C., Galindo-Zaldivar, J., López-Garrido, A. J., Alfaro, P., Pérez-Valera, F., Pérez-López, A., & García-Tortosa, F. J. (2006). La falla de Tíscar: su significado en la terminación sudoeste del Arco Prebético. *Revista de la Sociedad Geológica de España, 19*(3-4), 271-280.

Sanz de Galdeano, C., García-Tortosa, F. J., Peláez, J. A., Alfaro, P., Azañón, J. M., Galindo-Zaldivar, J., López Casado, C., López Garrido, A. C., Rodríguez-Farnández, J., & Ruano, P. (2012). Main active faults in the Granada and Guadix-Baza Basins (Betic Cordillera)/Principales fallas activas de las cuencas de Granada y Guadix-Baza (Cordillera Bética). *Journal of Iberian Geology, 38*(1), 209-223.

Schellart, W. P., Lister, G. S., & Toy, V. G. (2006). A Late Cretaceous and Cenozoic reconstruction of the Southwest Pacific region: Tectonics controlled by subduction and slab rollback processes. *Earth Sciences Review, 76*, 193-233.

Sengör, A. M. C. (1976). Collision of irregular continental margins: Implications for foreland deformation of Alpine-type orogens. *Geology, 4*(12), 779-782. https://doi.org//COICMI>2.0.CO;2

Serrano, I., Torcal, F., & Martín, J. B. (2015). High resolution seismic imaging of an active fault in the eastern Guadalquivir Basin (Betic Cordillera, Southern Spain). *Tectonophysics, 660*, 79-91. https://doi.org//10.1016/j.tecto.2015.08.020

Silva, P. G., Goy, J. L., Somoza, L., Zazo, C., & Bardají, T. (1993). Landscape response to strike-slip faulting linked to collisional settings: Quaternary tectonics and basin formation in the Eastern Betics, southeastern Spain. *Tectonophysics, 224*(4), 289-303. https://doi.org//10.1016/0040-1951(93)90034-H

Spakman, W., Chertova, M. V., van den Berg, A., & van Hinsbergen, D. J. J. (2018). Puzzling features of western Mediterranean tectonics explained by slab dragging. *Nature Geoscience, 11*, 211-216. https://doi.org/10.1038/s41561-018-0066-z

Stich, D., Serpelloni, E., Mancilla, F., & Morales, J. (2006). Kinematics of the Iberia–Maghreb plate contact from seismic moment tensors and GPS observations. *Tectonophysics, 426*(3), 295-317. https://doi.org//10.1016/j.tecto.2006.08.004

Tapponnier, P., Peltzer, G., Dain, A. Y. L., Armijo, R., & Cobbold, P. (1982). Propagating extrusion tectonics in Asia: New insights from simple experiments with plasticine. *Geology, 10*(12), 611-616. https://doi.org//PETIAN>2.0.CO;2

Telford, W. M., Geldart, L. P., & Sheriff, R. E. (1990). *Applied geophysics.* Cambridge, UK: Cambridge University Press.

Terrinha, P., Matias, L., Vicente, J., Duarte, J., Luís, J., Pinheiro, L., Lourenço, N., Diez, S., Rosas, F., Magalhães, V., Valadares, V., Zitellini, N., Roque, C., Mendes Víctor, L., & MATESPRO Team (2009). Morphotectonics and strain partitioning at the Iberia-Africa plate boundary from multibeam and seismic reflection data. *Marine Geology, 267*, 156-174. 10.1016/j.margeo.2009.09.012

Van der Beek, P A, & Cloetingh, S. (1992). Lithospheric flexure and the tectonic evolution of the Betic Cordilleras (SE Spain). *Tectonophysics, 203*, 325-344. https://doi.org//10.1016/0040-1951(92)90230-4

Waldhauser, F. (2001). *HypoDD: A computer program to compute double-difference earthquake locations* (Rep. 01-113). USGS Open File.

Waldhauser, F., & Ellsworth, W.F. (2000). A double-difference earthquake location algorithm: Method and application to the northern Hayward fault. *Bulletin of the Seismological Society of America, 90*, 1353-1368.

Waldhauser, F., & Richards, P.G. (2004). Reference events for regional seismic phases at IMS stations in China. *Bulletin of the Seismological Society of America, 94*, 2265-2279.

Wortel, M. J. R., & Spakman, W. (2000). Subduction and Slab Detachment in the Mediterranean-Carpathian Region. *Science, 290*(5498), 1910-1917. https://doi.org//10.1126/science.290.5498.1910

Yang, X., Guanghui, W., Yongliang, L., & Tingting, C. (2017). Analogue modeling of through-going process and development pattern of strike-slip fault zone. *Petroleum Exploration and Development, 44*(3), 368-376. https://doi.org//10.1016/S1876-3804(17)30043-5

Part III

9. General discussion

10. Conclusions/Conclusiones

CHAPTER 9

General discussion

The previous chapters collect the results of the five key zones that cover the aims proposed in the Ph.D. Thesis plan. The discussion of each chapter presents new insights about the geodynamic evolution of these zones based on a wide variety of methods applied on both sea and land structures, which provides a continuous view of marine and land geology. Although the geodynamic implications of the results are considered in each work, a comprehensive integration of all interpretations is needed, so it is presented in this chapter. Thus, the interaction of indentation tectonics and the ENE-WSW extension due to the slab roll-back is discussed through the analysis of strike-slip fault systems from the Betics front, in the Guadalquivir basin, to the Al Hoceima Bay, at the southern Alboran Sea coast. The geodynamic interpretation of these zones also sheds light on their seismicity distribution, being some of them areas with high seismic risk.

9.1 Strike-slip fault systems and indentation tectonics in the Alboran Sea evolution

The new geophysical data have improved the knowledge of the geodynamic history and the processes at the origin of the main reliefs of the Alboran Sea. The new magnetic models of the Alboran Sea presented in this Ph.D. Thesis have revealed the location of crustal, igneous bodies related to the rifting of the AlKaPeCa Domain. Although the association with the opening of the Algerian basin during Oligocene-Early Miocene has already been raised (Bouillin *et al.*, 1986; Jolivet *et al.*, 2021; Mauffret *et al.*, 2007; Romagny *et al.*, 2020; Rosenbaum *et al.*, 2002; Schettino and Turco, 2011), the presence of those igneous intrusions of crustal scale constitutes a record of the western tip of the rifting process of the AlKaPeCa Domain. These bodies have influenced the geodynamic evolution of the Alboran Sea, especially since Late Miocene. The STEP (Subduction Tear Edge Propagator) fault that accommodated the westward displacement of the Alboran Domain along its southern margin (d'Acremont *et al.*, 2020; Hidas *et al.*, 2019; Jolivet *et al.*, 2021) could be associated with the southern boundary of these igneous intrusions, as they may also constitute crust discontinuities.

When the STEP fault was deformed and curved by the NW-SE compression, the eastern part became the Yusuf fault that fragmented the igneous bodies and favored the emplacement of new ones in transtensional zones, like the Yusuf basin. The Yusuf fault represents a major crustal boundary because it limits the African crust from the Alboran Domain crust and the Algerian oceanic crust (d'Acremont *et al.*, 2020; Gómez de la Peña *et al.*, 2020). The Yusuf fault also connects the relict rift bodies of central Alboran Sea with the magnetic anomalies located along the Algerian margin, which are probably the continuation of that rift (Yelles *et al.*, 2009).

From Tortonian to Pliocene, the South Alboran Sea was attached to the African crust and started a north-westwards indentation favored by the Yusuf fault and NW-SE compression combined with ENE-WSW extension. The indentation generated the Al Idrissi fault to accommodate the displacement along its western boundary (Estrada *et al.*, 2018, Lafosse *et al.*, 2020). In this setting, the igneous intrusions of central Alboran Sea have acted as a backstop, which conditioned the elevation of the Alboran Ridge (Estrada *et al.*, 2018). The tectonic inversion of the central Alboran Sea basin is related to the decrease of the westward migration of the slab roll-back, while the Alboran Domain collided over Iberian and African margins (Chalouan *et al.*, 2008; d'Acremont *et al.*, 2020; Spakman *et al.*, 2018; Vitale *et al.*, 2015; Ziegler *et al.*, 1998).

The southern termination of the Al Idrisi fault zone generated a horsetail splay with normal and sinistral faults, like the Trougout fault, which formed the transtensional Nekor basin (d'Acremont *et al.*, 2014; Lafosse *et al.*, 2016; 2018). However, the development of these faults is also affected by the south-westward movement of the Rif Cordillera that GPS data show (Koulali *et al.*, 2011, Palano *et al.*, 2015). The analysis of their recent activity shows a westwards migration of tectonic activity into the Al Hoceima Bay (Nekor basin). This is coherent with the location of the major earthquakes of the region that are on the western part of the bay, where the Bokkoya fault is located and do not overlap the Trougout fault (Galindo-Zaldivar *et al.*, 2009; Van der Woerd *et al.*, 2014). The south-westward motion of the Rif Cordillera can be due to a dragging of the subducted slab still attached to the African crust (Faccena *et al.*, 2014; Spakman *et al.*, 2018), or to a mantle delamination after the subduction (Baratin *et al.*, 2016). In any case, the Al Hoceima Bay can be considered a place where

the ongoing indentation tectonics related to the inversion of the Alboran Sea basin is interacting with the active extension due to roll-back.

To the north, in the indented block, the central Alboran Sea indentation has generated a set of strike-slip faults on the northern part of the basin that propagates towards the coast (this Ph.D. Thesis, Estrada *et al.*, 2018). In fact, these faults are in continuity with the Al Idrissi fault zone and, since they are active, can be considered as the active Trans Alboran Shear Zone, or the Betic-Alboran shear zone (Stich *et al.*, 2006; Martín *et al.*, 2015). Some of them are tsunamigenic, as it has been recently recognized by the Averroes fault (Estrada *et al.*, 2021).

At the northern Alboran coast, the Campo de Dalías faults interact with ENE-WSW folds that appear near the coast and deform the cordillera since the Late Tortonian, and that are related to the NW-SE, regional compression (Marín-Lechado *et al.*, 2007; Pedrera *et al.*, 2015). On land, the studied faults are N-S to NW-SE extensional hybrid joints that should act as normal faults in line with the regional stress, but that are, in fact, oblique faults with dextral component (Marín-Lechado *et al.*, 2005; 2007; 2010). This regime is congruent with the combination of the propagation of the strike-slip faults generated in the indented block and with the extension that still experiments the central Betic Cordillera, associated with the roll-back (Galindo-Zaldivar *et al.*, 2015; González-Castillo *et al.*, 2015). Moreover, this is confirmed by the GNSS results of the Balanegra fault network: the westward displacement decreases southwards, whilst it should increase in a context of pure westward motion due to slab roll-back, and there is no radial pattern as it to be expected in the case of an indented block. Thus, the interaction of both processes can be observed between the central Alboran Sea indentation (Estrada *et al.*, 2018) and the extensional active faulting that characterize the central Betic Cordillera (Galindo-Zaldivar *et al.*, 2015; Martín *et al.*, 2015; Ruiz-Constán *et al.*, 2011).

9.2 Active and incipient indentation tectonics in the central-eastern sector of the Betic Cordillera

In the eastern Betic Cordillera, the indentation tectonics has been applied to explain the origin of the Águilas Arc and the nearby bended folds (Coppier *et al.*, 1989; Silva *et al.*, 1993) in combination with the tectonic activity of the Eastern Betic Shear Zone

(EBSZ, Bousquet, 1979). Earthquakes of Mw> 6.7 has been considered for the EBSZ due to fracture propagation along several fault planes or sections of the EBSZ, including the Palomares fault zone, PFZ (*e.g.*, Herrero-Barbero *et al.*, 2021; García-Mayordomo *et al.*, 2017). Nevertheless, the results provided in this Thesis show that the PFZ is disconnected from the Alhama de Murcia fault to the north and, consequently, from the EBSZ. The formation and evolution of the PFZ is mainly conditioned by the fold rotation and fragmentation that resulted from the indentation of an Algerian block into the Betics, so it is constrained to the displacement between the Cabrera Range and the Almagrera Range (this Ph.D. Thesis, Coppier *et al.*, 1989; Ercilla *et al.*, 2022; Silva *et al.*, 1993). As opposed to other tectonic indentations, in this case there is no development of large strike-slip systems that affect both the hinterland and the indenter flanks. In addition, the structure of the Guadalentín corridor between the Águilas Arc front and the Alhama de Murcia fault points to a north-westwards propagation of the deformation front. This is also supported by sealed Pleistocene faults located at the Águilas Arc front (Roquero *et al.*, 2019) and the GPS data, which show that the shortening is mainly accommodated by the Alhama de Murcia fault (Echeverria *et al.*, 2013; Palano *et al.*, 2015).

To the north-east of Águilas Arc, the EBSZ presents a transpressive regime (Alfaro *et al.*, 2012; Borque *et al.*, 2019; Stich *et al.*, 2010; 2020), and this includes the Alhama de Murcia fault, where the accommodation of the Eurasia-Africa convergence seems to be the main factor driving the active tectonics. Folding, the EBSZ and the indentation tectonics of the Águilas Arc, and its progression north-westwards are the main processes that manifest a response to the regional compression in the eastern Betics. Thus, the tectonic influence of the extension associated with the westward displacement of the Alboran Domain due to roll-back has decreased, or almost disappeared, in the eastern Betics.

Moreover, the propagation of compression and indentation tectonics from the central-eastern Betics may be affecting the Iberian foreland under the Betic External Zones. The seismicity of the Guadiana Menor valley is characterized by strike-slip moment tensors that cannot be associated with the surface structures. The evidence points to an active NNE-SSW, sinistral fault into the Iberian basement of the Guadalquivir foreland basin. This is contradictory with the surface structures, where

the fold and thrusts belt of the Prebetic Arc and the Tíscar fault (a NNW-SSE, dextral fault) are the most prominent structures that condition the relief. These results combined with previous ones on eastern Guadaqluivir basin, like the Torreperogil area (Marín-Lechado *et al.*, 2017; Morales *et al.*, 2015) support the transmission of compressive stress from the Alboran Domain (Betic Internal Zones) to the Iberian basement, which implies a high degree of coupling between them.

On the other hand, surface GPS data for the eastern Guadalquivir basin show a WSW displacement, smaller than those observed in central Betic Cordillera (Galindo-Zaldivar *et al.*, 2015). At present, this zone is still experimenting the westwards displacement of central and western Betics (Galindo-Zaldivar *et al.*, 2015; González-Castillo *et al.*, 2015; Ruiz-Constán *et al.*, 2011), while compression has started to deform the Iberian basement. Considering the compressive structures detected to the north in Marín-Lechado *et al.* (2017), the Guadiana Menor fault could be part of an indentation process in the Iberian crust. However, the Guadiana Menor fault seems to be in an initial phase and it has not clearly propagated to the surface yet, suggesting that this zone may be better considered as an incipient tectonic indentation. As it was proposed by Coppier *et al.* (1989), the transmission of compression to this zone may be related to the Águilas Arc indentation and its propagation, but it is only expressed in the basement.

9.3 Current roll-back influenced zones vs. indentation tectonics zones in the Betic Cordillera and the Alboran Sea: geodynamic implications

As the Alboran Domain and the slab are westward displaced, or blocked, it can be expected that the ENE-WSW related extension decreases its influence in favor of continental collision, like indentation and transpression tectonics, with an increase of the coupling between Alboran Domain and Iberian crusts. This is observed in the eastern Betics due to the tearing of the slab: Alboran Domain and Iberian crusts are attached under the eastern Betics, which has favored the stress transmission to Iberia (Mancilla *et al.*, 2013; 2015; Morales *et al.*, 2022). This is in contrast with the western Betics, where the oceanic slab is still attached to the Iberian crust and pushing downwards (Chertova *et al.*, 2014; Faccena *et al.*, 2014; Gutscher *et al.*, 2012; Spakman *et al.*, 2018). This lithospheric difference between eastern and western Betics can be associated with the surface displacements observed by GPS (Borque *et*

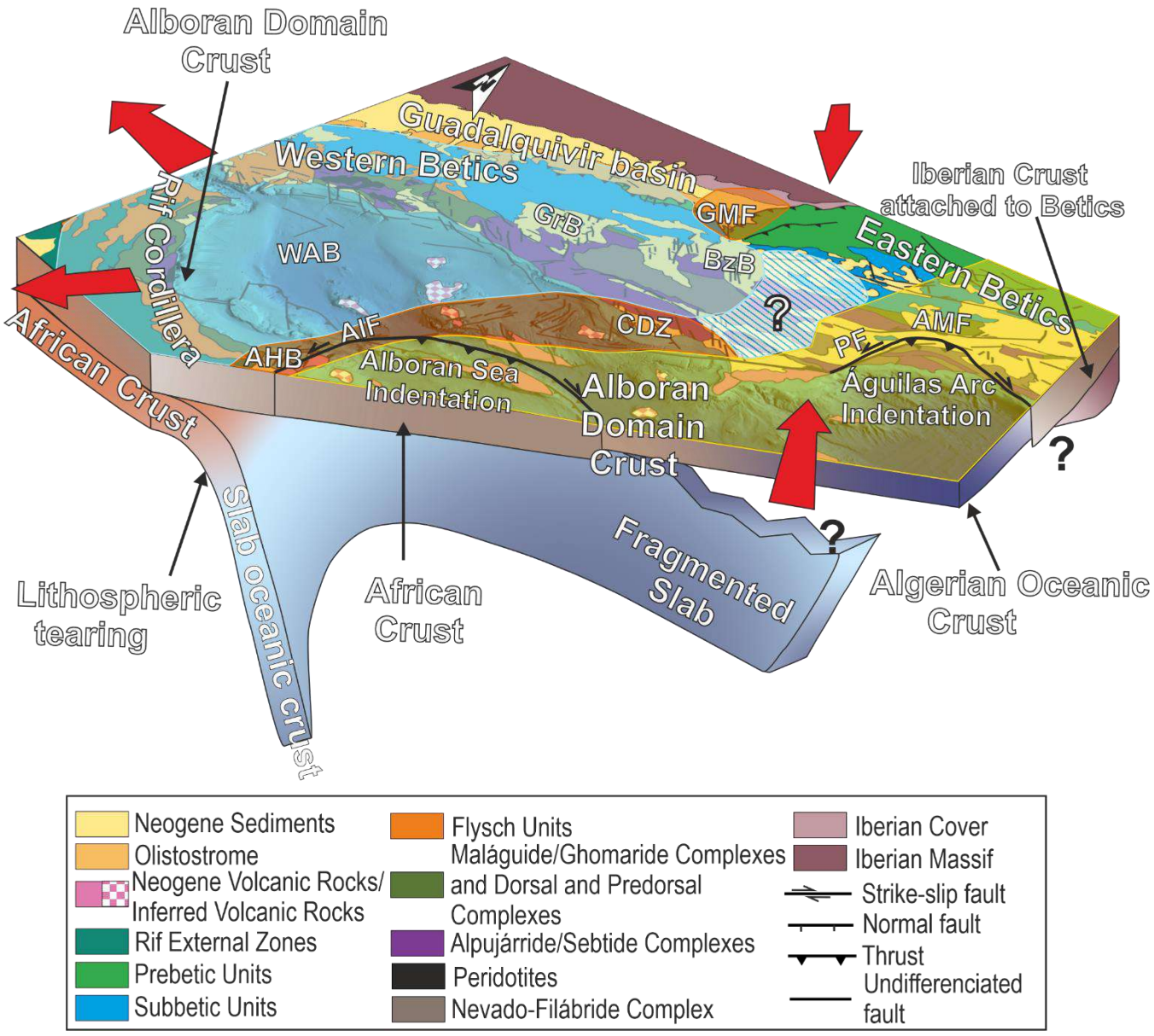

Figure 9.1. Geodynamic sketch f the Gibraltar Arc and the Alboran Sea. Pale blue area corresponds to roll-back dominated area, yellow area to the indentation-collision tectonics dominated zone, and orange area to transition zones. Red arrows represent the tectonic movementes. The striped area is tentative, see text for further discussion. AHB: Al Hoceima Bay; AIF: Al Idrissi fault; AMF: Alhama de Murcia fault; BzB: Baza basin; CDZ: Campo de Dalías Zone; GMF: Guadiana Menor fault; GrB: Granada Basin; PF: Palomares fault zone; WAB: West Alboran Basin.

al., 2019; Galindo-Zaldivar *et al.*, 2015; González-Castillo *et al.*, 2015; Koulali *et al.*, 2011; Palano *et al.*, 2015) and active faults distribution over the cordillera (Buforn *et al.*, 2004; García-Mayordomo *et al.*, 2017; Stich *et al.*, 2006; 2010; 2020). The main consequences of this difference are:

- The eastern Betics experience transpression with indentation tectonics due to Eurasia-Africa convergence accommodated in the margins of the rigid,

Algerian crust, which results in reverse and strike-slip faults in the margins and active folding. Where indentation tectonics takes place, radial patterns of surface displacement appear with conjugate systems of strike-slip faults.

- Conversely, western Betics are characterized by the westward displacement related to the slab roll-back (with or without delamination) combined with the regional compression caused by the continental convergence. The same dynamic can be applied to the Rif Cordillera.

This westward displacement has generated compression in the western part of the Betics and in the Rif, extension in the central Betics, and transtension in the north-eastern Rif (*e.g.*, Galindo-Zaldivar *et al.*, 2015; González-Castillo *et al.*, 2015; Martín *et al.*, 2015; Ruiz-Constán *et al.*, 2011). The Alboran Sea is mainly characterized by the inversion of the basin and the generation of tectonic indentation with active neoformed fault systems, such as the Al Idrissi faults, although most of the Western Alboran basin remains with low deformation (Comas *et al.*, 1992; d'Acremont *et al.*, 2020; Do Couto *et al.*, 2016; Estrada *et al.*, 2018). The western boundary zones of this indentation are very influenced by the ENE-WSW extension. These are the cases of the westward migration of the active faulting affecting the Al Idrissi fault zone (Galindo-Zaldivar *et al.*, 2018), its southern termination in the Al Hoceima Bay faults, and the Campo de Dalías faults (this Thesis). Therefore, the western boundary of the South Alboran indenter can be interpreted as a boundary zone between the zones tectonically controlled by convergence and tetonic indentation processes, and zones controlled by westward displacement (slab roll-back).

On the Betic Cordillera, the limits of this transition zone are more diffuse than in the Alboran Sea. On the one hand, the Águilas Arc shows tectonic indentation with transpression in its frontal part (Guadalentín corridor and the Alhama de Murcia fault). This zone can therefore be considered as having a similar stress as the rest of the eastern Betics. On the other hand, the central Betics are characterized by active normal faults, while strike-slip is active only in the Campo de Dalías zone and in the eastern Guadalquivir foreland basin. These zones also present extension that is interpreted as related to slab roll-back. Between these two zones, the Granada and Baza basins are the main seismic zones and are controlled by active normal faulting coherent with the ENE-WSW, regional extension (Alfaro *et al.*, 2021; Galindo-Zaldivar

et al., 2015; Madarieta-Txurruka *et al.*, 2021). Therefore, the zones affected by the slab roll-back westward displacement and indentation processes, or transpressional tectonics, that could be considered as transition zones in the Betic Cordillera do not seem to form a continuous band as it is the case in the Alboran Sea. In order to explain this, the zone located between the Baza basin and the Águilas Arc indentation (Fig. 9.1) can be interpreted in three different ways:

I. A progressive transition from indentation to roll-back. This zone may accommodate the compression by active E-W folding and orthogonal extension by normal faults in a transition to the eastern strike-slip faults related to indentation tectonics.

II. The zone is affected by another process that may have to do with the rupture of the slab, which some authors located under the central Betics (*e.g.*, Mancilla *et al.*, 2013; 2015; Morales *et al.*, 2022). This could generate a zone characterized by uplift and normal faulting similar to the activity in the central Betic Cordillera.

III. In the eastern-central Betics, a sharp boundary separates the areas tectonically controlled by indentation tectonics and by extension due to slab roll-back. The areas considered of transition could be restricted to the zones where the indentation is propagating (like the eastern Guadalquivir foreland basin) or its boundaries (*i.e.* the Campo de Dalías and Al Hoceima Bay).

The third one is, in my opinion, the most likely explanation. The continuous transition zone in the Alboran Sea is probably due to the bigger scale indentation. It is also the main active tectonic process that controls the present relief, especialy compared to the little deformed and adjacent West Alboran Basin. In contrast, in the Betics the indentation of the Águilas Arc is smaller and the forming relief processes of the Central Betics are still active. Thus, the influence of the Águilas Arc is restricted to the proximal and propagations areas. Moreover, the area where this transition could be located (eastward of Baza basin) presents similar active structures that the central Betics (E-W large folds and normal faulting with some E-W strike-slip faults).

CHAPTER 10

Conclusions

The Gibraltar Arc is an alpine orogen formed by the Betics and Rif cordilleras around the Alboran Sea developed in the frame of Eurasia-African convergence. It is an excellent place to study the interaction of the slab roll-back influence and the recent development of tectonic indentations related to the collision. The Alboran Domain has displaced westwards as a consequence of subduction with slab roll-back since the opening of the Algerian basin in the Oligocene-Early Miocene. This displacement has caused ENE-WSW extension that was simultaneous with the compression associated with the oblique Eurasia-Africa convergence and the collision of the Alboran Domain with the Iberian and African margins. Since the Tortonian, the compression led to the inversion of the Alboran Sea basin and the elevation of the main reliefs of the Betics and Rif cordilleras. Although the NW-SE compression with orthogonal extension has been constant since the Tortonian with minor variations, the active tectonics on the eastern Betics and Central Alboran Sea are characterized by strike-slip activity, whilst the central Betic Cordillera mainly presents active, normal faults and large, kilometric folds. This difference can be explained by lithospheric processes. The oceanic slab was ruptured and separated from the Iberian and African crusts from east to west, so that the Iberian crust separated from the slab got attached to the overlaid Alboran Domain in the eastern Betics. Meanwhile, the western Betics and the Rif still experiment westwards movement conditioned by the sinking of the slab attached to the Iberian and African crusts.

In the eastern Betics, the high degree of coupling between both crusts, combined with the reduction of the westwards displacement, originated transpression along the Eastern Betic Shear Zone combined with folding. In addition, indentation tectonics took place in the Águilas Arc, as a result of the compression of the rigid Algerian crust that indented the former E-W folds of the Betic Cordillera, which become NE-SW and were still active. The rotation and fragmentation of these folds generated the Palomares fault zone. In contrast with other tectonic indentations, the PFZ is constrained to the fold rotations and no large strike-slip faults are generated to accommodate the indenter displacement. Moreover, these faults are disconnected

from the strike-slip systems developed in the indented block. In recent times, the transmission of compression to the Betic front propagated into the Iberian basement of the Guadalquivir foreland basin, even as the area still experiences westwards displacement. The nucleation of strike-slip faulting in the Iberian crust has been caused by this stress propagation, while the folds and thrusts of the External Zones of the Cazorla Range present low activity.

In the Alboran Sea, the basin was inverted and tectonic indentation has taken place at least, since the Plio-Quaternary, in the central Alboran. The south Alboran block attached to the African crust collided and displaced the igneous intrusions generated during the rifting of the AlKaPeCa Domain. The indentation tectonics has been accommodated by the dextral Yusuf fault, probably inherited by the STEP fault related to the westwards motion of the Alboran Domain, and by the sinistral Al Idrissi fault, which was formed by the indentation during the Pleistocene. In the western margin of the indenter, the interaction between the indentation process, related to a continental collision phase, and the westwards displacement associated with the slab roll-back, has conditioned the westwards displacement of the active structures. The results of this Ph.D. underline that the interaction is significant in the Campo de Dalías zone, where the GNSS data show an interference of the radial pattern caused by an indentation with the WSW displacement of the central Betic Cordillera. In addition, the interaction is also determining during the Pleistocene westward migration of the activity of the Al Hoceima Bay faults, whose origin is the southern termination of the Al Idrissi fault. The migration is likely caused by the south-westwards displacement of the Rif Cordillera.

Altogether, it is possible to define a transition zone where the influence of the westward displacement of the slab roll-back and the indentation tectonics are, both, controlling processes of active faulting and folding along the western and northern boundary of the Alboran Sea indentation. However, this zone is not well-characterized in the central-eastern Betics, where a sharp boundary may occur. Alternatively, an area of progressive transition, eventually affected by other lithospheric processes related with the rupture of the slab, could be located between the western and eastern Betics.

Future perspectives

The definition of a transition zone influenced by both slab roll-back induced westward displacement and indentation tectonics related to a high degree of coupling of the Iberian and Alboran crusts in the eastern Betics, remains open. Even though in the previous chapter the absence of such a transition zone is argued, together with alternative explanations for the data presented, it is also necessary to undertake a proper discussion about the active and recent structures of these areas. Such a discussion should take into account the integration of previous data, as well as further geological and geophysical research. In this respect, local GPS networks could be very useful to better understand the present day real movements, as they have revealed in other cases such as that of the Balanegra fault.

Moreover, in areas where the plate displacements are slow, the geodynamic models of faulting migration have proved to be a useful tool to better understand the location of seismogenic faults, as it has been presented in the Al Hoceima Bay in this Ph.D. Thesis. The slow motion is also an opportunity to study the different stages of the orogeny that simultaneously affect wide areas of these arcuate belts. This improves the knowledge of how the influence of the different lithospheric processes changes as the sides of the orogen collide with the continental margins, while the front continues its displacement due to the slab roll-back. Further research combining geophysical, geodetical and geological data with this perspective may unveil significant implications in the framework of the geodynamic evolution of these type of orogens.

Finally, this Ph.D. Thesis highlights the importance of the integration of marine and terrestrial data, especially in contexts where the same crustal domain constitutes the back-arc basin and part of the arcuate orogen. The presented results show that the terrestrial and marine structures are commonly related and, for example, zones like the Campo de Dalías or the Águilas Arc need further research in both environments to comprehend their geodynamic history and possible future evolution. Future studies in deformed and active regions that involve coastal orogens and/or inverted marine basins should be multidisciplinary and involve both terrestrial and marine techniques in order to provide an entire view of the active tectonic structures and the associated geodynamic processes with implications in natural hazards assessment.

CAPÍTULO 10

Conclusiones

El Arco de Gibraltar es un orógeno alpino formado por las Cordilleras Béticas y el Rif que rodean del Mar de Alborán y desarrollado en el contexto de la convergencia Eurasia-África. Es un excelente lugar para estudiar la interacción de los procesos de slab roll-back con el reciente desarrollo de indentaciones tectónicas debidas a la colisión continental. El Dominio de Alborán se ha desplazado al oeste como consecuencia de la subducción con slab roll-back desde la apertura de la cuenca argelina en el Oligoceno-Mioceno Inferior. Este movimiento causa extensión ENE-OSO a la vez que el Dominio de Alborán experimenta compresión asociada a la convergencia oblicua Eurasia-África y colisiona con los márgenes de Iberia y África. Desde el Tortoniense, la compresión llevó a la inversión de la cuenca de Alborán y la elevación de los principales relieves de las cordilleras Bética y del Rif. Aunque la compresión NO-SE con extensión perpendicular han sido constantes desde el Tortoniense con pequeñas variaciones, la tectónica activa de las Béticas orientales y el centro del Mar de Alborán se caracterizan por fallas de salto en dirección, mientras que la Bética central presenta actividad fundamentalmente en fallas normales y grandes pliegues de escala kilométrica. Esta diferencia puede explicarse por los diferentes procesos litosféricos que las afectan. La slab oceánica se fue rompiendo y separando de la corteza ibérica y africana de este a oeste, así que en las Béticas orientales la corteza de Iberia está ya separada y quedó acoplada a la base del Dominio de Alborán. En cambio, las Béticas occidentales y el Rif aún experimentan ese movimiento hacia el oeste debido al hundimiento de la slab oceánica que sigue unida a África e Iberia en esta zona.

En las Béticas orientales, el alto grado de acoplamiento entre ambas cortezas en las Béticas orientales, combinado con la reducción del movimiento hacia el oeste, dio lugar a transpresión a lo largo de la Eastern Betic Shear Zone y plegamiento. Además, tuvo lugar la indentación tectónica del Arco de Águilas, como resultado de la compresión ejercida por la corteza argelina, que es rígida y que colisionó con los pliegues E-O de las Béticas, que se convirtieron en pliegues NE-SO mientras aún eran activos. La rotación y fragmentación de estos pliegues generó la zona de falla de

Palomares. A diferencia de otras indentaciones tectónicas, la PFZ está restringida a las rotaciones de los pliegues y no se han formado grandes fallas de salto en dirección que acomoden el desplzamiento del indentor, ni están conectadas con las fallas de salto en dirección generadas en el bloque indentado. Recientemente, la transmisión de la compresión al frente bético alcanzó el basamento ibérico de la cuenca de antepaís del Guadalquivir, aunque el área todavía experimenta desplazamientos hacia el oeste en superficie. La nucleación de fallas de salto en dirección en la corteza ibérica muestra la propagación de estos esfuerzos a la misma, mientras que los pliegues y cabalgamientos de las Zonas Externas de la Sierra de Cazorla presentan poca o nula actividad.

En el Mar de Alborán, la cuenca se invirtió y se formó una indentación tectónica en el sector central, al menos, desde el Plio-Cuaternario. El bloque del sur de Alborán se adhirió a la corteza africana y colisionó y desplazó a las intrusiones ígneas generadas durante el rift del Dominio AlKaPeCa. La indentación tectónica se acomoda por la falla dextra de Yusuf, que probablemente es una estructura heredada de la falla de STEP asociada al desplazamiento hacia el oeste del Dominio de Alborán, y por la falla sinistra de Al Idrissi, que se formó por la propia indentación durante el Pleistoceno. La interacción entre el proceso de indentación, relacionada con una fase de colisión continental, y el desplazamiento hacia el oeste asociado con el roll-back, puede observarse en el margen occidental del indentador, donde condiciona el desplazamiento al oeste de las estructuras activas. Los resultados de esta Tesis destacan esta interacción de la tectónica activa en el Campo de Dalías, donde los datos de GNSS muestran una interferencia entre el patrón radial causado por una indentación con el desplazamiento al OSO de la Bética central. La interacción de ambos procesos también determina la migración al oeste durante el Pleistoceno de la actividad de las fallas de la Bahía de Alhucemas, que constituyen la terminación sur de la falla de Al Idrissi. La migración está causada probablemente por el movimiento hacia el suroeste del Rif.

En conjunto, se puede definir una zona de transición donde la influencia del desplazamiento hacia el oeste causado por el roll-back y la tectónica de indentación y/o la transpresión controlan las fallas y pliegues activos; concretamente, a lo largo del borde occidental y septentrional de la indentación del Mar de Alborán. Sin

embargo, esta zona no queda bien caracterizada en el sector centro-oriental de las Béticas, donde puede haber un contacto neto entre ambos dominios. Alternativamente, podría haber un área de transición muy progresiva, eventualmente afectada por procesos litosféricos relacionados con la ruptura del slab entre las Béticas orientales y occidentales.

Perspectivas futuras

La definición de una zona de transición controlada tanto por el desplazamiento al oeste debido al slab roll-back y la tectónica de indentación relacionada con un alto acoplamiento de las cortezas ibéricas y de Alborán en las Béticas orientales permanece abierta. Aunque de las alternativas presentadas en el capítulo previo se argumenta la ausencia de una zona de transición, junto con otras explicaciones alternativas, es preciso una discusión más detallada integrando datos previos e investigación geológica y geofísica adiconal en las estructuras activas y recientes de estas áreas. Con respecto a ello, la instalación de redes locales de GPS podría ser muy útil para conocer mejor el movimiento real y actual de las mismas, como ha ocurrido en otros casos como la falla de Balanegra.

Además, en áreas en las que el movimiento de las placas es lento, los modelos geodinámicos de migración de las fallas han probado ser útiles para comprender mejor la posición de las fallas sismogénicas, como se muestra en esta Tesis para la Bahía de Alhucemas. El movimiento lento de las placas también supone una oportunidad para estudiar las diferentes etapas de la orogenia que afectan simultáneamente a amplias áreas de estos orógenos arqueados. Eso permite conocer mejor cómo la influencia de los diferentes procesos litosféricos cambia a medida que los laterales del orógeno chocan con los márgenes continentales, mientras que el frente del arco continúa su desplazamiento debido al slab roll-back. Futuras investigaciones que combinen datos geofísicos, geodéticos y geológicos con esta perspectiva podrían revelar aspectos signficativos de la evolución geodinámica de este tipo de orógenos.

Por último, esta tesis resalta la importancia de la integración de datos marinos y terrestres, especialmente en contextos en los que el mismo dominio cortical constituye la cuenca de back-arc y parte del orógeno arqueado. Los resultados

presentados muestran que las estructuras marinas y terrestres están normalmente relacionadas y, por ejemplo, en zonas como el Campo de Dalías o el Arco de Águilas se necesita investigación en tierra y mar para comprender por completo su historia geodinámica y su posible evolución. Las futuras investigaciones en regiones deformadas y tectónicamente activas que incluyen orógenos costeros o cuencas marinas invertidas deberían ser multidisciplinares e involucrar técnicas marinas y terrestres para proporcionar una visión completa de las estructuras tectónicas activas y los procesos geodinámicos asociaddos con implicaciones en la gestión de riesgos naturales.

References

ABEM (2006). *Instruction Manual Terrameter SAS 4000/SAS 1000*. Sundbyberg, Sweden: ABEM Instrument AB.

Aldaya, F., Alvarez, F., Galindo-Zaldivar, J., González-Lodeiro, F., Jabaloy, A., & Navarro Vilá, F. (1991). The Malaguide-Alpujarride contact (Betic Cordilleras, Spain): a brittle extensional detachment. *C. R. Acad. Sci. Paris, 313, Série II*(101), 1447-1453.

Alfaro, P., Delgado, J., de Galdeano, C. S., Galindo-Zaldívar, J., García-Tortosa, F. J., López-Garrido, A. C., ... & Borque, M. J. (2008). The Baza Fault: a major active extensional fault in the central Betic Cordillera (south Spain). *International Journal of Earth Sciences*, *97*(6), 1353-1365.

Alfaro, P., Sánchez-Alzola, A., Martin-Rojas, I., García-Tortosa, F. J., Galindo-Zaldívar, J., Avilés, M., ... & Gil, A. J. (2021). Geodetic fault slip rates on active faults in the Baza sub-Basin (SE Spain): Insights for seismic hazard assessment. *Journal of Geodynamics*, *144*, 101815.

Alken, P., Thébault, E., Beggan, C. D., Amit, H., Aubert, J., Baerenzung, J., ... & Zhou, B. (2021). International geomagnetic reference field: the thirteenth generation. *Earth, Planets and Space*, *73*(1), 1-25.

Alpert, L. A., Miller, M. S., Becker, T. W., & Allam, A. A. (2013). Structure beneath the Alboran from geodynamic flow models and seismic anisotropy. *Journal of Geophysical Research: Solid Earth*, *118*(8), 4265-4277.

Ammar, A., Mauffret, A., Gorini, C., & Jabour, H. (2007). The tectonic structure of the Alboran Margin of Morocco. *Revista de la Sociedad Geológica de España, 20,* 247–271.

Anahnah, F., Galindo-Zaldívar, J., Azzouz, O., Ruano, P., Chalouan, A., Pedrera, A., ... & Bouregba, N. (2009). The Nador dipole: one of the main magnetic anomalies of the NE Rif. *Trabajos de Geología*, (29).

Andrés, J., Marzán, I., Ayarza, P., Martí, D., Palomeras, I., Torné, M., ... & Carbonell, R. (2018). Curie point depth of the Iberian Peninsula and surrounding margins. A thermal and tectonic perspective of its evolution. *Journal of Geophysical Research: Solid Earth*, *123*(3), 2049-2068.

Andrieux, J., Fontbote, J. M., & Mattauer, M. (1971)a. Sur un modele explicatif de l'arc de Gibraltar. *Earth and Planetary Science Letters*, *12*(2), 191-198.

Andrieux, J. (1971)b. La structure du Rif Central. Étude des relations entre la tectonique de compression et les nappes de glissement dans un tronçon de la chaîne alpine. Ed. Notes et Mém. Serv. Géol. Maroc. 235, 1–155.

Ayala, C., Bohoyo, F., Maestro, A., Reguera, M. I., Torne, M., Rubio, F., ... & García-Lobón, J. L. (2016). Updated Bouguer anomalies of the Iberian Peninsula: a new perspective to interpret the regional geology. *Journal of Maps*, *12*(5), 1089-1092. https://doi.org/10.1080/17445647.2015.1126538

Ballesteros, M., Rivera, J., Muñoz, A., Muñoz-Martín, A., Acosta, J., Carbó, A., & Uchupi, E. (2008). Alboran Basin, southern Spain—Part II: Neogene tectonic implications for the orogenic float model. *Marine and Petroleum Geology*, *25*(1), 75-101.

Banda, E., Gallart, J., García-Dueñas, V., Dañobeitia, J. J., & Makris, J. (1993). Lateral variation of the crust in the Iberian Peninsula: new evidence from the Betic Cordillera. *Tectonophysics*, *221*(1), 53-66.

Baratin, L. M., Mazzotti, S., Chéry, J., Vernant, P., Tahayt, A., & Mourabit, T. (2016). Incipient mantle delamination, active tectonics and crustal thickening in Northern Morocco: Insights from gravity data and numerical modelling. *Earth and Planetary Science Letters, 454,* 113-120.

Blanco, M. J., & Spakman, W. (1993). The P-wave velocity structure of the mantle below the Iberian Peninsula: evidence for subducted lithosphere below southern Spain. *Tectonophysics*, *221*(1), 13-34.

Blumenthal, M. (1927). Versuch einer tektonischen Gliederung der Betischen Kordilleren von Central und Sùdwest Andalusien. *Eclogae Geol. Helv., 20,* 487-592

Borque, M. J., Sánchez-Alzola, A., Martin-Rojas, I., Alfaro, P., Molina, S., Rosa-Cintas, S., ... & Gil, A. J. (2019). How much Nubia-Eurasia convergence is accommodated by the NE end of the Eastern Betic Shear Zone (SE Spain)? Constraints from GPS velocities. *Tectonics*, *38*(5), 1824-1839.

Booth-Rea, G., Azañón, J. M., García-Dueñas, V., & Augier, R. (2003). Uppermost Tortonian to Quaternary depocentre migration related with segmentation of the strike-slip Palomares Fault Zone, Vera Basin (SE Spain). *Comptes Rendus Geoscience*, *335*(9), 751-761.

Booth-Rea, G., Azañón, J. M., Azor, A., & García-Dueñas, V. (2004). Influence of strike-slip fault segmentation on drainage evolution and topography. A case study: the Palomares Fault Zone (southeastern Betics, Spain). *Journal of Structural Geology*, *26*(9), 1615-1632.

Booth-Rea, G., Ranero, C. R., Martínez-Martínez, J. M., & Grevemeyer, I. (2007). Crustal types and Tertiary tectonic evolution of the Alborán Sea, western Mediterranean. *Geochemistry, Geophysics, Geosystems, 8*(10).

Bouillin, J. P., Durand-Delga, M., & Olivier, P. (1986). Betic-Rifian and Tyrrhenian arcs: distinctive features, genesis and development stages. In *Developments in Geotectonics* (Vol. 21, pp. 281-304). Elsevier.

Bourgois, J. (1978). La transversale de Ronda (Cordillères bétiques, Espagne): données géologiques pour un modèle d'évolution de l'arc de Gibraltar. Doctoral thesis, University of Besançon, Besançon, 445 pp.

Bousquet, J. C. (1979). Quaternary strike-slip faults in southeastern Spain. *Tectonophysics, 52,* 277-286.

Braga, J. C., Martín, J. M., & Quesada, C. (2003). Patterns and average rates of late Neogene–Recent uplift of the Betic Cordillera, SE Spain. *Geomorphology*, *50*(1-3), 3-26.

Buforn, E., Bezzeghoud, M., UdÍas, A., & Pro, C. (2004). Seismic sources on the Iberia-African plate boundary and their tectonic implications. *Pure and Applied Geophysics*, *161*(3), 623-646.

Calvert, A., Gomez, F., Seber, D., Barazangi, M., Jabour, N., Ibenbrahim, A., & Demnati, A. (1997). An integrated geophysical investigation of recent seismicity in the Al-Hoceima region of North Morocco. *Bulletin of the Seismological Society of America*, *87*(3), 637-651.

Calvert, A., Sandvol, E., Seber, D., Barazangi, M., Roecker, S., Mourabit, T., ... & Jabour, N. (2000). Geodynamic evolution of the lithosphere and upper mantle beneath the Alboran region of the western Mediterranean: Constraints from travel time tomography. *Journal of Geophysical Research: Solid Earth*, *105*(B5), 10871-10898.

Carbonell, R., Sallarès, V., Pous, J., Dan, J. J., Queralt, P., Ledo, J. J., & Duen, V. G. (1998). A multidisciplinary geophysical study in the Betic chain (southern Iberia Peninsula). *Tectonophysics*, *288*(1-4), 137-152.

Carminati, E., Wortel, M. J. R., Meijer, P. T., & Sabadini, R. (1998). The two-stage opening of the western–central Mediterranean basins: a forward modeling test to a new evolutionary model. *Earth and Planetary Science Letters*, *160*(3-4), 667-679.

Casas, A., & Carbo, A. (1990). Deep structure of the Betic Cordillera derived from the interpretation of a complete Bouguer anomaly map. *Journal of Geodynamics*, *12*(2-4), 137-147.

Catalán, M., Dyment, J., Choi, Y., Hamoudi, M., Lesur, V., Thébault, E., ... & Taylor, P. (2016). Making a better magnetic map. *Eos*, *97*. https://doi.org/10.1029/2016EO054645.

Chalouan, A., & Michard, A. (1990). The Ghomarides nappes, Rif coastal range, Morocco: a variscan chip in the Alpine belt. *Tectonics, 9,* 1565-1583.

Chalouan, A., Michard, A., Kadiri, K., Negro, F., Lamotte, D., Soto, J. I., & Saddiqi, O. (2008). The Rif Belt. In *Continental evolution: the geology of Morocco* (pp. 203-302). Springer, Berlin, Heidelberg.

Chapman, T. J., and Meneilly, A. W. (1991). The displacement patterns associated with a reverse-reactivated, normal growth fault. *The Geometry of Normal Faults. Geological Society, London, Special Publications,* 56, 183-191. https://doi.org/10.1144/GSL.SP.1991.056.01.12

Chertova, M. V., Spakman, W., Van den Berg, A. P., & Van Hinsbergen, D. J. J. (2014). Absolute plate motions and regional subduction evolution. *Geochemistry, Geophysics, Geosystems, 15*(10), 3780-3792.

Cloetingh, S. A. P. L., & Nieuwland, F. (1984). On the mechanics of lithospheric stretching and doming: a finite element analysis. *Geologie en Mijnbouw*, *63*, 315-322.

Comas, M.C., García-Dueñas, V., & Jurado, M.J. (1992). Neogene tectonic evolution of the Alboran Sea from MCS data. *Geo-Marine Lett., 12*, 157-164.

Comas, M. C., Platt, J. P., Soto, J. I., & Watts, A. B. (1999). 44. The origin and tectonic history of the Alboran Basin: insights from Leg 161 results. In *Proceedings of the Ocean Drilling Program Scientific Results* (Vol. 161, pp. 555-580).

Coppier, G., Griveaud, P., de Larouziere, F. D., Montenat, C., & Ott d' Estevou, P. (1989). Example of Neogene tectonic indentation in the Eastern Betic Cordilleras: the Arc of Águilas (southeastern Spain). *Geodinamica Acta*, *3*(1), 37-51.

Corsini, M., Chalouan, A., & Galindo-Zaldivar, J. (2014). Geodynamics of the Gibraltar Arc and the Alboran Sea region. *Journal of Geodynamics, 77,* 1-3. https://doi.org/10.1016/j.jog.2014.04.005

Coulon, C., Megartsi, M. H., Fourcade, S., Maury, R. C., Bellon, H., Louni-Hacini, A., ... & Hermitte, D. (2002). Post-collisional transition from calc-alkaline to alkaline volcanism during the Neogene in Oranie (Algeria): magmatic expression of a slab breakoff. *Lithos, 62*(3-4), 87-110.

Crespo-Blanc, A., Comas, M., & Balanyá, J. C. (2016). Clues for a Tortonian reconstruction of the Gibraltar arc: Structural pattern, deformation diachronism and block rotations. *Tectonophysics*, *683*, 308‑324. https://doi.org/10.1016/j.tecto.2016.05.045

d'Acremont, E., Gutscher, M. A., Rabaute, A., de Lépinay, B. M., Lafosse, M., Poort, J., ... & Gorini, C. (2014). High-resolution imagery of active faulting offshore Al Hoceima, Northern Morocco. *Tectonophysics*, *632*, 160-166.

d'Acremont, E., Lafosse, M., Rabaute, A., Teurquety, G., Do Couto, D., Ercilla, G., ... & Gorini, C. (2020). Polyphase tectonic evolution of fore-arc basin related to STEP fault as revealed by seismic reflection data from the Alboran Sea (W-Mediterranean). *Tectonics*, *39*(3), e2019TC005885. https://doi.org/10.1029/2019TC005885

Dañobeitia, J. J., Sallarès, V., & Gallart, J. (1998). Local earthquakes seismic tomography in the Betic Cordillera (southern Spain). *Earth and planetary science letters*, *160*(3-4), 225-239.

De Larouzière, F. D., Bolze, J., Bordet, P., Hernandez, J., Montenat, C., & Ott d'Estevou, P. (1988). The Betic segment of the lithospheric Trans-Alboran Shear Zone during the Late Miocene. *Tectonophysics*, *152*(1-2), 41–52. https://doi.org/10.1016/0040-1951(88)90028-5

DeMets, C., Gordon, R. G., & Argus, D. F. (2010). Geologically current plate motions. *Geophysical Journal International, 181*(1), 1-80. https://doi.org//10.1111/j.1365-246X.2009.04491.x

Dewey, J. F., Helman, M. L., Knott, S. D., Turco, E., & Hutton, D. H. W. (1989). Kinematics of the western Mediterranean. *Geological Society, London, Special Publications*, *45*(1), 265-283.

Díaz, J., & Gallart, J. (2014). Seismic anisotropy from the Variscan core of Iberia to the Western African Craton: New constrains on upper mantle flow at regional scales. *Earth and Planetary Science Letters*, *394*, 48-57.

Do Couto, D., Gumiaux, C., Augier, R., Lebret, N., Folcher, N., Jouannic, G., ... & Gorini, C. (2014). Tectonic inversion of an asymmetric graben: insights from a combined field and gravity survey in the Sorbas basin. *Tectonics*, *33*(7), 1360-1385.

Do Couto, D., Gorini, C., Jolivet, L., Lebret, N., Augier, R., Gumiaux, C., ... & Auxietre, J. L. (2016). Tectonic and stratigraphic evolution of the Western Alboran Sea Basin in the last 25 Myrs. *Tectonophysics*, *677*, 280-311.

Driussi, O., Briais, A., & Maillard, A. (2015). Evidence for transform motion along the South Balearic margin and implications for the kinematics of opening of the Algerian basin. *Bulletin de la Société Géologique de France*, *186*(4-5), 353-370.

Duggen, S., Hoernle, K., Bogaard, P., & Harris, C. (2004). Magmatic evolution of the Alboran Region: the role of subduction in forming the western Mediterranean and causing the Messinian Salinity Crisis. *Earth Planet Sci Lett, 218,* 91–108.

Duggen, S., Hoernle, K., van den Bogaard, P., & Garbe-Schönberg, D. (2005). Post-collisional transition from subduction-to intraplate-type magmatism in the westernmost Mediterranean: evidence for continental-edge delamination of subcontinental lithosphere. *Journal of Petrology*, *46*(6), 1155-1201.

Duggen, S., Hoernle, K., Klügel, A., Geldmacher, J., Thirlwall, M., Hauff, F., ... & Oates, N. (2008). Geochemical zonation of the Miocene Alborán Basin volcanism (westernmost Mediterranean): geodynamic implications. *Contributions to Mineralogy and Petrology, 156*(5), 577.

Durand-Delga, M., Rossi, P., Olivier, P., & Puglisi, D. (2000). Situation structurale et nature ophiolitique de roches basiques jurassiques associées aux flyschs maghrébins du Rif (Maroc) et de Sicile (Italie). *Comptes Rendus de l'Académie des Sciences-Series IIA-Earth and Planetary Science*, *331*(1), 29-38.

Echeverria, A., Khazaradze, G., Asensio, E., Gárate, J., Dávila, J. M., & Suriñach, E. (2013). Crustal deformation in eastern Betics from CuaTeNeo GPS network. *Tectonophysics*, *608*, 600-612.

Egeler, C. G. (1963). On the tectonics of the eastern Betic Cordilleras (SE Spain). *Geol. Rundsch., 52,* 260-269.

El Bakkali, S., Gourgaud, A., Bourdier, J. L., Bellon, H., & Gundogdu, N. (1998). Post-collision neogene volcanism of the Eastern Rif (Morocco): magmatic evolution through time. *Lithos*, *45*(1-4), 523-543.

El Moudnib, L., Villaseñor, A., Harnafi, M., Gallart, J., Pazos, A., Serrano, I., ... & Chourak, M. (2015). Crustal structure of the Betic–Rif system, western Mediterranean, from local earthquake tomography. *Tectonophysics*, *643*, 94-105.

Ercilla, G., Juan, C., Hernandez-Molina, F. J., Bruno, M., Estrada, F., Alonso, B., ... & Ammar, A. (2016). Significance of bottom currents in deep-sea morphodynamics: an example from the Alboran Sea. *Marine Geology*, *378*, 157-170.

Ercilla, G., Galindo-Zaldívar, J., Estrada, F., Valencia, J., Juan, C., Casas, D., ... & Yenes, M. (2022). Understanding the complex geomorphology of a deep sea area affected by continental tectonic indentation: The case of the Gulf of Vera (Western Mediterranean). *Geomorphology*, 108126.

Estrada, F., Galindo-Zaldivar, J., Vázquez, J. T., Ercilla, G., D'Acremont, E., Alonso, B., & Gorini, C. (2018). Tectonic indentation in the central Alboran Sea (westernmost Mediterranean). *Terra Nova, 30*(1), 24-33. https://doi.org//10.1111/ter.12304

Estrada, F., González-Vida, J. M., Peláez, J. A., Galindo-Zaldívar, J., Ortega, S., Macías, J., ... & Ercilla, G. (2021). Tsunami generation potential of a strike-slip fault tip in the westernmost Mediterranean. *Scientific reports*, *11*(1), 1-9.

Faccenna, C., Becker, T. W., Auer, L., Billi, A., Boschi, L., Brun, J. P., ... & Serpelloni, E. (2014). Mantle dynamics in the Mediterranean. *Reviews of Geophysics*, *52*(3), 283-332. doi:10.1002/2013RG000444

Fadil, A., Vernant, P., McClusky, S., Reilinger, R., Gomez, F., Ben Sari, D., ... & Barazangi, M. (2006). Active tectonics of the western Mediterranean: Geodetic evidence for rollback of a delaminated subcontinental lithospheric slab beneath the Rif Mountains, Morocco. *Geology*, *34*(7), 529-532.

Fernández-Soler, J., Martínez-Ruíz, F., Akhmanov, G., Akhmetzhanov, A., Stadnitskaya, A., Kozlova, E., … & Goncharov, D. (2000). Bottom sampling. In: *Multidisciplinary Study of Geological Processes on the North East Atlantic and Western Mediterranean Margins, Preliminary results of geological and geophysical investigations* during the TTR-9 of R/V Professor Logachev, June- July, 1999 (Ed. by N. H. Kenyon, M. K. Ivanov, A. M. Azhmetzhanov & G. G. Akhmanov), 56, 85–91, IOC Technical Series, UNESCO.

Fontboté, J. M. (1966). *Las Cordilleras Béticas. La depresión del Guadalquivir*. Madrid, Spain: Librería Paraninfo.

Frizon de Lamotte, D. (1982): Contribution à l'étude de l'évolution structurale du Rif oriental. *Notes Mém. Serv. Géol. (Morocco)*, 314: 239‑309.

Fullea, J., Fernàndez, M., & Zeyen, H. (2006). Lithospheric structure in the Atlantic–Mediterranean transition zone (southern Spain, northern Morocco): a simple approach from regional elevation and geoid data. *Comptes Rendus Geoscience*, *338*(1-2), 140-151.

Galdeano, A., Courtillot, V., Le Borgne, E., Le Mouel, J. L., & Rossignol, J. C. (1974). An aeromagnetic survey of the southwest of the western Mediterranean: Description and tectonic implications. *Earth and Planetary Science Letters*, *23*(3), 323-336.

Galindo-Zaldivar, J., Gonzalez-Lodeiro, F., & Jabaloy, A. (1989). Progressive extensional shear structures in a detachment contact in the western Sierra Nevada, (Betic Cordilleras, Spain). *Geodinamica Acta, 3*(1), 73-85.

Galindo-Zaldivar, J., González-Lodeiro, F., Jabaloy, A., Maldonado, A., & Schreider, A.A. (1998). Models of magnetic and Bouguer gravity anomalies for the deep structure of the central Alboran Sea basin. *Geo-Mar. Lett., 18*, 10-18.

Galindo-Zaldıvar, J., Gil, A. J., Borque, M. J., González-Lodeiro, F., Jabaloy, A., Marın-Lechado, C., ... & Sanz de Galdeano, C. (2003). Active faulting in the internal zones of the central Betic Cordilleras (SE, Spain). *Journal of Geodynamics*, *36*(1-2), 239-250.

Galindo-Zaldívar, J., Chalouan, A., Azzouz, O., Sanz de Galdeano, C., Anahnah, F., Ameza, L., ... & Chabli, A. (2009). Are the seismological and geological observations of the Al Hoceima (Morocco, Rif) 2004 earthquake (M= 6.3) contradictory? *Tectonophysics*, *475*(1), 59-67.

Galindo-Zaldivar, J., Gil, A. J., Sanz de Galdeano, C., Lacy, M. C., García-Armenteros, J. A., Ruano, P., ... & Alfaro, P. (2015). Active shallow extension in central and eastern Betic Cordillera from CGPS data. *Tectonophysics*, *663*, 290-301. https://doi.org/10.1016/j.tecto.2015.08.035

Galindo-Zaldivar, J., Ercilla, G., Estrada, F., Catalán, M., d'Acremont, E., Azzouz, O., ... & Gil, A. J. (2018). Imaging the growth of recent faults: the case of 2016–2017 seismic sequence sea bottom deformation in the Alboran Sea (Western Mediterranean). *Tectonics*, *37*(8), 2513-2530.

Galindo-Zaldívar, J., Braga, J. C., Marín-Lechado, C., Ercilla, G., Martín, J. M., Pedrera, A., ... & Alonso, B. (2019). Extension in the Western Mediterranean. In *The geology of Iberia: a geodynamic approach* (pp. 61-103). Springer, Cham. https://doi.org/10.1007/978-3-030-11190-8_3

Garate, J., Martin-Davila, J., Khazaradze, G., Echeverria, A., Asensio, E., Gil, A. J., ... & Harnafi, M. (2015). Topo-Iberia project: CGPS crustal velocity field in the Iberian Peninsula and Morocco. *GPS Solutions*, *19*(2), 287-295.

García-Castellanos, D., Fernández, M., & Torné, M. (2002). Modeling the evolution of the Guadalquivir foreland basin (southern Spain). *Tectonics*, *21*(3), C001339. https://doi.org/10.1029/2001TC001339

García-Dueñas, V., & Balanyá, J. C. (1986). Estructura y naturaleza del Arco de Gibraltar. *Maleo Bolletin. Societa Geologica de Portugal, 2*,1–23.

García-Dueñas, V., Balanyá, J.C., & Martínez-Martínez, J.M., (1992). Miocene extensional detachments in the outcropping basement of the Northern Alboran Basin (Betics) and their tectonic implications. *Geo-Mar. Lett.* 12, 88–95.

García-Dueñas, V., Banda, E., Torné, M., Córdoba, D., & ESCI-Béticas Working Group. (1994). A deep seismic reflection survey across the Betic Chain (southern Spain): first results. *Tectonophysics*, *232*(1-4), 77-89.

García-Hernández, M., López-Garrido, A. C., Rivas, P., Sanz de Galdeano, C., & Vera, J. A. (1980). Mesozoic palaeogeographic evolution of the external zones of the Betic cordillera. *Geologie en Mijnbouw*, *59*(2), 155–168.

García-Mayordomo, J., Martín-Banda, R., Insua-Arévalo, J. M., Álvarez-Gómez, J. A., Martínez-Díaz, J. J., & Cabral, J. (2017). Active fault databases: building a bridge between earthquake geologists and seismic hazard practitioners, the case of the QAFI v. 3 database. *Natural Hazards and Earth System Sciences*, *17*(8), 1447-1459.

Garrido, C. J. (1995). Estudio geoquimico de las capas maficas del macizo ultramafico de Ronda (Cordillera Betica, Espana). Doctoral dissertation, Universidad de Granada.

Gil, A. J., Galindo-Zaldívar, J., Sanz de Galdeano, C., Borque, M. J., Sánchez-Alzola, A., Martinez-Martos, M., & Alfaro, P. (2017). The Padul normal fault activity constrained by GPS data: Brittle extension orthogonal to folding in the central Betic Cordillera. *Tectonophysics*, *712*, 64-71.

Gill, R. C. O., Aparicio, A., El Azzouzi, M., Hernandez, J., Thirlwall, M. F., Bourgois, J., & Marriner, G. F. (2004). Depleted arc volcanism in the Alboran Sea and shoshonitic volcanism in Morocco: geochemical and isotopic constraints on Neogene tectonic processes. *Lithos, 78*(4), 363-388.

Gómez de la Peña, L., Grevemeyer, I., Kopp, H., Díaz, J., Gallart, J., Booth-Rea, G., ... & R. Ranero, C. (2020). The lithospheric structure of the Gibraltar Arc System from wide-angle seismic data. *Journal of Geophysical Research: Solid Earth*, *125*(9), e2020JB019854.

Gómez-Pugnaire, M. T., Rubatto, D., Fernández-Soler, J. M., Jabaloy, A., López-Sánchez-Vizcaíno, V., González-Lodeiro, F., ... & Padrón-Navarta, J. A. (2012). Late Variscan magmatism in the Nevado-Filábride Complex: U-Pb geochronologic evidence for the pre-Mesozoic nature of the deepest Betic complex (SE Spain). *Lithos*, *146*, 93-111.

González-Castillo, L. (2015). *Crustal structure and active deformation in the westernmost Betic Cordillera and its foreland*. Doctoral dissertation, Universidad de Granada, 190 pp.

González-Castillo, L., Galindo-Zaldívar, J., Ruiz-Constán, A., & Pedrera, A. (2014). Magnetic evidence of a crustal fault affecting a linear laccolith: The Guadiana Fault and the Monchique Alkaline Complex (SW Iberian Peninsula). *Journal of Geodynamics*, *77*, 149-157.

Gonzalez-Castillo, L., Galindo-Zaldivar, J., de Lacy, M. C., Borque, M. J., Martinez-Moreno, F. J., García-Armenteros, J. A., & Gil, A. J. (2015). Active rollback in the Gibraltar Arc: Evidences from CGPS data in the western Betic Cordillera. *Tectonophysics*, *663*, 310-321.

Gueguen, E., Doglioni, C., & Fernandez, M. (1998). On the post-25 Ma geodynamic evolution of the western Mediterranean. *Tectonophysics, 298*(1-3), 259-269. http://dx.doi.org/10.1016/S0040-1951(98)00189-9.

Gurrıa, E., & Mezcua, J. (2000). Seismic tomography of the crust and lithospheric mantle in the Betic Cordillera and Alboran Sea. *Tectonophysics*, *329*(1-4), 99-119.

Gutscher, M. A., Dominguez, S., Westbrook, G. K., Le Roy, P., Rosas, F., Duarte, J. C., ... & Bartolomé, R. (2012). The Gibraltar subduction: A decade of new geophysical data. *Tectonophysics*, *574*, 72-91.

Hatzfeld, D. (1976). Étude sismologique et gravimétrique de la estructure profonde de la mer d'Alborán: Mise en évidence d'un manteau anormal. *C. R. Acad. Sci., Ser. IIA Earth Planet. Sci., 5,* 483-500.

Herrero-Barbero, P., Álvarez-Gómez, J. A., Williams, C., Villamor, P., Insua-Arévalo, J. M., Alonso-Henar, J., & Martínez-Díaz, J. J. (2021). Physics-Based Earthquake Simulations in Slow-Moving Faults: A Case Study From the Eastern Betic Shear Zone (SE Iberian Peninsula). *Journal of Geophysical Research: Solid Earth*, *126*(5), e2020JB021133.

Hidas, K., Garrido, C. J., Booth-Rea, G., Marchesi, C., Bodinier, J. L., Dautria, J. M., ... & Azzouni-Sekkal, A. (2019). Lithosphere tearing along STEP faults and synkinematic formation of lherzolite and wehrlite in the shallow subcontinental mantle. *Solid Earth*, *10*(4), 1099-1121.

Hoernle, K., Bogaard, P., Duggen, S., Mocek, B., & Garbe-Schönberg, D. (1999). Evidence for Miocene subduction beneath the Alboran Sea: $^{40}Ar/^{39}Ar$ dating and geochemistry of volcanic rocks from Holes 977A and 978A. In: Zahn R, Comas MC, Klaus A (eds) Proceedings of the ocean drilling program 161, Scientific Results, vol 161, pp 357–373.

Houseman, G. A., McKenzie, D. P., & Molnar, P. (1981). Convective instability of a thickened boundary layer and its relevance for the thermal evolution of continental convergent belts. *Journal of Geophysical Research: Solid Earth*, *86*(B7), 6115-6132.

Instituto Geográfico Nacional (IGN) (1976). *Mapa de anomalías de Bouguer*. Madrid, Spain: IGN.

Jackson, C. A.-L., Bell, R. E., Rotevatn, A., & Tvedt, A. B. M. (2017). Techniques to determine the kinematics of synsedimentary normal faults and implications for fault growth models. *Geological Society, London, Special Publications,* 439. https://doi.org/10.1144/SP439.22

Jabaloy-Sánchez, A., Martín-Algarra, A., Padrón-Navarta, J. A., Martín-Martín, M., Gómez-Pugnaire, M. T., Sánchez-Vizcaíno, V. L., & Garrido, C. J. (2019). Lithological successions of the Internal Zones and Flysch Trough units of the Betic Chain. In *The Geology of Iberia: A Geodynamic Approach* (pp. 377-432). Springer, Cham. https://doi.org/10.1007/978-3-030-11295-0_8

Jolivet, L., Menant, A., Roche, V., Le Pourhiet, L., Maillard, A., Augier, R., ... & Canva, A. (2021). Transfer zones in Mediterranean back-arc regions and tear faults. *BSGF-Earth Sciences Bulletin*, *192*(1), 11.

Juan, C., Ercilla, G., Hernández-Molina, F. J., Estrada, F., Alonso, B., Casas, D., ... & Ammar, A. (2016). Seismic evidence of current-controlled sedimentation in the Alboran Sea

during the Pliocene and Quaternary: Palaeoceanographic implications. *Marine Geology*, *378*, 292-311. https://doi.org/10.1016/j.margeo.2016.01.006

Julivert, M., & Fontboté, J. M. (1977). *Memoria Mapa Tectónico de la Península Ibérica y Baleares*. Madrid, Spain: IGME-Servicio de Publicaciones del Ministerio de Industria.

Kane, M. F. (1962). A comprehensive system of terrain corrections using a digital computer. *Geophysics*, *27*(4), 455-462.

Kornprobst, J., (1974): Contribution à l' étude pétrographique et structurale de la Zone interne du Rif (Maroc septentrional), *Notes Mém. Serv. Géol. Maroc*, 251: 1–256.

Koulali, A., Ouazar, D., Tahayt, A., King, R. W., Vernant, P., Reilinger, R. E., ... & Amraoui, N. (2011). New GPS constraints on active deformation along the Africa–Iberia plate boundary. *Earth and Planetary Science Letters*, *308*(1-2), 211-217.

Lafosse, M., d'Acremont, E., Rabaute, A., de Lépinay, B. M., Tahayt, A., Ammar, A., & Gorini, C. (2016). Evidence of Quaternary transtensional tectonics in the Nekor basin (NE Morocco). *Basin Research*, *29*(4), 470-489.

Lafosse, M., Gorini, C., Le Roy, P., Alonso, B., d' Acremont, E., Ercilla, G., ... & Ammar, A. (2018). Late Pleistocene-Holocene history of a tectonically active segment of the continental margin (Nekor basin, Western Mediterranean, Morocco). *Marine and Petroleum Geology*, *97*, 370-389.

Lafosse, M., d'Acremont, E., Rabaute, A., Estrada, F., Jollivet-Castelot, M., Vazquez, J. T., ... & Gorini, C. (2020). Plio-Quaternary tectonic evolution of the southern margin of the Alboran Basin (Western Mediterranean). *Solid Earth*, *11*(2), 741-765.

Lesur, V., Hamoudi, M., Choi, Y., Dyment, J., & Thébault, E. (2016). Building the second version of the world digital magnetic anomaly map (WDMAM). *Earth, Planets and Space*, *68*(1), 1-13.

Li, C. F., Lu, Y., & Wang, J. (2017). A global reference model of Curie-point depths based on EMAG2. *Scientific reports*, *7*(1), 1-9.

Li, Q., Ruano, P., Pedrera Parias, A., & Galindo Zaldívar, J. (2012). Estructura de la cuenca sedimentaria de Tabernas-Sorbas mediante prospección gravimétrica y magnética (Zonas Internas, Cordillera Bética Oriental). *Geogaceta, 52,* 117-120.

Loke, M. H. (2014). *Tutorial: 2-D and 3-D Electrical Imaging Surveys. Geotomo Software Company*. Retrieved from www.geotomosoft.com

Lonergan, L., & White, N. (1997). Origin of the Betic-Rif mountain belt. *Tectonics*, *16*(3), 504-522.

Madarieta-Txurruka, A., Galindo-Zaldívar, J., González-Castillo, L., Peláez, J. A., Ruiz-Armenteros, A. M., Henares, J., ... & Gil, A. J. (2021). High-and Low-Angle Normal Fault Activity in a Collisional Orogen: The Northeastern Granada Basin (Betic Cordillera). *Tectonics*, *40*(7), e2021TC006715.

Malinverno, A., & Ryan, W. B. (1986). Extension in the Tyrrhenian Sea and shortening in the Apennines as result of arc migration driven by sinking of the lithosphere. *Tectonics*, *5*(2), 227-245.

Mancilla, F. d. L., Stich, D., Berrocoso, M., Martín, R., Morales, J., Fernandez-Ros, A., Páez, R., & Pérez-Peña, A. (2013). Delamination in the Betic Range: Deep structure, seismicity, and GPS motion. *Geology, 41*(3), 307-310. https://doi.org//10.1130/G33733.1

Mancilla, F. d. L., Booth-Rea, G., Stich, D., Pérez-Peña, J. V., Morales, J., Azañón, J. M., ... & Giaconia, F. (2015). Slab rupture and delamination under the Betics and Rif constrained from receiver functions. *Tectonophysics*, *663*, 225-237.

Marín-Lechado, C., Galindo-Zaldívar, J., Rodríguez-Fernández, L. R., Serrano, I., & Pedrera, A. (2005). Active faults, seismicity and stresses in an internal boundary of a tectonic arc (Campo de Dalías and Níjar, southeastern Betic Cordilleras, Spain). *Tectonophysics*, *396*(1-2), 81-96.

Marín-Lechado, C., Galindo-Zaldívar, J., Rodríguez-Fernández, L. R., & Pedrera, A. (2007). Mountain front development by folding and crustal thickening in the Internal Zone of the Betic Cordillera-Alboran Sea boundary. *Pure and Applied Geophysics*, *164*(1), 1-21.

Marín-Lechado, C., Galindo-Zaldívar, J., Gil, A. J., Borque, M. J., De Lacy, M. C., Pedrera, A., ... & Sanz de Galdeano, C. (2010). Levelling profiles and a GPS network to monitor the active folding and faulting deformation in the Campo de Dalias (Betic Cordillera, Southeastern Spain). *Sensors*, *10*(4), 3504-3518.

Marín-Lechado, C., Pedrera, A., Peláez, J. A., Ruiz-Constán, A., González-Ramón, A., & Henares, J. (2017). Deformation style and controlling geodynamic processes at the eastern Guadalquivir foreland basin (Southern Spain). *Tectonics*, *36*, 1072–1089. https://doi.org/10.1002/2017TC004556

Martín, J. M., Braga, J. C., Aguirre, J., & Puga-Bernabéu, Á. (2009). History and evolution of the North-Betic Strait (Prebetic Zone, Betic Cordillera): a narrow, early Tortonian, tidal-dominated, Atlantic–Mediterranean marine passage. *Sedimentary Geology*, *216*(3-4), 80-90.

Martín, R., Stich, D., Morales, J., & Mancilla, F. (2015). Moment tensor solutions for the Iberian-Maghreb region during the IberArray deployment (2009–2013). *Tectonophysics*, *663*, 261-274.

Martínez-García, P., Soto, J. I., & Comas, M. (2011). Recent structures in the Alboran Ridge and Yusuf fault zones based on swath bathymetry and sub-bottom profiling: evidence of active tectonics. *Geo-Marine Letters*, *31*(1), 19-36.

Martínez-Martínez, J. M. (2006). Lateral interaction between metamorphic core complexes and less-extended, tilt-block domains: the Alpujarras strike-slip transfer fault zone (Betics, SE Spain). *Journal of Structural Geology*, *28*(4), 602-620.

Martinez-Martinez, J. M., Soto, J. I., & Balanyá, J. C. (1997). Crustal decoupling and intracrustal flow beneath domal exhumed core complexes, Betics (SE Spain). *Terra Nova*, *9*(5-6), 223-227.

Martinez-Martos, M., Galindo-Zaldivar, J., Sanz de Galdeano, C., Garcia-Tortosa, F. J., Martinez-Moreno, F. J., Ruano, P., ... & Azañon, J. M. (2017). Latest extension of the Laujar fault in a convergence setting (Sierra Nevada, Betic Cordillera). *Journal of Geodynamics*, *104*, 15-26.

Martínez-Moreno, F. J., Galindo-Zaldívar, J., Pedrera, A., Teixido, T., Ruano, P., Peña, J. A., ... & Martín-Rosales, W. (2014). Integrated geophysical methods for studying the karst system of Gruta de las Maravillas (Aracena, Southwest Spain). *Journal of Applied Geophysics*, *107*, 149-162.

Mauffret, A., Ammar, A., Gorini, C., & Jabour, H. (2007). The Alboran Sea (Western Mediterranean) revisited with a view from the Moroccan margin. *Terra Nova*, *19*(3), 195-203.

Maury, R. C., Fourcade, S., Coulon, C., Bellon, H., Coutelle, A., Ouabadi, A., ... & Réhault, J. P. (2000). Post-collisional Neogene magmatism of the Mediterranean Maghreb margin: a consequence of slab breakoff. *Comptes Rendus de l'Académie des Sciences-Series IIA-Earth and Planetary Science*, *331*(3), 159-173.

Medina-Cascales, I., Martin-Rojas, I., García Tortosa, F. J., Peláez Montilla, J. A., & Alfaro García, P. (2020). Geometry and kinematics of the Baza Fault (central Betic Cordillera, South Spain): insights into its seismic potential. *Geodinamica Acta, 18*(11), 1-25. https://doi.org/10.1344/GeologicaActa2020.18.11

Michard A, Feinberg H, El Azzab D, BouybaoueneM, Saddiqi O (1992). A serpentinite ridge in a collisional paleomargin setting: the Beni Malek massif, External Rif, Morocco. *Earth Planet Sci Lett 113*, 435‑442.

Milliard, Y. (1959): Sur la présence d'assises carbonifères dans le massif paléozoique interne du Rif. *C.R. Acad. Sci. Paris* 249: 1688–1690.

Monié, P., Galindo-Zaldivar, J., González-Lodeiro, F., Goffe, B., & Jabaloy, A. (1991). Ar-40/Ar-39 geochronology of alpine tectonism in the Betic Cordilleras (Southern Spain). *Journal of the Geological Society, 148,* 289-297.

Monié, P., Torres-Roldan, R. L., & García-Casco, A. (1994). Cooling and exhumation of the Western Betic Cordilleras, 40Ar/39Ar thermochronological constraints on a collapsed terrane. *Tectonophysics, 238,* 353-379.

Monna, S., Argnani, A., Cimini, G. B., Frugoni, F., & Montuori, C. (2015). Constraints on the geodynamic evolution of the Africa–Iberia plate margin across the Gibraltar Strait from seismic tomography. *Geoscience Frontiers*, *6*(1), 39-48.

Morales, J., Serrano, I., Jabaloy, A., Galindo-Zaldivar, J., Zhao, D., Torcal, F., ... & Lodeiro, F. G. (1999). Active continental subduction beneath the Betic Cordillera and the Alboran Sea. *Geology*, *27*(8), 735-738.

Morales, J., Azañón, J. M., Stich, D., Roldán, F. J., Pérez-Peña, J. V., Martín, R., ... & González-Ramón, A. (2015). The 2012–2013 earthquake swarm in the eastern Guadalquivir basin (South Spain): A case of heterogeneous faulting due to oroclinal bending. *Gondwana Research*, *28*(4), 1566-1578. https://doi.org/10.1016/j.gr.2014.10.017

Morales, J., Molina-Aguilera, A., Mancilla, F., Stich, D., Azañon, J. M., Teixido, T., ... & Posadas, A. M. (2022). Preservation of the Iberian Tethys paleomargin beneath the eastern Betic mountain range. *Gondwana Research, 106*, 237-246.

Nagy, D. (1966). The gravitational attraction of a right rectangular prism. *Geophysics*, 3*1*(2), 362-371.

National Geographic Service of Spain, IGN. http://centrodedescargas.cnig.es/CentroDescargas/index.jsp

Neres, M., Carafa, M. M. C., Fernandes, R. M. S., Matias, L., Duarte, J. C., Barba, S., & Terrinha, P. (2016). Lithospheric deformation in the Africa-Iberia plate boundary: Improved neotectonic modeling testing a basal-driven Alboran plate. *Journal of Geophysical Research: Solid Earth*, *121*(9), 6566-6596. https://doi.org/10.1002/2016JB013012

Palano, M., González, P. J., & Fernández, J. (2015). The Diffuse Plate boundary of Nubia and Iberia in the Western Mediterranean: Crustal deformation evidence for viscous coupling and fragmented lithosphere. *Earth Planet. Sci. Lett. 430*, 439–447. doi: 10.1016/j.epsl.2015.08.040

Pedley, R. C., Busby, J. P., & Dabek, Z. K. (1993). GRAVMAG user manual–interactive 2.5 D gravity and magnetic modelling. British Geological Survey, Technical Report WK/93/26/R. 73.

Pedrera, A., Galindo-Zaldívar, J., Sanz de Galdeano, C., & López-Garrido, Á. C. (2007). Fold and fault interactions during the development of an elongated narrow basin: The Almanzora Neogene-Quaternary Corridor (SE Betic Cordillera, Spain). *Tectonics*, *26*(6).

Pedrera, A., Galindo-Zaldívar, J., Ruíz-Constán, A., Duque, C., Marín-Lechado, C., & Serrano, I. (2009). Recent large fold nucleation in the upper crust: Insight from gravity, magnetic, magnetotelluric and seismicity data (Sierra de Los Filabres–Sierra de Las Estancias, Internal Zones, Betic Cordillera). *Tectonophysics*, *463*(1-4), 145-160.

Pedrera, A., Galindo-Zaldívar, J., Marín-Lechado, C., García-Tortosa, F.J., Ruano, P., López-Garrido, A. C., … & Giaconia, F. (2012). Recent and active faults and folds in the central-eastern Internal Zones of the Betic Cordillera/Las fallas y pliegues recientes y activos de la parte centro-oriental de las Zonas Internas de la Cordillera Bética. *Journal of Iberian Geology*, *38*(1), 191-208.

Pedrera, A., Ruiz-Constán, A., Marín-Lechado, C., Galindo-Zaldivar, J., González, A., & Peláez, J. A. (2013). Seismic transpressive basement faults and monocline development in a foreland basin (eastern Guadalquivir, SE Spain). *Tectonics*, *32*, 1571–1586. https://doi.org/10.1002/2013TC003397

Pedrera, A., Marín-Lechado, C., Galindo-Zaldívar, J., & Lobo, F. J. (2015). Smooth folds favoring gypsum precipitation in the Messinian Poniente marginal basin (Western Mediterranean). *Tectonophysics*, *663*, 48-61.

Pérouse, E., Vernant, P., Chéry, J., Reilinger, R., & McClusky, S. (2010). Active surface deformation and sub-lithospheric processes in the western Mediterranean constrained by numerical models. *Geology*, *38*(9), 823-826.

Platt, J. P., & Vissers, R. L. M. (1989). Extensional collapse of thickened continental lithosphere: A working hypothesis for the Alboran Sea and Gibraltar arc. *Geology*, *17*(6), 540–543. https://doi.org/10.1130/0091613(1989)017%3C0540:ECOTCL%3E2.3.CO;2

Platt, J. P., Allerton, S., Mandeville, C., Mayfield, A., Platzman, E. S., & Rimi, A. (2003). The ultimate arc: Differential displacement, oroclinal bending, and vertical axis rotation in the external Betic-Rif arc. *Tectonics*, *22*(3), C001321. https://doi.org/10.1029/2001TC001321

Platt, J. P., Anczkiewicz, R., Soto, J.I., Kelley, S.P., & Thirlwall, M. (2006). Early Miocene continental subduction and rapid exhumation in the western Mediterranean. *Geology, 34,* 1981-1984.

Platt, J. P., Behr, W. M., Johanesen, K., & Williams, J. R. (2013). The Betic-Rif arc and its orogenic hinterland: a review. *Annual Review of Earth and Planetary Sciences*, *41*, 313-357.

Polyak, B. G., Fernàndez, M., Khutorskoy, M. D., Soto, J. I., Basov, I. A., Comas, M. C., ... & Banda, E. (1996). Heat flow in the Alboran Sea, western Mediterranean. *Tectonophysics*, *263*(1-4), 191-218.

Poujol, A., Ritz, J. F., Tahayt, A., Vernant, P., Condomines, M., Blard, P. H., ... & Idrissi, A. K. (2014). Active tectonics of the Northern Rif (Morocco) from geomorphic and geochronological data. *Journal of Geodynamics*, *77*, 70-88.

Reicherter, K. R., Jabaloy, A., Galindo-Zaldívar, J., Ruano, P., Becker-Heidmann, P., Morales, J., ... & González-Lodeiro, F. (2003). Repeated palaeoseismic activity of the Ventas de Zafarraya fault (S Spain) and its relation with the 1884 Andalusian earthquake. *International Journal of Earth Sciences*, *92*(6), 912-922.

Rodríguez-Cañero, R., Jabaloy-Sánchez, A., Navas-Parejo, P., & Martín-Algarra, A. (2018). Linking Palaeozoic palaeogeography of the Betic Cordillera to the Variscan Iberian Massif: new insight through the first conodonts of the Nevado-Filábride Complex. *International Journal of Earth Sciences*, *107*(5), 1791-1806.

Rodríguez-Fernández, J., Roldán, F. J., Azañón, J. M., & García-Cortés, A. (2015). El colapso gravitacional del frente orogénico alpino en el Dominio Subbético durante el Mioceno medio-superior: El Complejo Extensional Subbético. *Boletín Geológico y Minero*, *124*(3), 477–504. http://www.igme.es/boletin/2013/124_3/9_ARTICULO%208.pdf

Romagny, A., Jolivet, L., Menant, A., Bessière, E., Maillard, A., Canva, A., ... & Augier, R. (2020). Detailed tectonic reconstructions of the Western Mediterranean region for the last 35 Ma, insights on driving mechanismsReconstructions détaillées de la Méditerranée occidentale depuis 35 Ma, implications en terme de mécanismes moteur. *Bulletin de la Société Géologique de France*, *191*(1).

Roquero, E., Silva, P. G., Rodríguez-Pascua, M. A., Bardají, T., Elez, J., Carrasco-García, P., & Giner-Robles, J. L. (2019). Analysis of faulted fan surfaces and paleosols in the Palomares Fault Zone (Betic Cordillera, SE Spain): Paleoclimatic and paleoseismic implications. *Geomorphology*, *342*, 88-102.

Rosas, F. M., Duarte, J. C., Neves, M. C., Terrinha, P., Silva, S., Matias, L., Gracia, E., & Bartolomé, R. (2012). Thrust-wrench interference between major active faults in the Gulf of Cadiz (Africa-Eurasia plate boundary, offshore SW Iberia): Tectonic implications from coupled analog and numerical modeling. *Tectonophysics*, *548-549*, 1‑21. https://doi.org/10.1016/j.tecto.2012.04.013

Rosenbaum, G., Lister, G. S., & Duboz, C. (2002). Reconstruction of the tectonic evolution of the western Mediterranean since the Oligocene. *Journal of the Virtual Explorer*, *8*, 107-130.

Royden, L. H. (1993). Evolution of retreating subduction boundaries formed during continental collision. *Tectonics*, *12*(3), 629-638.

Ruano, P., & da S. Fernandes, R. M. (2020). Active Deformation in the Iberian Peninsula from Geodetic Techniques. In *The Geology of Iberia: A Geodynamic Approach* (pp. 5-9). Springer, Cham. https://doi.org/10.1007/978-3-030-10931-8_2

Ruiz-Constán, A., Galindo-Zaldívar, J., Pedrera, A., Célérier, B., & Marín-Lechado, C. (2011). Stress distribution at the transition from subduction to continental collision (northwestern and central Betic Cordillera). *Geochemistry, Geophysics, Geosystems*, *12*(12).

Ruiz-Constán, A., Pedrera, A., Galindo-Zaldívar, J., Pous, J., Arzate, J., Roldán-García, F. J., ... & Anahnah, F. (2012). Constraints on the frontal crustal structure of a continental collision from an integrated geophysical research: The central-western Betic Cordillera (SW Spain). *Geochemistry, Geophysics, Geosystems*, *13*(8).

Ruiz-Constán, A., Galindo-Zaldívar, J., Andrés-Martínez, M., Pedrera, A., & Martínez-Martos, M. (2013). Estructura de la Cuenca de Ugíjar a partir de datos gravimétricos y magnéticos (Zonas Internas, Cordillera Bética Central). *Geogaceta*, *54*, 95-98.

Sanz de Galdeano, C. (1983). Los accidentes y fracturas principales de las Cordilleras Béticas. *Estudios Geológicos (Madrid)*, *39*(3-4), 157-165.

Sanz de Galdeano, C. (1990). Geologic evolution of the Betic Cordilleras in the Western Mediterranean, Miocene to the present. *Tectonophysics*, *172*(1-2), 107‑119. https://doi.org/10.1016/00401951(90)90062-D

Sanz de Galdeano, C., & Vera, J. A. (1992). Stratigraphic record and palaeogeographical context of the Neogene basins in the Betic Cordillera, Spain. *Basin Research*, *4*(1), 21-36.

Sanz de Galdeano, C., Casado, C. L., Delgado, J., & Peinado, M. A. (1995). Shallow seismicity and active faults in the Betic Cordillera. A preliminary approach to seismic sources associated with specific faults. *Tectonophysics*, *248*(3-4), 293-302.

Sanz de Galdeano, C., & Alfaro, P. (2004). Tectonic significance of the present relief of the Betic Cordillera. *Geomorphology*, *63*(3-4), 175-190.

Schettino, A., & Turco, E. (2011). Tectonic history of the western Tethys since the Late Triassic. *Bulletin*, *123*(1-2), 89-105.

Seber, D., Barazangi, M., Ibenbrahim, A., & Demnati, A. (1996). Geophysical evidence for lithospheric delamination beneath the Alboran Sea and Rif–Betic mountains. *Nature, 379*(6568), 785‐790

Serpelloni, E., Vannucci, G., Pondrelli, S., Argnani, A., Casula, G., Anzidei, M., ... & Gasperini, P. (2007). Kinematics of the Western Africa-Eurasia plate boundary from focal mechanisms and GPS data. *Geophysical Journal International*, *169*(3), 1180-1200.

Serrano, I., Morales, J., Zhao, D., Torcal, F., & Vidal, F. (1998). P-wave tomographic images in the Central Betics-Alborán Sea (South Spain) using local earthquakes: Contribution for a continental collision. *Geophysical Research Letters*, *25*(21), 4031-4034.

Serrano, I., Hearn, T. M., Morales, J., & Torcal, F. (2005). Seismic anisotropy and velocity structure beneath the southern half of the Iberian Peninsula. *Physics of the Earth and Planetary Interiors*, *150*(4), 317-330.

Silva, P. G., Goy, J. L., Somoza, L., Zazo, C., & Bardají, T. (1993). Landscape response to strike-slip faulting linked to collisional settings: Quaternary tectonics and basin formation in the eastern Betics, southeastern Spain. *Tectonophysics*, *224*(4), 289–303. https://doi.org/10.1016/0040-1951(93)90034-H

Socias, I., & Mezcua, J. 2002. Mapa de Anomalías Magnéticas de la Península Ibérica. Instituto Geográfico Nacional (IGN), Madrid.

Spakman, W., & Wortel, R. (2004). A tomographic view on western Mediterranean geodynamics. In *The TRANSMED atlas. The Mediterranean region from crust to mantle* (pp. 31-52). Springer, Berlin, Heidelberg.

Spakman, W., Chertova, M. V., van den Berg, A., & van Hinsbergen, D. J. (2018). Puzzling features of western Mediterranean tectonics explained by slab dragging. *Nature Geoscience*, *11*(3), 211-216. https://doi.org/10.1038/s41561-018-0066-z

Stich, D., Serpelloni, E., Mancilla, F., & Morales, J. (2006). Kinematics of the Iberia-Maghreb plate contact from seismic moment tensors and GPS observations. *Tectonophysics 426*, 295–317. doi: 10.1016/j.tecto.2006.08.004

Stich, D., Martín, R., & Morales, J. (2010). Moment tensor inversion for Iberia–Maghreb earthquakes 2005–2008. *Tectonophysics*, *483*(3-4), 390-398.

Stich, D., Martínez-Solares, J. M., Custódio, S., Batlló, J., Martín, R., Teves-Costa, P., & Morales, J. (2020). Seismicity of the Iberian Peninsula. In *The geology of Iberia: A geodynamic approach* (pp. 11-32). Springer, Cham. https://doi.org/10.1007/978-3-030-10931-8_3

Suriñach, E., & Vegas, R. (1993) Estructura general de la corteza en una transversal del Mar de Alborán a partir de datos de sísmica de refracción-reflexión de gran ángulo. Interpretación geodinámica. *Geogaceta, 14,* 126-128.

Terrinha, P., Matias, L., Vicente, J., Duarte, J., Luis, J., Pinheiro, L., ... & Matespro Team. (2009). Morphotectonics and strain partitioning at the Iberia–Africa plate boundary from multibeam and seismic reflection data. *Marine Geology*, *267*(3-4), 156-174. https://doi.org/10.1016/j.margeo.2009.09.012

Thébault, E., Finlay, C. C., Beggan, C. D., Alken, P., Aubert, J., Barrois, O., ... & Zvereva, T. (2015). International geomagnetic reference field: the 12th generation. *Earth, Planets and Space*, *67*(1), 1-19.

Thiebot, E., & Gutscher, M. A. (2006). The Gibraltar Arc seismogenic zone (part 1): constraints on a shallow east dipping fault plane source for the 1755 Lisbon earthquake provided by seismic data, gravity and thermal modeling. *Tectonophysics*, *426*(1-2), 135-152.

Torné, M., Fernandez, M., Comas, M. C., & Soto, J. I. (2000). Lithospheric structure beneath the Alboran Basin: results from 3D gravity modeling and tectonic relevance. *Journal of Geophysical Research: Solid Earth*, *105*(B2), 3209-3228.

Van Bemmelen, R. W. (1927). Bijdrage tot de geologie der Betisch Ketens in de provincie Granada. Ph.D. Thesis, Univ. Delft, 176pp.

Van der Woerd, J., Dorbath, C., Ousadou, F., Dorbath, L., Delouis, B., Jacques, E., ... & Haessler, H. (2014). The Al Hoceima Mw 6.4 earthquake of 24 February 2004 and its aftershocks sequence. *Journal of Geodynamics*, *77*, 89-109.

Vernant, P., Fadil, A., Mourabit, T., Ouazar, D., Koulali, A., Davila, J. M., ... & Reilinger, R. (2010). Geodetic constraints on active tectonics of the Western Mediterranean: Implications for the kinematics and dynamics of the Nubia-Eurasia plate boundary zone. *Journal of Geodynamics*, *49*(3-4), 123-129.

Vitale, S., Zaghloul, M. N., El Ouaragli, B., Tramparulo, F. D. A., & Ciarcia, S. (2015). Polyphase deformation of the Dorsale Calcaire Complex and the Maghrebian Flysch Basin Units in the Jebha area (Central Rif, Morocco): New insights into the Miocene tectonic evolution of the Central Rif belt. *Journal of Geodynamics*, *90*, 14-31.

Weijermars, R. (1985). Uplift and subsidence history of the Alboran Basin and a profile of the Alboran Diapir (W-Mediterranean). *Geologie en Mijnbouw*, *64*(4), 349-356.

Weijermars, R., Roep, T. B., Eeckhout, B. V. D., Postma, G., & Kleverlaan, K. (2007). Uplift history of a Betic fold nappe inferred from Neogene-Quaternary sedimentation and tectonics (in the Sierra Alhamilla and Almeria, Sorbas and Tabernas Basins of the Betic Cordilleras, SE Spain). *Netherlands Journal of Geosciences/Geologie en Mijnbouw*, (Classic Papers).

Yelles, A., Domzig, A., Déverchère, J., Bracène, R., de Lépinay, B. M., Strzerzynski, P., ... & Djellit, H. (2009). Plio-Quaternary reactivation of the Neogene margin off NW Algiers, Algeria: the Khayr al Din bank. *Tectonophysics*, *475*(1), 98-116.

Zeck, H. P., Monié, P., Villa, I. M., & Hansen, B. T. (1992). Very high rates of cooling and uplift in the Alpine belt of the Betic Cordilleras, southern Spain. *Geology, 20,* 79-82.

Ziegler, P. A., Van Wees, J. D., & Cloetingh, S. (1998). Mechanical controls on collision-related compressional intraplate deformation. *Tectonophysics*, *300*(1-4), 103-129.

Appendix

Appendix A. Supplementary files of Chapter 4.

Appendix B. Supporting information of Chapter 8.

APPENDIX A

Supplementary files of Chapter 4

The supplementary files of Chaper 4 are provided in this section. These files are multichannel seismic reflection profiles that were used during the modeling of the magnetic profiles that constitute the main results of Chapter 4.

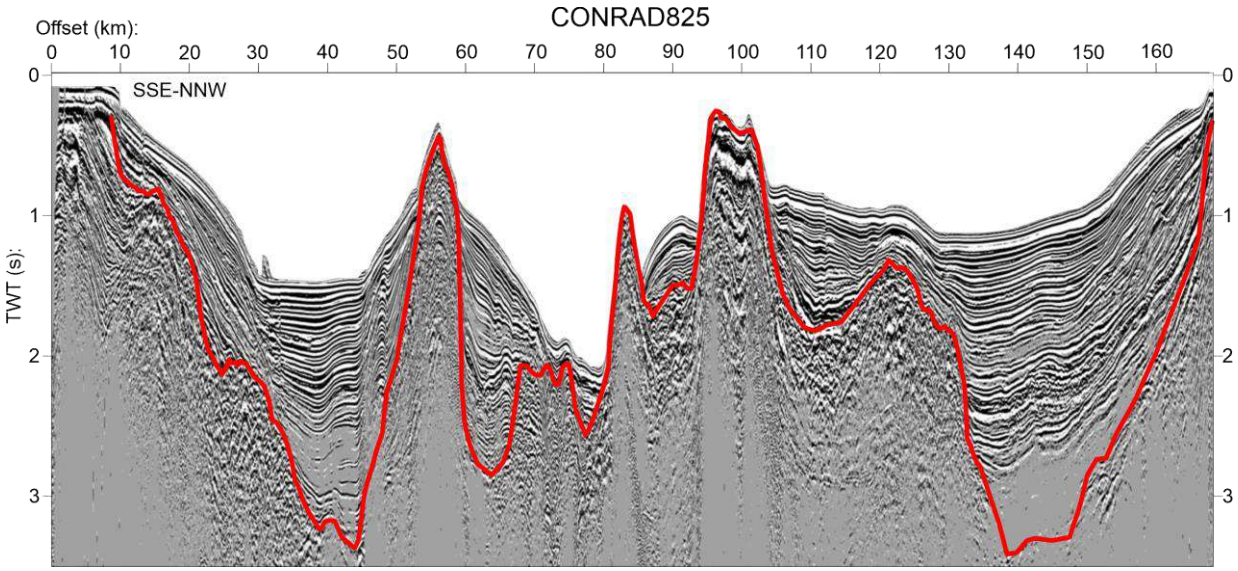

Figure A1. Seismic reflection profile CONRAD825. The sediments-basement contact is marked by the red line.

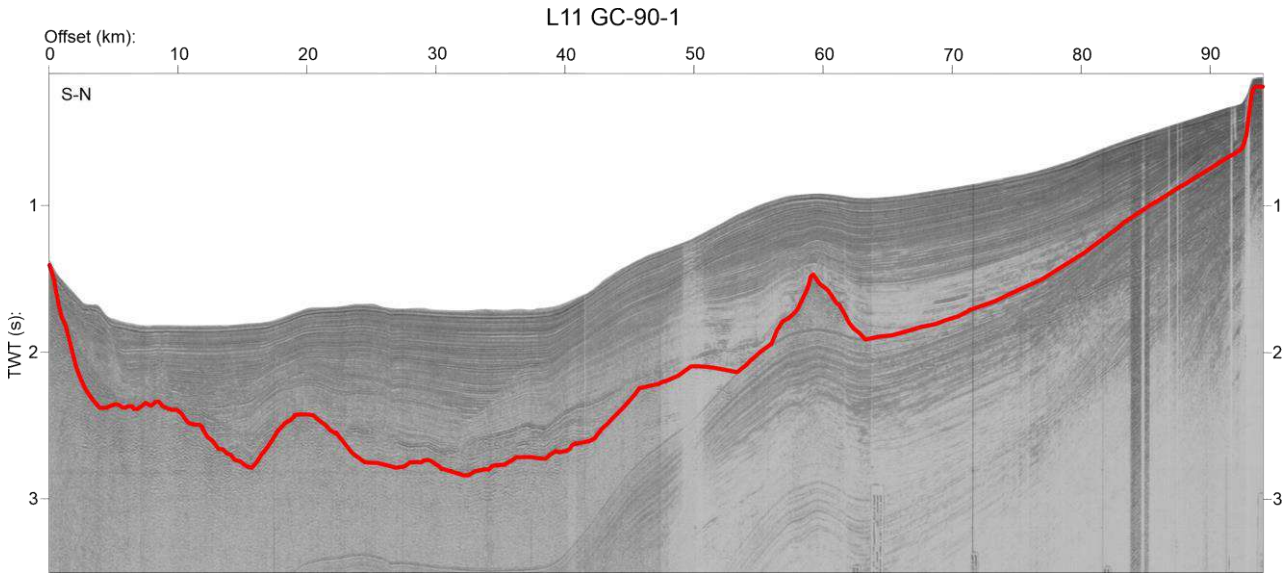

Figure A2. Seismic reflection profile L11 GC-90-1. The sediments-basement contact is marked by the red line.

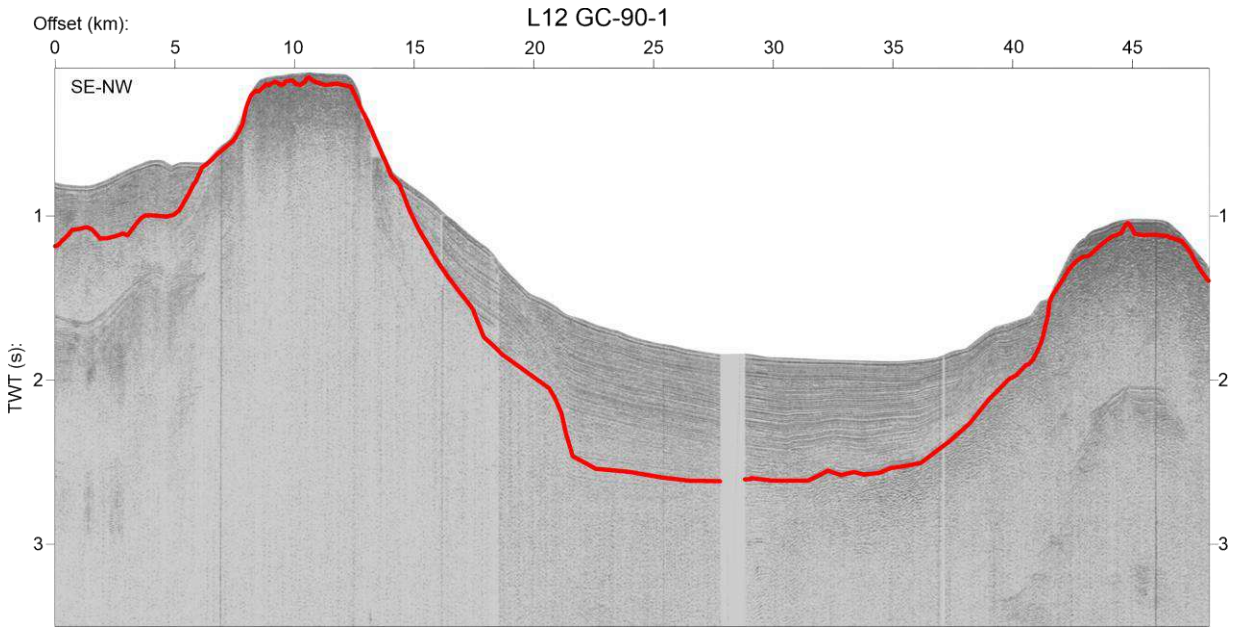

Figure A3. Seismic reflection profile L12 GC-90-1. The sediments-basement contact is marked by the red line.

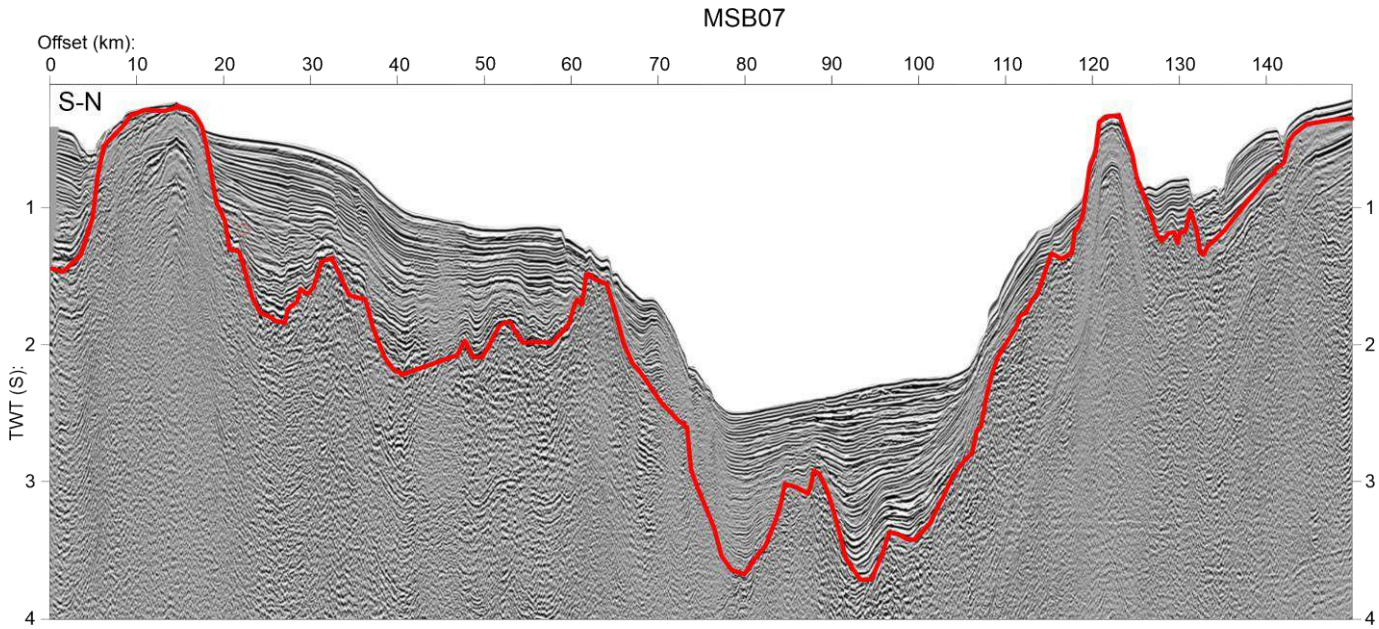

Figure A4. Seismic reflection profile MSB07. The sediments-basement contact is marked by the red line.

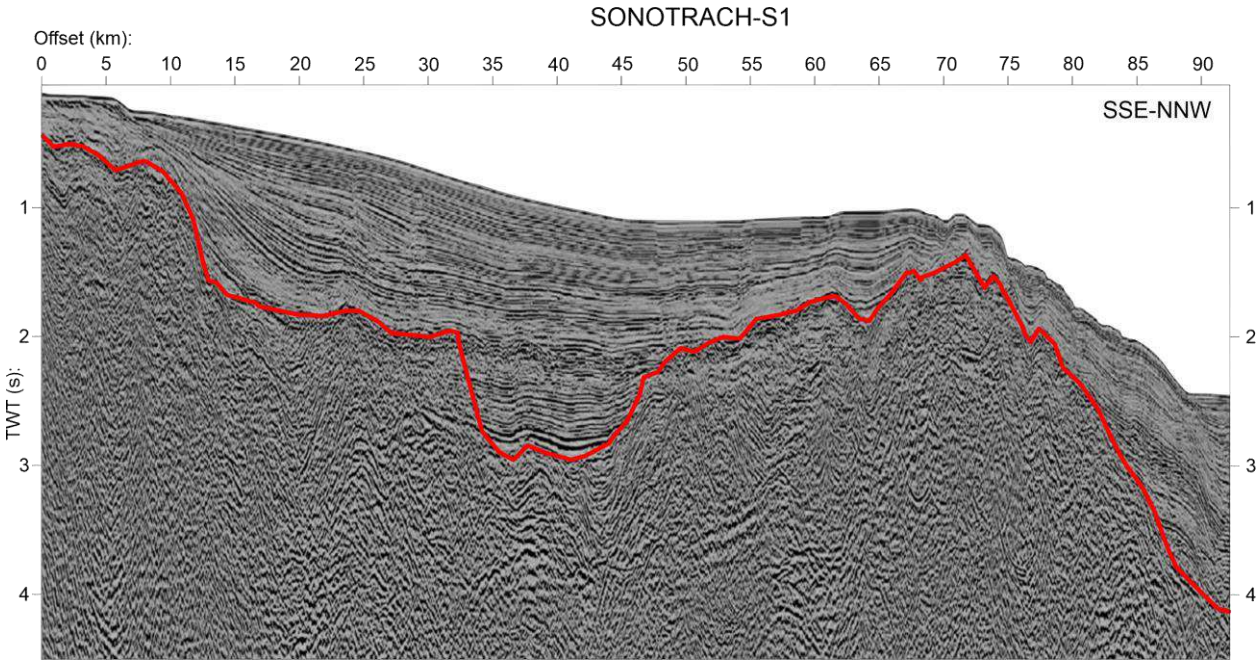

Figure A5. Seismic reflection profile SONOTRACH-S1. The sediments-basement contact is marked by the red line.

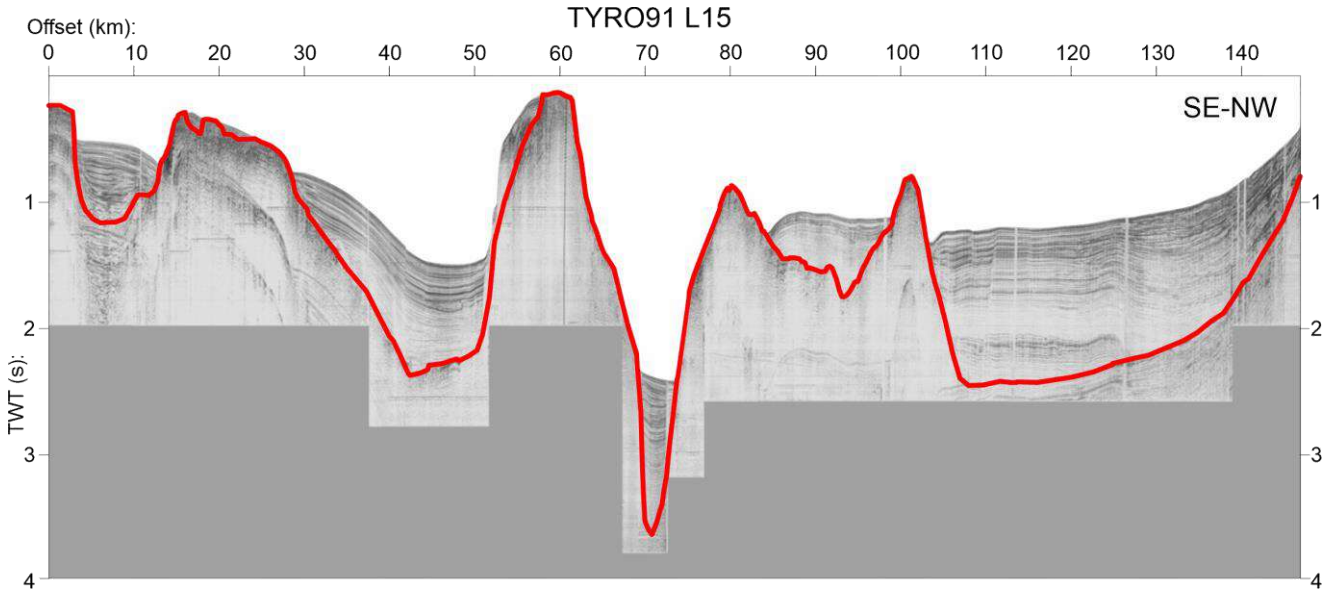

Figure A6. Seismic reflection profile TYRO91 L15. The sediments-basement contact is marked by the red line.

APPENDIX B

Supporting information of Chapter 8

The supporting information of Chapter 8 is provided in this section. This supporting information provides complementary explanations about the seismicity relocations. Figures comparing the earthquake locations before (IGN velocity model) and after the processing (our velocity model) are included. Finally, it is also included a figure (Fig. B8) with a photograph of the observed striae at the Tíscar fault.

In Figs. B1 and B2 the earthquakes locations made by IGN are depicted along two profiles (N-S and E-W respectively). This institution uses the code EVLOC and locates earthquakes individually. On the contrary, the code HypoDD used for relocations (Figs. B3 and B4) uses the difference in travel times for couples of events observed at one station and it obtains the relative position among them.

In Figs. B1 and B2 the 11-12 km level can be considered an artificial level because it coincides with a change in the shear velocity model used by this institution (see Table 8.1 in the main text, Chapter 8). After using HypoDD and our shear velocity model, we obtained a more diffuse earthquakes swarm where two clusters can be differentiated (Figs. B3 and B4). The appliance of this code have also reduced considerably the location mistakes (vertical and horizontal) as can be seen in figures B1, B2, B3, B4, B5 and B6. On the other hand, the depths of the clusters are close to changes in the shear velocity model (2 km and 12 km, see Table 8.1 in Chapter 8). Thus, we used another shear velocity model, the one presented in Palomeras *et al.* (2014). In this model, the changes of shear velocity located in the upper crust are at 5 km and 15 km (see table 8.1 in Chapter 8). Figure B7 shows a comparison between the results obtained with these models and the clusters maintained their position. Only the shallow cluster is more diffuse (although at the same depth) and the deep one appears in the same position.

Figure B8 show an example of the striae found in the fault plane of the Tíscar fault. They show a clear strike-slip kinematics with some downthrowing of the eastern block.

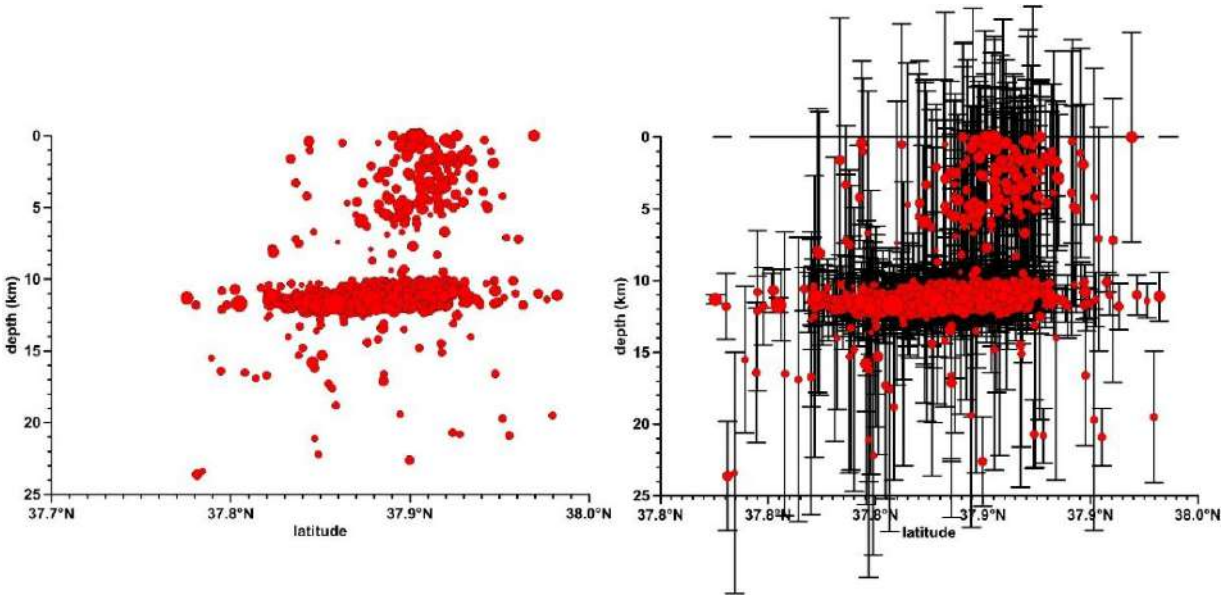

Figure B1. N-S profile of the locations computed by the Spanish IGN. Left: without depth error. Right: showing depth error provided by the institution.

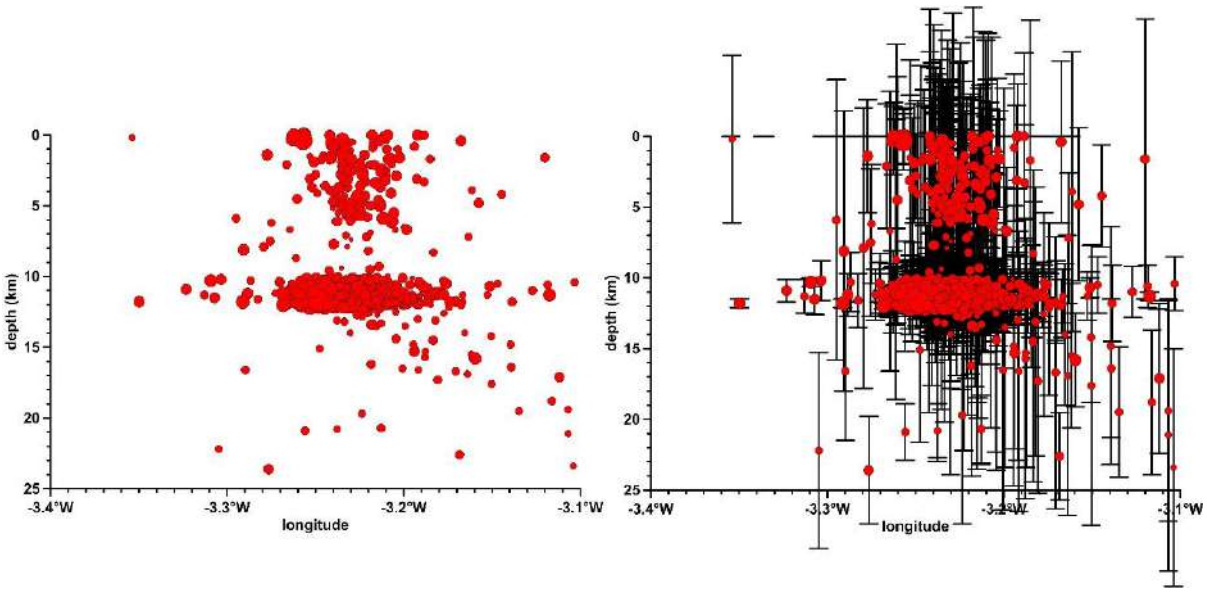

Figure B2. E-W profile of the locations computed by the Spanish IGN. Left: without depth error. Right: showing depth error provided by the institution.

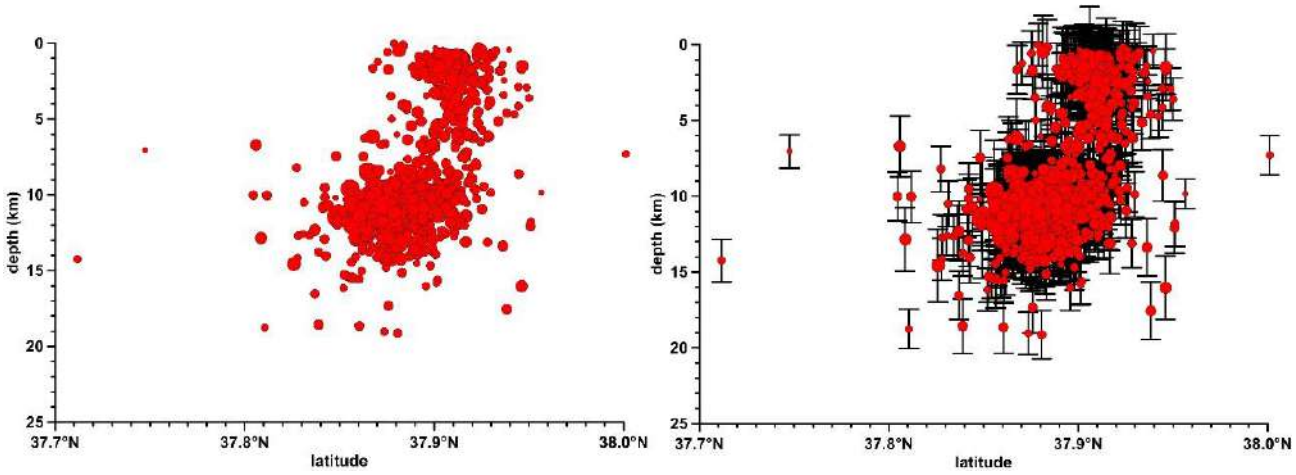

Figure B3. N-S profile of the locations computed in our work using HypoDD. Left: without depth error. Right: showing depth error computed by HypoDD.

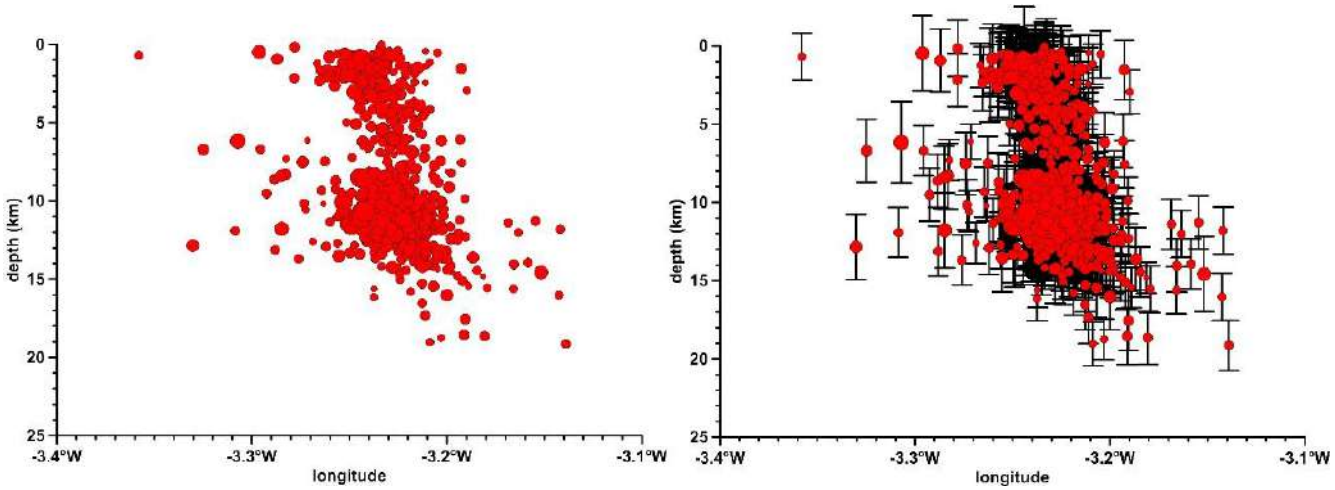

Figure B4. E-W profile of the locations computed in our work using HypoDD. Left: without depth error. Right: showing depth error computed by HypoDD.

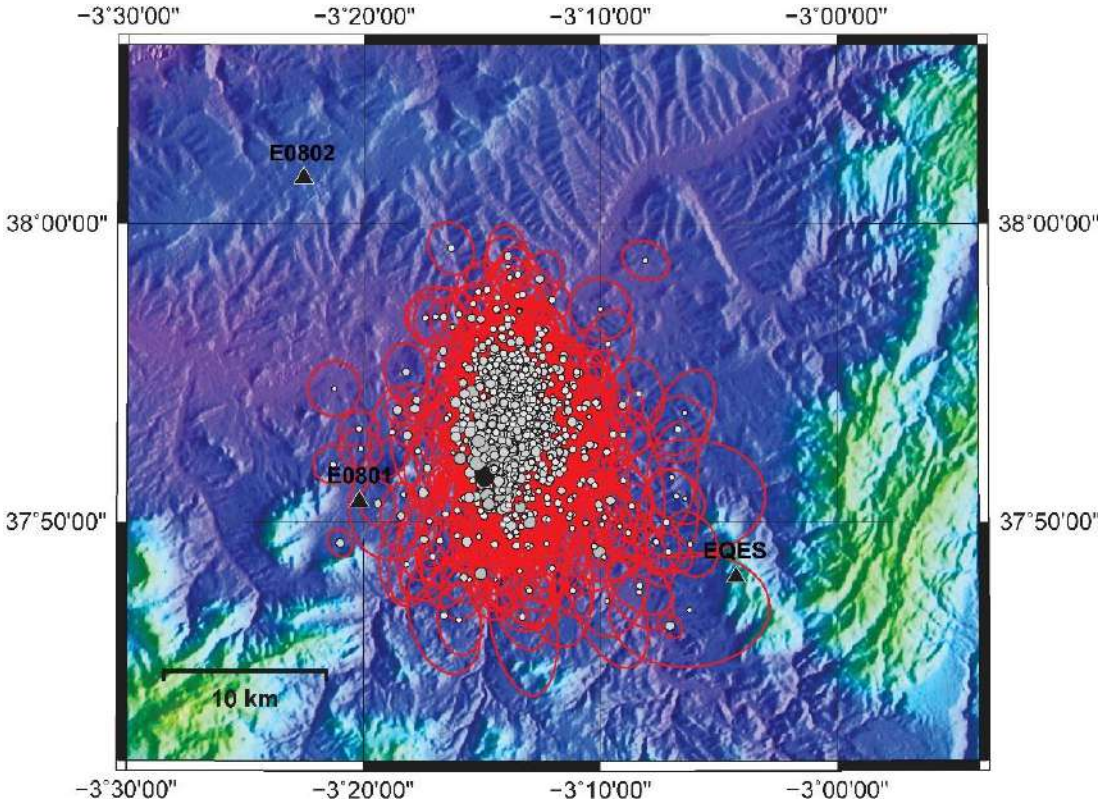

Figure B5. Locations computed by the Spanish IGN, showing error ellipses provided by the institution. Black triangles mark the position of the IGN seismic stations in the area.

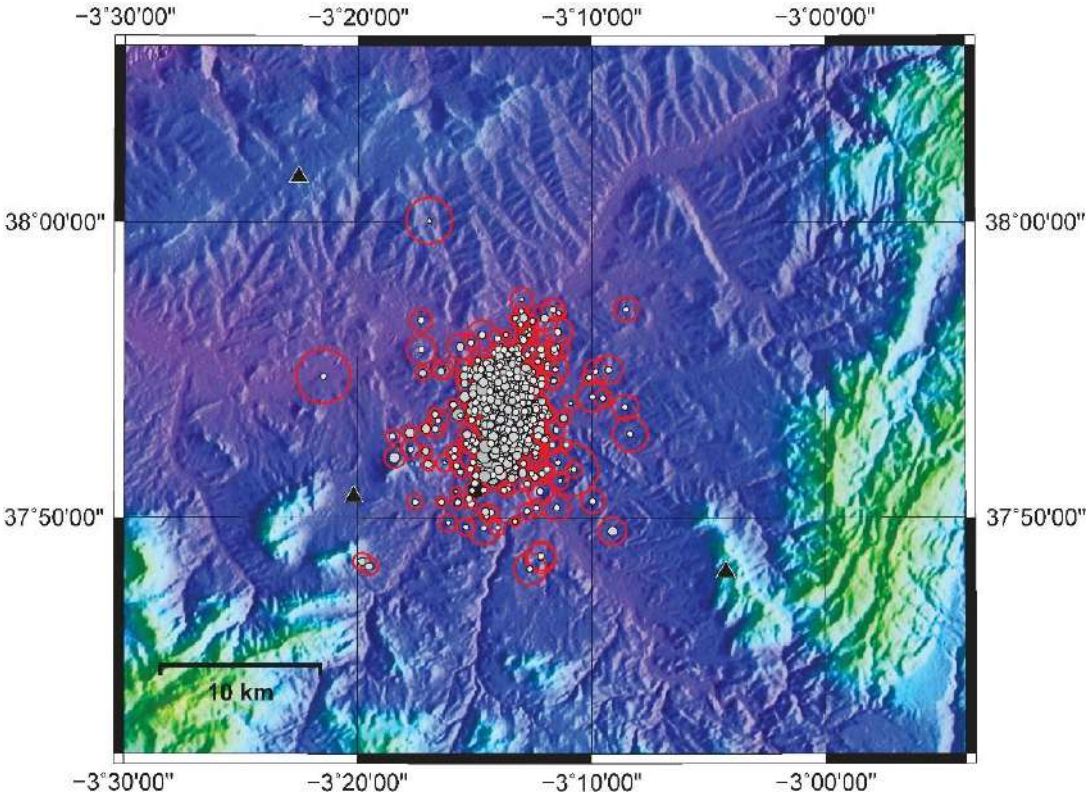

Figure B6. Locations computed in our work using HypoDD, showing computed mean errors. Black triangles mark the position of the IGN seismic stations in the area.

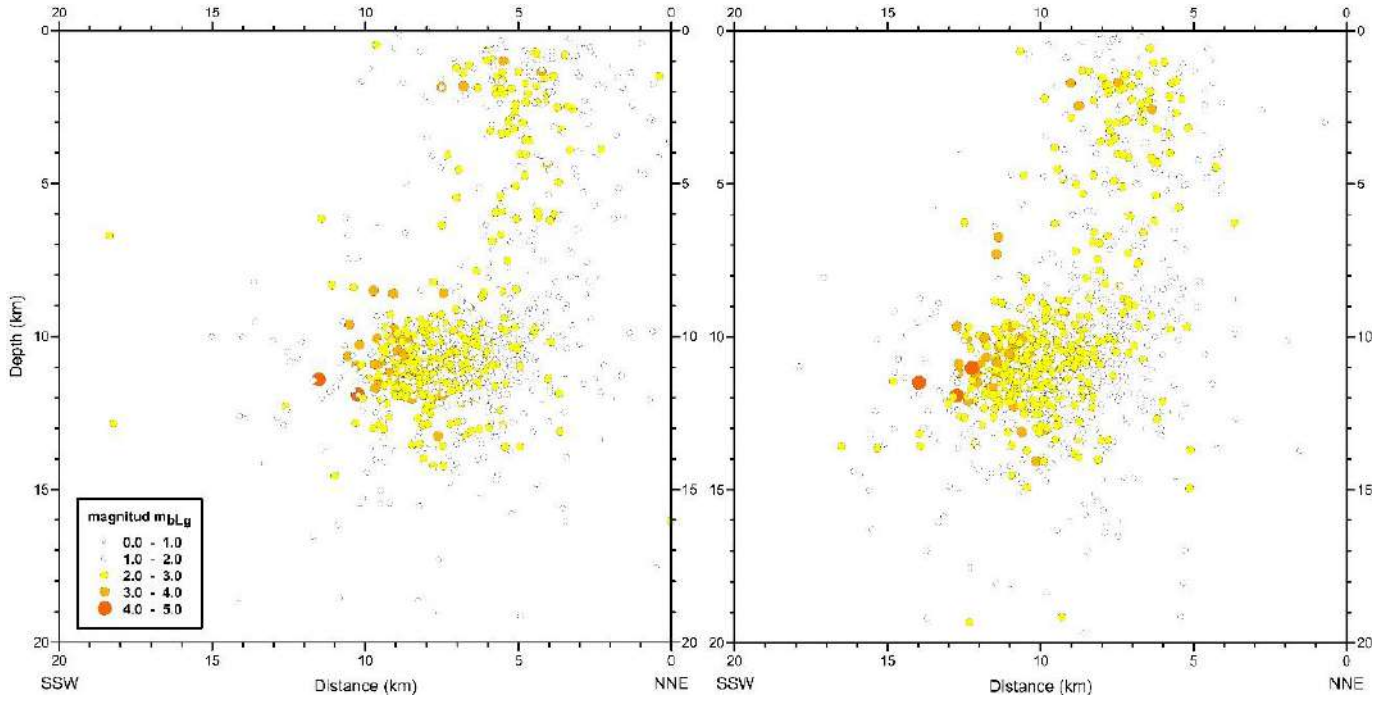

Figure B7. Relocated seismicity at depth along a SSW-NNE profile. Left: assessed relocation presented in our manuscript. Right: relocation carried out using the velocity model of Palomeras *et al.* (2014).

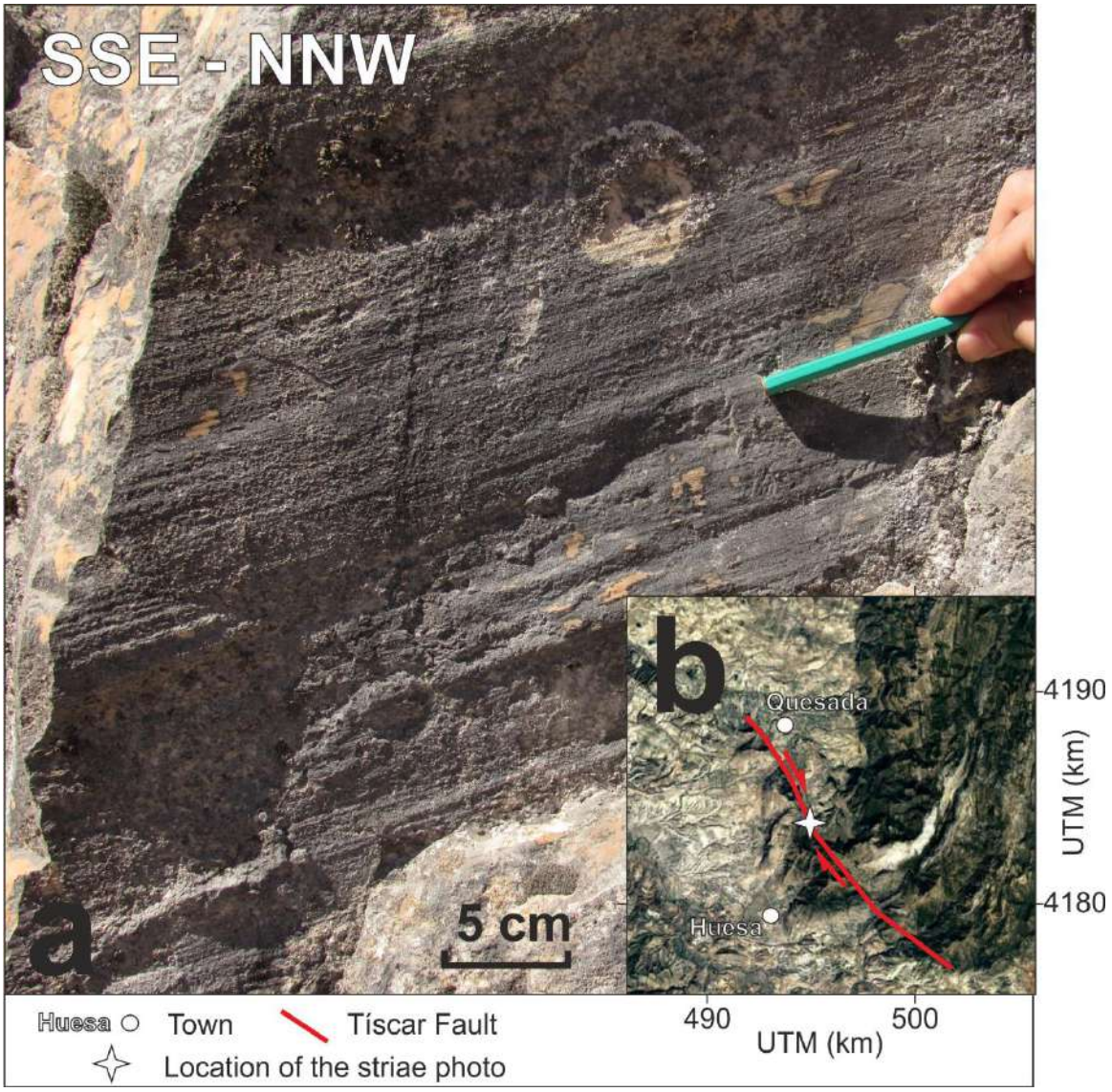

Figure B8. Striae observed at the Tíscar Fault plane (a) and location of the photograph (b).